ENHANCING THE ROBUSTNESS AND PRACTICALITY OF NANOFILTRATION MEMBRANES FOR WASTEWATER TREATMENT AND RESOURCE RECOVERY

Qieyuan Gao

Supervisor:

Prof. Bart Van der Bruggen (KU Leuven)

Prof. Peter Van Puyvelde (KU Leuven)

Members of the Examination Committee:

Prof. Robert Puers (Chair, KU Leuven)

Prof. Christian Clasen (Secretary, KU Leuven)

Prof. Pedro Fardim (KU Leuven)

Prof. Yumeng Zhao (Harbin Institute of Technology)

Prof. Asim Laeeq Khan (COMSATS University Islamabad)

Dissertation presented in partial fulfilment of the requirements for the degree of Doctor of Engineering Science (PhD):

Chemical Engineering

Feburary 2025

© Qieyuan Gao

Uitgegeven in eigen beheer, Qieyuan Gao, Celestijnenlaan 200F , 3001 Leuven

Alle rechten voorbehouden. Niets uit deze uitgave mag worden vermenigvuldigd en/of openbaar gemaakt worden door middel van druk, fotokopie, microfilm, elektronisch of op welke andere wijze ook zonder voorafgaandelijke schriftelijke toestemming van de uitgever.

All rights reserved. No part of the publication may be reproduced in any form by print, photoprint, microfilm, electronic or any other means without written permission from the publisher.

Dedication

For Prof. Bart Van der Bruggen, who have the same birthday as me.

For Prof. Yongtian Wang in heaven, who loved my story.

For my parents and my wife who gave me life, my present and my future.

For you who are reading, thank you for taking the time to participate in my life.

Acknowledgments

Engineers have always been artists, just like *Leonardo da Vinci* when he wrote to the *Duke of Milan* in 1482. Eleven years ago, I accidentally chose to study engineering, giving up my dream of becoming a chef. In 2021, amid the special circumstances of the pandemic, I arrived in the small European town of Leuven, embarking on a magical journey. Time flies, and when I suddenly look back, I realize that as the number of Asian supermarkets on *Brusselsestraat* has grown, and I have already spent several years here. The university hall on *Naamsestraat* remains quietly there, coldly observing the comings and goings of people like me, quietly waiting for its 600th birthday. This university has brought me more than just Erasmus and Mercator, the so-called "light of humanity". They are just cold names to me. KU Leuven has brought me warm knowledge, friendship, and even love. Likewise, Leuven, this international Flemish city, has given me a warm doctoral journey. This warmth would not have been possible without the support of my family, friends, promoters, and my homeland.

First and foremost, I want to thank my promoter, *Prof. Bart Van der Bruggen*, who has the same birthday as me. As the Flemish say, "A person who has the same birthday as you are very important in your life." He has been a significant figure involved in the two most important events of my life so far. First, as my Ph.D. promoter, he witnessed the entire process of my doctoral journey. Secondly, as the best man at my wedding, he added much meaning to my life. In fact, he is the best Ph.D. promoter I have ever met. At a time when news of conflicts between promoters and students is becoming more frequent, Bart and I can still raise our glasses—whether it's vodka, whiskey, or the finest Belgian beer, we can happily cheer together. In my life, Bart is not only my Ph.D. promoter and wedding best man but also an important friend. I still remember when a paper was rejected for the sixth time, Bart would still tell me, "Your research abilities are not wrong; it is just the review rules that are stupid." I believe in fate; I believe it is a mysterious force in the universe, perhaps as enigmatic as the Bhagavad Gita or the Quran, that brought me together with this person who is very important in my life. I am very grateful to Bart for his help, companionship, and the encouragement he gave me during my life's low points.

I would like to thank my co-promoter, *Prof. Peter Van Puyvelde* (Department of Chemical Engineering, KU Leuven). Peter is a very responsible person. Whenever I need help, no matter how busy he is, he always responds positively. I would also like to thank my assessors, Prof. Christian Clasen

(Department of Chemical Engineering, KU Leuven) and *Prof. Pedro Fardim* (Department of Chemical Engineering, KU Leuven). You participated in all essential points in my Ph.D. progress and gave me valuable comments and profound suggestions. Furthermore, I would like to express my gratitude to *Prof. Robert Puers* (Department of Electrical Engineering, KU Leuven) for being the chairman of my Ph.D. defense, *Prof. Yumeng Zhao* (Department of Chemical Engineering, Harbin Institute of Technology), and *Prof. Asim Laeeq Khan* (Department of Chemical Engineering, COMSATS University Islamabad) for agreeing to be my jury members.

At this point, I want to express my gratitude to my master's supervisor, *Prof. Yongtian Wang*. Although he passed away while working in his beloved field of research, his legacy has continuously inspired me and has been a driving force for me to keep moving forward in my engineering career. Here, I also want to thank an important person, our technician, *Herman Tollet* (Department of Chemical Engineering, KU Leuven). As an important friend, he has always warmed my heart in his own way. Whether it's discussing the history of ancient Rome or the weather in Belgium, we always seem to have common topics to talk about. I can't believe that a Flemish man of the same age as my father shares so many interests with me. If I could choose the Secretary-General of the United Nations, I would definitely vote for this person who has crossed nationalities, generational gaps, and religions to become my friend! Additionally, I want to express my heartfelt gratitude to *Christine Wouters*, *Hanne Geunes*, *Michèle Vanroelen*, *Kim Natus*, and *Alexander Volodine* for their tremendous help with my experiments and work during my doctoral journey.

I also want to thank my colleagues, whose companionship made my nearly perfect doctoral journey possible. I am grateful to *Dr. Pengrui Jin*, who taught me how to prepare my first membrane. I also want to thank *Dr. Junfeng Zheng*, who captured many beautiful moments of my travels in Europe with his camera. Additionally, I want to thank *Dr. Yan Zhao* for his help with my research and academic work. I am also grateful to another best man, *Stef Depuydt*, and the members of the "Komen eten" group, including *Gilles Van Eygen, Julieta Garcia Chirino, Diego Acevedo,* and their partners and families. They provided a lot of support for my life and studies. I also want to thank my other colleagues: *Daliang Xu, Yue Wang, Yanyan Liu, Rui Zhao, Junwei Li, Riri Liu, Lei Jiang, Qin Chen,* and others. There are too many names to list, and I apologize for not being able to mention everyone individually. I want to thank each one of you for your support during my doctoral studies. A friend will joyfully sing with you when

you are on the mountain top, and silently walk beside you through the valley. I also want to express my gratitude to all the friends who have silently supported me behind my back. We are fortunate to have met in Leuven, regardless of nationality, gender, race, or faith. May our friendship forever!

At this moment, I cannot forget my homeland and the support from the China Scholarship Council (CSC) under the Ministry of Education. It is through their support that I was given the opportunity to study in Belgium. The CSC provides Chinese students like myself with the chance to study at world-class universities abroad, and we have all greatly benefited from it. Including myself, Chinese international students must express gratitude for the support our homeland provides us with. Here, I want to say, “感谢祖国！”

Last but not least, I want to express my gratitude to my family and my wife. Especially to my wife, I still remember how we looked on our wedding day last year. It was the "De langste dag", as we registered our marriage in the City Hall of Leuven. We met, grew to know each other, and fell in love in Leuven. There's a Chinese saying that goes, "First establish a family, then pursue a career." Thank you for enabling me to embody this ancient Chinese wisdom passed down for thousands of years. As I write these words, you are still by my side, and no matter what I do, my greatest honor is seeing you beside me. I am grateful that we chose each other to spend our lives together! Here, I want to say, my dear *Jiahui*, I love you!

Qieyuan Gao



Leuven, May 2024

Table of contents

Acknowledgments ..... **I**

Abstract ..... **IX**

Samenvatting ..... **XIII**

List of abbreviations ..... **XVI**

Chapter 1: General introduction and research outline **1**

1.1 Background **1**

1.2 Thesis outline **4**

1.3 Motivation and objective of this thesis **6**

1.4 Technical background and theoretical framework of nanofiltration **7**

1.4.1 Characteristics of nanofiltration membranes 8

1.4.2 Separation mechanism of nanofiltration membrane 8

1.5 Manufacturing and synthesis of nanofiltration membranes **11**

1.5.1 Phase inversion 11

1.5.2 Layer-by-layer self-assembly 12

1.5.3 Interfacial polymerization 13

1.6 Application of nanofiltration membrane in water treatment **15**

1.6.1 Textile wastewater 15

1.6.2 Surface/groundwater treatment 16

1.6.3 Brackish water treatment 19

1.6.4 Wastewater reuse and resource recovery 20

1.7 Limitations of nanofiltration membranes **21**

1.7.1 Robustness in nanofiltration membranes 21

1.7.2 Practicality concerns in nanofiltration applications 23

Chapter 2: Materials and methods **25**

2.1 Chemicals and materials **25**

2.2 Membrane Preparation Procedure **27**

2.2.1 Preparation of PEI-THPC-AMN membranes (Chapter 3) 27

2.2.2 Preparation of pDA/β-cyclodextrin/GA (PBG) membranes (Chapter 4) 28

2.2.3 Preparation of dye/salt separation membranes (DSM) (Chapter 5) 30

2.2.4 Preparation of AMN- Cu-TiO_2/CuO membranes (Chapter 6) 32
2.3 Characterization 34
2.3.1 Surface chemistry 34
2.3.2 Morphology 34
2.3.3 Surface properties 35
2.3.4 Photocatalytic performance characterization 35
2.4 Filtration performance measurement 36
2.4.1 Membrane separation performance 36
2.4.2 Anti-(bio)fouling and robustness performance 39
2.4.3 Pore size distribution 42
2.5 Photocatalytic conversion performance evaluation 42
2.6 Computational simulations 43
2.6.1 Molecular dynamics (MD) simulations of membranes 43
2.6.2 The density functional theory (DFT) calculations of membranes 44
2.6.3 The density functional theory (DFT) calculations of photocatalyst 44
Chapter 3: Positively charged nanofiltration membranes based on Mannich reaction and prebiotic chemistry for anti-(bio)fouling 45
3.1 Introduction 45
3.2 Results and discussion 47
3.2.1 Chemical composition characterization of the membranes surface 47
3.2.2 Morphology of the membranes 49
3.2.3 Hydrophilicity and surface potential characteristics of the membranes 50
3.3.4 Filtration performance of the membranes 51
3.2.5 Antifouling and antibacterial performance of the membranes 57
3.3 Conclusion 59
Chapter 4: Robust loose nanofiltration membrane with fast solute transfer for dye/salt separation 61
4.1 Introduction 61
4.2 Results and discussion 63
4.2.1 Chemical composition characterization of the membrane surface 63

4.2.2 Morphology of the membrane 65
4.2.3 Hydrophilicity and surface potential characteristics of the membrane 67
4.2.4 Membrane filtration performance 68
4.2.5 Stability and self-cleaning properties of the membrane 72
4.2.6 pH stability and antibacterial properties of the membrane 74
4.3 Conclusion 76
Chapter 5: Robust self-cleaning membrane based on host-guest interaction combined with photocatalyst loading 77
5.1 Introduction 77
5.2 Results and discussion 79
5.2.1 Chemical composition characterization of DSM surface 79
5.2.2 Morphology of DSM 82
5.2.3 Hydrophilicity and surface potential characteristics of DSM 85
5.2.4 DSM filtration performance 86
5.2.5 Self-cleaning and photocatalytic properties of DSM 92
5.3 Conclusion 97
Chapter 6: Tailoring fast mass transfer membrane: zero discharge of wastewater using visible light to increase practicality 99
6.1 Introduction 99
6.2 Results and discussion 100
6.2.1 Membrane simulation predictions 100
6.2.2 Insertion of AMN into PIP/pDA selection layer 103
6.2.3 Bifunctional Cu-TiO_2/CuO photocatalyst on the membrane 105
6.2.4 Membrane separation performance 107
6.2.5 Membrane self-cleaning and photocatalytic properties 112
6.2.6 Photocatalytic mechanism 115
6.3 Conclusion 117
Chapter 7: General conclusions and further research 119
7.1 General Conclusions 119
7.2 Recommendations and future research 121

References **125**

Curriculum Vitae **153**

Abstract

Water scarcity represents a global challenge, affecting over one-third of the world's population. Human-induced water pollution, particularly from industrial sources, exacerbates this crisis. Nanofiltration (NF) membrane technology offers promising solutions to mitigate water scarcity issues. However, the robustness and practicality of NF membranes significantly limit their widespread adoption. Among these limitations, membrane robustness plays a pivotal role in addressing pollution concerns and impacting separation efficiency in practical scenarios. Understanding the factors and mechanisms underlying fouling is essential, considering the complex physical and chemical interactions influenced by contaminant properties, operational parameters, and membrane characteristics. Additionally, enhancing membrane stability and recyclability through the incorporation of antibacterial or self-cleaning properties is crucial. Besides fouling, challenges related to membrane stability, necessitating mechanical and chemical robustness, must be addressed to ensure sustained performance. Concerns regarding the practicality of membrane synthesis underscore the need for evaluating materials for large-scale deployment and considering cost implications. Despite advancements in integrating nanomaterials, careful examination of the feasibility of mass production and long-term environmental impacts is imperative. Shifting research focus towards prioritizing the practicality of membrane development is vital for achieving sustainable water treatment solutions. This thesis will propose solutions focusing on enhancing membrane robustness and practicality, aiming to provide technical support for the widespread application of NF technology in water treatment processes.

The emergence of increasingly permeable nanofiltration membranes for dye/salt separation has prompted exploration into synthesis approaches employing interfacial polymerization and bio-inspired materials such as polydopamine (pDA). However, the protracted polymerization duration of pDA poses significant constraints on the efficient fabrication and utilization of rapid dye/salt separation membranes. In this study, leveraging prebiotic chemistry principles, aminomalononitrile (AMN) was utilized as a binding agent for co-depositing tetrakis(hydroxymethyl)phosphonium chloride (THPC) and polyethyleneimine (PEI) via the Mannich reaction, facilitating the swift formation of a positively charged selective layer. The optimized membrane exhibited a water permeance of 30.7 LMH bar^{-1} and demonstrated rejection of 99.5% for positively charged Victoria blue B (VBB, 200 ppm) and 9.9% for

Na_2SO_4 (1g/L). Furthermore, practical application testing underscored its outstanding separation efficacy across various positively charged dyes and salts, alongside demonstrating a commendable long-term stability. Notably, the membrane exhibited remarkable antibacterial and antifouling properties, as corroborated by subsequent antibacterial assessments, including confirmation of its efficacy against *E. coli.* This proposed preparation methodology offers valuable technical insights for advancing the development of novel dye/salt separation membranes.

Furthermore, in the treatment of textile wastewater, the utilization of a membrane possessing enhanced solute transport properties enables selective solute removal at a consistent energy input, thereby promoting energy savings. Moreover, given the challenging nature of typical textile wastewater, it is imperative for membranes to exhibit a certain level of robustness. In this thesis, β-cyclodextrin (β-cyclodextrin) and mussel-inspired polydopamine (pDA) were synergistically integrated via host-guest chemistry, subsequently cross-linked using glutaraldehyde to engender a resilient yet permeable separation layer. Results indicate that membranes fabricated through this approach demonstrate a dye rejection exceeding 99% and a salt rejection of approximately 16%. Notably, the surface's substantial cross-linking endows the membrane with exceptional resilience in corrosive media across varying pH ranges. Additionally, the heightened cross-linking density on the surface imparts commendable anti-fouling and antibacterial properties to the modified membrane. Filtration experiments employing diverse concentrations of dye/salt mixtures underscore the membrane's stability in filtering highly concentrated salt solutions. Furthermore, a protracted stability assessment confirmed the membrane's operational consistency for over 60 hours, preserving its selectivity. This robust membrane holds promise for offering practical guidance and theoretical underpinnings for the widespread implementation of loose nanofiltration membranes on an industrial scale.

The extraction of dyes and salts from textile wastewater is imperative for resource reutilization. In this study, a highly selective and permeable photocatalytic membrane was developed utilizing supramolecular β-cyclodextrin and mussel-inspired polydopamine pDA as foundational elements. The membrane featured a stable intermediate layer of AgBr-Ag_3PO_4 photocatalyst, formed *in-situ* through host-guest interaction between β-cyclodextrin and pDA, facilitating the creation of honeycomb microstructures. The optimized photocatalytic membrane exhibited exceptional separation efficacy, boasting a water permeance of 101.3 LMH bar^{-1}, alongside achieving a remarkable dye rejection of up

to 99% and efficient salt transport from synthetic dye textile wastewater. Under visible light, the AgBr-Ag_3PO_4 layer allowed for a nearly complete degradation of dyes adhering to the membrane surface, thus imparting outstanding self-cleaning photocatalytic properties to the membrane. Through comprehensive material and membrane characterization, the superior separation performance of the membrane was elucidated, highlighting the benefits of host-guest interaction between β-cyclodextrin and pDA, as well as the *in-situ* photocatalytic functionalization approach. This investigation provides valuable insights for expediting the separation of Angström-sized molecules in membrane separation processes.

In response to the imperative to address pollution and recover resources in industrial settings, there has been a pioneering approach: the integration of separation membranes and advanced photocatalysts. This thesis introduces a catalyzed mass-transfer membrane designed to enhance the treatment of heavy metal salts and dyes in wastewater. The research reveals a significant development—the incorporation of AMN into a polydopamine (pDA)/piperazine (PIP) selective layer, altering its structure and improving the membrane permeance. The AMN-pDA/PIP selective layer demonstrates notable self-cleaning and anti-biofouling properties, maintaining effectiveness over prolonged real-world applications. Additionally, the introduction of Cu-TiO_2/CuO heterojunction photocatalyst results in simultaneous membrane modification, leading to reduced Cr^{6+} levels during oxidative degradation of dye species. This approach achieves impressive removal rates of approximately 70% for Cr^{6+} and 100% for dye, as demonstrated in authentic textile wastewater conditions. The mechanism behind the exceptional photocatalytic performance is elucidated through comprehensive simulations and pollutant filtration tests.

Samenvatting

Waterschaarste vormt een wereldwijde uitdaging en treft meer dan een derde van de wereldbevolking. Door de mens veroorzaakte watervervuiling, met name door industriële bronnen, verergert deze crisis. Nanofiltratie (NF) membraantechnologie biedt veelbelovende oplossingen om de problemen van waterschaarste te verminderen. De robuustheid en praktische bruikbaarheid van NF-membranen beperken echter de brede adoptie ervan aanzienlijk. Onder deze beperkingen speelt de robuustheid van het membraan een cruciale rol bij het aanpakken van vervuilingsproblemen en het beïnvloeden van de scheidingsefficiëntie in praktische scenario's. Het begrijpen van de factoren en mechanismen die ten grondslag liggen aan vervuiling is essentieel, gezien de complexe fysieke en chemische interacties die worden beïnvloed door de eigenschappen van verontreinigingen, operationele parameters en membraaneigenschappen. Bovendien is het verbeteren van de membraanstabiliteit en recycleerbaarheid door de opname van antibacteriële of zelfreinigende eigenschappen cruciaal. Naast vervuiling moeten uitdagingen met betrekking tot de stabiliteit van het membraan, die mechanische en chemische robuustheid vereisen, worden aangepakt om een duurzame prestatie te waarborgen. Zorgen over de praktische bruikbaarheid van membraansynthese onderstrepen de noodzaak om materialen te evalueren voor grootschalige inzet en kostenoverwegingen in overweging te nemen. Ondanks vooruitgang bij de integratie van nanomaterialen, is zorgvuldige beoordeling van de haalbaarheid van massaproductie en de langetermijneffecten op het milieu noodzakelijk. Het verschuiven van de onderzoeksfocus naar het prioriteren van de praktische bruikbaarheid van membraanontwikkeling is essentieel voor het bereiken van duurzame waterzuiveringsoplossingen. Deze scriptie zal oplossingen voorstellen die zich richten op het verbeteren van de robuustheid en praktische bruikbaarheid van membranen, met als doel technische ondersteuning te bieden voor de brede toepassing van NF-technologie in waterzuiveringsprocessen.

De opkomst van steeds doorlatendere nanofiltratie membranen voor kleurstof/zoutscheiding heeft geleid tot onderzoek naar synthesebenaderingen waarbij interfaciale polymerisatie en bio-geïnspireerde materialen zoals polydopamine (pDA) worden gebruikt. De langdurige polymerisatieduur van pDA vormt echter aanzienlijke beperkingen voor de efficiënte fabricage en het gebruik van snelle kleurstof/zoutscheidingsmembranen. In deze studie, gebruikmakend van prebiotische chemieprincipes, werd aminomalononitrile (AMN) gebruikt als bindmiddel voor de co-depositie van tetrakis(hydroxymethyl)fosfoniumchloride (THPC) en polyethyleenimine (PEI) via de Mannich-reactie, wat de snelle vorming van een positief geladen selectieve laag faciliteert. Het geoptimaliseerde membraan vertoonde een waterpermeabiliteit van 30,7 LMH bar^{-1} en toonde een afwijzing van 99,5% voor positief geladen Victoria blue B (VBB, 200 ppm) en 9,9% voor Na_2SO_4 (1g/L). Bovendien benadrukten praktische toepassingsproeven de uitstekende scheidingsefficiëntie over verschillende positief geladen kleurstoffen en zouten, naast het aantonen van een bewonderenswaardige langdurige stabiliteit. Opmerkelijk is dat het membraan opmerkelijke antibacteriële en anti-vervuilingseigenschappen vertoonde, zoals bevestigd door daaropvolgende antibacteriële beoordelingen,

waaronder de bevestiging van de werkzaamheid tegen *E. coli*. Deze voorgestelde bereidingsmethode biedt waardevolle technische inzichten voor het bevorderen van de ontwikkeling van nieuwe kleurstof/zoutscheidingsmembranen.

Bovendien, bij de behandeling van textielafvalwater, maakt het gebruik van een membraan met verbeterde oplosmiddeltransporteigenschappen selectieve verwijdering van oplosmiddelen mogelijk bij een constant energieverbruik, waardoor energiebesparing wordt bevorderd. Daarnaast, gezien de uitdagende aard van typisch textielafvalwater, is het van essentieel belang dat membranen een bepaald niveau van robuustheid vertonen. In deze scriptie werden β-cyclodextrine en door mosselen geïnspireerde polydopamine synergetisch geïntegreerd via gast-gastheerchemie, en vervolgens gekruislinkt met glutaraldehyde om een veerkrachtige maar doorlaatbare scheidingslaag te creëren. Resultaten geven aan dat membranen die door deze aanpak zijn vervaardigd, een kleurstofafwijzing van meer dan 99% en een zoutafwijzing van ongeveer 16% vertonen. Opmerkelijk is dat de aanzienlijke kruislinking van het oppervlak het membraan uitzonderlijke veerkracht geeft in corrosieve media over verschillende pH-bereiken. Bovendien verleent de verhoogde kruislinkdichtheid op het oppervlak het gemodificeerde membraan uitstekende anti-vervuiling en antibacteriële eigenschappen. Filtratie-experimenten met verschillende concentraties van kleurstof/zoutmengsels benadrukken de stabiliteit van het membraan bij het filteren van sterk geconcentreerde zoutoplossingen. Bovendien bevestigde een langdurige stabiliteitsbeoordeling de operationele consistentie van het membraan gedurende meer dan 60 uur, waarbij de selectiviteit behouden bleef. Dit robuuste membraan biedt veelbelovende praktische richtlijnen en theoretische onderbouwingen voor de brede implementatie van losse nanofiltratiemembranen op industriële schaal.

De extractie van kleurstoffen en zouten uit textielafvalwater is essentieel voor hergebruik van hulpbronnen. In deze studie werd een zeer selectief en doorlaatbaar fotokatalytisch membraan ontwikkeld met behulp van supramoleculaire β-cyclodextrine en door mosselen geïnspireerde polydopamine (pDA) als fundamentele elementen. Het membraan had een stabiele tussenlaag van AgBr-Ag_3PO_4-fotokatalysator, in-situ gevormd door gast-gastheerinteractie tussen β-cyclodextrine en pDA, wat de creatie van honingraat-microstructuren faciliteerde. Het geoptimaliseerde fotokatalytische membraan vertoonde uitzonderlijke scheidingsefficiëntie, met een waterpermeabiliteit van 101,3 LMH bar^{-1}, naast een opmerkelijke kleurstofafwijzing tot 99% en efficiënte zouttransport uit synthetisch kleurstof textielafvalwater. Onder zichtbaar licht zorgde de AgBr-Ag_3PO_4-laag voor een bijna volledige afbraak van kleurstoffen die aan het membraanoppervlak kleven, waardoor het membraan uitstekende zelfreinigende fotokatalytische eigenschappen kreeg. Door uitgebreide materiaal- en membraankarakterisering werd de superieure scheidingsprestatie van het membraan verduidelijkt, waarbij de voordelen van gast-gastheerinteractie tussen β-cyclodextrine en pDA, evenals de in-situ fotokatalytische functionalisatiebenadering werden benadrukt. Dit onderzoek biedt waardevolle inzichten voor het versnellen van de scheiding van Angström-grootte moleculen in membraanscheidingsprocessen.

In reactie op de noodzaak om vervuiling aan te pakken en hulpbronnen te herwinnen in industriële omgevingen, is er een baanbrekende benadering ontwikkeld: de integratie van scheidingsmembranen en geavanceerde fotokatalysatoren. Deze scriptie introduceert een gekatalyseerd massatransportmembraan dat is ontworpen om de behandeling van zware metaalzouten en kleurstoffen in afvalwater te verbeteren. Het onderzoek onthult een significante ontwikkeling—de incorporatie van AMN in een polydopamine (pDA)/piperazine (PIP) selectieve laag, waardoor de structuur wordt gewijzigd en de doorlaatbaarheid van het membraan wordt verbeterd. De AMN-pDA/PIP selectieve laag vertoont opmerkelijke zelfreinigende en antibiofilm-eigenschappen, waardoor de effectiviteit gedurende langdurige toepassingen in de praktijk behouden blijft. Bovendien resulteert de introductie van Cu-TiO_2/CuO heterojunctie-fotokatalysator in gelijktijdige membraanmodificatie, wat leidt tot verlaagde Cr^{6+}-niveaus tijdens de oxidatieve afbraak van kleurstofsoorten. Deze benadering bereikt indrukwekkende verwijderingspercentages van ongeveer 70% voor Cr^{6+} en 100% voor kleurstof, zoals aangetoond onder authentieke textielafvalwateromstandigheden. Het mechanisme achter de uitzonderlijke fotokatalytische prestaties wordt verduidelijkt door middel van uitgebreide simulaties en verontreinigingsfiltratietests.

List of abbreviations	
AC	Alternating current
AMN	Aminomalononitrile
AFM	Atomic force microscopy
CFU	Colony forming units
CB	Conduction band
CR	Congo red
DFT	Density functional theory
DCM	Dichloromethane
DMPO	5,5-Dimethyl-1-pyrroline-Noxide
DMSO	Dimethyl sulfoxide
DR23	Direct red 23
DA	Dopamine
DSM	Dye/salt separation membranes
EIS	Electrochemical impedance spectroscopy
ESR	Electron spin resonance
E. coli	Escherichia coli
FRR	Fouling resistance ratio
FT-IR	Fourier transform infrared spectrometer
GGA	Generalized gradient approximation
GA	Glutaraldehyde
ITO	Indium tin oxide
IP	Interfacial polymerization
JGB	Janus green B
LNMs	Loose nanofiltration membranes
LB	Luria-Bertani broth
MSD	Mean square displacement
MO	Methyl orange
MB	Methylene blue

MF	Microfiltration
MD	Molecular dynamics
MWCO	Molecular weight cut-off
MPD	m-phenylenediamine
NF	Nanofiltration
NR	Neutral Red
PBVF	Patent blue VF
PBG	pDA/β-cyclodextrin/GA
PBE	Perdew-Burke-Ernzerhof
PBS	Phosphate-buffered saline
PIP	Piperazine
PEG	Poly (ethylene glycol)
PAN	Polyacrylonitrile
pDA	Polydopamine
PES	Polyethersulfone
PE	Polyethylene
PEI	Polyethyleneimine
PP	Polypropylene
RDFs	Radial distribution functions
RB5	Reactive black 5
RB2	Reactive blue 2
RO16	Reactive orange 16
RESP	Restrained electrostatic potential
RO	Reverse osmosis
RhB	Rhodanile blue
SEM	Scanning electron microscopy
AgNPs	Silver nanoparticles
SDS	Sodium dodecyl sulfate
SDFs	Spatial distribution functions

TBAPF6	Tetrabutylammonium hexafluorophosphate
THPC	Tetrakis(hydroxymethyl)phosphonium chloride
TOC	Total organic carbon
TEM	Transmission electron microscopy
TMC	Trimesoyl chloride
VB	Valence band
UF	Ultrafiltration
VBB	Victoria blue B
WCA	Water contact angle
WP	Water permeance
XRD	X-ray diffractometer
XPS	X-ray photoelectron spectrometer

Chapter 1: General introduction and research outline

Adapted from: *"Gao, Q., Li, J., Jin, P., Zheng, J., Xu, D., van der Bruggen, B. with Gao, Q. (corresp. author), van der Bruggen, B. (corresp. author) (2023). The Practical Application Value of a Sustainable Water Purification Process Is Crucial. ACS ES&T WATER, 3 (8), 1990-1993. doi: 10.1021/acsestwater.3c00301"*

1.1 Background

With the relentless advancement of industrialization and the persistent expansion of the global population, the issue of water scarcity has burgeoned into a pervasive challenge impeding worldwide economic progress [1]. Presently, merely a fraction, approximately 2.5%, of the available water reservoirs is deemed suitable for direct human consumption and utilization in various productive endeavors [2]. Alarmingly, as reported by the World Resources Institute, 41% of the Earth's inhabitants reside in regions afflicted by water scarcity, a figure projected to surge to 62% by the onset of 2025 [3]. Projections based on the latest statistical analyses forewarn that nearly a quarter of the global populace will grapple with acute water shortages by the year 2030 [4]. Human activities, particularly those associated with industrial production processes, have significantly contributed to water pollution and exacerbated the global water scarcity crisis [5]. Diverse industrial sectors generate substantial volumes of effluent containing a myriad of contaminants, encompassing heavy metals, organic compounds, pesticides, pharmaceuticals, and nutrients [6]. Notably, industrial activities such as mining, metallurgy, and manufacturing are principal sources of heavy metal discharge, including lead, mercury, cadmium, and arsenic, into aquatic ecosystems [7, 8]. These metals possess notable water solubility and exhibit a prolonged persistence in the environment [8]. Furthermore, organic pollutants such as polycyclic aromatic hydrocarbons and polychlorinated biphenyls originate from industrial emissions, urban runoff, and agricultural practices, manifesting characteristics of enduring presence, toxicity, and potential bioaccumulation within aquatic biota [9]. Agricultural effluents, comprising pesticides, herbicides, and fertilizers, compound water pollution challenges by inducing eutrophication, harmful algal proliferation, and contamination of potable water supplies through leaching into watercourses [10]. Similarly, pharmaceuticals and personal care products, encompassing antibiotics, hormones, and fragrances, infiltrate water bodies via wastewater discharges, posing hazards to aquatic ecosystems and human well-being [11]. Additionally, improper management of solid waste, including plastic residues, electronic

discards, and hazardous materials, engenders water pollution through leaching and runoff pathways [12]. Notably, the widespread prevalence of microplastics in global water bodies underscores a concerning threat to aquatic biodiversity and potential integration into the food web [13-15].

In response to this escalating crisis, there has been a mounting acknowledgment of the multifaceted social and ecological benefits that accrue from ensuring adequate water resources, spanning economic prosperity, ecological integrity, and public health [16]. Furthermore, within the EU, significant strides were made in 2024 to address water management concerns. In January of that year, the European Parliament ratified an agreement with the Council aimed at revising the EU's regulations pertaining to water management and urban wastewater treatment [17]. This revision was undertaken with the overarching goal of enhancing safeguards for public health and environmental preservation [18, 19]. As part of this agreement, EU member states will be mandated to actively promote the reuse of all treated wastewater, with a particular emphasis on regions facing acute water stress. Consequently, there has been a burgeoning quest for technological interventions to alleviate water scarcity [20]. Advanced treatment methodologies for municipal and industrial wastewater, coupled with the widespread adoption of desalination techniques and water reuse strategies, stand out as indispensable pathways toward fostering sustainable development in contemporary industries and ameliorating the prevailing water crisis [21-23].

Within the realm of advanced water treatment methodologies, membrane separation technology stands out as a novel approach utilizing external pressure or disparities in chemical potential energy to facilitate the permeation of solvent through a semi-permeable membrane, thereby effecting the segregation of solute and solvent constituents. This technology presents advantages including streamlined processes, heightened integration, cost-efficiency, and potential for automation. Its applications span diverse domains such as potable water purification, wastewater handling, seawater desalination, and wastewater reclamation, thus serving as a cornerstone in establishing technical frameworks for upholding water quality, mitigating water pollution, enhancing aquatic ecosystems, and mitigating water scarcity. Membrane processes are categorized based on multiple criteria encompassing membrane composition, material properties, driving forces, separation mechanisms, and the size range of targeted components for removal. Presently, predominant water treatment modalities involve pressure-driven membranes, which are classified into four primary categories contingent upon pore size or molecular weight cut-off: microfiltration, ultrafiltration, nanofiltration, and reverse osmosis membranes.

Among these membranes, nanofiltration membranes function akin to loosely configured reverse osmosis membranes, boasting exceptional pollutant removal capabilities for smaller contaminants [24, 25]. Moreover, nanofiltration membranes can operate at moderately lower pressures while yielding substantially higher wastewater fluxes, rendering them a prime option for enhancing the efficacy and efficiency of water treatment processes [26]. During nanofiltration membrane separations, solute retention is influenced by various repulsion phenomena, including size screening, Donnan repulsion, and dielectric repulsion [27]. Typically, nanofiltration membranes demonstrate proficiency in rejecting over 95% of divalent ions with charges akin to the membrane surface, while monovalent ion rejection typically falls within the range of 20% to 80% [28-30]. Furthermore, nanofiltration membrane technology assumes a pivotal role in resource recovery [31-33]. Specifically, within the domain of wastewater treatment, nanofiltration membranes exhibit a notable effectiveness in eliminating prevalent pollutants present in industrial effluents, encompassing organic matter, heavy metals, and salts, thereby facilitating their reclamation and subsequent utilization [34]. Simultaneously, wastewater treated through nanofiltration membranes can be repurposed, thus diminishing reliance on natural reservoirs and fostering the reuse of water resources [1]. It merits attention that this technology not only finds extensive application in industrial settings but also exerts a significant impact in urban water treatment, agricultural water conservation, and related domains, thereby affirming its contributions to sustainable development and environmental preservation [35].

Nevertheless, nanofiltration membranes do not represent a panacea and confront several hurdles. Despite generally necessitating lower operating pressures compared to reverse osmosis membranes, nanofiltration membranes demand a certain energy input to facilitate solvent penetration through their pores [36, 37]. This energy consumption is contingent not only upon operating pressure but also closely tied to membrane material composition and structural attributes [38]. With global energy expenses on the rise, reducing the energy footprint of nanofiltration membranes has become an increasingly pressing imperative. Addressing this challenge mandates achieving swift mass transfer rates while meeting wastewater treatment [39]. In addition, nanofiltration membranes are susceptible to membrane fouling, prone to contamination by diverse pollutants such as organic compounds and particulate matter, leading to surface precipitation or pore penetration, thereby inducing fouling and performance degradation [40-42]. Membrane fouling escalates cleaning and upkeep expenses, while also impairing membrane

longevity and operational robustness [42-44]. Moreover, the feasibility and sustainability of nanofiltration membranes pose pivotal considerations [45]. The preparatory and operational costs associated with these membranes are relatively elevated, encompassing outlays linked to membrane material selection and preparation, energy consumption, and maintenance and cleaning protocols [46, 47]. These cost limitations have hindered the widespread adoption of nanofiltration membrane technology. Furthermore, in alignment with burgeoning sustainability imperatives, there is a mounting imperative to prioritize the environmental sustainability and eco-friendliness of membrane materials [48]. Hence, there exists an urgent imperative to explore and advance more environmentally benign and sustainable membrane materials and fabrication processes. Thus, despite substantial strides in nanofiltration membrane technology, it grapples with myriad challenges. Overcoming these hurdles necessitates ongoing technological innovation and refinement, alongside astute policy frameworks and market incentives to foster broader deployment and sustained advancement of nanofiltration membrane technology in water treatment.

1.2 Thesis outline

In view of the limitations of nanofiltration membranes in robustness and practicality, this thesis conducted in-depth research and proposed several specific solutions. Specifically, this thesis comprises seven chapters organized as follows:

Chapter 1 offers a concise examination of the pervasive issue of water scarcity, succeeded by a comprehensive investigation into nanofiltration membrane technology. The emphasis is on elucidating the fundamental principles, state-of-the-art manufacturing methodologies, and varied applications of nanofiltration membranes. Furthermore, extant constraints associated with the flexibility and applicability of nanofiltration membranes are rigorously examined. **Chapter 2** delineates the material information utilized in this thesis, encompassing membrane preparation methodologies, analytical testing techniques, membrane performance evaluation, and computational simulation methods. **Chapter 3** documents the Mannich reaction with AMN for the synthesis of positively charged membranes tailored for desalination purposes in dye solutions. Utilizing a one-step co-deposition approach, PEI and THPC undergo the Mannich reaction, culminating in the formation of a positively charged selective layer adept at repulsing positively charged dyes while facilitating the rapid transport of salts. The selective layers

were affixed onto polyacrylonitrile (PAN) substrates employing AMN. The efficacy of the membranes was assessed through separation testing involving positively charged dyes and two salts commonly found in textile wastewater, namely Na_2SO_4 and NaCl. Additionally, investigations were conducted into the self-cleaning attributes of the membrane and the commendable bio-antifouling properties attributed to prebiotic-inspired AMN. **Chapter 4** delves into the utilization of host-guest coordination between pDA/β-cyclodextrin, coupled with glutaraldehyde in chemical cross-linking, to expedite solute transport for the attainment of swift dye/salt separation and resource recovery. This endeavor not only proposes a synthetic methodology for the fabrication of membranes conducive to rapid dye/salt separation but also elucidates the capacity of glutaraldehyde-cross-linked supramolecular β-cyclodextrin and pDA to configure a transport channel structure. Furthermore, the robustness of the membrane was scrutinized with respect to acid-base stability, antifouling performance, bacterial resistance, and long-term stability, thereby furnishing theoretical insights and technical underpinnings to bolster its practical deployment. **Chapter 5** introduces a novel high-flux membrane for dye/salt separation, characterized by rapid solute transfer channels facilitated through host-guest interactions. This membrane exhibits efficient dye rejection alongside rapid salt transport. Furthermore, an in-situ photocatalyst layer is synthesized on the membrane surface, which effectively degrades pollutants via photocatalysis, endowing the membrane with commendable antifouling and self-cleaning properties. The primary objective of this chapter is twofold: firstly, to propose a synthetic strategy for the development of efficient dye/salt separation membranes featuring rapid solute transfer; and secondly, to underscore the novelty of photocatalyst-supported membranes with enduring operational stability over the long term. **Chapter 6** elucidates the concept of a catalytic membrane system distinguished by a synergistic effect that enhances the permeability of the selective layer, thereby promoting accelerated mass transport. This augmentation is achieved through the incorporation of small molecule AMN. Moreover, by integrating photocatalytic components into the conventional PIP/pDA selective layer, the membrane exhibits self-cleaning properties and mitigates the concentration of heavy metal ions. This innovative membrane represents a significant advancement in enhancing the practical utility of nanofiltration membranes, thus harboring considerable potential for optimizing wastewater treatment processes. **Chapter 7** gives the final conclusions drawn from the research findings and offering insights into future prospects. The conclusion synthesizes the key outcomes and contributions of the study, highlighting the significance and implications of the research within the broader context of the field. Furthermore, this chapter outlines

potential avenues for future research and development, identifying areas for further exploration and innovation, by providing a comprehensive summary of the study's findings and suggesting directions for future inquiry.

1.3 Motivation and objective of this thesis

The primary objective of this study is to address the pressing need to tackle the multifaceted challenges inherent in wastewater treatment and resource recovery, particularly in the realm of nanofiltration membranes. Although nanofiltration membranes present promising avenues for pollutant removal and the retrieval of valuable resources from wastewater streams, they frequently encounter significant hurdles concerning their durability and applicability in real-world scenarios. In recent years, global attention, including that of the European Union, has remained steadfastly focused on sustainable objectives, with a particular emphasis on water pollution mitigation and resource recuperation. Consequently, the principal aim of this research is to optimize the design and synthesis of pragmatic and resilient nanofiltration membranes adaptable to diverse contexts, effectively segregating pollutants within water bodies and refining resource retrieval processes to address challenges stemming from water scarcity induced by pollution. This endeavor endeavors to fundamentally mitigate water shortages precipitated by contamination. To this end, the research objectives of this thesis are delineated as follows:

(1) In order to improve the fouling resistance and selectivity of the membrane, surface modification methods are used to achieve this using advanced chemical monomers.
(2) Develop polymers with enhanced mechanical strength, chemical resistance and resistance to contamination. Polymer reinforcement, cross-linking or the incorporation of additives gives the membrane the potential for durability.
(3) Integration of nanoparticles or nanocomposites into the membrane matrix can bolster mechanical attributes, augment surface hydrophilicity, and furnish supplementary functionalities like antibacterial or antifouling properties.
(4) Synergizing technologies from disparate domains to engineer and synthesize membranes aims to yield more pragmatic nanofiltration membranes.

1.4 Technical background and theoretical framework of nanofiltration

Nanofiltration (NF) came into prominence in the late 1970s (Fig. 1.1) [49]. Unlike its predecessors, NF membranes are primarily thin film composites, a structural feature shared with RO membranes [50]. However, NF membranes demonstrate a nuanced performance discrepancy in effectively segregating smaller and less charged ions, such as sodium and chloride ions, when juxtaposed with RO membranes [51]. The fundamental differentiator of NF membranes lies in their nanoporous structure, typically characterized by pore sizes below 2 nm. This nanoarchitecture imparts NF membranes with a unique molecular weight cutoff (MWCO) typically ranging from 150 to 800 Da [52]. Such selective permeability facilitates NF's pivotal role as an intermediary between UF and RO, facilitating the partial removal of salts from water [53]. This selective removal is predominantly achieved through mechanisms of size exclusion and charge repulsion [52, 53]. Notably, NF exhibits a distinct capacity to target specific ionic species, notably sulfate ions and hardness ions, contributing to its efficacy in water treatment processes. This selectivity is particularly advantageous in scenarios requiring targeted ion removal while preserving essential water constituents. Moreover, NF's operational advantages further underscore its utility in various applications [52]. These benefits include a lower requirement for operational pressure, reduced energy consumption, and augmented flux rates compared to traditional RO processes [54, 55]. The intricate nanoporous structure of NF membranes, coupled with their selective permeability and operational efficiencies, positions NF as a versatile and effective tool in water treatment processes, with implications spanning industrial, environmental, and public health domains [54].

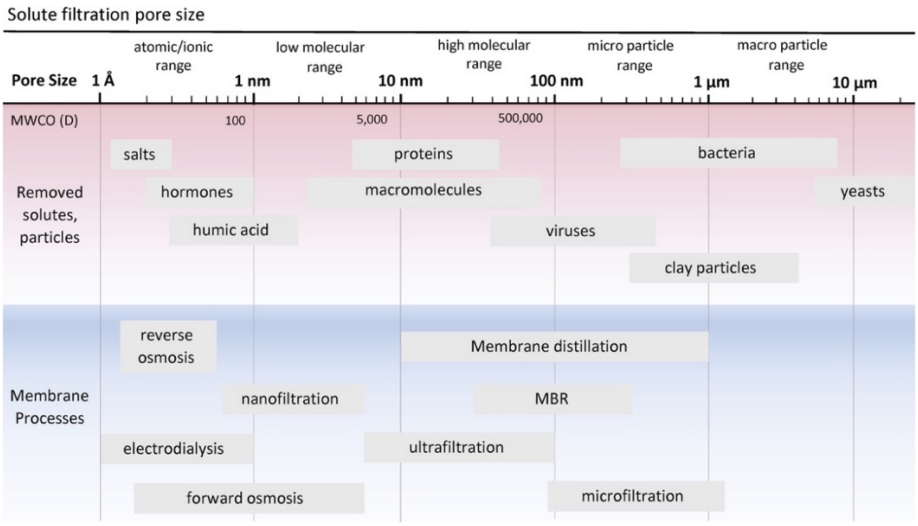

Figure 1.1 Membrane separation processes, pore sizes, molecular weight cut-off (MWCO): Classification and use of various membranes [56].

1.4.1 Characteristics of nanofiltration membranes

In typical scenarios, nanofiltration membranes exhibit negative surface charges under neutral or alkaline conditions, while they become positively charged under acidic conditions [57]. This surface charge attribute confers a beneficial role in selectively intercepting multivalent ions [58]. The prevalent negative charge characterizing most commercial nanofiltration membranes stems from the presence of negative fixed charges on the polymer backbone, such as sulfonic and carboxylic acids [59]. Conversely, positively charged nanofiltration membranes find utility in separating cations due to their positively charged surface. Furthermore, a noteworthy phenomenon known as the "trade-off" effect governs the interplay between the permeability and selectivity of nanofiltration membranes [53, 60]. The nanostructured topography on the membrane surface proves instrumental in enhancing membrane permeability while ensuring sustained selectivity [61]. Nanostructures leverage external stimuli to modulate the diffusion kinetics of aqueous monomers, such as the introduction of inhibitors into the aqueous phase or precise adjustments to the matrix's hydrophilicity [62]. Enhanced hydrophilicity contributes to heightened rejections, permeate flux, and anti-fouling properties of the membrane. Supramolecular chemistry interventions wield influence over the spatial dimensions of monomers via host-guest interactions, thereby eliciting changes in their diffusion kinetics [63]. Furthermore, the selectivity of NF membranes can be fine-tuned through alterations in surface charge. When the membrane carries a charge, ions are retained, whereas when the membrane is neutralized, ions permeate through the membrane [64]. One approach to modulating the surface charge of nanofiltration membranes involves the deposition of a metal oxide layer [65]. The surface charge of metal oxides is contingent upon the pH of the aqueous solution, and the formation of metal oxide layers typically occurs through atomic or molecular layer deposition techniques [59, 66].

1.4.2 Separation mechanism of nanofiltration membrane

Nanofiltration mass transfer is a pressure-driven process predicated on the pressure differential across the membrane. Given its intricate nature, numerous researchers persist in proposing and refining relevant models. Notably, surface interfacial interactions of the membrane and the influence of microfluidic motion proximal to the membrane surface contribute to this complexity (Fig. 1.2). Moreover, the internal structure of the membrane exerts a substantial impact on mass transfer. Consequently,

drawing from the characteristics shared between nanofiltration membranes and those of ultrafiltration and reverse osmosis membranes, mass transfer mechanisms akin to those utilized in ultrafiltration and reverse osmosis can be applied to elucidate nanofiltration membrane mass transfer phenomena. A frequently model often employed is the "pore flow model" originating from ultrafiltration membranes, grounded in the convection-driven mass transfer across the membrane. Notably, the size discrepancy between solutes and membrane pores predicates size exclusion steric hindrance. The water flux of porous membranes can be quantified utilizing equations such as the Hagen-Poiseuille equation or the Kozeny-Carman equation, given by Equation (1.1) and Equation (1.2), respectively:

$$J = \left(\frac{\varepsilon r_p^{\,2}}{8\tau l}\right)\left(\frac{\Delta P}{\eta}\right) = \frac{\Delta P}{\eta R_m} \tag{1.1}$$

where J is the water flux; ε is the membrane porosity; rp is the membrane pore radius; τ is the membrane tortuosity; l is the thickness of the rejection layer; ΔP is the trans-membrane pressure; η is the viscosity of water and R_m is the membrane hydraulic resistance.

$$J = \left(\frac{\varepsilon^3}{K_{KC} l S_m^2 (1-\varepsilon)^2}\right)\left(\frac{\Delta P}{\eta}\right) \tag{1.2}$$

where K_{KC} is the Kozeny-Carman coefficient; S_m is the specific surface area.

RO membranes typically comprise a dense functional layer known as the rejection layer. The mass transfer phenomenon across RO membranes is commonly expounded using the "Solution-diffusion model". In this model, both solute and solvent molecules permeate into the nonporous rejection layer, subsequently diffusing across it under the influence of their respective concentration gradients, and eventually desorbing at the permeate side. The separation process hinges upon disparities in solubility and diffusivity inherent in RO membrane materials. The mass transfer dynamics of water and solute within the framework of the "solution-diffusion model" can be mathematically represented by equations (1.3) and (1.4), respectively.

$$J = A(\Delta P - \Delta \pi) \tag{1.3}$$

and

$$J_S = B\Delta C \tag{1.4}$$

where ΔC is the concentration difference across the membrane; Δπ is the osmotic pressure difference across the membrane; A and B are the water permeability coefficient and solute permeability coefficient, respectively. The transport coefficients (A and B) can be determined based on the membrane characteristics, as elucidated in Equation (1.5) and Equation (1.6) respectively.

$$A = \frac{D_{wm} C_{wm} V_w}{R_g T l} \tag{1.5}$$

and

$$B = \frac{D_{sm} K_{sm}}{l} \tag{1.6}$$

where D_{wm} is the diffusion coefficient of water; D_{sm} is the diffusion coefficient of the solute inside the rejection layer; C_{wm} is the concentration of water inside the rejection layer; V_w is the molar volume of water; R_g is the universal gas constant (8.31 $J \cdot mol^{-1}K^{-1}$); K_{sm} is the solute partioning coefficient into the rejection layer.

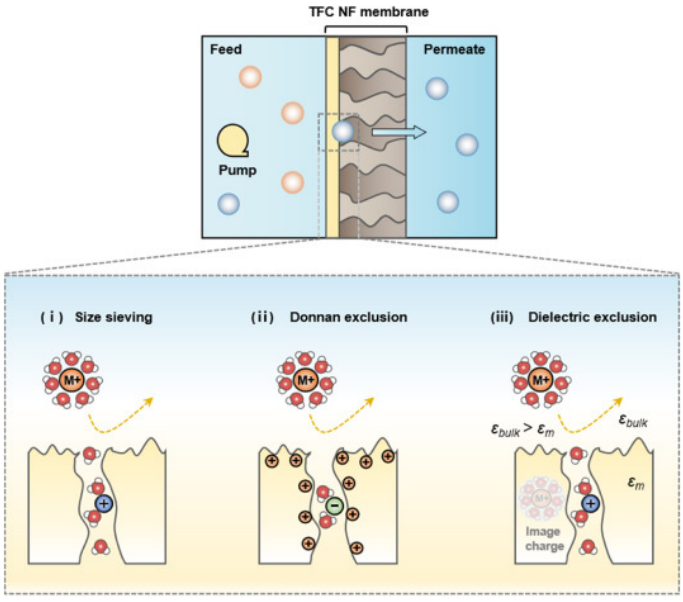

Figure 1.2 Schematic diagram of the ion separation mechanism of TFC nanofiltration membrane, including size sieving, Donnan exclusion and dielectric exclusion effects [27].

1.5 Manufacturing and synthesis of nanofiltration membranes

1.5.1 Phase inversion

The phase inversion technique stands as a prevalent method in the fabrication of nanofiltration membranes within academic discourse (e.g., Fig. 1.3). Originally associated with the inception and conventional industrial production of ultrafiltration membranes, this technique has evolved significantly [67]. Through meticulous optimization of membrane preparation parameters, the phase inversion method can be adeptly tailored to yield nanofiltration membranes characterized by symmetric structures [68]. Notably, this methodology transcends conventional flat membranes to encompass the fabrication of hollow fiber nanofiltration membranes. The employment of phase inversion techniques widens the spectrum of polymer materials viable for nanofiltration membrane synthesis, catering to diverse water quality conditions [69]. Central to the phase inversion process lies the formulation of the casting solution, a pivotal determinant of the resultant nanofiltration membrane's performance attributes [69, 70]. Typically, organic polymers, organic solvents, and porogens are judiciously blended in specific proportions before being uniformly cast onto a non-woven substrate [68]. Subsequent polymer solidification into a nanofiltration membrane is achieved through solvent exchange induced by methodologies such as non-solvent soaking, thermal conditioning, and steam exposure [71]. Nanofiltration membranes fabricated via the phase inversion method exhibit a compact surface morphology conducive to selective separation, concurrently ensuring robust mechanical support with minimal influence on mass transfer resistance [60]. However, the integrated nature of nanofiltration membranes produced via the phase inversion approach poses challenges in precisely characterizing the separation layer thickness [72]. This limitation impedes accurate cross-sectional measurements through conventional microscopy modalities like scanning electron microscopy (SEM) or transmission electron microscopy (TEM). The optimization of phase inversion-derived membranes necessitates meticulous experimentation encompassing variables such as polymer composition, solvent selection, and porogen characteristics, all of which impact membrane performance [73]. Moreover, the integration of diverse additives into the casting solution, ranging from salts and alcohols to surfactants and nanoparticles, offers avenues to further fine-tune the functional attributes of resultant nanofiltration membranes. A comprehensive evaluation delineates nanofiltration membranes manufactured via phase inversion methodologies, typified by enlarged pore size, diminished flux rates, and attenuated surface charge

density [68]. Despite inherent constraints, the burgeoning demand for nanofiltration membranes underscores their indispensable role in addressing myriad water quality challenges.

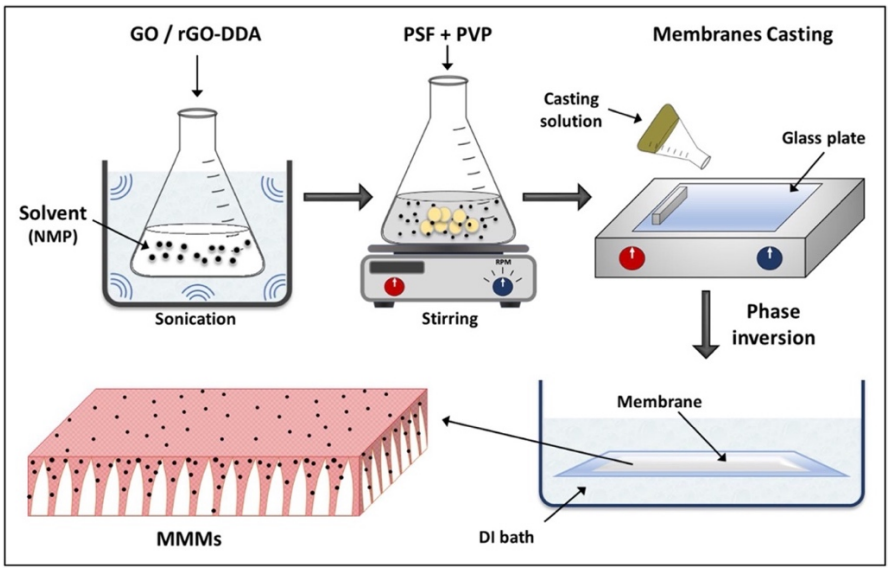

Figure 1.3 Schematic diagram of the preparation of GO-based MMMs using phase inversion technology, where nanomaterials were incorporated into a casting solution containing organic solvents and polymer materials, and then additives were added and the mixture was prepared by phase inversion [74].

1.5.2 Layer-by-layer self-assembly

The layer-by-layer self-assembly method is a technique wherein positively and negatively charged polyelectrolytes are sequentially deposited onto a base membrane, resulting in the formation of thin layers termed polyelectrolyte layers (Fig. 1.4) [75]. This method has garnered widespread adoption in membrane manufacturing because of its simplicity and cost-effectiveness. Static deposition, a variant of the layer-by-layer method, involves the deposition of polyelectrolytes onto a base membrane without the application of external forces [76]. Consequently, this approach exhibits lower production costs and greater versatility in its application to various nanofiltration membranes and supporting substrates [77]. One notable advantage of static deposition lies in its capability to achieve precise control over the thickness of polyelectrolyte layers by modulating the number of deposited layers [78]. This attribute enhances the tunability of membrane properties, catering to specific separation requirements. As researchers delve deeper into the intricacies of layer-by-layer self-assembly methods, the scope of interlayer interactions has expanded beyond mere electrostatic forces to encompass covalent bonds, hydrogen bonding, complexation, and other molecular interactions [79]. This broadening understanding of interlayer interactions not only enriches the theoretical foundation of layer-by-layer self-assembly but

also enhances the practical feasibility of this approach [77]. By leveraging diverse intermolecular interactions, researchers can tailor the properties of polyelectrolyte layers with greater precision, thereby opening avenues for the development of advanced membrane materials with enhanced performance characteristics [77, 78].

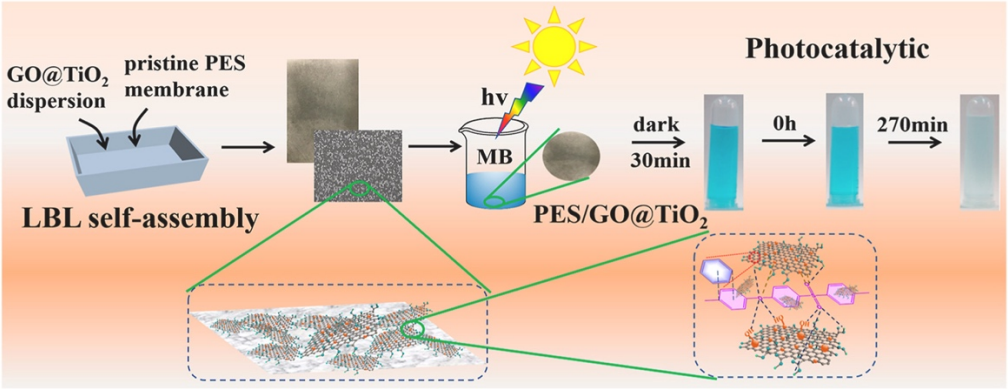

Figure 1.4 A method for preparing a photocatalytic nanofiltration membrane by layer-by-layer self-assembly, wherein the photocatalyst is between layers and catalysed the decomposition of dyes by light. [80]

1.5.3 Interfacial polymerization

Interfacial polymerization (IP) technology stands out as a prominent method in the realm of nanofiltration membrane fabrication, earning the moniker of the "star method" and emerging as the primary technique for commercial nanofiltration membrane production [63]. This process entails the polycondensation reaction of two monomers occurring at the interface of two immiscible solutions [81]. Practically, the implementation involves utilizing a porous matrix membrane to adsorb an aqueous solution containing a monomer such as piperazine (PIP) or m-phenylenediamine (MPD) [82]. Typically, the concentration of PIP in the aqueous phase ranges from 1% to 2%, while the MPD concentration hovers around 2% [33]. Following this, the porous matrix membrane laden with the aqueous phase monomer is immersed in an organic phase solution containing trimesoyl chloride (TMC), with TMC concentration typically between 0.1% and 0.2% (Fig. 1.5) [34, 63]. Upon interaction of the two monomers at the interface, a dense polyamide layer forms at the boundary between the aqueous and organic phases, impeding further monomer reactions. Consequently, nanofiltration membranes produced via interfacial polymerization typically exhibit a reduced separation layer thickness [83]. This reduction in thickness concurrently diminishes the overall resistance of the nanofiltration membrane, thereby augmenting water flux. Subsequently, the prepared nanofiltration membrane undergoes heat treatment to

elevate the cross-linking degree of the polyamide layer, enhancing the adhesion between the polyamide layer and the base membrane [84]. This step fortifies the structural integrity and durability of the membrane, ensuring its suitability for prolonged operational use in various filtration applications.

Throughout the IP process, the performance attributes of resultant nanofiltration membranes can be finely tuned by manipulating a plethora of parameters. Key factors for adjustment include the type of monomer utilized, its concentration, the nature of the organic solution, duration of the polymerization reaction, temperature during heat treatment, and post-treatment conditions [60]. Through meticulous optimization of these variables, significant impacts on membrane characteristics were have observed. PIP and MPD emerge as prevalent aqueous phase monomers in nanofiltration membrane fabrication. While PIP enjoys widespread use, controlled conditions with MPD can yield denser nanofiltration membranes [85, 86]. Incremental augmentation of monomer concentration typically correlates with enhanced water flux and desalination capacity [86, 87]. However, surpassing the optimal monomer concentration threshold precipitates a notable reduction in water flux, albeit with minimal effect on desalination efficiency [60]. Accurate determination of the optimal monomer concentration poses challenges due to the multifaceted interplay of factors such as aqueous phase additives, organic solvent composition, and heat treatment methodologies [77]. Moreover, the characteristics inherent to the substrate membrane, encompassing pore size, porosity, hydrophobicity, and chemical properties, wield substantial influence over the interfacial polymerization reaction and ensuing membrane performance [88]. Consequently, any substitution of the substrate membrane necessitates a recalibration of membrane preparation parameters to ensure an optimal performance [89]. This nuanced interplay of parameters underscores the intricate nature of interfacial polymerization in nanofiltration membrane fabrication and underscores the importance of systematic optimization to achieve desired membrane properties for specific applications.

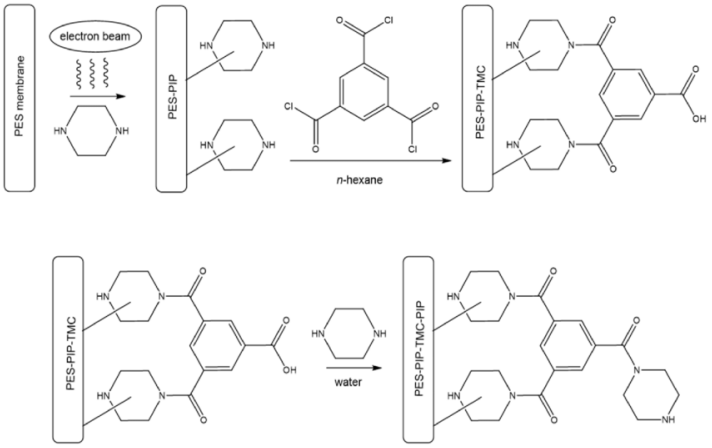

Figure 1.5 Interfacial polymerization of PIP/TMC on PES support substrate.

1.6 Application of nanofiltration membrane in water treatment

Given the diverse array of pollutants present in industrial wastewater, the issue stands as a global environmental menace with profound implications for human health [90]. Industries such as textiles, food processing, petroleum refining, mining, tanneries, pharmaceuticals, and paper production are notable water consumers, generating copious amounts of wastewater as a byproduct of their manufacturing processes [91]. Against the backdrop of dwindling freshwater resources and escalating environmental concerns, there has been a concerted push within the industrial sector towards water recycling, reuse, and resource recovery [92]. Nanofiltration membranes have emerged as a compelling technology for addressing these imperatives. This section delves into the specific application of nanofiltration membranes within the realm of water treatment.

1.6.1 Textile wastewater

The textile industry is recognized for its substantial water consumption and significant generation of wastewater, estimated at 200–350 m^3 per ton of finished product [93]. This wastewater comprises various pollutants, including dyes, chemical oxygen demand (COD), inorganic salts, suspended solids, and trace heavy metals, with dyes presenting notable challenges due to their persistent, carcinogenic, and poorly biodegradable nature [93, 94]. Discharge of untreated textile wastewater not only jeopardizes aquatic ecosystems but also exacerbates the scarcity of clean water resources [95]. Thus, the implementation of advanced treatment methodologies is imperative to manage textile wastewater effectively and recuperate valuable resources.

Nanofiltration (NF) membranes emerge as a promising avenue for the sustainable recovery of dyes and salts from textile wastewater [93]. The NF process facilitates the segregation of dyes and salts into distinct streams, enabling resource recuperation while mitigating environmental contamination [96]. Research demonstrates the efficacy of NF membranes in segregating dye/salt mixtures, achieving high rejections for dyes such as Congo red while permitting efficient passage of salts like sodium chloride [97-99]. Moreover, NF processes aid in diminishing other impurities such as turbidity and COD, thus enhancing the quality of reclaimed water [100]. The effectiveness of NF in treating textile wastewater can be attributed to mechanisms such as size exclusion and Donnan exclusion. NF membranes generally exhibit a superior rejection of larger molecular weight dyes via size exclusion, while electrostatic repulsion (Donnan effect) aids in the repulsion of oppositely charged dyes [101]. Despite the promising performance of NF membranes, fouling remains a significant challenge, necessitating a comprehensive approach to mitigate its impact. Integration with pretreatment technologies such as electrocoagulation holds promise in minimizing fouling and enhancing membrane performance, thereby facilitating the achievement of water reuse objectives in the textile industry [102].

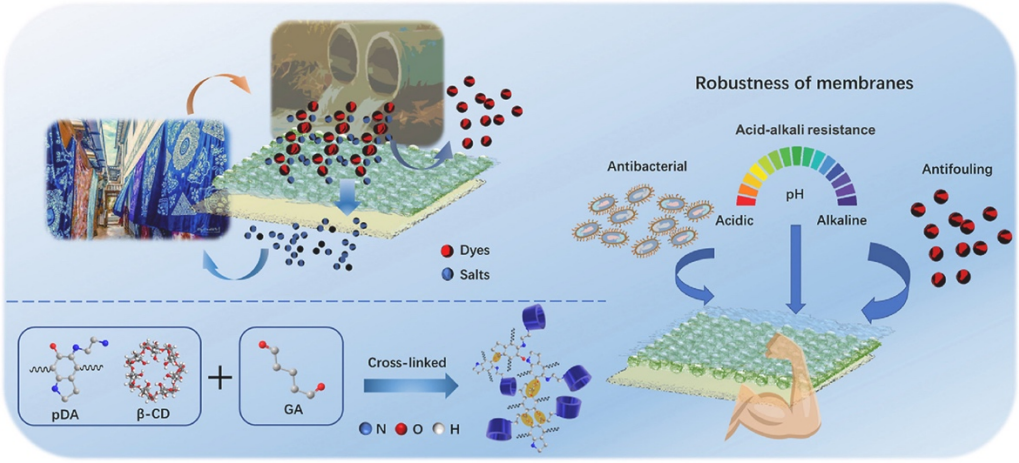

Figure 1.6 Nanofiltration membrane purification and resource recovery of textile wastewater uses stronger cross-linking agents to improve the robustness of nanofiltration membranes and is suitable for a variety of applications.

1.6.2 Surface/groundwater treatment

At present, surface water stands as the primary source of potable water; however, its quality remains susceptible to various factors, including precipitation, point source pollution, non-point source pollution, and seasonal fluctuations (Table. 1.1) [103]. Conventional treatment methods, such as coagulation,

sedimentation, filtration, and disinfection, are commonly employed in surface water treatment [104]. Nevertheless, these traditional combined treatment processes primarily target particulate matter and microorganisms within the water column, displaying limited efficacy in eliminating dissolved organic pollutants. Notably, dissolved organic pollutants act as precursors to disinfection by-products, which, post-disinfection, may yield carcinogenic and teratogenic compounds, such as trihalomethanes, halo acetic acids, and related substances [105]. Additionally, certain low molecular weight organic micropollutants pose additional health hazards [105]. Given the diverse molecular weight distribution of dissolved organic pollutants, the utilization of membranes featuring smaller molecular weight cutoffs offers a promising approach to address these challenges [73]. Nanofiltration membranes, characterized by molecular weight cutoffs ranging from 200 to 2000 Da, exhibit proficiency in effectively removing the majority of dissolved organic pollutants, thereby enhancing water quality and mitigating associated health risks[106].

Groundwater serves as a vital resource for agricultural irrigation and potable water supply globally, with abundant groundwater reservoirs playing a pivotal role in supplying drinking water to various regions in my country [107]. However, the majority of groundwater sources exhibit high hardness levels and contain elevated concentrations of calcium and magnesium ions. Concurrently, escalating chemical usage and industrial wastewater discharge have variably compromised groundwater quality [108]. Emerging contaminants such as arsenic, perfluoroalkyl compounds, and polyfluoroalkyl compounds have been detected in groundwater, posing significant risks to human health [109]. Nanofiltration technology, renowned for its capacity to eliminate divalent salt ions and the majority of dissolved organic matter, presents a promising avenue for groundwater treatment [72]. By leveraging nanofiltration, it is anticipated that the removal of these contaminants can be achieved, thereby enhancing the suitability of groundwater for various applications while safeguarding public health [72, 110].

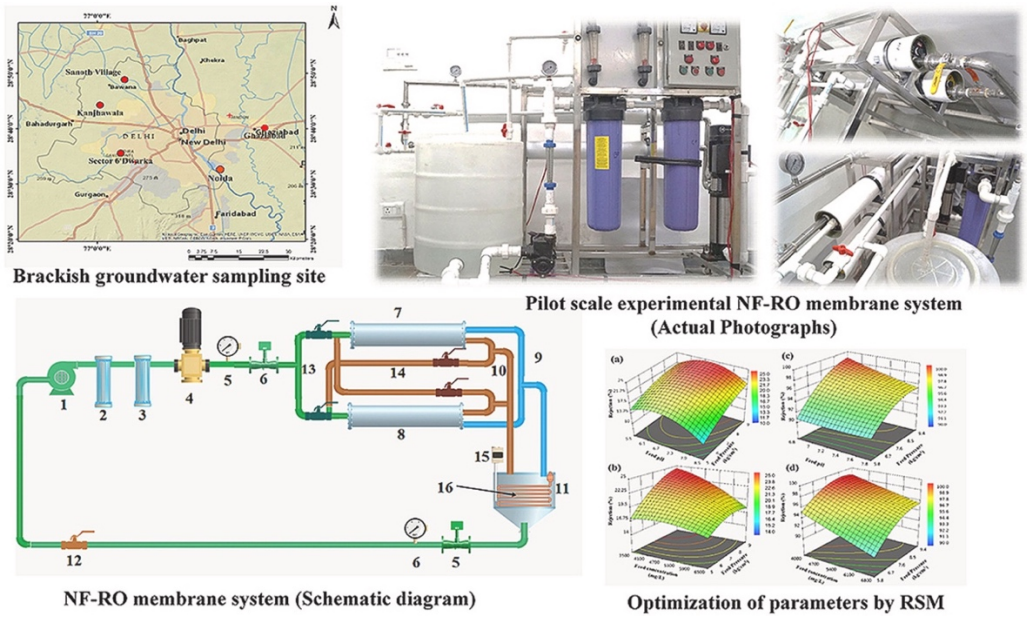

Figure 1.7 A groundwater treatment pilot system based on NF/RO was developed, and multi-scale optimization of the process was performed [111].

Table 1.1 One of surface water quality as average values ± standard deviation during the experiment.

Indicators	**Value**
Temperature, °C[a]	18.1±0.4
pH	5.9±0.1
Conductivity, mS/m	14.3±0.7
Turbidity, FTU	0.14±0.07
Alkalinity, mmol/l	0.09±0.01
Hardness, mmol/l	0.10±0.01
TOC, mg/l	2.17±0.11
UVA, cm^{-1}	0.024±0.002
HPC, CFU/ml	4200±2400
Al^{3+}, µg/l	17.5±14.3
Ca^{2+}, mg/l	13.1±1.1
Mg^{2+}, mg/l	1.39±0.00
Na^{+}, mg/l	7.28±0.16
Cl^{-}, mg/l	12.3±0.3
SO_4^{2-}, mg/l	33.5±2.7

1.6.3 Brackish water treatment

Brackish water, a saline water source with salinity levels ranging between freshwater and seawater, presents unique challenges for drinking water production [112]. It contains a diverse range of constituents, including calcium ions, magnesium ions, fluoride ions, nitrate ions, sulfate ions, and dissolved organic matter [113]. Among these constituents, salts pose significant treatment challenges due to their varying ionic properties. Nanofiltration membranes are designed with medium and high retention properties for monovalent and divalent salts, respectively, allowing for effective removal of complex ions found in brackish water (Fig. 1.8) [114]. However, the interception efficiency of traditional commercial nanofiltration membranes for monovalent salts can be inconsistent, potentially jeopardizing water quality. To overcome this limitation, integrating nanofiltration membranes with other membrane processes such as reverse RO and forward osmosis FO offers a promising solution [115]. RO and FO membranes are known for their robust interception properties, particularly for monovalent salt ions. In this integrated approach, nanofiltration membranes serve as a pretreatment step, prioritizing the removal of divalent salt ions from brackish water [60]. This sequential arrangement provides several benefits. Firstly, it helps to mitigate subsequent operational loads by pre-treating the water and reducing the workload on downstream membrane processes. Additionally, it addresses membrane fouling issues in subsequent membrane processes, thereby improving overall process efficiency and prolonging membrane lifespan [116]. By synergistically integrating these membrane processes, the treatment of brackish water is enhanced, ensuring the production of high-quality potable water while optimizing operational effectiveness [117].

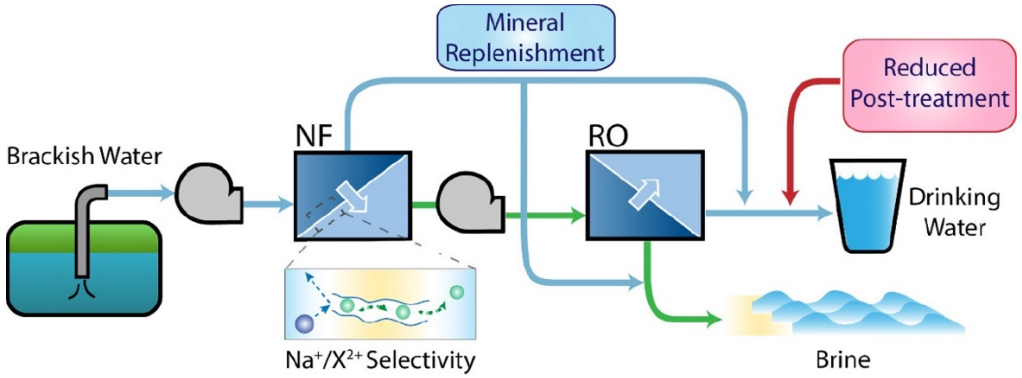

Figure 1.8 Schematic diagram of the process of desalination of brackish water by NF/RO[114].

1.6.4 Wastewater reuse and resource recovery

In addition to conventional surface water and groundwater sources for potable water supply, municipal and industrial wastewaters present opportunities for membrane-based treatment processes, thereby augmenting freshwater resources and mitigating wastewater discharges (Fig. 1.9) [21]. In regions grappling with water scarcity, wastewater reclamation has been integrated into potable water supply systems to alleviate local water deficits. Nanofiltration and reverse osmosis technologies play pivotal roles in purging water bodies of deleterious pollutants, constituting indispensable components of wastewater reclamation processes aimed at ensuring the quality of reclaimed water [21, 100, 118]. While reverse osmosis membranes excel in interception capabilities and afford high-quality drinking water, nanofiltration membranes serve as effective barriers in wastewater reclamation endeavors [119]. Notably, nanofiltration membranes entail lower transmembrane pressure differences and higher water fluxes compared to reverse osmosis membranes, rendering them economically and operationally more viable alternatives[120].

Moreover, nanofiltration membranes facilitate resource recovery during wastewater treatment by adeptly segregating valuable dissolved substances such as organic compounds, inorganic salts, and metal ions from wastewater streams [121]. Through modulation of membrane retention properties, these substances can be selectively retained on one side of the membrane while purified water is separated [122]. Additionally, nanofiltration membranes enable the concentration of dissolved substances in wastewater into reduced volumes, thereby curtailing treatment costs and resource consumption [77]. By judiciously adjusting membrane retention properties and operational parameters, efficient concentration of valuable substances within wastewater streams can be realized [123]. Furthermore, nanofiltration membranes offer avenues for the retrieval of valuable solid particles present in wastewater, such as granular sludge and suspended matter [124]. Through appropriate manipulation and subsequent processing, these solid particles can be repurposed for beneficial applications, including soil enhancement and energy production [50]. In summary, nanofiltration membranes facilitate resource recovery in wastewater treatment through the selective separation of valuable substances, concentration of wastewater streams, recycling of water resources, and reclamation of solid particles. Thus, they furnish critical technological avenues for harnessing wastewater resources and advancing sustainability in water management practices.

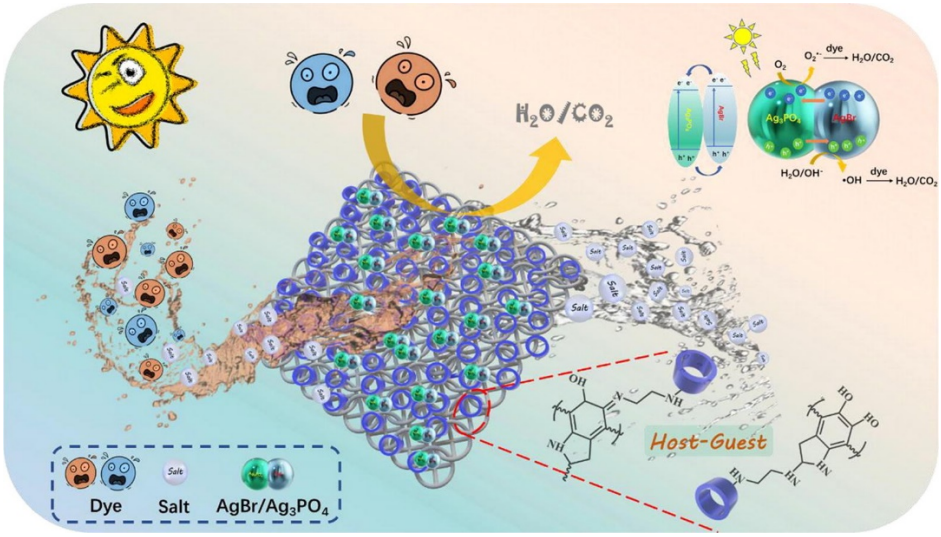

Figure 1.9 The nanofiltration membrane for textile wastewater reuse and resource recovery uses photocatalysts generated in situ on the surface to achieve the self-cleaning and anti-fouling capabilities of the membrane.

1.7 Limitations of nanofiltration membranes

1.7.1 Robustness in nanofiltration membranes

The primary concern regarding membrane robustness pertains to membrane fouling, which constitutes the foremost impediment to the efficient separation efficacy of membrane technology in real-world applications [125]. Membrane fouling significantly undermines membrane permeability, escalates energy consumption, and diminishes membrane longevity [51, 126]. Hence, comprehending the causative factors and mechanisms underpinning membrane fouling during the filtration process is imperative, alongside endeavors to control and mitigate its adverse ramifications. Fundamentally, the origins of membrane fouling stem from physical and chemical interactions, chiefly influenced by three facets: the physicochemical attributes of pollutants (including charge, molecular conformation, and dissolution state), operational parameters (such as feed solution pH, cross-flow velocity, and salt concentration), and membrane characteristics (encompassing surface charge, hydrophobicity, and roughness) (Fig. 1.10) [50, 127, 128]. Furthermore, categorization of fouling into hydrophilic reversible and irreversible types has been proposed, wherein reversible fouling can be readily eliminated through water rinsing, whereas irreversible fouling poses challenges for removal [129]. Additionally, concentration polarization and osmotic pressure elevation are intricately linked to the formation of filter cake and gel layers, fostering bacterial adhesion to the membrane surface [51]. Concentration

polarization entails solute entrapment leading to elevated solute concentrations, further contributing to adsorption, filter cake, and gel layer formation, thereby complicating scale deposition processes [130]. Specifically, for nanofiltration membranes characterized by heightened permeability and reduced pressure requirements, separation mechanisms primarily hinge upon the Donnan effect and size exclusion [131]. For instance, fouling of loose nanofiltration membranes utilized in dye/salt separations is notably influenced by feed characteristics and dye-membrane surface interactions[132]. At low salt concentrations, filter cake layer formation predominates, whereas adsorption becomes dominant at elevated salt concentrations[133]. Organic fouling poses significant challenges for membranes with larger pore sizes, resulting in diminished permeate flux, exacerbated by dye-induced pore clogging and bacterial proliferation within filter cake and gel layers[133]. Consequently, an optimal loose nanofiltration membrane for dye/salt separation necessitates a precise pore size, superior hydrophilicity, electroneutrality, and abundant hydrogen bond acceptors to mitigate adsorption and pore clogging[134]. Incorporating antimicrobial or self-cleaning properties addresses biofouling concerns and enhances membrane stability and long-term recyclability in practical applications.

Comparable to membrane fouling, membrane stability poses another unavoidable challenge in membrane technology. The stability of membranes intricately correlates with their separation efficacy and the operational conditions of the feed solution[135]. Typically, membrane performance stability is assessed through prolonged testing under identical conditions to filtration experiments, yet the intrinsic stability of membranes remains incompletely understood[50]. Intrinsic membrane stability encompasses both mechanical and chemical aspects, including thermal, acid, and alkali resistance, crucial for ensuring sustained performance and prolonged membrane lifespan[77]. Mechanical stability represents a fundamental requirement for conventional membranes. However, the thermal stability of membranes becomes particularly pertinent when dealing with high-temperature dye wastewater, which generates considerable heat and thus challenges membrane performance[136]. Though typically processed at approximately 60°C, well-managed utilization of high-temperature dye wastewater can enhance permeability and mitigate membrane fouling[28]. Consequently, thermally stable membranes capable of withstanding heat fluctuations without stringent temperature control offer potential cost savings and facilitate sustainable industrial chemical processes[50, 137]. Furthermore, industrial wastewater often exhibits a wide pH range (pH=2-10), necessitating membranes to withstand harsh acidic and alkaline

conditions[42]. Additionally, commercial polyamide membranes frequently experience notable performance deterioration when exposed to trace amounts of chlorine[138]. Consequently, understanding the corrosion mechanisms of chlorine on aromatic polyamides and developing strategies to mitigate chlorination-induced degradation are imperative. Given the prevalent use of chlorination and chemical cleaning in pretreatment and separation processes, the development of chlorine-resistant membranes has garnered increased attention as a crucial research avenue in water treatment[139]. Ultimately, cultivating comprehensive membrane stability is indispensable for sustaining membrane operation and ensuring enduring performance in practical applications[136]. Efforts toward enhancing mechanical and chemical stability are paramount for the long-term viability of membrane-based processes in various industrial contexts.

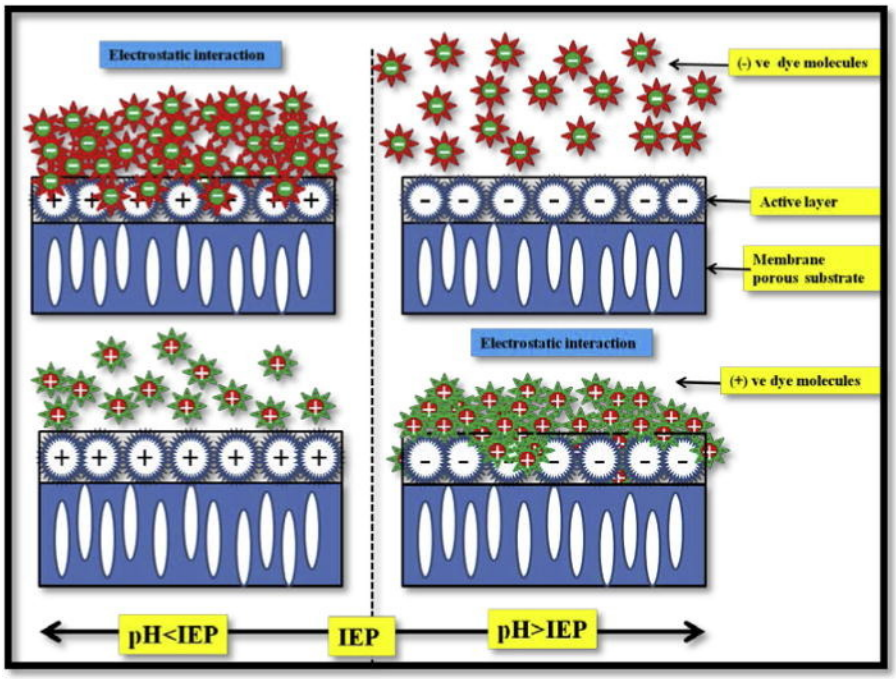

Figure 1.10 The fouling mechanism of nanofiltration membranes, taking electrostatic action as an example, pollutant molecules gather on the surface of the membrane, and different membrane surface potentials and the electrical properties of pollutant molecules show different performances[140].

1.7.2 Practicality concerns in nanofiltration applications

In the realm of nanofiltration membrane synthesis, researchers frequently employ interfacial polymerization technology, which emerged approximately two decades ago[69]. This method allows for the continuous evolution of membrane substrates to create more sophisticated membranes. However, the focus of researchers seems to lean more towards arranging and combining compounds containing amino,

hydroxyl, and acid chloride groups to synthesize membranes, rather than emphasizing practical applicability[141]. Although these membranes often exhibit a superior performance in laboratory settings, researchers must diligently assess their potential for practical deployment. For instance, a study in 2011 highlighted the potential use of graphene with controllable ripples in nanofiltration[142]. Over a decade since this discovery, numerous advanced one- and two-dimensional (2D) nanomaterials have been integrated into membrane designs, with some even exploring the concept of using graphene as "ink" and a supporting substrate akin to "printing paper" for nanofiltration membrane preparation[143]. While these innovations show promise in laboratory-scale experiments, their translation into practical applications remains elusive. In the pursuit of new water purification materials, it is imperative to consider the practicality of these materials for large-scale implementation[144]. Furthermore, the cost implications of synthesizing advanced materials for nanofiltration membranes are often overlooked. Is the synthesis of nanofiltration membranes justified at any cost[73]? Take the example of 2D MXene materials, which have garnered significant attention in water purification membrane research due to their exceptional water permeability compared to traditional commercial nanofiltration membranes[145]. However, the exorbitant prices listed on platforms like 2dsemiconductors.com raise concerns about the feasibility of mass-producing these membranes, with prices exceeding those of gold. Moreover, the long-term stability and environmental impact of these materials during usage are critical considerations. While researchers strive to enhance chemical and contamination resistance, there is a growing concern about the persistence of these materials in the environment, akin to the concept of "permanent chemicals" [146]. Materials that adhere to support matrices through simple intermolecular forces may pose risks if released into water bodies, with potential implications for human health that demand attention[147]. In the light of these challenges, researchers must shift their focus from solely pursuing advanced materials to prioritizing practicality in water purification membrane development[148]. Rather than solely emphasizing laboratory-based observations, efforts should be directed towards developing membrane technologies applicable to real-world water purification plants. This shift in research focus will not only facilitate the advancement of water purification technologies but also address the pressing need for practical and sustainable solutions in water treatment.

Chapter 2: Materials and methods

Adapted from: "*Gao, Q., Zhu, Q., Zheng, J., Yuan, S., Wang, Y., Zhao, R., Liu, Y., Gui, X., Wang, C., Volodine, A., Jin, P., Van der Bruggen, B. with Jin, P. (corresp. author), Van der Bruggen, B. (corresp. author) (2022). Positively charged membranes for dye/salt separation based on a crossover combination of Mannich reaction and prebiotic chemistry. JOURNAL OF HAZARDOUS MATERIALS, 440, Art.No. ARTN 129744. doi: 10.1016/j.jhazmat.2022.129744"*

"*Gao, Q., Bouwen, D., Yuan, S., Gui, X., Xing, Y., Zheng, J., Ling, H., Zhu, Q., Wang, Y., Depuydt, S., Li, J., Volodine, A., Jin, P., Van der Bruggen, B. with Jin, P. (corresp. author), Van der Bruggen, B. (corresp. author) (2023). Robust loose nanofiltration membrane with fast solute transfer for dye/salt separation. JOURNAL OF MEMBRANE SCIENCE, 674, Art.No. ARTN 121518. doi: 10.1016/j.memsci.2023.121518"*

"Gao, Q., Weng, B., Jin, P., Yuan, S., Gui, X., Zheng, J., Xu, D., Wang, Y., Volodine, A., Sun, L., Van der Bruggen, B. with Jin, P. (corresp. author), Van der Bruggen, B. (corresp. author) (2022). Rapid solute transfer photocatalytic membrane: The combination of host-guest interaction and photocatalyst load. CHEMICAL ENGINEERING JOURNAL, 446, Art.No. ARTN 137316. doi: 10.1016/j.cej.2022.137316"

"Gao, Q., Ding, Y., Li, J., Jin, P., Xu, D., Fang, L., Wang, Y., Liu, B., Xie, Y., Bao, X., Jiang, L., Du, J., Zhu, J., Zheng, L., Su, B-L., Ng, Y.H., Xing, Y., Gui, X., Wang, C., van der Bruggen, B. with Li, J. (corresp. author), Xing, Y. (corresp. author), Wang, C. (corresp. author), van der Bruggen, B. (corresp. author) (2025). Tailoring fast mass transfer membrane: Zero discharge of wastewater using visible light. JOURNAL OF MEMBRANE SCIENCE, 717, Art.No. ARTN 123632. doi: 10.1016/j.memsci.2024.123632"

2.1 Chemicals and materials

A polypropylene/polyethylene (PP/PE) nonwoven blend (Novatexx 2471) was used as the support for membrane synthesis. Polyethersulfone (PES) powder was purchased from BASF Co., Ltd. The commercial polyacrylonitrile ultrafiltration membrane (PAN, Mw=50 kDa) as the support substrate was provided by RisingSun Membrane Co. Ltd. (Beijing, China).

Polyethyleneimine (PEI), tetrakis(hydroxymethyl)phosphonium chloride (THPC) and AMN were purchased from Sigma-Aldrich. The solvent used for the casting solution was dimethyl sulfoxide (DMSO, 99.5%) purchased from Sigma-Aldrich (Belgium). Hydrogen peroxide (H_2O_2, 35 wt%), copper sulfate ($CuSO_4$, 99%), sodium hydroxide (NaOH, >97%), hydrochloric acid (HCl, 0.5M), tris(hydroxymethyl) aminomethane (Tris, 99.8%), and dopamine hydrochloride (DA, 99%) were obtained from Sigma-Aldrich (Diegem, Belgium). β-Cyclodextrin was purchased from Aladdin (Shanghai, China). Commercial polyacrylonitrile ultrafiltration membranes (PAN, Mw=50 kDa) were provided by

RisingSun Membrane Co. Ltd. (Beijing, China). The cross-linking agent was glutaraldehyde (glutaraldehyde, 50% aqueous solution) purchased from Aladdin (China). Trimesoyl chloride (TMC, 98%), poly (ethylene glycol) (PEG, Mw=300-6000 Da), and n-hexane (95%) were purchased from Sigma-Aldrich (Belgium). The piperazine (PIP, 99 wt%) used to form the selective layer of loose nanofiltration with pDA was purchased from Sigma-Aldrich (Diegem, Belgium). Aminomalononitrile (AMN) used for insertion into the selection layer was also purchased from Sigma-Aldrich (Diegem, Belgium). Copper nitrate pentahydrate ($Cu(NO_3)_2•5H_2O$, 99%), and analytically pure titanium (IV) butanol used for the synthesis of photocatalysts were purchased from Aladdin Co., Ltd. The surfactant used to prepare the photocatalyst dispersion was sodium dodecyl sulfate (SDS, >99 %), purchased from Sigma-Aldrich (Diegem, Belgium). Phosphate-buffered saline (PBS) with a concentration of 100 mM was used, and the preparation method and chemicals used were based on a previous study by Chen et al. [149].

Neutral Red (NR), methylene blue (MB), methyl orange (MO), Victoria blue B (VBB), Janus green B (JGB), patent blue VF (PBVF), direct red 23 (DR23) and reactive black 5 (RB5), reactive orange 16 (RO16), congo red (CR), and reactive blue 2 (RB2), and rhodanile blue (RhB) were used as dyes in textile wastewater to explore the separation performance of membranes for dyes. The membranes were investigated for the separation of salts using sodium chloride (NaCl, 99%) and sodium sulfate (Na_2SO_4, 99%) from Sigma-Aldrich (Belgium). Sodium hydroxide (NaOH, >97%) and hydrochloric acid (HCl, 0.5M) were purchased from Sigma-Aldrich (Belgium). Potassium dichromate ($K_2Cr_2O_7$, >99 wt%), sodium chloride (NaCl, >99 wt%), sodium sulfate (Na_2SO_4, >99 wt%), magnesium chloride ($MgCl_2$, >99 wt%), magnesium sulfate ($MgSO_4$, >99 wt%), and $(NH_4)_2SO_4$ (>99 wt%) used in the salt rejection study were purchased from Sigma-Aldrich (Diegem, Belgium). Poly (ethylene glycol) (PEG, >99 wt%, Mw=300-6000 Da) was used to test molecular weight cut-off (MWCO) and was purchased from Sigma-Aldrich (Diegem, Belgium).

Sodium bromide (NaBr, 99%), silver nitrate ($AgNO_3$, 99%), and disodium phosphate (Na_2HPO_4, 99%) were purchased from Sigma-Aldrich (Belgium) as raw materials for the synthesis of photocatalysts. Ammonium oxalate ($(NH_4)_2C_2O_4•H_2O$), benzoquinone ($C_6H_4O_2$), and tert-butyl alcohol ($(CH_3)_3COH$) were also purchased from Sigma-Aldrich (Belgium) for quenching experiment. 5,5-Dimethyl-1-pyrroline-Noxide (DMPO) was provided by Cayman Chemical Company (Ann Arbor, USA).

2.2 Membrane Preparation Procedure

2.2.1 Preparation of PEI-THPC-AMN membranes (Chapter 3)

PEI and THPC were used as raw materials for the Mannich reaction to prepare selective layers, and AMN was used with one-step co-deposition to prepare positively charged membranes. The reaction and synthesis processes involved are shown in Fig. 2.1. A certain amount of PEI and THPC was dissolved in 10 ml of PBS buffer in a certain proportion. The ratio was denoted as T_x-P_x, where P is PEI, T was THPC, and x is the mass concentration of each composition (wt%). Meanwhile, 40 mg of AMN or pDA was dissolved in 10 ml of PBS buffer, stirred well, and recorded as T_x-P_x-AMN or T_x-P_x-pDA. After that, the two solutions were mixed and poured into a lab-made holder (Fig. 2.2) loaded with a commercial PAN membrane. The liquid-laden holder was covered with plastic wrap and shaken (70 rpm) for a certain period for co-deposition. After the co-deposition step, the membrane surface was washed with DI water, air-dried, and then heat-treated at 60°C for 15 minutes. Finally, the membrane surface was rinsed and the membrane was refrigerated in DI water at 4°C overnight. For specific preparation conditions, please refer to Table 2.1.

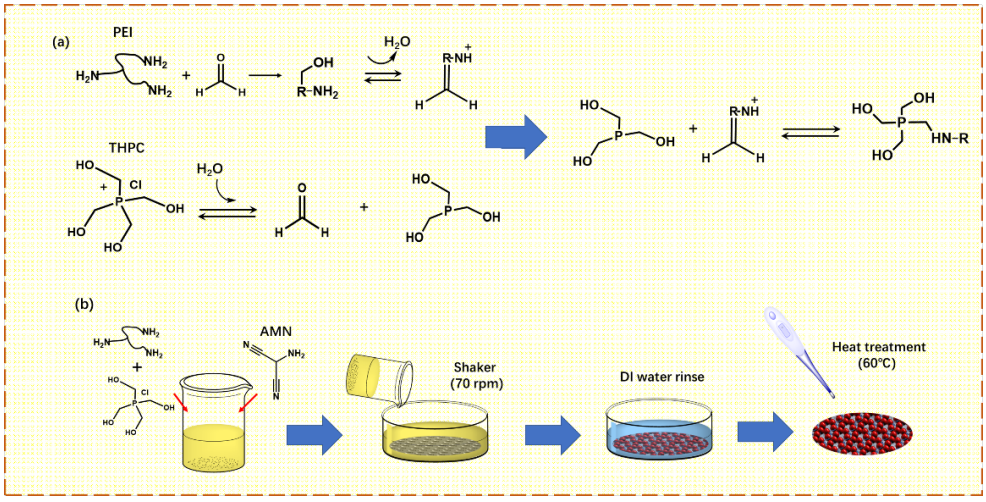

Figure 2.1 (a) Chemical reaction of PEI and TPHC via the Mannich reaction; (b) the membrane synthesis process.



Figure 2.2 The co-deposition membrane holder.

Table 2.1 The synthesis conditions of the membranes.

	Membrane	PEI concentration (wt%)	THPC concentration (wt%)	co-deposition time (min)	AMN /pDA
1	PAN	0	0	0	AMN
2	P_1-T_0-AMN	1	0	60	AMN
3	P_0-T_1-AMN	0	1	60	AMN
4	**$P_{0.5}$-$T_{0.5}$-AMN**	**0.5**	**0.5**	**60**	**AMN**
5	$P_{0.5}$-$T_{0.5}$-pDA	0.5	0.5	60	**pDA**
6	AMN	0	0	60	AMN
7	$P_{0.25}$-$T_{0.75}$-AMN	**0.25**	**0.75**	60	AMN
8	$P_{0.75}$-$T_{0.25}$-AMN	**0.75**	**0.25**	60	AMN
9	$P_{0.875}$-$T_{0.125}$-AMN	**0.875**	**0.125**	60	AMN
10	$P_{0.125}$-$T_{0.875}$-AMN	**0.125**	**0.875**	60	AMN
11	$P_{0.5}$-$T_{0.5}$-AMN	0.5	0.5	**20**	AMN
12	$P_{0.5}$-$T_{0.5}$-AMN	0.6	0.2	**40**	AMN
13	$P_{0.5}$-$T_{0.5}$-AMN	0.6	0.2	**80**	AMN

2.2.2 Preparation of pDA/β-cyclodextrin/GA (PBG) membranes (Chapter 4)

The casting solution was prepared by dissolving 18% (w/w) PES particles in DMSO by vigorous stirring at 25 °C ± 3 °C for 12 h. The obtained casting solution was put into a 4000-rpm centrifuge and degassed for 10 min to eliminate air bubbles in the casting solution. The phase inversion method was used to draw the membrane, and a casting knife with a thickness of 250 μm was used to uniformly cast the casting liquid onto the surface of the non-woven fabric. Several indentations with a certain thickness were laser etched on the casting knife. The thickness of the membrane is expected to roughly correlate with the casting knife. Subsequently, the initial membrane was placed in a water bath for solvent/non-solvent exchange to complete the phase inversion process. Finally, the resulting PES membrane was immersed in deionized water and stored in a refrigerator at 4°C.

The pDA self-polymerization buffer was prepared by a method reported elsewhere [63]. As shown in Fig. 3.1, 50 mM Tris and 5.0 mM $CuSO_4$ were dissolved in deionized water, and the pH was adjusted to pH=8.5 [63]. Then, a certain concentration of β-cyclodextrin (0, 0.4, 0.8, and 1.2 wt%) and a certain concentration of dopamine hydrochloride (0, 0.15, 0.2, and 0.25 wt%) were mixed and dissolved in the previously mentioned buffers and stirred well. Rapid aggregation of dopamine was induced by the oxidizing properties of H_2O_2 (19.6 mM). The specific operational procedure was as follows: the co-deposition solution containing H_2O_2 was in contact with the PES support substrate for a certain period of time (0, 45, 60, 75 minutes), during which pDA can undergo self-polymerization, and make the pDA/β-cyclodextrin structure assembly evenly deposited on the PES support substrate. To make the membrane robust, the cross-linking agent selected in the supramolecular interface polymerization process is glutaraldehyde. Aqueous glutaraldehyde solutions at certain concentrations (0, 0.1, 0.2, and 0.4 wt%) were poured into the holder carrying the previously described membranes and allowed to cross-link for a certain time (0, 2, 6, and 10 min). After that, the glutaraldehyde solution was removed, and the surface was washed with deionized water until the solution was completely removed. In order to make the cross-linking reaction and the evaporation of the solution more complete, thermal cross-linking was carried out using heat treatment at 60 °C for 15 min. The membranes were then rinsed five times and stored submerged in deionized water at 4°C. The specific synthesis process is shown in Fig. 2.2. The synthesis conditions and codes of the membranes are shown in Table 2.2.

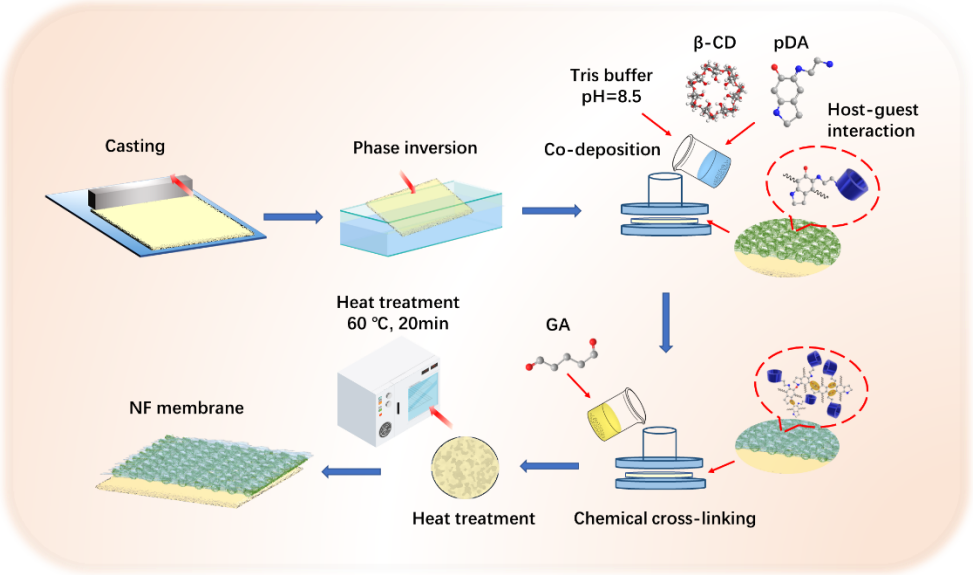

Figure 2.3 Schematic diagram of the membrane synthesis applied.

Table 2.2 The synthesis conditions of the membranes.

Membrane	β-cyclodextrin concentration (wt%)	pDA concentration (wt%)	co-deposition time (min)	Crosslink time	GA concentration (wt%)
PES	0	0	0	0	0
PBG-1	**0**	0.2	60	6	0.2
PBG-2	**0.4**	0.2	60	6	0.2
PBG-3	**0.8**	**0.2**	**60**	**6**	**0.2**
PBG-4	**1.2**	0.2	60	6	0.2
PBG-5	0.8	**0**	60	6	0.2
PBG-9	0.8	**0.15**	60	6	0.2
PBG-7	0.8	**0.25**	60	6	0.2
PBG-8	0.8	0.2	**45**	6	0.2
PBG-9	0.8	0.2	**75**	6	0.2
PBG-10	0.8	0.2	60	**0**	0
PBG-11	0.6	0.2	60	**2**	0.2
PBG-12	0.6	0.2	60	**10**	0.2
PBG-13	0.6	0.2	60	6	**0.1**
PBG-14	0.6	0.2	60	6	**0.4**

2.2.3 Preparation of dye/salt separation membranes (DSM) (Chapter 5)

The commercial PAN membrane needs to be hydrolyzed in NaOH aqueous solution (1 M) at 60°C for 1 h before the selective layer can be synthesized. The PAN membrane was hydrolyzed in the aqueous solution rich in OH^-, and the HPAN membrane was obtained, exposing the -COOH group and increasing hydrophilicity. The resulting HPAN membrane was then stored in DI water at 4°C before using. All membranes mentioned in this work were stored via this method.

Tris (50 mM) and $CuSO_4$ (5.0 mM) in DI water were dissolved to prepare a Tris-buffer/$CuSO_4$ solution and adjust the pH of the solution to 8.5. A certain concentration of dopamine hydrochloride (0, 0.1, 0.2, 0.3, and 0.4 wt%) and β-cyclodextrin (0, 0.3, 0.6, 0.9, and 1.2 wt%) were added into the Tris-buffer/$CuSO_4$ solution and stirred well. H_2O_2 (19.6 mM) was added to start the rapid polymerization of dopamine. Then the co-deposition solution was obtained. The previously prepared HPAN membrane was taken in DI water, and the experimental preparation was carried out in a clean assembly room. Then, the resulting co-deposition solution (20 ml) was gently poured into the membrane holder loaded with the HPAN membrane, so that only the dry HPAN membrane was in contact with the co-deposition solution for a certain period of 30 minutes. The purpose of this step was to realize the rapid self-polymerization

of pDA and the assembly and uniform deposition of the pDA/β-cyclodextrin structure on the HPAN membrane. After the co-deposition, the membrane was rinsed with DI water to clean the residual co-deposition solution in the membrane holder and dried in the air. In order to make the selective layer more stable and denser, TMC (in n-hexane, 0.1 wt%) was poured into the membrane holder and allowed it to undergo crosslinking reaction for a certain time (0, 1, 2, and 3 min). After that, the TMC on the membrane surface was poured off. The heat treatment was performed at 60°C for 15 minutes to make the crosslinking reaction on the membrane surface proceed more fully and allow the solvent on the membrane to evaporate better. Membranes were rinsed five times and submerged in DI water overnight at 4°C. AgBr-Ag_3PO_4 photocatalytic membranes were prepared by an alternate dipping method[150]. Solution P1 is a solution of $AgNO_3$. $AgNO_3$ was dissolved in DI water to form a solution with a certain concentration (2, 4, and 9 mM). Solution P2 was a mixed solution of NaBr (0.5, 1, and 9 mM) and Na_2HPO_4 (1.5, 3, and 2 mM) with a certain concentration. The pDA/β-cyclodextrin membrane was immersed in solution P1 for 1 min, then transferred in solution P2 for 1 min. Each dipping into both solutions was counted as one alternate dipping. In addition, different dipping times (3, 6, and 9 times) were used to optimize the photocatalytic membrane to explore the influence of dipping times on the membrane performance. Membranes were rinsed five times and submerged in DI water overnight at 4°C. The preparation conditions of all membranes are shown in Table 2.4, and the preparation process is shown in Fig. 2.3.

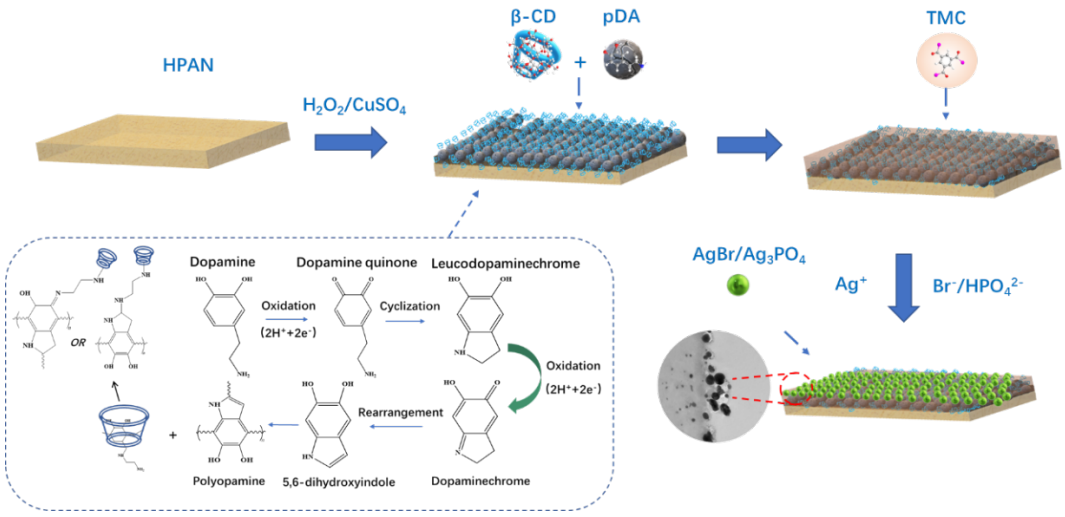

Figure 2.4 Schematic diagram of photocatalytic dye/salt separation membrane synthesis.

Table 2.3 Preparation conditions of dye/salt separation membranes (DSM).

Membrane	β-cyclodextrin concentration (wt%)	pDA concentration (wt%)	IP time (min)	P1 solution concentration (mM)	P2 solution concentration (mM)	Dipping times
HPAN						
DSM-1	**0**	0.2	2			
DSM -2	**0.3**	0.2	2			
DSM -3	**0.6**	0.2	2			
DSM -4	**0.9**	0.2	2			
DSM -5	0.6	**0**	2			
DSM -6	0.6	**0.1**	2			
DSM -7	0.6	**0.4**	2			
DSM -8	0.6	0.2	**0**			
DSM -9	0.6	0.2	**1**			
DSM -10	0.6	0.2	**3**			
DSM -11	0.6	0.2	2	**9**	**9+2**	6
DSM -12	0.6	0.2	2	**4**	**1+3**	6
DSM -13	0.6	0.2	2	2	0.5+1.5	**3**
DSM -14	0.6	0.2	2	**2**	**0.5+1.5**	**6**
DSM -15	0.6	0.2	2	2	0.5+1.5	**9**

2.2.4 Preparation of AMN- Cu-TiO_2/CuO membranes (Chapter 6)

The commercial PAN membrane was hydrolyzed in NaOH aqueous solution (1 M) at 60°C for 1 h before the selective layer can be synthesized. The procedure involves the hydrolysis of polyacrylonitrile (PAN) within an aqueous solution rich in OH^- to yield a high-performance PAN (HPAN) membrane characterized by the presence of exposed -COOH groups and enhanced hydrophilic properties. The resulting HPAN membrane was then stored in DI water at 4 °C until use. The construction of the membrane selective layer was carried out in Tris-buffer through a co-deposition reaction. The preparation process was to dissolve Tris (50 mM) and $CuSO_4$ (5.0 mM) in deionized water to prepare a Tris buffer/$CuSO_4$ solution. The pH of the solution was adjusted to 8.5. Then, certain concentrations of DA (0, 0.1, 0.2, and 0.4 wt%) and PIP (0, 0.15, 0.3, and 0.45 wt%) were added into the Tris-buffer/$CuSO_4$ solution and the mixture was stirred. Hydrogen peroxide (19.6 mM) was added to start the rapid polymerization of dopamine. At the same time, a certain concentration (0, 0.2, 0.4, and 0.6 wt%) of AMN was added to complete the insertion of AMN into the pDA/PIP structure. Then, a co-deposition solution containing the PIP/pDA-AMN structure was obtained. The co-deposition process of the membranes was carried out in a clean fume hood. The previously prepared HPAN membrane was taken out and used as

a supporting substrate to be loaded into a special membrane holder. Then, the resulting co-deposition solution (20 ml) was gently poured into the membrane holder containing the HPAN membrane, such that only the dry HPAN membrane was in contact with the co-deposition solution for a certain period of time (20, 40, and 60 min). The purpose of this process is to realize self-polymerization of pDA and uniform deposition of the selective layer of PIP/pDA-AMN in one step. After the co-deposition process was complete, the membrane on the membrane holder was washed with deionized water to remove the co-deposition solution on the membrane surface and then left to dry in a clean fume hood. The heat treatment process was carried out in a preheated vacuum oven at 60°C for 15 min to allow better evaporation of water on the membrane surface. The specific synthesis conditions are shown in Table 2.4. The membrane was then rinsed five times and immersed in deionized water at 4°C overnight.

The photocatalyst was prepared by first dissolving 4 g of $Cu(NO_3)_2•5H_2O$ in deionized water at room temperature[151]. After the solid was completely dissolved, 5 mL of titanium (IV) butoxide was slowly dropped into the reaction flask containing the $Cu(NO_3)_2$ solution, and the mixture was stirred vigorously for 1 h. The precipitate was collected using a Buchner funnel and then dried in air at 40°C for 1 h. The light blue powder obtained was calcined in an oven at 550°C for 6 h, and the gray sample obtained was the final Cu-TiO_2/CuO. Similarly, we used the same steps during an experiment without addition of Cu $(NO_3)_2•5H_2O$ and obtained a pure TiO_2 sample. Then, 2 mg of photocatalyst powder was dissolved in 20 ml of solution containing 0.1 wt% SDS and treated ultrasonically for 2 h to obtain a photocatalyst dispersion. After obtaining dispersion of the photocatalyst, we loaded the photocatalyst onto the surface of the previously prepared membrane using the vacuum filtration method.

Table 2.4 The synthesis conditions of the membranes.

Membrane	DA concentration (wt%)	AMN concentration (wt%)	PIP concentration (wt%)	co-deposition time (min)	
PAN	0	0	0	0	
NF-1	**0**	0.4	0.3	40	
NF-2	**0.1**	0.4	0.3	40	
NF-3	**0.2**	**0.4**	**0.3**	**40**	
NF-4	**0.4**	0.4	0.3	40	
NF-5	0.2	**0**	0.3	40	
NF-6	0.2	**0.2**	0.3	40	
NF-7	0.2	**0.6**	0.3	40	
NF-8	0.2	0.4	**0**	40	
NF-9	0.2	0.4	**0.15**	40	
NF-10	0.2	0.4	**0.45**	40	
NF-11	0.2	0.4	0.3	**20**	
NF-12	0.2	0.4	0.3	**60**	
NF-13	0.2	0.4	0.3	40	TiO_2
NF-14	0.2	0.4	0.3	40	Cu-TiO_2/CuO

2.3 Characterization

2.3.1 Surface chemistry

Each membrane sample was dried in a dust-free fume hood for at least 48 hours and degassed prior to characterization. The surface functional groups were analyzed by NEXUS670 Fourier transform infrared spectrometer (FT-IR, Thermo Fisher, USA). A Kratos ULFRA X-ray photoelectron spectrometer (XPS, Shimadzu Corporation, Japan) was used to analyze the elemental composition of the membranes, the functional group distribution on the surface, and the functional group variation of the nanoparticles. The crystal phase characteristics of the photocatalyst powder synthesized using a Bruker D8 Advance X-ray diffractometer (XRD).

2.3.2 Morphology

The surface morphology was obtained by scanning electron microscopy (SEM), atomic force microscopy (AFM) and transmission electron microscopy (TEM). Before SEM (FEI Nova NanoSEM 450) observation, each sample needs to be sputtered with gold (Au), and the AFM equipment (Dimension Icon SPM, Veeco Instruments Inc) with a size of 3100 was used under environmental conditions to

determine the surface roughness. A JEOL model JEM 2010 EX instrument was used to obtain transmission electron TEM images at an accelerating voltage of 200 kV to further determine the surface morphology of the membrane. The hydrophilicity of polyester membranes was evaluated by a contact angle goniometer (OCA20, Dataphysics Instruments, Germany) with 2 μL water droplets at 5 random locations.

2.3.3 Surface properties

The charge properties of membrane surface were investigated using an Electrokinetic Analyzer (SurPASS 3, Anton Paar, Austria). Membranes were cut into two pieces with a dimension of 1 cm × 2 cm for each measurement. The pH was adjusted by standard NaOH and HCl aqueous solutions ranging from 3.0 to 10.0. The water contact angle test of the membrane was used to determine the hydrophilicity and hydrophobicity of the membrane surface, using 2 μL water droplets at five random locations on the membrane and then measuring using a contact angle meter (OCA20, Dataphysics Instruments, Germany). The pH of the liquid used should be controlled consistent with the pH of the corresponding membrane.

2.3.4 Photocatalytic performance characterization

UV-4800 UV–Vis spectrophotometer (Perkin Elmer Lambda 350) was used to determine the UV diffuse reflectance of the membrane to characterize the photo responsiveness of the membrane. For the quenching experiment of photocatalytic membrane degradation of DR23, a reactive oxygen species scavenger was added to explore the impact of free radicals on the photocatalytic process. Here, tert-butanol, p-benzoquinone, and ammonium oxalate are used as hydroxyl radical scavengers, superoxide radical scavengers, and hole scavengers, respectively. Mineralization efficiency was monitored by total organic carbon (TOC) measurement, determined by injecting 50 mL of sample via thermostatic oxidation at 680 °C using a Multi N/C 2100 Analytikjena analyzer equipped with a manual injector. The calibration curve of the analyzer was established using a standard potassium hydrogen phthalate solution (99.5%). The membrane test before FT-IR, XRD, SEM, TEM, and UV-Vis testing of the catalyst powder was conducted in the same laboratory using the same equipment. Electrochemical impedance spectroscopy and photocurrent responses were performed using a standard three-electrode setup. An Ag/AgCl electrode was used as the reference electrode and a platinum plate was used as the counter electrode. The working electrode was deposited on a clean indium tin oxide (ITO) substrate. More specifically, first, 10

mg of powdered photocatalyst was fully dispersed in 1 mL of toluene by ultrasonic treatment. Then 20 μL of the slurry solution was dropped on the ITO substrate, and the exposed area of the working electrode was fixed at 0.25 cm^2 with transparent tape to protect the boundary of the ITO substrate, and dried at 80 °C for 2 h to improve adhesion. Afterwards, the clear tape was removed and the uncoated electrodes were isolated with epoxy. The connections of the CsPbBr3 working electrode were immersed into the electrolyte solution. Tetrabutylammonium hexafluorophosphate (TBAPF6, 0.1 M) dissolved in dichloromethane (DCM) solution was used as the electrolyte. An alternating current (AC) voltage (amplitude 5 mV) with a frequency range from 10 kHz to 5 MHz and an open circuit potential of 0.2 V was applied on the electrochemical workstation, and electrochemical impedance spectra were obtained under simulated sunlight. Photocurrent response measurements were performed following impedance spectroscopy. Photocurrent response measurements were performed as those of impedance spectra. Electron spin resonance (ESR) spectra were recorded using a Bruker A300 EPR electron paramagnetic resonance spectrometer and the irradiation wavelength was 350±15 nm, the same light source as that for the photocatalytic degradation.

2.4 Filtration performance measurement

2.4.1 Membrane separation performance

Generally, the calculation formula of water permeance (WP, L m^{-2} h^{-1} bar^{-1}) was as follows:

$$WP = \frac{V}{A \cdot \Delta t \cdot \Delta p} \tag{2.1}$$

where *V* is the volume of permeate solution (L) collected by filtration at a certain time t (h), A is the effective membrane area provided by the cross-flow device, and p is the pressure across the membrane. The rejection (R) was calculated as follows:

$$R = \left(1 - \frac{C_p}{C_f}\right) \times 100\% \tag{2.2}$$

where Cp and C_f (g L^{-1}) are the concentrations in the feed and permeate solution, respectively.

The specific tests involved in each chapter are as follows:

(Chapter 3) A laboratory-scale cross-flow setup was used to examine the filtration performance of the membranes. Specifically, the effective area of each tested membrane was 7.1 cm^2. To ensure the stability of the testing process, all dye/salt separation membranes to be tested were pre-pressurized with deionized water at 3 bar for 30 minutes until the water permeance was stable. When the water permeance was stable, the pressure was adjusted to 2 bar and the tests were carried out with different feeds. The water permeance was calculated according to Equation 2.1. The rejection of salts (Na_2SO_4 and NaCl, 1 g L^{-1}) and different positive dyes (200 ppm) was calculated according to Equation 2.2. The dye concentration was measured with a UV-Vis spectrophotometer (Shimadzu, Japan), and the salt concentration was measured with an Orion Star A212 conductivity meter (Thermo Fisher, USA). The dye in the dye/salt mixed solution was removed using a Dionex AG 9-HC ion chromatography column (Dionex, USA), and the salt concentration was measured through the conductivity. All membrane tests were repeated three times to ensure the repeatability of the results. The dye/salt separation experiments were carried out with the previously mentioned equipment. Na_2SO_4 with different concentrations (1, 10, 20, 30, and 40 g/L) and a specific concentration of Victoria blue B (VBB, 200 ppm) were used. Then the method mentioned before was used to test the permeance and rejection. A mixed solution containing 200 ppm VBB and 1 g/L Na_2SO_4 was filtered through a cross-flow system at 2 bar for 60 h for stability testing of the membranes, and the permeance and rejection were calculated similarly.

(Chapter 4) Before the filtration test, all the tested membranes were pre-pressurized at 3 bar for more than 30 min until their permeance was stable. Before starting the test, reduce the pressure to 2 bar, change the different feed, and carry out the corresponding filtration test. Among them, the calculation formula of water permeance is Equation 2.1. At the same time, if the feed solution is the dye/salt, then the water permeance was replaced by solution permeance. The calculation formula remained the same. The rejection (R) for Na_2SO_4 and NaCl (1 g L^{-1}) and DR23 (200 ppm) was calculated using Equation 2.2. The dye concentrations in the simulated dye contaminants were measured with a UV-Vis spectrophotometer (Shimadzu, Japan), and the concentrations of inorganic salts were measured with a conductivity meter (Star A212, Thermo Fisher, USA). For the mixed salt/dye solution, the dye was first removed with a Dionex AG 9-HC ion chromatography column (Dionex, USA). The salt concentration was measured by the conductometric method. Long-term stability was assessed using dye/salt (200 ppm DR23 and 1 g/L NaCl) mixtures filtered through the system at 2 bar for 60 hours through a lab-scale

cross-flow setup. The permeance and rejection of the long-term stability test were calculated similarly to the previous experiments.

(Chapter 5) A laboratory-scale cross-flow device was used to test the filtration performance of the membrane at room temperature and pressure. Specifically, the effective area of each tested membrane was 7.1 cm^2. Before the DSM filtration test, all membranes needed to be pre-pressed with DI water and N_2 for 30 min at 2 bar until a stable water permeability was obtained. After pre-pressing for 30 minutes, the pressure across the membrane was adjusted to 1 bar and tested with different feeds at room temperature (20 ± 5 °C). The calculation method of water permeability was as Equation 2.1. The rejection of salts and dyes (DR23 and RB5, 200 ppm) was calculated using Equation 2.2. All the dye concentrations were measured with a UV-Vis spectrometer (Shimadzu, Japan). Conductivity measurement equipment was used for a single salt concentration measurement (Thermo Scientific Orion Star A212). For the measurement of the salt concentration in the salt/dye mixed solution, it was necessary to remove the dye in advance, using ion chromatography (DX-120, Dionex, USA) with an anionic chromatographic column (Dionex AG 9-HC), and the conductivity measuring device was used. All membrane tests were repeated three times to ensure the repeatability of the results. Different Na_2SO_4 concentrations (1, 10, 20, 30, and 40 g/L) and a certain concentration of DR23 (200 ppm) were used. Then the method mentioned before was used to test the permeability and rejection. For the stability test of the membrane, a mixed solution containing 200 ppm DR 23 and 1 g/L Na_2SO_4 was filtered for 60 h by the cross-flow system at 1 bar. Then, permeability and rejection were measured, as mentioned before.

(Chapter 6) A laboratory-scale cross-flow device was used to test the filtration performance of the membrane at room temperature and normal pressure (25°C, 101 kPa). All filtration tests in this study were performed using this device. Specifically, the effective area of each membrane module tested w as 7.1 cm^2. Before each membrane filtration, all membranes were pre-pressurized with deionized water at 2 bar for 30 min until a stable permeance was achieved. The purpose of this process is to make the selected layer more stable during the water permeance process. Subsequently, the pressure of the device was adjusted to 1 bar and tests were performed with different feeds. The calculation method of water permeance was according to Equation 2.1. The rejection of salts and dyes was calculated with Equation 2.2. Conductivity measurement equipment (Thermo Scientific Orion Star A212) was used for single salt (except Cr^{6+}) concentration measurement. For the measurement of the salt concentration in the salt/dye

mixed solution, it was necessary to remove the dye in advance using ion chromatography (DX-120, Dionex, USA) with an anionic chromatographic column (Dionex AG 9-HC) and then use the conductivity measuring device. All membrane tests were repeated three times to ensure the repeatability of the results. The previously mentioned equipment was used to conduct dye and salt separation experiments with different concentrations. Specifically, different $K_2Cr_2O_7$ concentrations (1, 10, 20, 30, 40, and 50 g/L) and a concentration of DR23 (200 ppm) were used. Then, the permeance and rejection were tested using the methods mentioned earlier. For the membrane stability test, a mixed solution containing 200 ppm DR 23 and 1 g/L $K_2Cr_2O_7$ was filtered for 60 h using the cross-flow system at 1 bar. Then, the permeance and rejection were measured as described above.

2.4.2 Anti-(bio)fouling and robustness performance

In general, a higher fouling resistance ratio (FRR) and lower summary fouling rate (R_t) could indicate the antifouling ability of the membrane. The calculation method follows:

$$FRR = \left(\frac{J_{w,4}}{J_{w,1}}\right) \times 100\% \tag{2.3}$$

$$R_t = \left(1 - \frac{J_{p,1}}{J_{p,4}}\right) \times 100\% \tag{2.4}$$

irreversible fouling (R_{ir}), expressed by:

$$R_{ir} = R_t - R_r \tag{2.5}$$

which refers to the fouling formed by adsorption or molecular deposition. Reversible fouling (R_r) is caused by concentration polarization during membrane operation. It can be expressed as follows:

$$R_r = \frac{J_{w,4} - J_{p,1}}{J_{w,1}} \times 100\% \tag{2.6}$$

For the anti-biofouling test, the typical gram-negative bacterium *Escherichia coli (E. coli*) was used as a biological contamination for antibacterial testing. *E. coli* cells were grown overnight at 37 °C with LB (Luria-Bertani broth), then inoculated with 1 ml of 50 ml of pre-warmed LB overnight and allowed to grow for 2-3 hours with shaking until OD = 0.5-0.8, where 108 colony forming units (CFU)·mL^{-1} were found. The cut 2.5 cm^2 test piece was sterilized with 75% ethanol. Then 5 mL of the *E. coli* suspension was taken in contact with the membrane for 3 hours at 37 °C with shaking at 200 rpm. Bacterial

suspensions were plated on LB agar plates by standard dilution and incubated overnight at 37°C. The Plate Colony Forming Unit (CFU) Count method uses plates from 3 to 1000 CFU to determine the number of colonies on a plate. Among them, the number of colonies in the control group was 100, and the bacteriostatic efficiency of the dye/salt separation membrane under different conditions was calculated.

The specific tests involved in each chapter are as follows:

(Chapter 3) An antifouling test was carried out using $P_{0.5}$-$T_{0.5}$-AMN. The dyes used were victoria blue B (VBB) and patent blue VF (PBVF) (200 ppm) at 2 bar with the cross-flow device. After the system was stabilized, DI water was used for filtering and data were recorded every ten minutes within 1 hour. $J_{w,1}$ was used to record the average water permeance of the first cycle. After one hour, the DI water was changed to the dye solution. Then, the membrane was washed with DI water for 30 min. This was repeated four times to calculate the permeance of the membrane. A higher fouling resistance ratio (FRR) and a lower summary fouling rate (R_t) indicates the antifouling ability of the membrane. The calculation method is Equation 2.3 and 2.4. Irreversible fouling (R_{ir}), expressed by Equation 2.5, refers to the fouling formed by adsorption or molecular deposition. The phenomenon of concentration polarization during membrane operation can cause reversible fouling (R_r) of the membrane, which is expressed as Equation 2.6.

(Chapter 4) For the anti-fouling and robustness testing of NF-3, experiments were performed in a cross-flow setup using DR23 (200 ppm) as the contaminant at a pressure of 2 bar. Likewise, the membrane was pre-pressed with deionized water at a pressure of 3 bar until the system stabilized. Then, it was filtered with deionized water for 1 hour, during which permeance and rejection data were recorded at regular intervals. $J_{w,1}$ was the average permeance of the first cycle. After one hour, the deionized water in the feed was changed to DR23 (200 ppm), and the permeance and rejection ($J_{p,1}$) data were recorded at intervals. Then, the membrane was washed with DI water for 30 min. Then, the membrane was filtered with deionized water for 30 min for cleaning purposes. The above experiment was repeated four times, and recorded as $Jw_{1\text{-}4}$ and $Jp_{1\text{-}4}$ fouling resistance ratio (FRR) and total fouling rate (R_t) to make the membrane anti-fouling and self-cleaning ability the most important index. The calculation was based on Equation 2.3 and 2.4. Irreversible fouling (R_{ir}) was expressed by Equation 2.5, which refers to the fouling formed on the membrane surface through intermolecular interaction. Since the concentration polarization

phenomenon occurs during the filtration process of the membrane, it will also cause reversible fouling (R_r) of the membrane, expressed by Equation 2.6.

For pH robustness, the prepared NF-3 was treated with pH=1 and pH=13 acid-base solutions for 24 h. Then, a mixed solution of DR23 (200 ppm) and NaCl (1g/L) was used to conduct a 48 h long-term stability filtration experiment to confirm the robustness of the membrane under extremely acidic and alkaline conditions.

(Chapter 5 and 6) The dye DR23 (200 ppm) was used to test the visible light catalytic performance of the membrane. The visible light source used a 300 W xenon lamp (using a 400 nm filter to remove ultraviolet rays, PLSSXE 300, Beijing Perfectlight Co. Ltd.), which was placed 10 cm away from the membrane. For the static catalytic degradation experiment of DR23, the photocatalytic membrane was immersed into a DR23 solution (100 mL, 200 ppm) at room temperature (20±5°C). The solution and the membrane were kept under the initial dark condition for 90 minutes to ensure the adsorption equilibrium of the membrane to DR23. Then, the solution was irradiated with visible light. After that, a sample (3 mL) was taken every 30 minutes and used UV-Vis spectrophotometry to measure the absorbance of the solution to calculate the degradation rate (C/C_0). The filter-visible-filter method was used to evaluate the self-cleaning performance of the membranes. The dye DR23 was used in the self-cleaning experiment of the membrane, in which the membrane module with quartz transparency was used to improve the membrane module of the previous cross-flow experiment, using a transparent quartz glass membrane assembly. During the operation, visible light can pass through the quartz glass on the membrane module and directly irradiate the membrane surface loaded in the membrane module. The initial feed is DI water, and the average permeability for 1 h is recorded as $J_{w,1}$. Then the feed solution was replaced with DR23 for one hour, and the average permeate permeability was recorded as $J_{p,1}$. At this time, the surface of the membrane was covered with dye, then irradiated with visible light; the permeability was replaced with DI water. The test was carried out for 1 h, and its average permeability $J_{w,2}$. This was repeated four times to obtain $J_{w,4}$ and $J_{p,4}$. Then, in order to determine the permeation recovery of the membrane, the water permeability of the membrane was measured through the same procedure in section 2.4. A higher permeability recovery rate (FRR) and a lower summary fouling rate (R_t) could indicate the antifouling ability of the membrane. The calculation was based on Equation 2.3 and 2.4. Irreversible fouling (R_{ir}), expressed by Equation 2.5 refers to the fouling formed by adsorption or molecular deposition. Reversible

fouling (R_r) is caused by concentration polarization during membrane operation. It can be expressed by Equation 2.6.

2.4.3 Pore size distribution

For the pore size distribution, the feed solutions were changed as 100 ppm PEGs (300-6000 g mol^{-1}). The dissolved organic carbon was measured using a total organic carbon (TOC) analyzer (Multi N/C 2100, Analytikjena). Based on the PEGs rejections (R, %), the pore size distribution of the PA-SSL membrane was obtained via the following equation[152]:

$$\frac{dR(d_p)}{dd_p} = \frac{1}{d_p \ln \sigma_p \sqrt{2\pi}} exp\left[-\frac{(\ln d_p - \ln \mu_p)^2}{2(\ln \sigma_p)^2}\right] \quad (2.7)$$

where d_p, μ_p, and σ_p are the stokes diameter (nm), mean pore radius (nm) and the geometric standard deviation of the PEGs, respectively. The charge properties of membrane surface were investigated using an Electrokinetic Analyzer (SurPASS 3, Anton Paar, Austria).

2.5 Photocatalytic conversion performance evaluation

(Chapter 6) To demonstrate the photocatalytic conversion performance of the membrane, the same cross-flow device used for the photocatalytic self-cleaning test was implemented. Specifically, the Cr^{6+} content in actual textile wastewater is approximately 1–10 mg/L[153]. Therefore, when selecting the feed concentration, a certain concentration of DR23 and Cr^{6+} was used (10, 30, 50, 70, 90 mg/L), with a concentration ratio of 1:1. The membrane rejection results were then obtained using the same approach as used for the previous filtration test. To explore the effect of the concentration ratio of DR23 and Cr^{6+} in the feed on membrane rejection, it was made similar to that of the concentration test. The feed was adjusted to 50 ml/L of DR23 and Cr^{6+} at a certain concentration ratio (0.1, 0.2, 1, 2, and 10). The rejection result test was the same as the previous filtration experiment. The feed materials for the actual catalytic conversion test were DR23 and Cr^{6+} with a concentration of 50 mg/L, and the tests were conducted continuously on the same device for 60 h. Membrane permeance and rejection were measured using a method similar to the one used before.

2.6 Computational simulations

2.6.1 Molecular dynamics (MD) simulations of membranes

All molecular dynamics (MD) simulations were performed using the GROMACS 2019.6 CPU package on a parallel Linux cluster[154]. Water molecules were modeled using the OPC3 potential, whereas other molecules were characterized using the general AMBER force field（GAFF. The geometry of membrane molecules was optimized by ORCA software (version 5.0.2) at the B97-3c level. The average of the restrained electrostatic potential (RESP) charges of the membrane molecules was computed in the liquid and gas phases by ORCA, which is called $RESP2_{0.5}$. The $RESP2_{0.5}$ charges were calculated by Multiwfn (version 3.8)[155]. The topology file simulations were prepared by Sobtop. The steepest descent method was used to minimize the energy of initial configurations[156]. An isothermal–isobaric (NPT) ensemble with a 1.0 fs time step was employed to obtain a stable box size. MD simulation with a time step of 2 fs at 298 K in the NVT ensemble was performed. For all dynamics runs, the temperature was controlled using the v-rescale thermostat, and the pressure was controlled with the Berendsen barostat. The LINCS method was used to restrict the h-bond lengths. Periodic boundary conditions were applied in all three dimensions. The cut-off approach was used to compute van der Waals interactions using a cut-off distance of 1.0 nm, whereas the particle mesh Ewald method was used to calculate electrostatic interactions. The simulation results were visualized using VMD 1.9.3.

MD simulations were carried out to calculate the diffusion rate of PIP molecules in different system. The diffusion coefficients of the PIP molecules can be estimated from the slope of the mean square displacement (MSD) curves, using the Einstein relationship. With a constant pDA:PIP:AMN quantity ratio of 33:100:133, the PIP and water molecules were randomly packed in a cubic simulation box with side length of 50 Å. Then, the box was filled with water molecules according to the density of water. In other separate analogous simulations, the same PIP containing cubic simulation box was constructed, but pDA and AMN molecules were also added.

With a constant PDA: PDA/PIP: PDA/PIP/AMN quantity ratio of 270:70:60, the membrane molecules were packed in same cubic simulation boxes with side length of 50 Å. Then, the box was filled with water molecules according to the density of water. Energy minimization、NPT and NVT ensemble were performed for the above three systems. Then, Zeo++ was used to analyze pore size distribution with

a probe radius of 0.5 Å. Radial distribution functions (RDFs) of water molecules with different segments were extracted by GROMACS. In addition, the free volume was calculated by Multiwfn[157]. From the MD simulations, spatial distribution functions (SDFs) of water molecules were obtained by GROMACS. The SDF data were then visualized using the VMD.

2.6.2 The density functional theory (DFT) calculations of membranes

The Quantum ESPRESSO distribution[158] was utilized for conducting DFT calculations. The interactions between nuclei and core electrons were elucidated employing the ultrasoft pseudopotential within the framework of the generalized gradient approximation (GGA) with the Perdew-Burke-Ernzerhof (PBE) functional. A kinetic energy cutoff of 30 Ry along with a charge-density cutoff of 300 Ry were used to ensure energy convergence. Additionally, Fermi-surface effects were addressed using the Methfessel and Paxton smearing technique, employing a smearing parameter of 0.02 Ry. For Brillouin-zone sampling, a k-point mesh of 3×3×1 was employed. A vacuum layer of ~ 10 Å was included to mitigate slab interactions along the z-direction. The models of pDA-PIP and pDA-PIP/AMN had been relaxed (the process of gradually returning to equilibrium) before calculated to optimize the structure. The adsorption energy (ΔE_a) of water was calculated by the following Equation:

$$\Delta E_a = E_{total} - E_{water} - E_{substrate} \quad (2.8)$$

where E_{total} is the total energy of the compound, E_{water} is the energy of H_2O, and $E_{substrate}$ is the energy of the corresponding molecule.

2.6.3 The density functional theory (DFT) calculations of photocatalyst

The density functional theory (DFT) calculations were performed using the Vienna Ab initio Simulation Package code. The electron-nuclei interactions are described using the projector augmented wave method. The exchange-correlation was described using the GGA of a PBE functional. The DFT-D3 method was used to describe the van der Waals interaction. The total energy and all forces on atoms were converged to 1×10^{-4} eV and 0.01 eV/Å, respectively. The plane-wave cutoff was set to 450 eV and the Brillouin zone was set to Monkhorst-Pack 5×5×1 meshes.

Chapter 3: Positively charged nanofiltration membranes based on Mannich reaction and prebiotic chemistry for anti-(bio)fouling

Adapted from: "*Gao, Q., Zhu, Q., Zheng, J., Yuan, S., Wang, Y., Zhao, R., Liu, Y., Gui, X., Wang, C., Volodine, A., Jin, P., Van der Bruggen, B. with Jin, P. (corresp. author), Van der Bruggen, B. (corresp. author) (2022). Positively charged membranes for dye/salt separation based on a crossover combination of Mannich reaction and prebiotic chemistry. JOURNAL OF HAZARDOUS MATERIALS, 440, Art.No. ARTN 129744. doi: 10.1016/j.jhazmat.2022.129744*"

3.1 Introduction

More than 224 national flags worldwide cover almost all common colors, among which purple is rarely used (except for *El Salvador*, *The Republic of Nicaragua* and *Dominica*) due to its high cost, even more than gold in the past [159]. In 1856, this problem was solved by an eighteen-year-old man, *Sir William Henry Perkin* (1838-1907), who synthesized the world's first synthetic purple dye, 'Mauveine' [160]. In less than two hundred years, more artificially synthesized dyes have been filling our lives and making our life almost a world 'dyed with dyes'. However, the large amount of dye-containing textile wastewater that comes along is detrimental for the environment and threatens human health and safety. For this reason, researchers extensively explored the treatment of textile wastewater, among which advanced oxidation [161], photocatalysis [162], adsorption [163, 164] , and membrane separation [165] are the most promising treatment methods. Nanofiltration membranes with pore sizes smaller than dye molecules are generally considered 'star players' in dye/salt separation due to their high efficiency [166-169]. It is worth noting that NaCl and Na_2SO_4 are accelerators that make dyes adsorb on textiles during the dyeing process, so in the process of treating textile wastewater, the separation of dyes and salts allows to recover both from waste.water, which yields a sustainable process [163, 170]. Conventional polyamide-based nanofiltration membranes, however, also reject Na_2SO_4 and NaCl present in textile wastewater, which undoubtedly negatively impacts the desalination efficiency [99, 171, 172]. In addition, based on the Donnan effect, positively charged membranes are favorable for rejecting positively charged dyes while ensuring the high efficiency of desalination [169, 173-175]. Currently, most dye/salt separation membranes with positively charged dyes are synthesized by the biomimetic material pDA and interfacial polymerization. Although this method can separate positively charged dyes to a certain extent, due to the long polymerization time of pDA and the low electrical potential of such membranes, they

have generally a poor selectivity and poor permeance [169, 176]. Therefore, efficiently retaining dyes from textile wastewater while recovering salts through rapid desalination is a standing challenge.

Branched polyethyleneimine (PEI) is one of the most common monomers in positively charged membranes [99, 169, 177]. As a water-soluble polymer composed of various amino groups, PEI often reacts with other compounds to form corresponding selective layers through surface finishing [178], interfacial polymerization [169] or coating [179]. As early as 2009, researchers used PEI and trimesoyl chloride (TMC) to prepare traditional polyamide nanofiltration membranes [34, 180, 181]. This reaction was intensively repeated in the ensuing decade to produce high-quality nanofiltration membranes in large quantities [34, 180, 181]. However, the reactions of the monomers may not only depend on this 'one-trick pony'. Interestingly, PEI is also popular in flame retardant synthesis due to its abundant amino groups, which promote nucleophilic substitution reactions to form denser flame-retardant layers. Recently, researchers have identified a reaction method of tetrakis(hydroxymethyl)phosphonium chloride (THPC), driven by the base-promoted polycondensation of THPC and amines, for commercializing flame-retardant cotton [182, 183]. Due to the amino groups, PEI easily pairs with THPC followed by a Mannich reaction, an amine methylation condensation reaction discovered by *Carl Mannich* in 1912 [184]. The combination of PEI and THPC through the Mannich reaction is a potential alternative to the fixed collocation of PEI and TMC to prepare positively charged membranes.

In membrane modification and synthesis, some bio-inspired materials (e.g., pDA) are commonly used as "bio-glue" to bind support substrates and selective layers [185-187]. However, its long deposition time (over 20 h) leads to defects and inhomogeneous aggregates on the membrane surface, which strongly affect the mass transfer efficiency of the membrane [187, 188]. Although some researchers have introduced oxidants (such as $CuSO_4/H_2O_2$) that enable rapid deposition of pDA, the addition of these chemicals makes the synthesis process difficult to control and increases the cost and burden on the environment [188]. Instead of pDA, bioinspired AMN is considered prebiotic chemistry and applied to form antimicrobial coatings [189, 190]. Coatings inspired by such theory are admired in biochemistry, but their application in membrane synthesis is rarely reported. AMN can spontaneously polymerize without initiating oxidants, the coating deposition time is shorter than pDA, and the formed selective layer is more stable [191]. Additionally, the antibacterial activity of AMN has also been confirmed in

many studies [149, 190, 192, 193]. With these merits, AMN can serve as underlying biomimetic material for membrane modification and synthesis.

Here, the Mannich reaction was employed with AMN to prepare positively charged membranes for desalination of dye solutions. By one-step co-deposition, PEI and THPC form a positively charged selective layer through a Mannich reaction capable of rejecting positive dyes and allowing fast transport of salts. The selection layer was adhered to a polyacrylonitrile (PAN) substrate with AMN. Positively charged dyes and two salts (Na_2SO_4 and NaCl) commonly found in textile wastewater were selected for separation testing. In addition, antifouling and antibacterial tests were carried out.

3.2 Results and discussion

3.2.1 Chemical composition characterization of the membranes surface

To explore the chemical composition of the newly synthesized membranes, FT-IR spectra are shown in Fig. 3.1a. The characteristic peak at ~3362 cm^{-1} is the -OH vibration, which may come from the support substrate or the -OH generated through the Mannich reaction[194]. The vibration of the -C≡N functional groups in the PAN support substrate and AMN coating is located at ~2243 cm^{-1} [195]. The characteristic peaks of $-CH_2$ are resolved at ~2933 cm^{-1}, 1662 cm^{-1} and 1453 cm^{-1} [196]. The characteristic peaks of -C=O and -C-O-C appear at ~1734 cm^{-1} and ~1061 cm^{-1}, respectively [197, 198]. It is worth noting that a new peak is generated at ~1061 cm^{-1}, making the peak shape of the membrane slightly different from the new membrane substrate, which is attributed to the stretching of the C-O bond on the ester group and the -C-O-C on the primary alcohol in the THPC molecule [199]. Fig. 3.1b and Fig. 3.1c show XPS wide-scan spectra. In addition to the obvious C, N, O peaks, the peaks of P element are present in the spectra of THPC-AMN, $P_{0.5}$-$T_{0.5}$-AMN and $P_{0.5}$-$T_{0.5}$-PDA, which shows that THPC was successfully added to the surface of the membrane. To further demonstrate the introduction of THPC and the occurrence of the Mannich reaction, Fig. 3.1d shows the elemental composition. It can be seen that the P element of THPC is present in the membranes. It can be observed that after the introduction of THPC, the content of O element increases, which is contributed by the -OH group in THPC [199]. Fig. 3.2 shows the XPS core-level spectra of O 1s and P 2p of PAN, PEI-AMN and $P_{0.5}$-$T_{0.5}$-AMN. In Fig. 3.2a, the spectrum of O 1s in PAN shows that the oxygen elements mainly exist in the form of N-C=O and O-C=O, and the content of N-C=O is high, which is similar to that of PEI-AMN (Fig. 3.2b). In contrast, a peak of -OH appeared

in $P_{0.5}$-$T_{0.5}$-AMN due to the intervention of THPC and the occurrence of the Mannich reaction [200] (Fig. 3.2c). This further proves the success of the introduction of THPC. Fig. 3.2d shows the XPS core-level spectra of P element for the three membranes; consistent with the previous elemental composition analysis, a peak of P element arises in $P_{0.5}$-$T_{0.5}$-AMN, but not in the other two membranes [201]. It also demonstrates that the participation of TPHC in the reaction leads to the presence of P on the membrane surface.

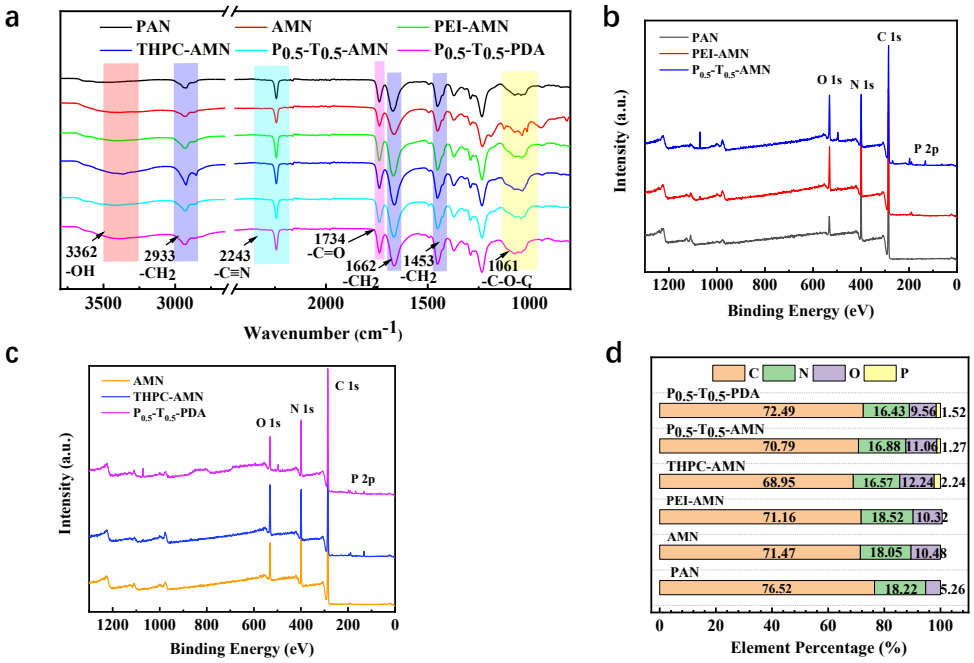

Figure 3.1 Chemical composition characterization of membranes: (a) FT-IR spectra; (b-c) XPS wide-scan spectra; (d) elemental composition analysis.

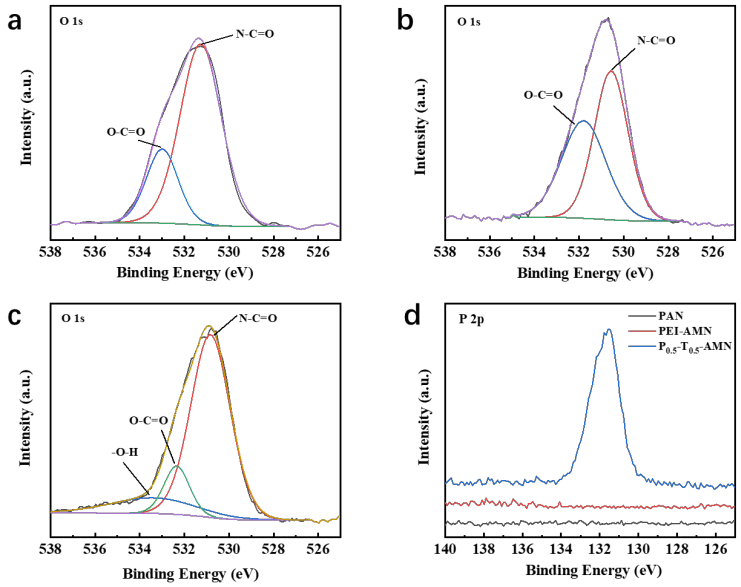

Figure 3.2 Core-level XPS spectra of O 1s: (a) PAN; (b) PEI-AMN; (c) P0.5-T0.5-AMN; (d) core-level XPS spectra of P 2p.

3.2.2 Morphology of the membranes

Fig. 3.3 shows the surface morphology and roughness of membranes in which the morphology of the PAN support substrate (Fig. 3.3a) and the modified layer can be observed. After AMN modification (Fig. 3.3b), the surface becomes smooth because AMN is combined with the support substrate to form a dense AMN layer [189]. After further modification with PEI, the roughness of the PEI-AMN membrane increased slightly due to the combination of PEI and AMN. Likewise, the roughness of TPHC-AMN (Fig. 3.3c-d) increased to a small extent compared with the AMN-modified membrane. Through the Mannich reaction, the -OH of THPC was substituted by -NH of PEI [34]. As shown in Fig. 3.3e, a flocculent structure was formed and adhered to the AMN layer, which renders the roughness of $P_{0.5}$-$T_{0.5}$-AMN membrane higher than that of the membrane mentioned above. However, the surface of the membrane modified with PDA instead of AMN showed many inhomogeneous structures and an increased roughness (Fig. 3.3f). This hints that AMN is more stable than PDA under similar modification conditions [194]. From the cross section of the membrane, the thickness of the selective layer of PEI-AMN can be obtained at ~101 nm (Fig. 3.3h) by comparison with PAN support substrates (Fig. 3.3g-j), while that of THPC-AMN is ~158 nm. Surprisingly, after the Mannich reaction occurred, the thickness of the selective layer did not change significantly, which indicated that the Mannich reaction between

PEI and THPC was moderate. This phenomenon advocates TPHC for membrane modification, which was also mentioned in a previous report [202].

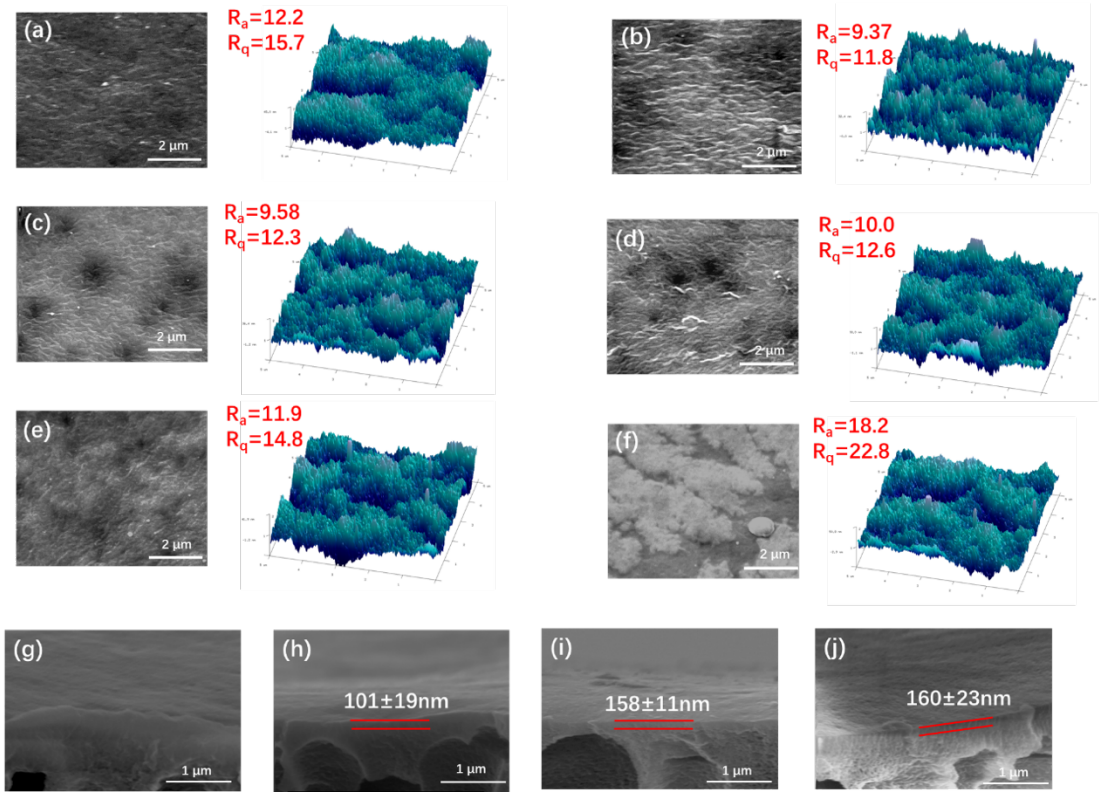

Figure 3.3 The surface morphology and the roughness by SEM and AFM of (a) PAN, (b) AMN, (c) PEI-AMN, (d) THPC-AMN, (e) $P_{0.5}$-$T_{0.5}$-AMN, (f) $P_{0.5}$-$T_{0.5}$-PDA; cross-sectional morphology by SEM of (g) PAN, (h)AMN, (i)THPC-AMN, (j) $P_{0.5}$-$T_{0.5}$-AMN.

3.2.3 Hydrophilicity and surface potential characteristics of the membranes

The water contact angles of the PAN substrate and the modified membranes prepared under different conditions are shown in Fig. 3.4a, which is closely related to the hydrophilicity and hydrophobicity of the membranes. The experimental results showed that the water contact angle of the PAN support substrate was increased after being modified by AMN, PEI-AMN and THPC-AMN, respectively. These modifications can form dense selective layers on PAN support substrates with high water transport resistance [194]. However, the Mannich reaction between THPC and PEI linked PEI to THPC, thus exposing more hydroxyl groups and the appearance of more amine and hydroxyl groups increased the hydrophilicity of the membrane, giving a smaller water contact angle [149]. Compared with the other .reports, the membrane synthesized by this method has a smaller contact angle, which shows that it has a better hydrophilicity[169, 199, 203]. In addition, the increased hydrophilicity of the membrane is more conducive to the permeance and provides a rapid mass transfer.

The zeta potential of the membranes surface is shown in Fig. 3.4b. It can be seen that after the PEI modification, the negative charges on the PAN support substrate are converted to positive charges in the lower pH range. This can be ascribed to the protonation of the amine group in PEI. Likewise, membranes with only AMN on the surface also exhibited higher potentials as a result of protonation of the amine groups in AMN. By comparing PEI-AMN with $P_{0.5}$-$T_{0.5}$-AMN, the introduction of TPHC slightly decreases the potential but still retains the positive charge in a certain pH range. This means that after TPHC modification, the membrane's separation performance may not be significantly affected due to a slight change in the surface charge of the membranes [199, 204].

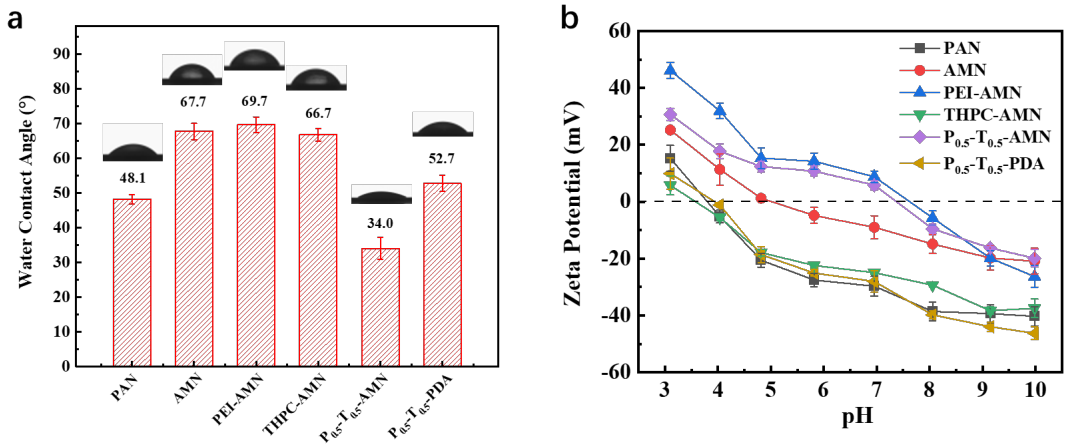

Figure 3.4 (a) Water contact angle of membranes; (b) Zeta potential measurements of membranes.

3.3.4 Filtration performance of the membranes

Figs. 3.5 to 3.7 summarize the filtration performance of the membranes. As shown in Fig. 3.5a, the water permeance of the PAN-based membrane is the highest (326.0 LMH bar^{-1}), and it significantly decreases after modification with AMN (105.8 LMH bar^{-1}). Furthermore, after modification with PEI or THPC together with AMN, the water permeance was slightly improved, as PEI or THPC could occupy some sites of AMN, providing a mass transfer channel for water permeation. When both PEI and THPC were introduced, the Mannich reaction occurred on the membrane surface, and the water permeance decreased to 30.7 LMH bar^{-1} ($P_{0.5}$-$T_{0.5}$-AMN). This is because a relatively dense selective layer was formed on the membrane surface, hindering the transport of water molecules [149, 200]. The same result also appeared in the optimization of the PEI/THPC ratio (Fig. 3.6a). When the PEI/THPC concentration ratio was 1, the water permeance of the membrane was lower, indicating that the Mannich reaction

occurred sufficiently and a dense selective layer was formed on the membrane surface. Similarly, when the deposition of PEI and THPC was prolonged, the water permeance of the prepared membranes decreased, and the platform was reached with deposition of 60 min (Fig. 3.7a). The comparable water permeance of PDA-modified membrane and AMN-modified membrane strongly proves the feasibility of AMN in replacing PDA [186].

A concentration of 200 ppm of Victoria blue B (VBB) was used to test the performance of the membrane for dye/salt separation. The PAN support substrate had a high water permeance (309 LMH bar^{-1}) and a poor dye rejection (65.6%) due to the presence of pores on the surface (Fig. 3.5b). After modification with AMN, the membrane with a denser surface showed a decreased permeance (98.5 LMH bar^{-1}) and a significantly increased rejection of dye (92.6%). Since the membrane potential is not high, positively charged dyes were adsorbed, so the membrane also has a higher rejection after AMN modification. Further, after the modification with PEI or THPC, the permeance of the dye slightly recovered compared with that of the membrane with AMN alone, as PEI/THPC combined with AMN occupying the original AMN site made the layer less dense [188]. Interestingly, PEI-AMN had a slightly higher permeance but also an improved rejection compared to AMN, which seems to break the “trade-off” between permeance and rejection. Due to the higher surface potential of PEI-AMN (Fig. 3.5b), the positively charged dye was more easily repulsed by the co-charged membrane surface based on the Donnan effect, and a higher rejection was obtained [169]. After the Mannich reaction, although the $P_{0.5}$-$T_{0.5}$-AMN membrane retained a positive potential, a denser selective layer was formed, resulting in a higher dye rejection (99.5%) and a low dye permeance (26.3 LMH bar^{-1}). The "star player" PDA did not have the expected victory: compared with $P_{0.5}$-$T_{0.5}$-AMN, although $P_{0.5}$-$T_{0.5}$-PDA has a slightly higher permeance, the dye rejection is lower at only 97.3%. A similar phenomenon was found during membrane optimization (Fig. 3.6b and 2.10b).

NaCl and Na_2SO_4, two salts commonly present in textile wastewater, were used here (1 g/L) to test the salt separation performance of the membranes. Fig. 3.5c shows that the PAN support substrate with larger pore size has a higher water permeance (Na_2SO_4, 315.6 LMH bar^{-1}; NaCl, 320.5 LMH bar^{-1}) and a lower salt rejection (Na_2SO_4, 4.5%; NaCl, 3.7%). Similar to the separation results of dyes, after AMN modification, the permeance of the membrane decreased. For salt rejection, a higher rejection of Na_2SO_4 was obtained because the hydrated ionic radius of Na_2SO_4 is larger than that of NaCl (sulfate (0.38 nm)

> sodium (0.36 nm)> chloride (0.33 nm))[194]. Interestingly, the Na_2SO_4 rejection did not appear to be associated with an increase or decrease in salt permeance (PEI-AMN (107.0 LMH bar^{-1}, 17.2%), THPC-AMN (147.0 LMH bar^{-1}, 17.5%), and $P_{0.5}$-$T_{0.5}$-AMN (27.0 LMH bar^{-1}, 9.9%)). Thus, not only the sieving effect but also the Donnan effect are playing [205]. Since Na_2SO_4 tends to be negatively charged in an aqueous solution, a positively charged membrane is more favorable for its transmembrane transport. Likewise, the NaCl separation of $P_{0.5}$-$T_{0.5}$-AMN is lower than that of $P_{0.5}$-$T_{0.5}$-PDA, which can be explained by the lower potential of $P_{0.5}$-$T_{0.5}$-AMN resulting from a more negative charge provided by PDA; vice versa for Na_2SO_4. Similar conclusions can be drawn from those membranes prepared for optimization. (Fig. 3.6c and 2.10c). It can be seen that the 'sieving effect' and 'Donnan effect', the basic theories of membrane separation, are fully exerted by the 'crossover combination' of the Mannich reaction (PEI/THPC) and prebiotic chemistry (AMN). A higher repulsion of positively charged dyes can be obtained, but the "trade-off" can be broken, with lower repulsion of negatively charged salts and higher permeance (Fig. 3.5c). Therefore, the membrane synthesized by this method has great potential in the field of dye/salt separation and has a sustainable application prospect in resource recovery.

The test results of dye/salt separation using a solution of 200 ppm VBB and different concentrations of Na_2SO_4 are shown in Fig. 3.8a. It can be seen that in the concentration range of 10-40 g/L Na_2SO_4, the separation performance of the membrane is stable. With the salt concentration in the feed solution increasing from trace to 10 g/L, the permeance of the membrane decreased slightly, while the salt rejection slightly increased, and the dye rejection remained unchanged because with the increase of concentration, the salt solution can interact with the positive charge at high concentration. The dye is coupled, and the diffusion of the dye molecule in the aqueous solution increases [203]. Moreover, the mixed solution with high salt concentration is likely to cause concentration polarization during the filtration process, thereby increasing the salt concentration in the feed solution and affecting the separation process. Several common positively charged dyes with different molecular weights including NR (Mw=288.78), MB (Mw=319.85), MO (Mw=327.33), VBB (Mw=506.08), JGB (Mw=511.06), PBVF (Mw=566.66), RhB (Mw=778.38) were applied for studying the newly developed membranes (200 ppm). As shown in Fig. 3.8b, the membrane is better for the separation of dye molecules with larger molecular weight (VBB, JGB, PBVF, and RhB) than for those with smaller molecular weight (NR, MB, and MO). This has a certain correlation with the pore structure of the membrane, but it is noted that the

diffusion effect and the hydration radius of the dye also should be taken into consideration rather than simply focusing on the molecular .weight of the dye [206]. Based on the rejections obtained for each dye, it is roughly estimated that at a molecular weight of 338 Da, the membrane rejects 90% of the dye. This shows that this membrane is suitable for the separation of most macromolecular dyes and has broad application prospects. Furthermore, the stability of the membrane was verified by a continuous experiment lasting for 60 h (Fig. 3.8c). The permeance decreased from 28.4 to 23.1 LMH bar^{-1} in the first hour due to the adsorption of the dye on the membrane surface but levelled off in the subsequent tests. During the whole long-cycle stability experiment, the separation performance of the dye/salt separation membrane remained stable: the rejection of Victoria blue B was almost kept at around 99.5% and the rejection of Na_2SO_4 at around 15%. It is worth mentioning that a water permeance of 30.7 LMH bar^{-1}, a decolorization rate of 99.5%, and a desalination rate of 9.9% were obtained. For difficult-to-separate positively charged dyes, it has certain advantages compared with some studies in the past three years (Table 3.1).

With the increasing number of interfacial polymerization (IP) polyamide membranes available today, innovative membrane synthesis methods are challenging. Especially for the difficult-to-separate wastewater containing positively charged dyes, the dye/salt separation membrane does not use the traditional IP method, but is obtained by the deposition method based on the cross-border combination of Mannich reaction and prebiotic chemistry. It showed good performance in the test. This shows that the membrane synthesized by this method has a good stability during the operation. At the same time, this also shows that the dye/salt separation membrane has excellent potential in practical large-scale industrial applications.

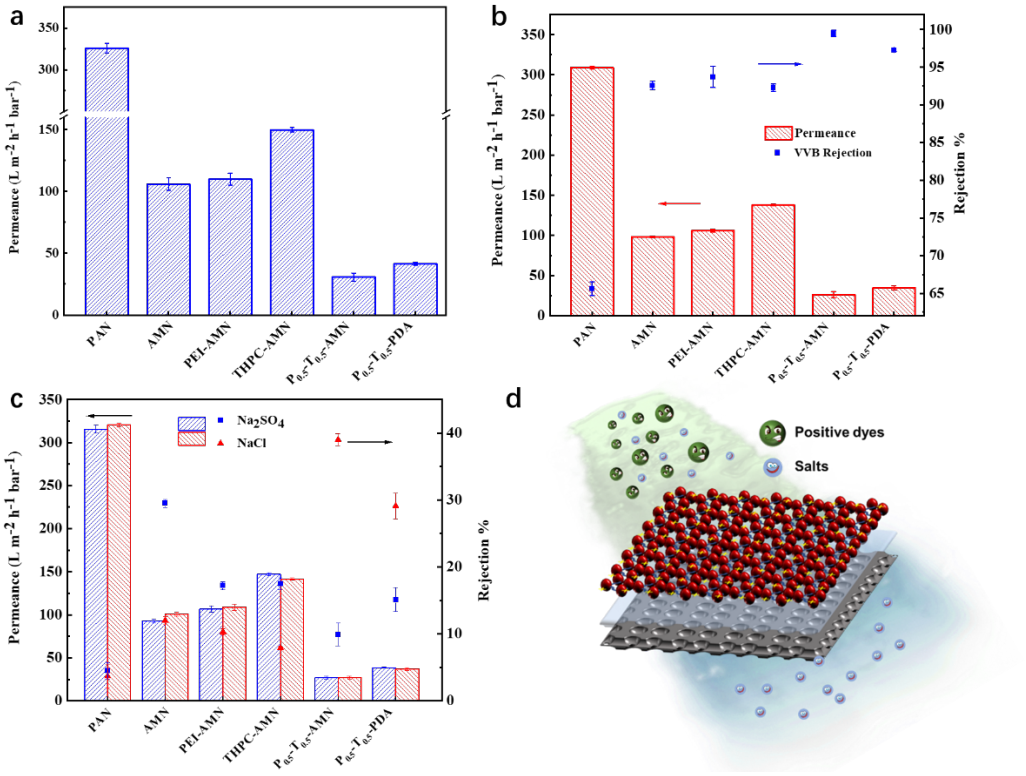

Figure 3.5 (a) DI water permeance of membranes; (b) dye solution permeance and rejection of membranes; (c) salt solution permeance and rejection of membranes; (d) schematic diagram of membranes separation of dye/salt.

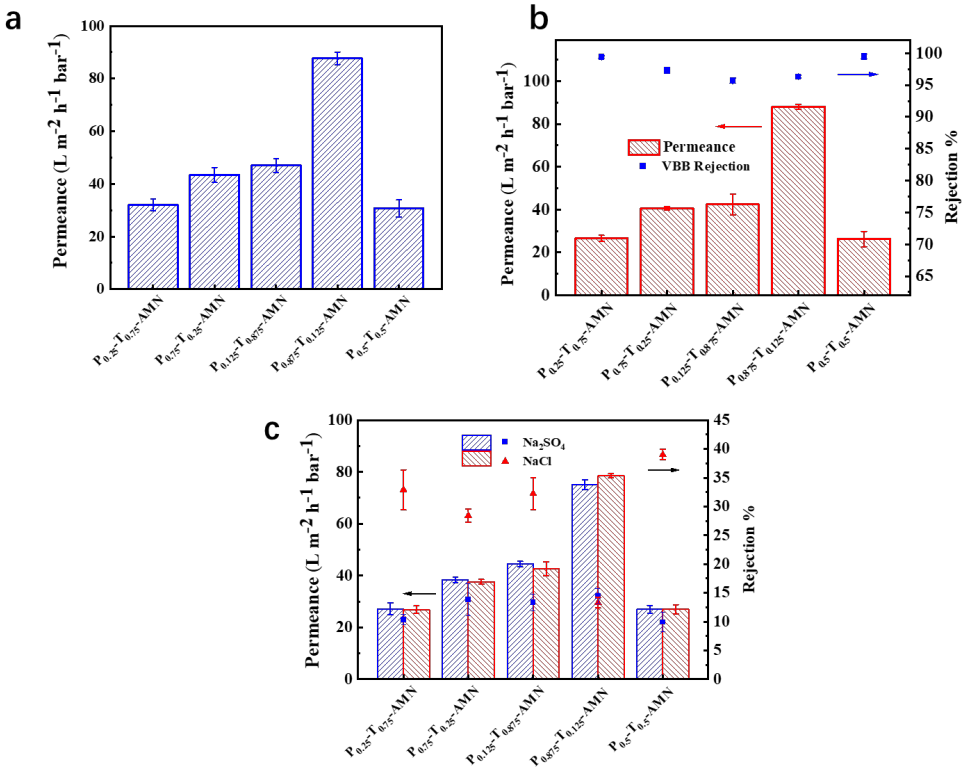

Figure 3.6 Separation performance of membranes with different concentrations of THPC/PEI: (a) water permeability; VBB separation performance; (c) Na_2SO_4/NaCl separation performance

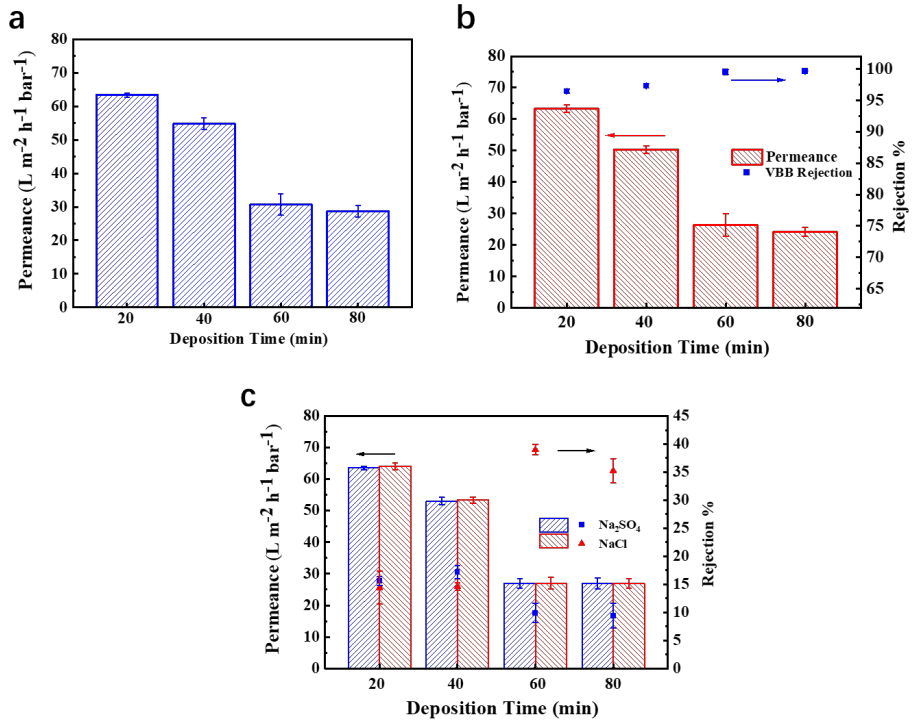

Figure 3.7 Separation performance of membranes with different deposition time: (a) water permeability; VBB separation performance; (c) Na_2SO_4/NaCl separation performance.

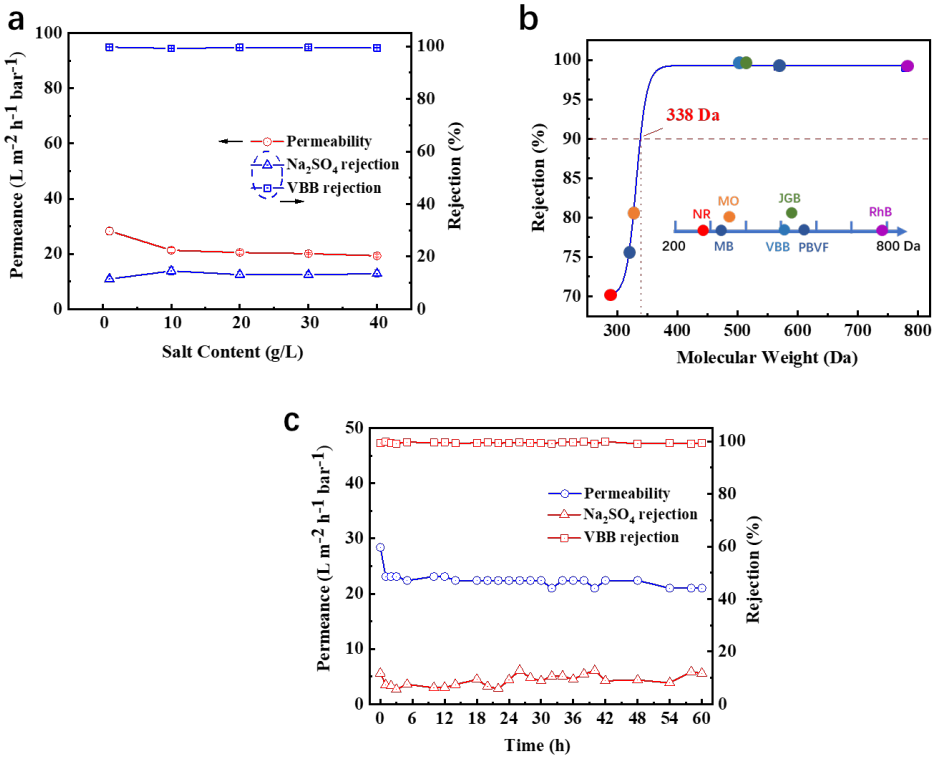

Figure 3.8 (a) effect of salt content on filtration performance of dye/salt mixture solution; (b) different dye solution (200 ppm) rejection of membranes; (c) long-term stability of the prepared membranes, 0.2 g/L dye + 1 g/L Na_2SO_4.

Table 3.1 Comparison of dye/salt separation membrane performance.

Membrane	Method	Permeance (LMH bar^{-1})	Types of dye	Dye rejection (%)	Types of salts	Salt Rejection (%)	Refs.
PAI/PEI	In-situ self-assembly	18.5	Methyl green	95.0	NaCl	11.3	[176]
Cationic nanoporous COF	Interfacial growth	24.0	Methylene blue	99.0	NaCl Na_2SO_4 $MgSO_4$	3.2 2.6 9.4	[207]
PAN-DHM	Chemical grafting	22.6	Victoria blue	>99	NaCl	<4.0	[208]
EGCg/PEI	Co-deposited	19.0	Congo Red	99.0	Na_2SO_4	4.1	[209]
EIP	IP	20.2	Congo red	99.6	NaCl	6.3	[210]
TFN-QCQDs	IP	23.8	Rhodamine B Methylene blue	98.9 98.4	$MgCl_2$	95.7	[211]
$P_{0.5}$-$T_{0.5}$-AMN	Co-Deposition/ Mannich reaction	30.7	Victoria blue B	99.5	Na_2SO_4	9.9	This work

3.2.5 Antifouling and antibacterial performance of the membranes

In applications, membrane fouling occurs due to hydrophobic interactions, electrostatic interaction, van der Waals forces, and hydrogen bonding. Especially for positively charged dyes, it is easy to adsorb on the surface of the membrane during the separation process, resulting in membrane fouling, so antifouling performance is an important parameter. To study the antifouling performance of new membranes, two positively charged dyes (VBB and PBVF, 200 ppm) were selected as fouling sources. Fig. 3.9a shows the permeance of $P_{0.5}$-$T_{0.5}$-AMN before and after dye filtration. The permeance of $P_{0.5}$-$T_{0.5}$-AMN membrane decreased slightly during dye filtration, mainly due to concentration polarization and membrane fouling. After rinsing with DI water, the permeance of membranes fouled by different dyes can be restored to various levels. The fouling resistance ratio (FRR) of the membrane is shown in Fig. 3.9b. The FRR values of the membrane for the two dye solutions were above 90%, indicating that the membrane has an excellent antifouling performance. Prepared based on the Mannich reaction, the hydrophilic selective layer of the dye/salt separation membrane allows water molecules to adsorb on the membrane surface and form a certain water molecule layer, thereby hindering the adsorption of dyes. Furthermore, the electrostatic repulsion between the positively charged dyes and the electropositive membrane surface can provide a higher rejection during the separation process and improve the

membrane's antifouling performance. The total fouling rate (R_t) of the dye/salt separation membrane is the sum of reversible fouling (R_r) and irreversible fouling (R_{ir}) as shown in Fig. 3.9b. The R_{ir} values for the two dyes were 6.7% (VBB) and 8.5% (PBVF), respectively. This indicates that the dye/salt separation membrane exhibits an excellent antifouling performance during the dye separation process.

Fig. 3.9c and 3.9d depict the antimicrobial properties of new membranes. In order to quantitatively analyze the bactericidal ability, the live cell technology was employed. The results showed that AMN, PEI, and THPC, and the product between them through the Mannich reaction all have a certain inactivation ability on *E. coli*. For AMN coating, the quaternary ammonium it provides can destroy the cell structure of bacteria and has a certain sterilization effect [190]. At the same time, THPC can break the stability of bacterial cell walls, thus inactivating *E. coli* [199, 202]. In some reports, the 'star product' pDA also demonstrated excellent antibacterial properties [212-214]. However, in this study, the better antibacterial performance of $P_{0.5}$-$T_{0.5}$-AMN than $P_{0.5}$-$T_{0.5}$-pDA obtained under the same conditions using pDA makes it a veritable antibacterial 'star product'. However, the antibacterial performance of the optimal membrane was only 13.1% compared with the control, but *E. coli* still remained, so the antibacterial performance of the membrane surface needs to be further improved.

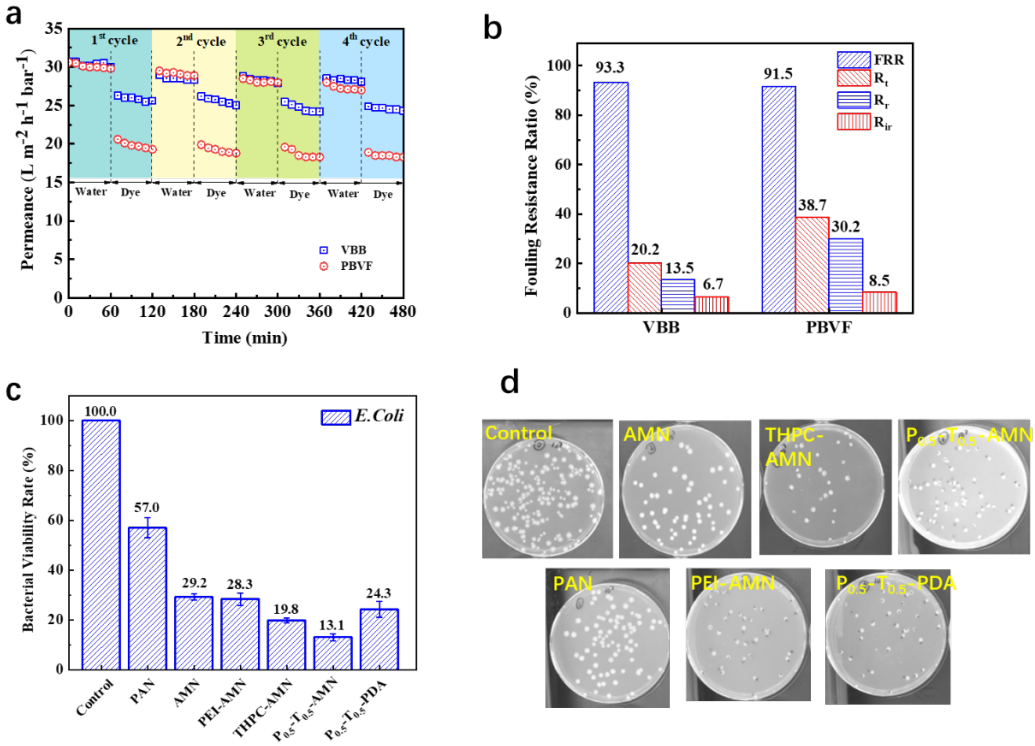

Figure 3.9 (a) antifouling performance of $P_{0.5}$-$T_{0.5}$-AMN (200 ppm VBB and PBVF); (b) fouling resistance ratio of $P_{0.5}$-$T_{0.5}$-AMN; (c) quantified antibacterial lability of membranes; (d) antibacterial effect of membranes.

3.3 Conclusion

In conclusion, a positively charged membrane for dye/salt separation was developed in a simple procedure based on the prebiotic chemistry-inspired AMN coating and the Mannich reaction between PEI and THPC. Based on fast mass transfer at 30.7 LMH bar^{-1} water permeance, the membrane can achieve up to 99.5% dye removal and less than 10% salt rejection, enabling resource recovery in textile wastewater treatment. After a 60 h long-term stability test, the membrane was found to have a long-term stable dye/salt separation performance and can achieve a good separation in dye/salt mixed solutions with high salt concentration. Moreover, the antifouling and antibacterial properties of the membrane have been confirmed, and the membrane has good antifouling and antibacterial properties. Today, when pDA-based and interfacial polymeric membranes are highly welcome in the treatment of textile wastewater, this 'crossover combination' strategy brings forth new ideas to the fabrication of membranes for dye/salt separation. Today, when pDA-based and interfacial polymeric membranes are highly welcome in the treatment of textile wastewater, this 'crossover combination' strategy brings forth new ideas to the fabrication of membranes for dye/salt separation.

Chapter 4: Robust loose nanofiltration membrane with fast solute transfer for dye/salt separation

Adapted from: "*Gao, Q., Bouwen, D., Yuan, S., Gui, X., Xing, Y., Zheng, J., Ling, H., Zhu, Q., Wang, Y., Depuydt, S., Li, J., Volodine, A., Jin, P., Van der Bruggen, B. with Jin, P. (corresp. author), Van der Bruggen, B. (corresp. author) (2023). Robust loose nanofiltration membrane with fast solute transfer for dye/salt separation. JOURNAL OF MEMBRANE SCIENCE, 674, Art.No. ARTN 121518. doi: 10.1016/j.memsci.2023.121518*"

4.1 Introduction

At present, there are about seven million colors that humans can see [215]. Before the invention of chemical dyes, people were more likely to find suitable animals, plants, minerals, or metals from nature to extract pigments [216]. For example, the traditional Chinese tie-dyeing process emerged very early (about 200 BC) and was mass-produced during the *Jin Dynasty* (266-420 AD) [217]. The dye used in the traditional Chinese tie-dye process is indigo from the leaves of the bluegrass plant [217, 218]. It was not until 1856 that "mauveine" was born, which marked the beginning of the synthetic dye industry [219]. With the advent of alizarin in 1868 and the application of artificial indigo technology in 1880, dyes gradually became an essential part of this colorful world [220, 221]. However, the continuous development of the dyeing industry has also brought a large amount of colored dye wastewater, which has produced many potential threats to public health [31, 63, 94]. Therefore, the treatment of colored dyeing wastewater has been extensively studied in recent years, such as developing materials with high adsorption capacity, developing advanced oxidation processes, and preparing photocatalytic materials [163, 222, 223]. The flourishing dyeing industry produces large volumes of colored dyeing wastewater where high concentrations of salt (such as NaCl and Na_2SO_4) are present as an adhesion promoter between the dyes and the fiber in the dyeing process [169, 203]. In this way, due to the suitable pore size of the nanofiltration membrane, not only can the printing and dyeing wastewater be treated efficiently, but also the salt in it can be recovered [224, 225]. On the other hand, the membrane needs to be driven by pressure in the actual application process, which is energy consuming. Therefore, a membrane with fast solute transport is required to have specific applicability in dealing with the energy crisis today [226]. In addition, the life of the membrane in the service cycle is one of the factors that must be considered, which means that the membrane should have a certain robustness in practical applications (e.g., pH range, long-term stability, anti-fouling, and antibacterial properties) [227]. Therefore, in dyeing

wastewater treatment, membranes with fast solute transport and good robustness have application advantages.

Various membrane preparation methods are considered to realize resource recovery during dyeing wastewater treatment, such as surface coating, adding functional layers, nanomaterial loading, co-deposition [94, 228-230]. Among these methods, the interfacial polymerization (IP) method is a widely used preparation method for nanofiltration membranes [231]. However, traditional IP enables membranes with generally small pore sizes and a compact internal structure, which limits salt transport due to the high reactivity between amines and acid chlorides (e.g., trimesoyl chloride (TMC)/piperazine (PIP) and TMC/polyethyleneimine (PEI))[94]. For this issue, supramolecules with cavity structures are a potential solution: these can act as channels for fast solute transport on the membrane surface. β-Cyclodextrin, a compound with a cavity, has been reported many times in the synthesis of membranes [63, 232]. Its cavity (6.0-7.8 Å) can act as a "host", and other compounds can act as "guests" through host-guest interaction [233]. One option for the "guest" is mussel-inspired polydopamine (pDA). This is because pDA is not only a bio-adhesive, but also its amine, catechol and imine groups can "assemble" with β-cyclodextrin through non-covalent bonds [63, 234, 235]. Therefore, using the robust biomimetic glue pDA as a guest, a layer of supramolecular solute transport channels can firmly adhere to some support substrate (e.g., PES) through the host-guest interaction between pDA and β-cyclodextrin. This is crucial for the membrane's ability to cope with harsh environments during practical applications. For this challenge, researchers have started from various aspects in recent years, such as improving the hydrophilic and hydrophobic properties of the surface of the membrane [236], using photocatalysts to manufacture self-cleaning membranes [63], modulation of membrane surface charge [237], and using denser cross-linking agents to form selective layers [238]. Among them, using a suitable cross-linking agent to make the selective layer on the surface of the membrane denser is a way to fundamentally improve the robustness of the membrane [239, 240]. However, as for supramolecules, chemical cross-linking usually occurs in a homogeneous medium; this requires that supramolecules and monomers can be dissolved in the same solvent [241]. For the β-cyclodextrin/pDA system, in previous study, the conventional cross-linker TMC needs to be dissolved in the oil phase, so crosslinking can only take place between pDA and TMC [63]. Glutaraldehyde (GA) is a water-soluble cross-linking agent and is widely used in the cross-linking of membranes [242]. In addition, glutaraldehyde can react

with alcohol groups and amino groups for cross-linking. These hydroxyl groups and amino groups widely exist in the host-guest structure of β-cyclodextrin and pDA [241]. Therefore, water-soluble glutaraldehyde provides a possibility for cross-linking. At the same time, the membrane structure formed after the chemical cross-linking has a certain firmness [235].

Herein, the host-guest coordination of pDA/β-cyclodextrin was exploited, with the addition of glutaraldehyde to chemical cross-linking based on fast solute transport for fast dye/salt separation and resource recovery. The purpose of this chapter is not only to propose a synthetic strategy for rapid dye/salt separation membranes, but also to demonstrate that supramolecular β-cyclodextrin and pDA cross-linked by glutaraldehyde can form a structure of transport channels. Furthermore, the robustness of the membrane is also investigated in terms of acid-base stability, anti-fouling properties, bacterial resistance, and long-term stability, which provides theoretical guidance and technical support for its practical application.

4.2 Results and discussion

4.2.1 Chemical composition characterization of the membrane surface

Fig. 4.1a shows the Fourier transform infrared (FT-IR) spectra of membranes modified under different conditions. When comparing the used sample with the unmodified PES membrane, a peak appeared around ~3282 cm^{-1}. This is due to the presence of -OH in β-cyclodextrin and -NH in pDA [243]. PBG-1 has a more pronounced -OH/-NH (~3282 cm^{-1}) peak intensity than the optimal membrane PBG-3 because the -OH or -NH in PBG-3 is bound to glutaraldehyde. In addition, PBG-5 without pDA, mainly because of the appearance of -OH in β-cyclodextrin, there is no -NH peak of pDA. In PBG-10 without glutaraldehyde, the same situation occurs due to the absence of a cross-linker. Therefore, it could be demonstrated that glutaraldehyde was cross-linked with pDA and β-cyclodextrin structures. The cross-linking reaction between pDA/β-cyclodextrin and glutaraldehyde occurred in the amino group and hydroxyl group of pDA and the hydroxyl group of β-cyclodextrin. The related structural schematic diagram is shown in Fig. 4.2. The cross-linking reaction can well cross-link pDA and β-cyclodextrin molecules without destroying the cavity in β-cyclodextrin. In addition, peaks at ~1578 and ~1486 cm^{-1}, which are attributed to the aromatic ring of pDA. After pDA was attached to β-cyclodextrin, the peak

at ~3282 cm^{-1} changed, which was the result of residual hydroxyl groups in β-cyclodextrin. The spectrum occurring at ~1029 cm^{-1} for the pDA/β-cyclodextrin refers to the –C–O–C– stretching vibration of β-cyclodextrin. At the same time, due to the lack of cross-linking, the complete β-cyclodextrin /pDA was exposed, and a unique peak appeared, which confirmed that β-cyclodextrin was cross-linked with pDA on the membrane surface through host-guest interaction[195]. At ~1578-1486 cm^{-1} and ~872-718 cm^{-1}, it is the characteristic peak of a benzene ring, which is obviously different due to the different selective layer formed compared with PES and the interaction with glutaraldehyde [244]. The number of aromatics on the surface is reduced due to the coupling, so the characteristic peaks of the benzene ring appear differently. Furthermore, at ~1150-1010cm^{-1}, the characteristic peak of C-O appeared [245]. This is induced by PES neutralizing the aldehyde groups in glutaraldehyde. However, a difference appeared in PBG-10 without glutaraldehyde at ~1010. This is because the structure of pDA/β-cyclodextrin through host-guest combination appeared on the surface of the membrane, which changed the C-O on the surface [63].

Fig. 4.1b shows the XPS broad-scan spectra of membranes under different conditions where the presence of C, N, O, and Cu elements could be observed. It is worth mentioning that the Tris-$CuSO_4$ buffer provided Cu element, while C, N, and O elements were from the selection layer [235]. The XPS spectrum for the core-level XPS spectra of the N element is shown in Fig. 4.1c. The presence of the N element was not found in the PBG-5 without pDA. The N element in the rest of the membrane is provided by pDA, which indicates that the pDA-containing structure is present on the selective layer of the membrane [63, 235]. The core-level XPS spectra of element C can also prove that chemical cross-linking has occurred. In Fig. 4.1d and e, compared with PBG-10 without glutaraldehyde cross-linking, the cross-linked PBG-3 has one more C=O peak, which the aldehyde group provides in glutaraldehyde.

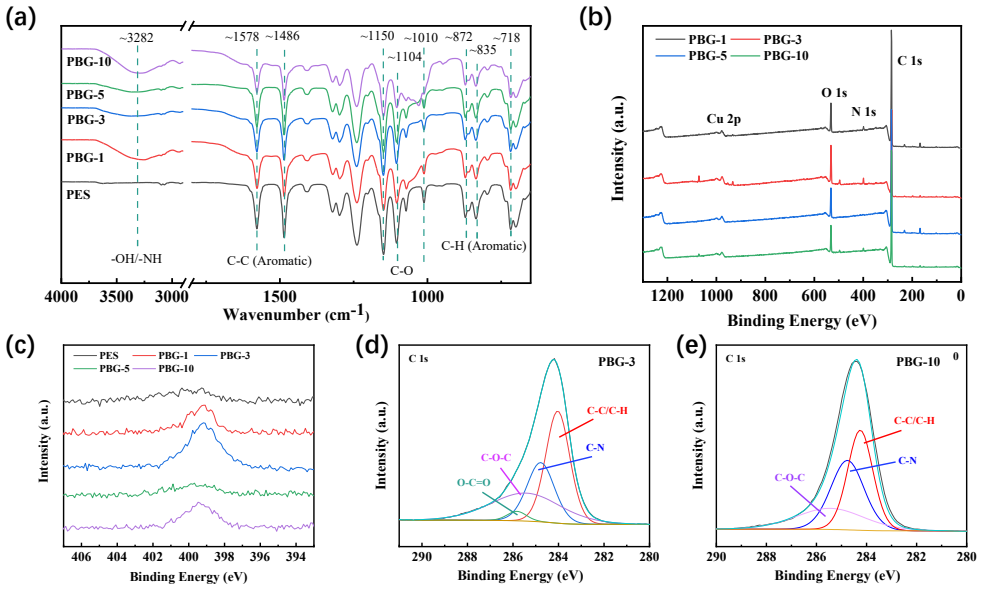

Figure 4.1 (a) FT-IR spectra of PES, PBG-1, PBG-3, PBG-5, and PBG-10; (b) XPS wide-scan spectra of PES, PBG-1, PBG-3, PBG-5, and PBG-10; (c) N1s core-level XPS spectra of of PES, PBG-1, PBG-3, PBG-5, and PBG-10; (d) C1s core-level XPS spectra of the PBG-3 membrane; (e) C1s core-level XPS spectra of the PBG-10 membrane.

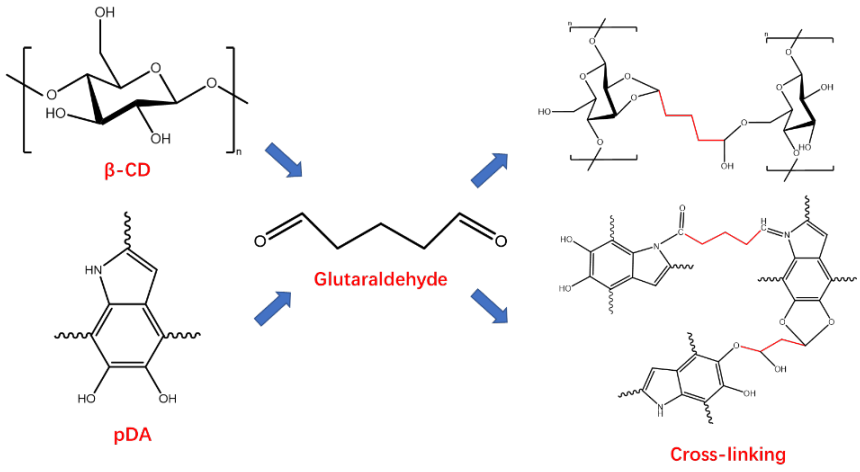

Figure 4.2 Structural diagram of cross-linking reaction of pDA/β-cyclodextrin with glutaraldehyde.

4.2.2 Morphology of the membrane

Fig. 4.3 and Fig. 4.4 show the morphology of the membrane. In Fig. 4.3a, since there is no β-cyclodextrin in PBG-1, only pDA and glutaraldehyde are cross-linked, so fewer cross-linked structures appear on the surface. Similarly, in Fig. 4.3c, PBG-5 without pDA, no large cross-linked structure was found on the surface, but from the roughness point of view, the membrane surface became rough because of cross-linked β-cyclodextrin and glutaraldehyde (Fig. 4.4) [246]. On PBG-3 and PBG-10 (Fig. 4.3b and Fig. 4.4b) where host-guest interaction occurs, the structure bound by host-guest interaction could

be observed. Moreover, compared with PBG-10, PBG-3 is cross-linked with glutaraldehyde, so its roughness is significantly smaller than that of PBG-10. At the same time, from the image of PBG-10 (Fig. 4.3f and Fig. 4.4i), larger particles with uneven distribution can also be seen, which is the structure of the pDA/β-cyclodextrin combination. Interestingly, in Fig. 4.3 and Fig. 4.4, when comparing the roughness, the roughness of PBG-3 was not much different from that of the PES-based membrane, which is due to the higher degree of cross-linking of glutaraldehyde with the pDA/β-cyclodextrin structure, resulting in a relatively smooth membrane surface [247]. When observing the cross-section (Fig. 4.3 and Fig. 4.4), it could be seen that after cross-linking with glutaraldehyde, the formed selection layer is relatively uniform. In Fig. 4.4e, PBG-10 without cross-linking reaction, noticeable particles can be seen. Moreover, when comparing PBG-1 and PBG-3 (Fig. 4.3d and e), it is found that the membrane thickness is higher. However, the change is insignificant, showing that after the introduction of β-cyclodextrin supramolecules, the structure of pDA/β-cyclodextrin can stably exist on the membrane [63, 94].

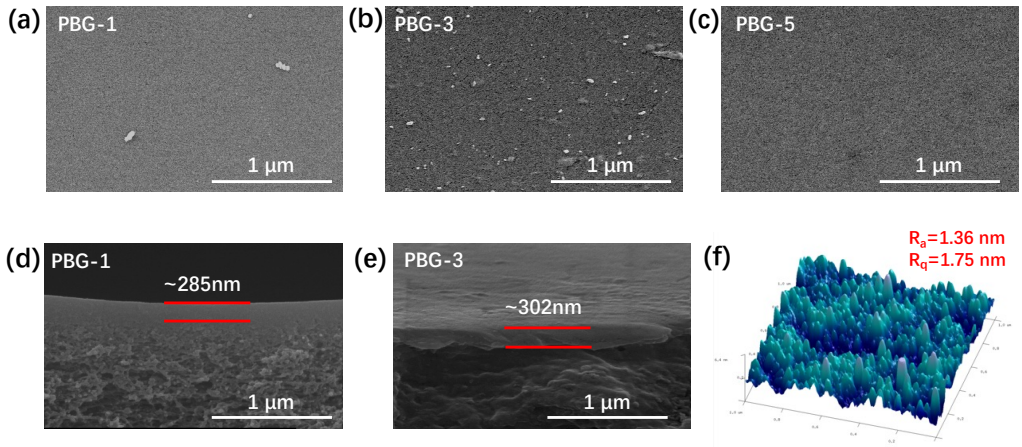

Figure 4.3 The surface morphology of NF membrane of (a) PBG-1, (b) PBG-3, (c) PBG-5; Cross-sectional morphology of (d) PBG-1, (e) PBG-3; (f) The surface roughness of PBG-3.

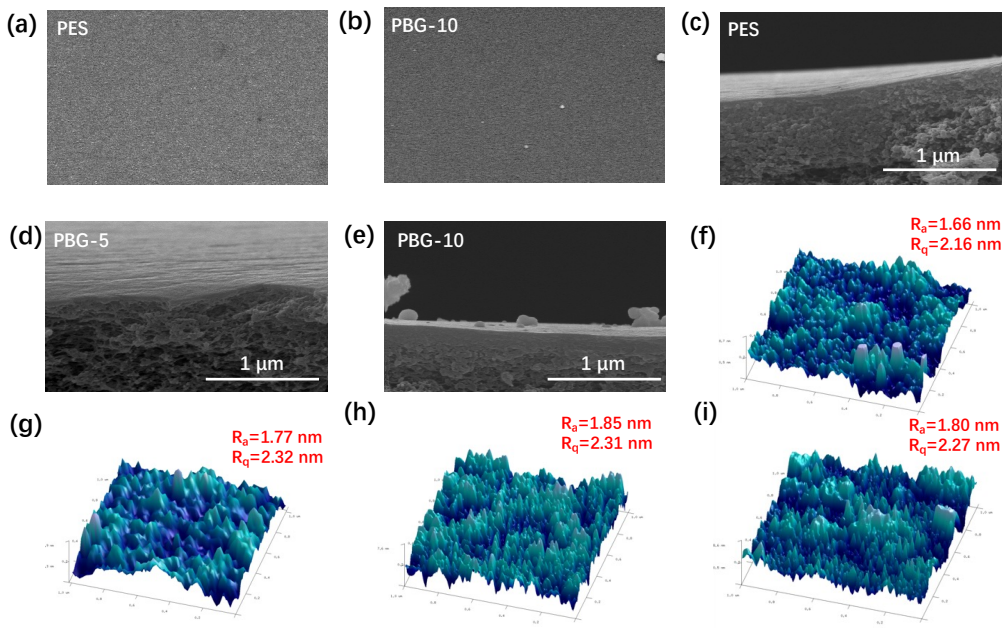

Figure 4.4 The surface morphology of (a) PES, (b) PBG-10; cross-sectional morphology of (c) PES, (d) PBG-5, (e) PBG-10; the surface roughness of (f) PES, (g) PBG-1, (h) PBG-5, (i) PBG-10.

4.2.3 Hydrophilicity and surface potential characteristics of the membrane

According to the Donnan effect, the surface zeta potential of a membrane is an important factor determining its separation properties [248]. Fig. 4.5a shows the surface zeta potential of the PES support substrate and the membrane. The results show that both the optimal membrane and other NF membranes showed a lower zeta potential. The PES support substrate exhibits a negative potential over a wide pH range because of the presence of S=O bonds on its surface [249]. PBG-1 does not contain β-cyclodextrin, but after pDA is cross-linked with glutaraldehyde, due to the presence of amino groups on the surface, it also shows a negative potential in a wider pH range [250]. Similarly, in PBG-5, since only β-cyclodextrin and glutaraldehyde undergo a cross-linking reaction, the hydroxyl groups on the surface of β-cyclodextrin also show negative charge after cross-linking [251]. The pDA/β-cyclodextrin binding structure of PBG-3 through the host-guest interaction shows a lower potential because it has a large number of amino groups and hydroxyl groups for cross-linking. Moreover, the slight gap can be seen, and its potential is roughly located between PBG-1 and PBG-5, because the newly formed structure of pDA/β-cyclodextrin can be cross-linked with glutaraldehyde. Furthermore, compared with PBG-10, the potential of PBG-3 after cross-linking with glutaraldehyde was further decreased due to the introduction of aldehyde groups in glutaraldehyde [252]. Because the membrane has a lower zeta potential in a wide pH range, it can better reject negatively charged particles from water, according to the Donnan effect.

The water contact angle was used to test the hydrophilicity and hydrophobicity of the membrane. Fig. 4.5b shows the water contact angle of the PES support substrate and NF membrane. The water contact angle of the PES support substrate is 60.1°. It can be seen that the water contact angle of PBG-1 without β-cyclodextrin is reduced to 19.9° because the amino groups in pDA can form hydrogen bonds with water molecules [253]. Similarly, in PBG-5, where only β-cyclodextrin participates in the cross-linking reaction, due to the supramolecular β-cyclodextrin on the surface, the outer side of the cavity shows a higher hydrophobicity, so a larger water contact angle is obtained, which is 68.9° [63, 254]. PBG-3 and PBG-10 have a pDA/β-cyclodextrin structure, and due to the cross-linking of PBG-3 with glutaraldehyde with aldehyde groups on the surface, a larger water contact angle (30.9°) representing a hydrophobicity enhancement was obtained, which was greater than that of PBG-10 without crosslinking. An appropriate hydrophobicity can induce the formation of a relatively fast mass transfer hydration layer, which is beneficial to the transport of solutes[195].

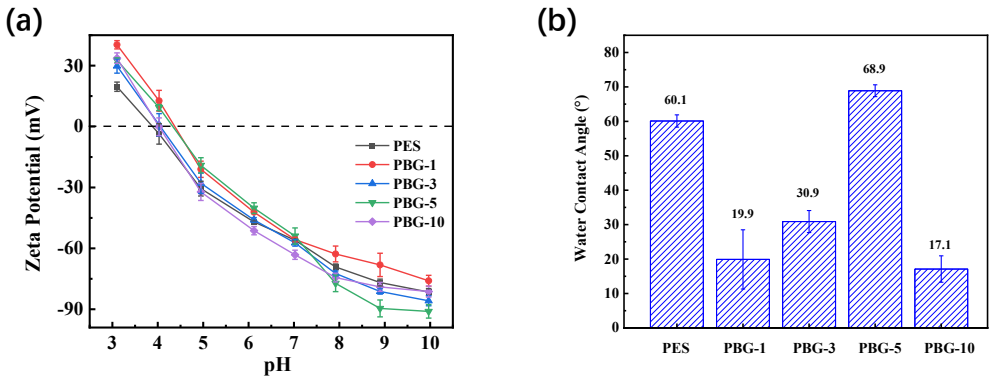

Figure 4.5 (a) Water contact angle of the membrane; (b) Zeta potential measurements for the membrane.

4.2.4 Membrane filtration performance

Fig. 4.6 and Fig. 4.7 show the PES support substrate and the membrane filtration performance. The permeance of the membrane is shown in Fig. 4.6a and Fig. 4.7, and the PES substrate has a greater permeance of 415.2 L m^{-2} h^{-1} bar^{-1}due to its greater porosity. The supramolecular β-cyclodextrin /pDA combined structure played an important role in NF membranes. PBG-1 without β-cyclodextrin had a smaller permeance of only 25.6 L m^{-2} h^{-1} bar^{-1}. This is because pDA has good adhesion, and its amino groups can be cross-linked with glutaraldehyde [235, 255]. However, PBG-5 with only β-cyclodextrin had a larger permeance of more than 200 L m^{-2} h^{-1} bar^{-1}. With the presence of supramolecular β-cyclodextrin, after cross-linking with glutaraldehyde, not only the cavities in the β-cyclodextrin molecule

but also gaps exist in the cross-linking between macromolecules, so a higher permeance was obtained [85]. After host-guest interaction, PBG-3 with β-cyclodextrin /pDA structure had a moderate permeance of 62.0 L m^{-2} h^{-1} bar^{-1}. However, compared with PBG-10 without glutaraldehyde cross-linking, a higher permeance was obtained because the membrane surface was looser, which might be a manifestation of the instability of the selective layer on the membrane surface [63]. For the cavities produced after cross-linking with glutaraldehyde, PBG-1 is a membrane in which only pDA and glutaraldehyde are cross-linked. Since pDA and glutaraldehyde can be well cross-linked, a denser selective layer was obtained with lower permeance and smaller cavities than in PBG-5 where only β-cyclodextrin was present. However, with the introduction of β-cyclodextrin, part of pDA performs host-guest interaction with β-cyclodextrin. Moreover, the cross-linking of β-cyclodextrin and glutaraldehyde can form larger cavities, while the cross-linking degree of pDA and glutaraldehyde can form smaller cavities. In this way, when the concentration of pDA and β-cyclodextrin was optimized, the cavity formed by the secondary cross-linking can have a synergistic effect with the cavity in β-cyclodextrin, in order to obtain a better separation performance. The results of the optimization process of the membrane are shown in Fig. 4.7. For the added amount of β-cyclodextrin (Fig. 4.7a), as the content of β-cyclodextrin increased, the permeance of the membrane increased, which was caused by the increased number of cavities in the β-cyclodextrin supramolecule [195]. However, the opposite is true for the amount of pDA added (Fig. 4.7b) because the amino groups in pDA could be cross-linked with glutaraldehyde to form a denser selective layer. As the content of pDA increases, the permeance of the membrane decreases [256]. The co-deposition time (Fig. 4.7c) had little effect on the permeance of the membrane and had a slight change trend; 60 min was found to be the optimal value. For the cross-linking time, the longer the cross-linking time (Fig. 4.7d), the denser the selective layer of the membrane, but when the time is longer than 6 min, there is little change, so the best cross-linking time is 6 min. For the cross-linker glutaraldehyde (Fig. 4.7e), more cross-linker makes the selective layer of the membrane denser, so the permeance of the membrane decreases with the increase of glutaraldehyde.

From the perspective of sustainability in textile wastewater treatment, salt recovery is an important issue. Fig. 4.6b shows the filtration performance of the PES support substrate and the NF membrane for Na_2SO_4 and NaCl (1 g/L), two common salts in textile wastewater (Fig. 4.6b). Since the hydration radius of Na_2SO_4 is larger than that of NaCl, the permeance of Na_2SO_4 during membrane filtration is lower than

that of NaCl. In addition, according to the Donnan effect, for PES support substrates and NF membranes with negative charges on the surface, the negatively charged Na_2SO_4 in an aqueous solution is not easy to transport across the membrane. Hence, the permeance was low, and the rejection was high. Like the water permeance of the membrane, PBG-1 has a low permeance because the amino group of pDA on the surface can cross-link with glutaraldehyde to form a denser selective layer (23.8 L m^{-2} h^{-1} bar^{-1} for Na_2SO_4 and 24.3 L m^{-2} h^{-1} bar^{-1} for NaCl). However, PBG-5 with only β-cyclodextrin has a higher permeance of Na_2SO_4 (224.1 L m^{-2} h^{-1} bar^{-1}) and NaCl (231.3 L m^{-2} h^{-1} bar^{-1}) because of its large number of molecular transport channels [63]. For PBG-3 and PBG-10 with β-cyclodextrin/pDA structure, PBG-3 cross-linked with glutaraldehyde has a lower permeance because it has a denser selective layer. For the rejection of the two salts, both the PES substrate and the NF membrane have a low rejection (~15%), which is conducive to the recovery of salt from textile wastewater [257]. It is worth mentioning that in PBG-3, although there is a relatively dense selective layer, due to the molecular transport channels in β-cyclodextrin, the salt with a hydration radius smaller than the cavity of β-cyclodextrin is rapidly transported across the membrane.

DR23 and RB5 (200 ppm) were selected as compounds simulating pollutants in textile wastewater to evaluate the filtration performance of membranes for dyes (Fig. 4.6c). Because both dyes contain sulfonic acid groups, and the dye ions are negatively charged after ionization in aqueous solution. For permeance, the overall trend is the same as for salt permeance, with a slight decrease in permeance because the size of the dye in the aqueous solution is larger than that of the salt [258]. The optimized PBG-3 shows better filtering characteristics. Not only does it have high permeance, but it also shows near-complete dye rejection. This is because the pDA/β-cyclodextrin structure of the membrane surface selection layer has a denser structure [259]. Moreover, the cavity of the β-cyclodextrin supramolecular structure is a transport channel between the size of the dye and the salt (Fig. 4.6d). Therefore, for PBG-3, salt permeates quickly, while retaining a good rejection of the dye. The β-cyclodextrin /pDA-based supramolecular interfacial polymeric structures capable of rapid solute transport have been identified as having certain advantages in similar studies over at least the past five years (Table 4.1).

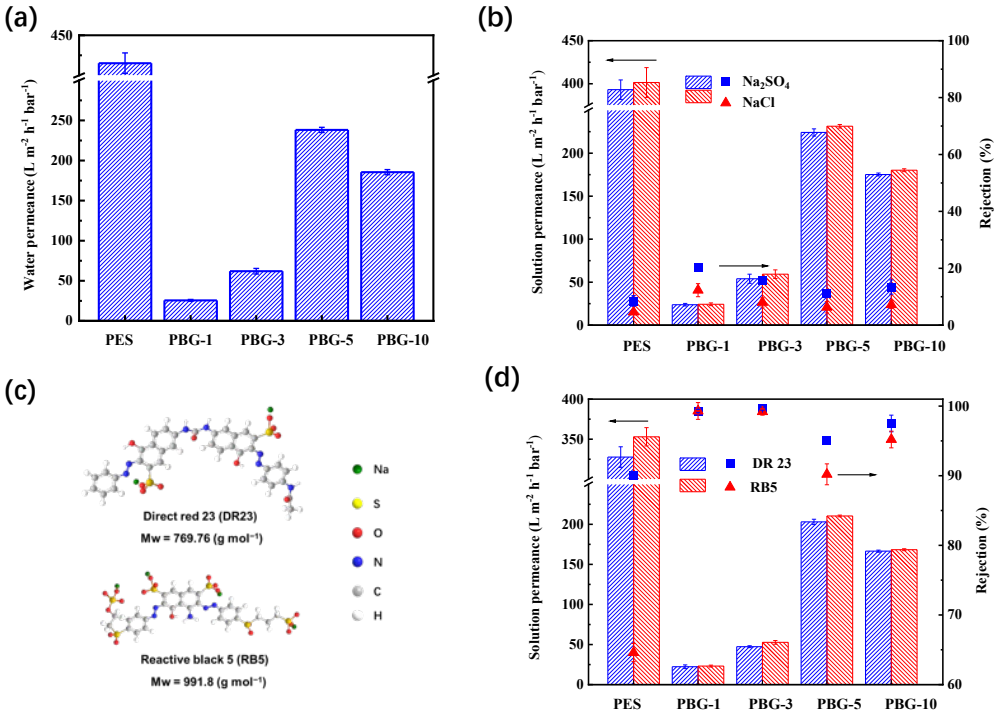

Figure 4.6 (a) DI water permeance of PES support substrate and NF membranes; (b) Salt solution permeance and rejection of PES support substrate and NF membranes; (c) Molecular structures and molecular weights of DR23 and RB5; (d) Dye solution permeance and rejection of PES support substrate and NF membranes.

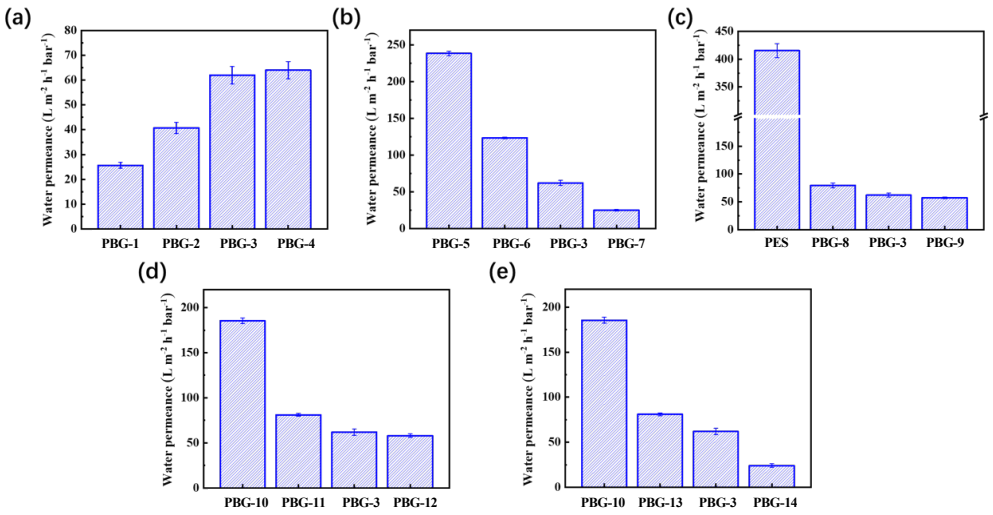

Figure 4.7 DI water permeance of PES support substrate and NF membranes, (a) with different concentration of β-cyclodextrin; (b) with different concentration of pDA; (c) with different concentration of co-deposition time; (d) with different concentration of cross-linking time; (e) with different concentration of concentration.

Table 4.1 Comparison of dye/salt filtration performance.

Membrane	Method	Permeability (LMH bar^{-1})	Types of dye	Dye rejection (%)	Types of salts	Salt Rejection (%)	Refs.
Sugar-based	IP	33.7	Direct red 23 Direct red 80 Reactive black 5 Reactive orange 16 Methyl orange	99.6 99.8 98.9 97.4 91.3	Na_2SO_4 $MgSO_4$ NaCl $MgCl_2$	95.0[a] 40.0[a] 60.0[a] 18.0[a]	[87]
Erythritol-based	IP	53.23	Congo red Direct red 23 Reactive blue 2	99.6 95.2 99.6	Na_2SO_4 NaCl	11.0 5.6	[203]
POP/TMC	IP	31.28	Reactive black 5	99.1	RB5/Na_2SO_4	15.4	[260]
Tannic acid/PEI	Co-deposition	41.5	Congo red	99.5	Na_2SO_4 NaCl	6.00 8.00	[261]
Catechol/PEI-$CuSO_4/H_2O_2$	Co-deposition	24.5	Congo red Reactive black 5 Methyl blue	99.8 99.7 99.3	Na_2SO_4 NaCl $MgCl_2$	12.5 2.0 0.6	[262]
Fe^{3+}-PEI@HPAN	In-situ self-assembly	6.0	Congo red Methyl blue Acid fuchsin Crystal violet	99.5 99.9 99.0 92.9	Na_2SO_4 NaCl $MgCl_2$ $MgSO_4$	5.9 7.5 30.5 20.6	[263]
PBG-3	Chemical cross-linking	62.0	Direct red 23 Reactive black 5	99.6 99.2	Na_2SO_4 NaCl	20.3 12.3	This work

([a]Estimated from published figures.)

4.2.5 Stability and self-cleaning properties of the membrane

The robustness of the membrane is an important factor that must be investigated in the process of bringing the membrane from the laboratory to industrial applications [264]. The stability and self-cleaning performance of the membrane are critical points that directly affect the service life of the membrane [265]. Fig. 4.8a shows the filtration performance of PBG-3 for different concentrations of salt (NaCl, 1-50 g/L) and dye (DR23, 200 ppm). It can be seen from the figure that for a high concentration of salt, PBG-3 has a stable separation of dye/salt. However, in the range of 1-20 g/L, the permeability of the membrane decreased slightly. This is due to the coupling of DR23 molecules with NaCl in an aqueous solution. Moreover, during the separation process, high-concentration salt is prone to concentration polarization [203]. As the concentration of salt increases, the separation process is affected [63, 94, 203].

However, in the high salt concentration range (>50 g/L), the separation process of the membrane is no longer affected by the increase in salt concentration.

During the actual application of the membrane, it is inevitable that different degrees of membrane fouling occurs in the hydration layer of the membrane due to intermolecular forces and electrostatic interactions [259]. Therefore, the self-cleaning performance of the membrane must be considered in the actual application process [266]. The self-cleaning performance of PBG-3 is shown in Fig. 4.8b. During the process of filtering the dye, the permeance of the membrane decreased slightly, mainly due to the fouling and concentration polarization on the surface of the membrane [267]. After rinsing with DI water, the permeance of the membrane can be recovered effectively. Specifically, the fouling resistance ratio (FRR) of the membrane is shown in Fig. 4.8c. Due to the dense ground selective layer on the surface of the PBG-3 membrane, the FRR values for both DR23 and RB5 dyes can reach more than 90%. This can fully explain why the PBG-3 membrane has good self-cleaning properties for the two dyes. In addition, the total fouling rate (R_t) of PBG-3 is in a lower range of reversible fouling (R_r) and irreversible fouling (R_{ir}). The long-term stability of the membrane was investigated using DR23 (200 ppm) and NaCl (1 g/L). Fig. 4.8d shows the long-term stability of the membrane for 60 h. In the first 6 hours of filtration, the permeance of the PBG-3 membrane decreased slightly because the surface of the membrane was fouled and some membrane pores were blocked [268]. Over time, the permeance of the membrane gradually stabilized and remained stable for a long time. Regarding rejection, PBG-3 membranes had nearly 100% rejection of DR23 and remained stable for 60 h. The NaCl rejection of the PBG-3 membrane was always lower than 20% during the long-term stable operation of 60 hours, which can ensure the uninterrupted resource recovery of the membrane during long-term operation.

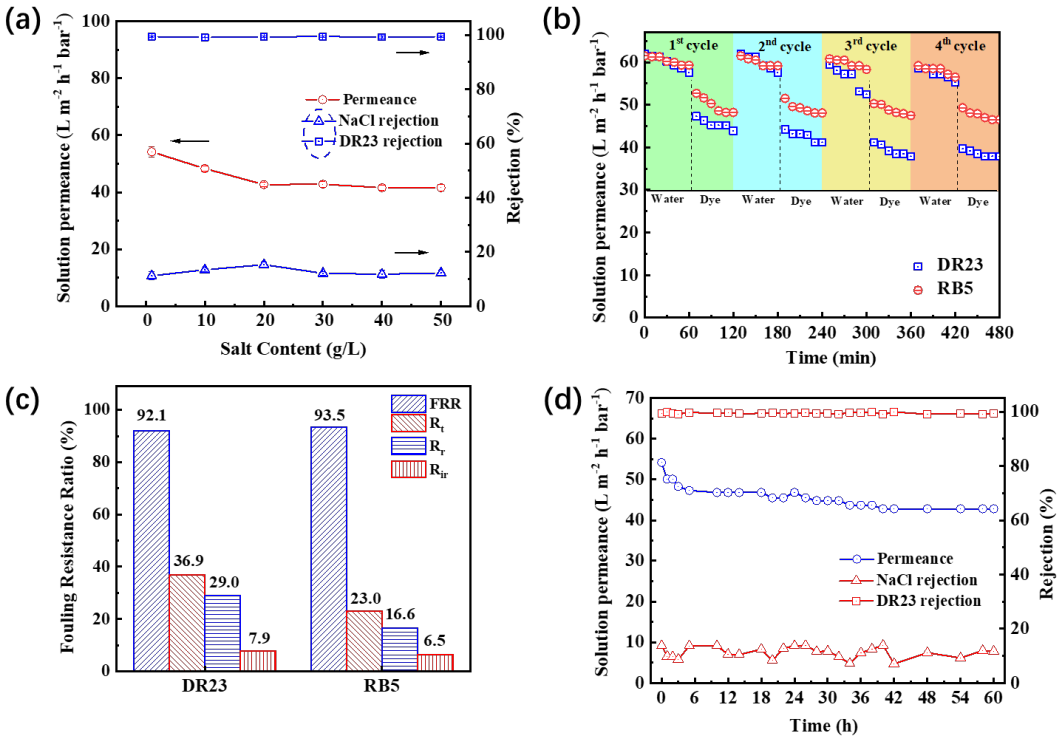

Figure 4.8 (a) Influence of salt content in dye/salt mixed solution on filtration performance; (b) Self-cleaning performance of PBG-3 (200 ppm DR23); (c) Fouling resistance ratio of PBG-3; (d) Long-term stability of the prepared membranes, 200 ppm DR23 + 1 g/L Na_2SO_4.

4.2.6 pH stability and antibacterial properties of the membrane

In the actual application process of the membrane, pH stability of acid and alkali resistance are essential [269]. Fig. 4.9a shows the stability experiments of the PBG-3 membrane after acid and alkali treatment. The permeance increased after acid and alkaline treatment, and the dye rejection decreased slightly. In addition, it can be seen that acidic treatment gives less change in permeance and rejection than alkaline treatment. This is because under alkaline conditions, a partial structure undergoes a hydrolysis reaction, resulting in a change in the structure of the membrane surface. However, since the selective layer on the surface of the membrane is relatively dense and the basic framework has a good robustness, the basic structure of PBG-3 is not affected. This allows to maintain a fast solute transport, good dye rejection and fast passage of salt [270]. The antibacterial properties of the membrane are important in practical applications [271]. PES, PBG-3, and PBG-10 were selected to explore the resistance of the membrane to *E. coli* and *B. subtilis*, and the results are shown in Fig. 4.9b and c. Compared with the PES support substrate, PBG-3 and PBG-10 with pDA/β-cyclodextrin results have good antibacterial properties. This is because the antibacterial properties of pDA, a mussel-inspired

biomimetic material, have been demonstrated many times [63, 235]. Moreover, after cross-linking with glutaraldehyde, PBG-3 showed strong antibacterial properties, and compared with the control group, the number of colony stocks was only 22.1% for *E. coli* and 14.0% for *B. subtilis* of the original. This is because after glutaraldehyde is cross-linked, a dense selective layer is formed on the surface of the membrane, and the hydrophobicity of the membrane increases (Fig. 4.9b), making it difficult for the colony to contact the surface of the membrane, thereby improving the antibacterial performance of the membrane [272]. However, although the number of *E. coli* and *B. subtilis* colonies in the optimal membrane decreased to a certain extent compared with the control, there were still residual colonies. Therefore, how to further improve the antibacterial properties of the membrane is the next research direction. Fig. 4.9c shows the colonies in the actual Petri dish, and the distribution of the colony can be seen more intuitively from the figure. Moreover, the SEM image of PBG-3 membrane after a 60-h test is shown in Fig. 4.9d. The adsorption of some solute molecules after aggregation can be seen on the surface of the membrane. This is because dye molecules can be adsorbed on the membrane surface through intermolecular interactions, thereby affecting the separation performance of the membrane. However, it can be seen from the figure that this adsorption is slight and there is still a large uncontaminated area on the membrane surface. Combined with the robust performance test of the membrane, when the membrane reaches the adsorption equilibrium when the permeability is constant, the maximum contaminated area of the membrane is still much smaller than the uncontaminated area. Therefore, the robust performance of the membrane is confirmed.

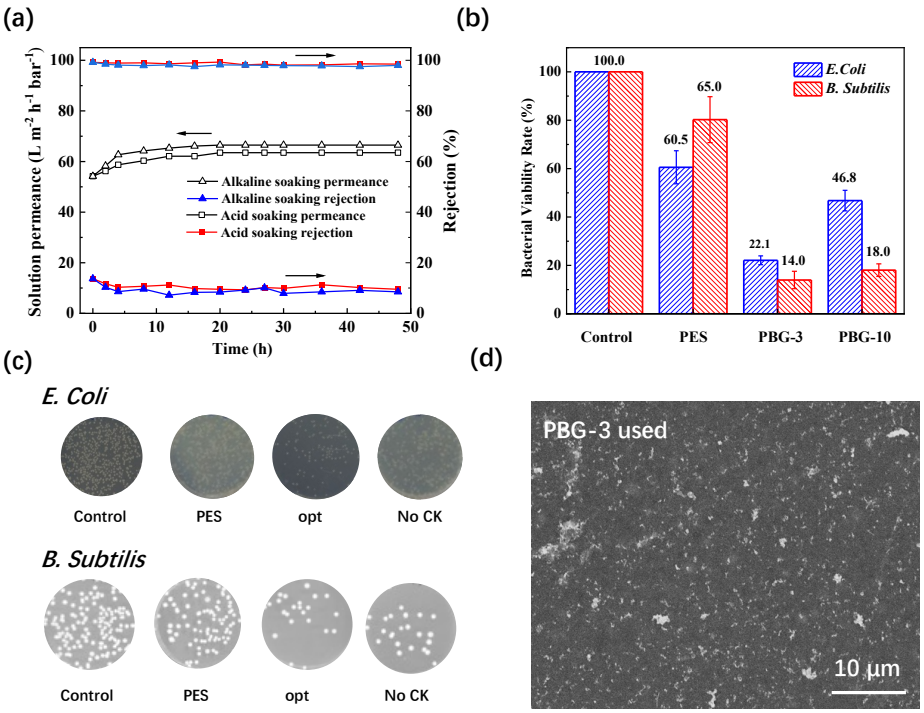

Figure 4.9 (a) stability experiments of the PBG-3 membrane after acid and alkali soaking; (b) quantified antibacterial lability of PBG-3 membrane; (c) antibacterial effect of PBG-3 membrane; (d) PBG-3 after filtration test 60h.

4.3 Conclusion

In conclusion, a robust and rapid solute transport membrane was developed via chemical cross-linking utilizing pDA/β-cyclodextrin combined with host-guest interactions. It was found that dyes/salts in textile wastewater be separated quickly, and the developed membranes have a good robustness to adapt to different applications. The membrane allows to recycle resources in the treatment of textile wastewater, and can also operate stably for a long time in a broad pH range. These membranes also have an excellent self-cleaning and antibacterial performance. The membrane can use specific molecular transport channels to maximize the rapid transport of solutes under the same energy input and recycle the available resources in textile wastewater. In this way, it has certain advantages regarding sustainability and energy saving, and the membrane has an unparalleled robustness. It can be used in various applications, providing the possibility for further large-scale applications.

Chapter 5: Robust self-cleaning membrane based on host-guest interaction combined with photocatalyst loading

Adapted from: *"Gao, Q., Weng, B., Jin, P., Yuan, S., Gui, X., Zheng, J., Xu, D., Wang, Y., Volodine, A., Sun, L., Van der Bruggen, B. with Jin, P. (corresp. author), Van der Bruggen, B. (corresp. author) (2022). Rapid solute transfer photocatalytic membrane: The combination of host-guest interaction and photocatalyst load. CHEMICAL ENGINEERING JOURNAL, 446, Art.No. ARTN 137316. doi: 10.1016/j.cej.2022.137316"*

5.1 Introduction

In the fifteenth century, the *Van Eyck* brothers from *Ghent, Belgium*, started painting with oil-melted dyes (e.g., *the Lamb of God, 1425-1432*) and revealed the secret of perpetuation of people's bright colors last forever [273]. Coincidentally, in 1856, *Sir William Henry Perkin* invented the first synthetic dye "Mauveine". Today, dyes have been widely used in various industrial sectors such as textiles, plastics, and paper [274]. A large amount of colored wastewater of dyes damages the environment and threatens human health[275]. At the same time, in the dyeing process, some inorganic salts are essential to promote absorption of by fabric fibers. For example, in the dyeing process of the textile industry, NaCl (~6.0 wt%) and Na_2SO_4 (~5.6 wt%) are usually added in the dyeing process [276]. Therefore, from the viewpoint of sustainability, the treatment of dye wastewater should shift from removing dyes to separating dyes and salts [277, 278]. Compared with conventional separation technologies [279-281], membrane separation has an excellent efficiency, which renders it a sought-after technology for dye/salt separation in recent years [166, 167]. Unfortunately, due to the limitation of modification methods, the current membranes suffer from some deficiencies, mainly that the synthesized membranes are dense, which leads to a low permeability during dye/separation. Therefore, traditional surface modification methods (interfacial polymerization [282], coating [179] and surface finishing [283]) alone are not sufficient to achieve dye/salt separation.

The inherent cavity structure of supramolecules can be a candidate for the rapid construction of separation membranes. Among the numerous supramolecules, β-cyclodextrin has been extensively reported many times to synthesize separation membranes [232]. The cavity (6.0-7.8 Å) of β-cyclodextrin can be used as the "host" to encapsulate various size-matched compounds through the host-guest interaction [232]. Inspired by the phenomenon of mussels adhering to reefs, many studies have explored

mussel-inspired polydopamine (pDA) as a “guest” and surface-modifying adhesive [284, 285]. The structure of pDA contains a variety of functional groups (amines, catechols, and imines), so it can be assembled with the “host” by non-covalent bonds, and due to the adhesion properties of pDA [286]. In addition, due to the adhesion of pDA, it can work as a sturdy bionic glue to firmly adhere the selected nanomaterials to the surface of the support layer of the membrane without any negative impact on the membrane surface. Therefore, utilizing the host-guest interaction between β-cyclodextrin and pDA the bio-adhesiveness of pDA, not only a structure combining β-cyclodextrin and pDA can be well loaded on the substrate of the membrane. The host-guest interaction based on β-cyclodextrin and pDA has shown good filtration performance in a few membrane applications, but till now it has not been used in the preparation of membrane for dye/salt separation [287]. In addition, the hydroxyl groups from β-cyclodextrin and amine groups from pDA can undergo interfacial polymerization (amide condensation reaction or esterification reaction) with trimesoyl chloride (TMC) to form a stable membrane structure. Furthermore, the remaining hydroxyl groups can also increase the hydrophilicity of the membrane surface [225, 288].

The membrane formed in this way, however, is not an "all-rounder". Membrane fouling, which comprises irreversible dye fouling and biofilm fouling caused by microbial proliferation, is the main hindrance of practical filtration applications [167]. It can result in a significant reduction in flux and therefore, a significant rise in energy consumption during separation. Conventional simple washing is incapable of removing biofouling, implying that the lifetime of the membrane is also greatly shortened. As a result, when regulating the structure of a dye/salt separation membrane to improve its separation performance, the self-cleaning and antibacterial properties of membranes should be simultaneously considered [210]. Photocatalytic technology has been widely used to degrade organic pollutants due to its high catalytic efficiency, good structural stability, and non-toxicity [289, 290]. The strategy of incorporating P and C elements into simple metal oxides (e.g., Ag_2O) with a narrow band gap has been taken to synthesize new types of visible-light-driven photocatalysts (e.g., Ag_3PO_4 and Ag_2CO_3) [291, 292]. In recent years, Ag_3PO_4 has been recognized as one of the most effective visible-light-driven photocatalysts [293]. However, Ag_3PO_4 in water is not stable, and encounters unpredictable photo-decomposition [150]. Some researchers found that AgBr-Ag_3PO_4 exhibiting a higher catalytic activity and stability is easily synthesized *via* the *in-situ* formation method [150, 294]. However, there is no

research on combining photocatalysts and host-guest interactions to endow the membranes with photocatalytic performance for textile wastewater treatment.

In this chapter, a novel high-throughput dye/salt separation membrane with a rapid solute transfer channel achieved via the host-guest interaction is described. In addition, a photocatalyst layer is generated *in-situ* on the surface of the dye/salt separation membrane, in order to effectively degrade the contaminants on the membrane surface by photocatalysis, imparting good antifouling and self-cleaning properties to the membrane. The purpose of this chapter is not only to put forward a synthesis strategy for high-efficiency dye/salt separation membranes with rapid solute transfer but also to highlight the novelty of a photocatalyst-supported membrane with long-term and stable operating performance.

5.2 Results and discussion

5.2.1 Chemical composition characterization of DSM surface

Fig. 5.1a and Fig. 5.2 show the Fourier transform infrared (FT-IR) spectra of the membranes, the HPAN support substrate comes from the hydrolysis of PAN and thus shows two typical characteristic peaks at ~2243 cm^{-1} and ~1453 cm^{-1}, corresponding to the bending vibration of the -C≡N and -CH_2 groups, respectively. In addition, compared with HPAN, the stronger peak at ~3362 cm^{-1} of other membranes (e.g., DSM-1) corresponds to the stretching vibration of amine-N-H and phenol-OH derived from the pDA matrix, and the stretching vibration of alcohol-OH in β-cyclodextrin [195] (Fig. 5.1a and Fig. 5.2). The peak at ~2933 cm^{-1} is the characteristic peak of -CH_2, and the peak at ~1662 cm^{-1} can be attributed to the aromatic ring of pDA [196]. The enhanced spectral intensity of the pDA/β-cyclodextrin membrane at ~1061 cm^{-1} can prove the -C-O-C stretching vibration of β-cyclodextrin, which in turn proves the synergistic effect of β-cyclodextrin on the surface of the membrane. After adding TMC (DSM-3), there is not only a typical peak of amide I bond (C=O) at 1654 cm^{-1}, but also a weak peak at 1554 cm^{-1} and a peak at 1734 cm^{-1}. This may because TMC has undergone an amide reaction with the selective layers of the membrane [198]. For the photocatalytically modified membrane, it can be seen from Figure 3b that the peaks at ~1450 cm^{-1} and ~1380 cm^{-1} are characteristic peaks of AgBr [295]. Moreover, ~1045 cm^{-1} and ~1495 cm^{-1} are the characteristic peaks of Ag_3PO_4, which can prove the presence of AgBr and Ag_3PO_4 on the membrane surface [295].

Through X-ray Photoelectron Spectrometer (XPS) analysis, the formation of pDA and pDA/β-cyclodextrin selective layers were further verified (Fig. 5.1c, Fig. 5.3, and Table 5.1). The C/N and O/N atomic ratios in the DSM formed by the pDA layer (DSM-1) were 8.19 and 2.47, respectively, while in the DSM formed by the combination of β-cyclodextrin and pDA (DSM-3), the C/N atomic ratio and O/N were 14.75 and 4.91. Compared with the pristine support layer of the membrane, those decorated by the β-cyclodextrin layer (DSM-5, Table S1) shows a reduced proportion of N atoms and an increased proportion of O atoms and this was caused by the hydroxyl group in β-cyclodextrin [195]. This can indicate that β-cyclodextrin was bound to the surface of the membrane selective layer. Interestingly, compared with the HPAN support layer, the Cu 2p3 peak appeared in the DSM spectrum (Fig. 5.1c, Fig. 5.3, and Table 5.1, which suggests that Cu nanoparticles (CuNPs) have also been incorporated in the selective layer of the membrane. For the photocatalyst modified membrane (DSM-14), the spectrum shows (Fig. 5.3c and Table 5.1) an Ag 3d peak, manifesting that the photocatalyst was loaded on the membrane. Fig. 5.1d and Fig. 5.1e are the narrow scan spectra of the Ag and Br elements of DSM-14, respectively. Ag^{+} is from AgBr-Ag_3PO_4, and there may be a small amount of Ag^0 represented by the peak at 374.1eV [296]. There were two characteristic peaks in the narrow scan spectrum of Br 3d at about 68.1eV and 69.1eV, corresponding to the binding energy of Br 3d5/2 and Br 3d3/2, which are consistent with the Br element peak in AgBr [297]. This shows that the photocatalyst has been loaded on the DSM. In addition, in the narrow scan spectrum of DSM-14 for C, O, N, and P, it can also prove that AgBr-Ag_3PO_4 has been loaded on the surface of the membrane (Fig. 5.3).

Fig. 5.1f shows the X-ray diffractometer (XRD) diffraction patterns of DSM-3, DSM-14, and AgBr-Ag_3PO_4 synthesized with the concentration of solution A and B in DSM-14. Among them, DSM-3 and DSM-14 have HPAN diffraction peaks in the range of 15°-27°. Compared with DSM-3 without photocatalyst modification, DSM-14 shows new diffraction peaks at 33.0° and 36.6°, which match well to that of the synthesized AgBr-Ag_3PO_4 powder. This corresponds well to the peak of silver phosphate here, indicating that this method can synthesize not only Ag_3PO_4 (PDF#70-0720) but also silver phosphate on the surface of the photocatalyst-modified membrane. Simultaneously, the diffraction pattern of DSM-14 has two AgBr (PDF#79-0149) peaks at 31.1° and 44.5°, which indicates that AgBr was generated *in-situ* on the photocatalyst modified membrane. In addition, the powders directly

synthesized by the concentration of solution A and B for photocatalytic modification of the membrane can well also correspond well to the characteristic peaks of AgBr and Ag_3PO_4.

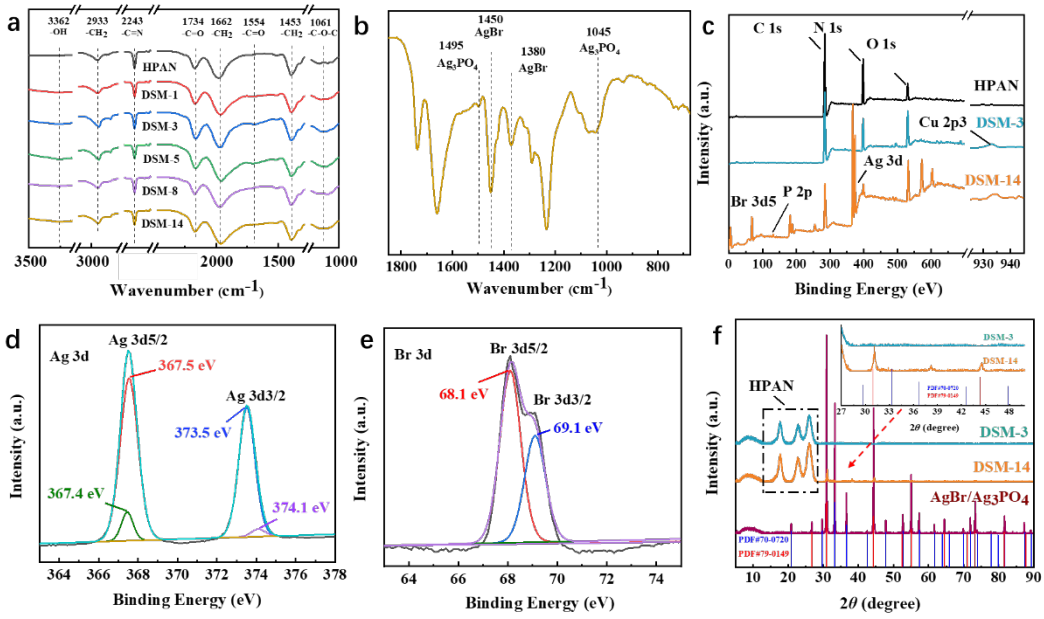

Figure. 5.1 (a, b) FT-IR and (c) XPS spectra of the DSM membrane. (d) Ag 3d XPS spectra of the DSM-14. (e) Br 3d XPS spectra of DSM-14. (f) XRD spectra of the DSM-3, DSM-14 and AgBr/Ag3PO4 powder.

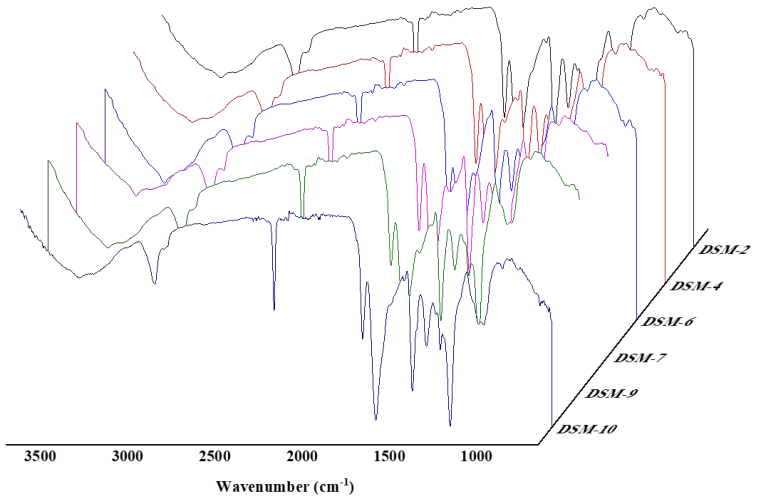

Figure 5.2 FT-IR spectra of the DSM-2, DSM-4, DSM-6, DSM-7, DSM-9, DSM-10.

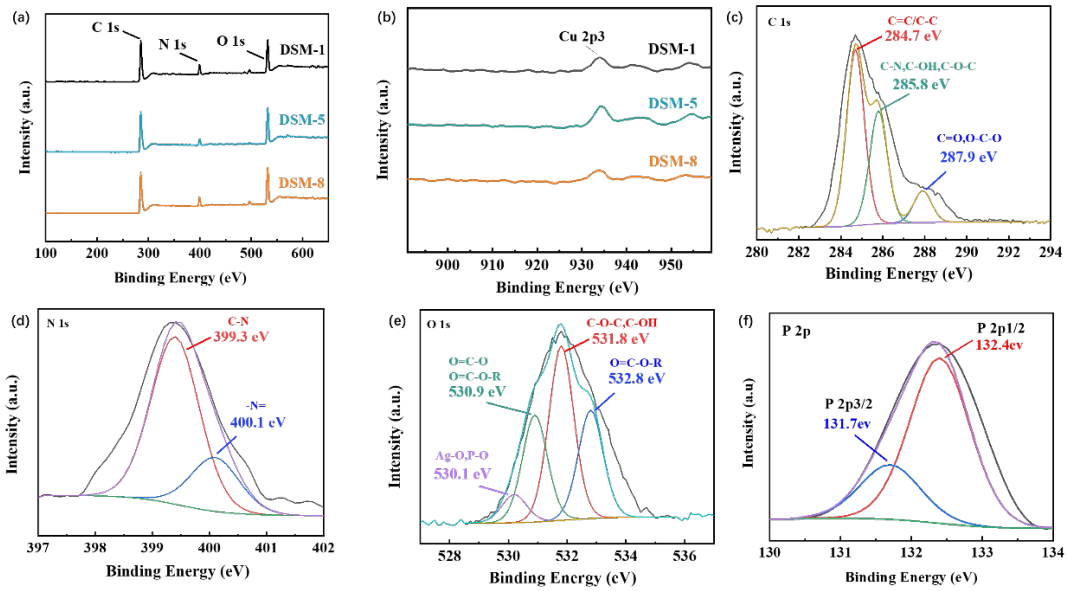

Figure 5.3 XPS spectra of the membrane: (a,b) DSM-1, DSM-5, DSM-8; (c,d,e,f) C 1s, N 1s, O 1s, and P 2p of DSM-14.

Table 5.1 XPS result of the DSM-1, DSM-5, DSM-8, and DSM-14.

Item	C (%)	N (%)	O (%)	Cu (%)	Ag (%)	P (%)	Br (%)	C/N	O/N
HPAN	73.62	19.41	6.19	-	-	-	-	3.79	0.32
DSM-1	69.25	8.46	20.89	0.91	-	-	-	8.19	2.47
DSM-3	70.49	4.78	23.49	0.63	-	-	-	14.75	4.91
DSM-5	69.68	4.90	24.28	0.73	-	-	-	14.22	4.96
DSM-8	69.90	7.62	22.72	0.63	-	-	-	9.17	2.98
DSM-14	52.61	9.80	16.76	1.11	7.31	3.74	8.03	5.37	1.71

5.2.2 Morphology of DSM

The surface morphology of DSM is shown in Fig. 5.4 and 5.5. Compared with the HPAN substrate, after pDA modification (DSM-1), many nano-nodules could be observed on the membrane surface in the scanning electron microscope (SEM) image on the surface of the membrane (Fig. 5.4a and 5.5b). In addition, the average roughness (R_a) of the membrane surface measured by atomic force microscopy (AFM) increased from 4.99 nm to 6.16 nm. This could be attributed to the rapid initiation of the non-covalent and covalent self-polymerization process of pDA by $H_2O_2/CuSO_4$ [298]. The surface of the membrane modified with β-cyclodextrin (DSM-5) is smoother, and R_a decreases to 3.71nm (Fig. 5.4d). For the membrane modified by pDA/β-cyclodextrin (DSM-8), clusters and honeycomb structures appeared on the surface of the membrane, and R_a was increased to 7.25 nm (Fig. 5.4e and Fig. 5.5) [195]. Fig. 5.4c (DSM-3) compares with Fig. 5.4f (DSM-14), after using TMC for interfacial polymerization,

R_a decreased from 7.25 to 4.37 nm, which shows that the interfacial polymerization can effectively cover the membrane and make the structure of the membrane more stable and denser. Nanoparticles can be observed on the surface of the photocatalyst modified membrane, and R_a raised significantly to 19.2. It could also be observed from the cross-sectional morphology of the membrane after pDA/β-cyclodextrin modification that a selective layer of approximately 58±1.55 nm was formed. Based on the host-guest interaction, the inclusion interaction of β-cyclodextrin occurs simultaneously during the formation of the pDA layer, resulting in pDA/β-cyclodextrin binding to each other, thereby forming a molecular transport pathway [195] (Fig. 5.4h). After the membrane was modified with photocatalyst, it was obvious that a photocatalyst layer appeared, and the thickness also increased to 103±3.72 nm (Fig. 5.4i). Interestingly, since the photocatalyst was generated *in-situ* on the surface of the membrane using solutions P1 and P2, nanoparticles also appeared in the matrix. In addition, a cavity could be seen around the nanoparticles, which is conducive to the rapid transport of solutes and compensating for the permeability loss caused by photocatalyst loading [299]. The result of EDS elemental mapping of DSM-14 is shown in Fig. 5.4k. As a result, there are distributions of Ag, P, Br, and O elements in the particles where DSM-14 is present. This can further illustrate that AgBr-Ag_3PO_4 is distributed on the surface of DSM-14, and the photocatalytic modification makes the photocatalyst well supported on the membrane.

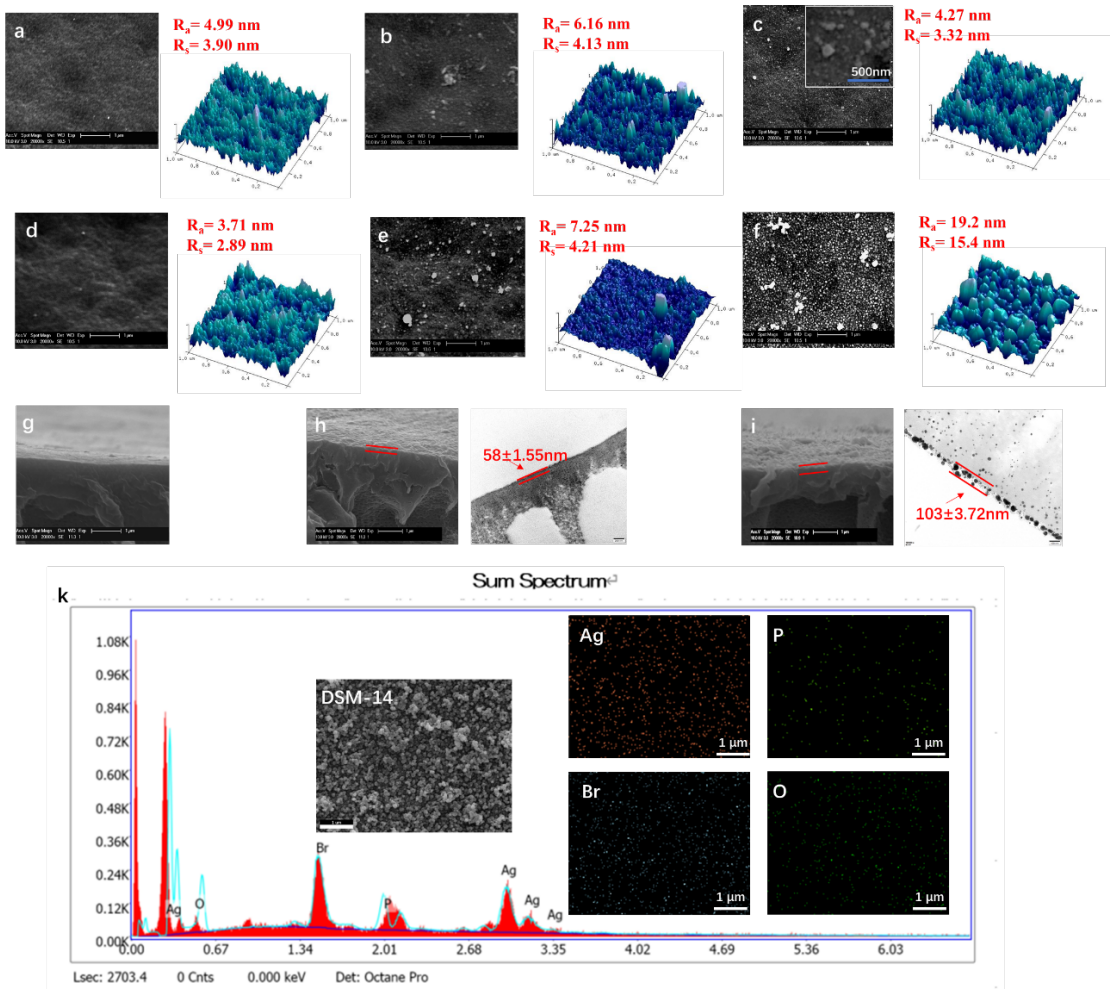

Figure 5.4 The surface morphology and the roughness by SEM and AFM of (a) HPAN, (b) DSM-1, (c) DSM-3, (d) DSM-5, (e) DSM-8, (f) DSM-14; cross-sectional morphology by SEM and TEM of (g) HPAN, (h) DSM-3, (i) DSM-14 (The attached picture (right side) shows the transmission electron microscope (TEM) results; (k) EDS elemental mapping of DSM-14.

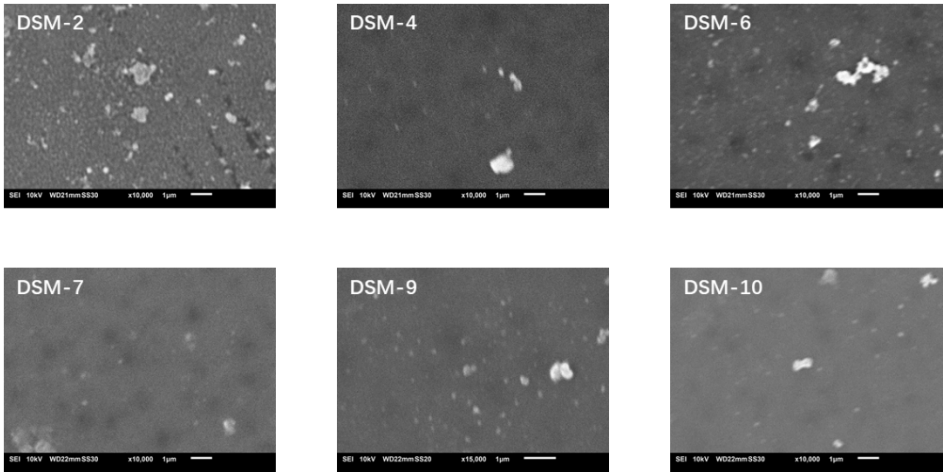

Figure 5.5 SEM of the DSM-2, DSM-4, DSM-6, DSM-7, DSM-9, DSM-10.

5.2.3 Hydrophilicity and surface potential characteristics of DSM

The water contact angle was used to evaluate the surface wettability of DSM to explore the hydrophilic/hydrophobic properties of DSM (Fig. 5.6a). There are many hydrophilic -COOH groups on the surface of HPAN, so the water contact angle was 29.7°, showing good hydrophilicity. After the introduction of pDA (DSM-1) and β-cyclodextrin (DSM-5), the hydrophilicity of the membrane surface decreases (46.6° and 53.0°, respectively). However, pDA/β-cyclodextrin modified membranes (DSM-3), the water contact angle was between the two materials used alone to modify (DSM-1 and DSM-5) (48.5°). Compared with the β-cyclodextrin membranes, the water contact angle was in between. Due to the occurrence of the amide condensation reaction, amide groups were formed on the surface of the membrane after TMC modification, which increased the water contact angle of the membrane from 42.7° to 48.5°. After loading the photocatalyst (DSM-14), the membrane exhibits a similar water contact angle value to that before the modification (DSM-3, 48.5°, and DSM-14, 50.1°), which indicated that the introduction of the photocatalyst did not change the hydrophilicity and hydrophobicity of the membrane (shown in Fig. 5.6e and 5.6f).

DSM has a large negative zeta potential in a wide pH range (4.0-10.5) (Fig. 5.6b). Compared with the HPAN substrate, the zeta potential of modified membranes decreased. During interfacial polymerization, TMC crosslinks had many amine groups and carboxyl groups[300]. After photocatalytic modification, there is a slight increase in the zeta potential. This is because the negative charge exhibited by the phosphoric acid group in Ag_3PO_4 leads to the potential of Ag_3PO_4 and AgBr powder being about -35.0 and 9.0 mV (pH=7), respectively. This is higher than the potential before modification (DSM-3), and the photocatalyst is supported on the surface of the membrane, so there is a slight increase in the zeta potential of the modified membrane [301, 302]. However, due to the strongly negative potential on the membrane surface, the photocatalyst-modified membrane still had a relatively large negative potential in a wide pH range. The zeta potential results show the potential of DSM in the rejection of anionic molecules [303].

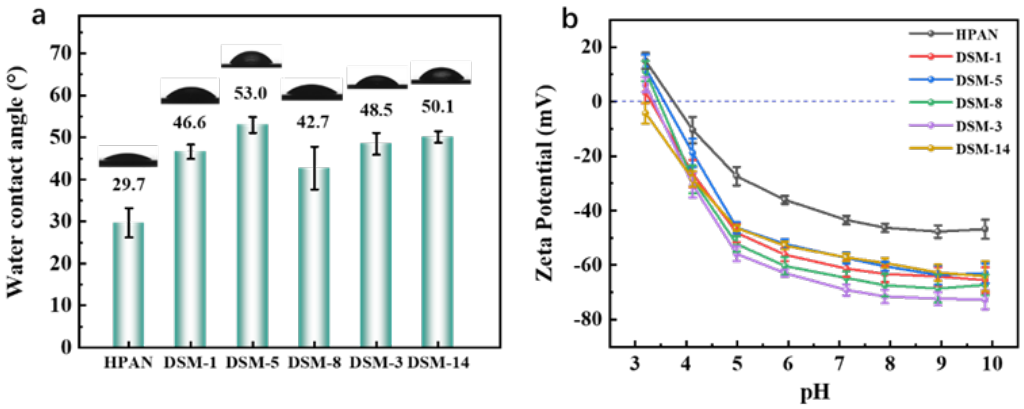

Figure 5.6 (a) Water contact angle of DSM; (b) Zeta potential measurements for DSM.

5.2.4 DSM filtration performance.

The water permeability of DSM is shown in Fig. 5.7a and Fig. 5.8. After pDA modification (DSM-1), the pDA on the surface underwent an amide condensation reaction with TMC to form a dense selective layer through interfacial polymerization, so the water permeability decreased. For the membrane modified with β-cyclodextrin alone (DSM-5), the hydroxyl groups could interact with the highly reactive acid chloride group of TMC to obtain a highly cross-linked polyester network selective layer [304]. Therefore, the water permeability of DSM modified with β-cyclodextrin is low at 45.5 LMH bar^{-1}. The DSM modified with β-cyclodextrin/pDA structure had different results. Interestingly, DSM modified with β-cyclodextrin/pDA and then modified with TMC had a significant increase in water permeability compared to DSM modified with β-cyclodextrin or pDA alone. Compared with the hydroxyl group in β-cyclodextrin, the amine group in pDA has a higher reactivity to the acid chloride group in TMC. TMC first undergoes an amide condensation reaction with the amine group in pDA, thus the substance transmission channel of β-cyclodextrin was retained, and a greater water permeability was obtained. After the photocatalytic modification, the water permeability of DSM dropped from 133.7 LMH bar^{-1} to 101.3 LMH bar^{-1}. The photocatalytic particles attached to the surface of the membrane (Fig. 5.7i), which caused a small amount of blockage of the transmission channel formed by β-cyclodextrin, resulting in a decrease in permeability.

As shown in Fig. 5.7b and Fig. 5.9, the rejection of DR23 (96.9%) by the HPAN substrate is better than that of RB5 (64.6%). After adding pDA to the membrane, the permeability dropped rapidly (20.6 LMH bar^{-1}), but the rejection of RB5 increased (89.2%). This was caused by the interfacial polymerization of pDA and TMC on the membrane surface. In addition, the potential of the membrane

was lowered (Fig. 5.7b), which was beneficial to the separation of these two negatively charged dyes. After modification with β-cyclodextrin, a higher rejection of the two dyes was obtained (DR23, 99.2% and RB5, 99.2%), but the flux was not high (DR23, 36.8 LMH $bar^{-1,}$ and RB5, 34.2 LMH bar^{-1}). Because the -OH of β-cyclodextrin underwent an esterification reaction with the acid chloride group of the TMC the selective layer of the membrane is denser. After modification with β-cyclodextrin/pDA, the membrane was equipped with a selective layer with a lower potential so that the rejection of the two dyes (DR23, 96.2% and RB5, 88.0%). This can be explained by the Donnan effect, since both dyes used in this study, either DR23 or RB5, are negatively charged dyes in aqueous solution. Moreover, compared with a membrane modified with only β-cyclodextrin or pDA, a larger permeability was obtained (DR23, 99.5 LMH $bar^{-1,}$ and RB5, 98.7 LMH bar^{-1}), because the host-guest interaction formed molecular transport channels and achieved rapid solute transport. The same situation occurred in DSM prepared with various β-cyclodextrin concentrations, pDA concentrations, and IP times, which could also be explained well by the density of the membrane surface (sieving effect) and the surface potential (Fig. 5.9). After the photocatalyst was modified, the permeability of the two dyes was slightly reduced (DR23, 88.0 LMH $bar^{-1,}$ and RB5, 95.6 LMH bar^{-1}), but the rejection was not changed substantially (DR23, 99.4% and RB5, 98.9%), which was caused by the decrease of the hydrophilicity of the membrane surface and the slight blockage of the membrane surface pore size. However, it has been reported in the literature that when silver nanoparticles (AgNPs) were generated *in-situ*, a hole appears around the generated particles[299]. Holes around the particles were indeed observed by TEM (Fig. 5.7i). This can make up for the decrease in dye permeability caused by the decrease in pore size and hydrophilicity.

For the salt permeability of DSM, two kinds of salts (Na_2SO_4 and NaCl) were used in a concentration of 1 g/L, and the results are shown in Fig. 5.7c and Fig. 5.9. The rejection of all DSMs for the two salts followed the salt rejection order Na_2SO_4> NaCl. It proves that the DSM surface has a negative potential. After the modification with β-cyclodextrin and pDA, the permeability of the membrane to the salt solution is reduced. The permeability of Na_2SO_4 and NaCl of the β-cyclodextrin modified membrane was 26.1 LMH bar^{-1} and 34.2 LMH bar^{-1}, respectively, and the rejections were 53.8% and 13.6%, respectively. Simultaneously, the permeability of Na_2SO_4 and NaCl of the pDA modified membrane was 33.6 LMH bar^{-1} and 33.7 LMH bar^{-1}, respectively, and the rejections were 67.3% and 14.7%, respectively. After modification with β-cyclodextrin/pDA, salt could quickly pass through the channels formed by β-

cyclodextrin, and the diameter of the channel cavity was 0.60-0.78 nm [305], which was larger than the hydration radius of these ions (sulfate (0.38 nm) > sodium (0.36 nm)> chloride (0.33 nm)) [300]. Therefore, a larger permeability (Na_2SO_4, 235.3 LMH $bar^{-1}$and NaCl, 249.3 LMH bar^{-1} without TMC; Na_2SO_4, 100.1 LMH bar^{-1} and NaCl, 100.4 LMH bar^{-1} within TMC) and a lower rejection was obtained (Na_2SO_4, 25.3% and NaCl, 8.6% without TMC; Na_2SO_4, 24.2 % and NaCl, 5.0% within TMC). After the modification of the photocatalyst, there is a slight decrease in the permeability of the salt solution due to the *in-situ* generation of the photocatalyst on the membrane surface. It can be seen from Fig. 5.7c that the permeability of Na_2SO_4 before modification (DSM-3) was 100.1 and 100.4 LMH bar^{-1}, respectively, and after modification (DSM-14) decreased to 84.4 and 95.0 LMH bar^{-1}. In addition, due to the slight decrease in the potential of the membrane surface, the permeability of the salt solution slightly decreased (Na_2SO_4, 84.4 LMH $bar^{-1}$and NaCl, 95.0 LMH bar^{-1}). This could be explained by the combined Gibbs-Donnan effect and sieving effect, as the rejection of Na_2SO_4 increased because the zeta potential of the membrane increased after photocatalyst modification. Moreover, the loading of the photocatalyst also makes the surface of the membrane denser, thereby increasing the rejection of salts. The same situation also appeared in the filtration experiment of changing different β-cyclodextrin concentrations, different pDA concentrations, IP time, photocatalytic solution concentration, and dipping times.

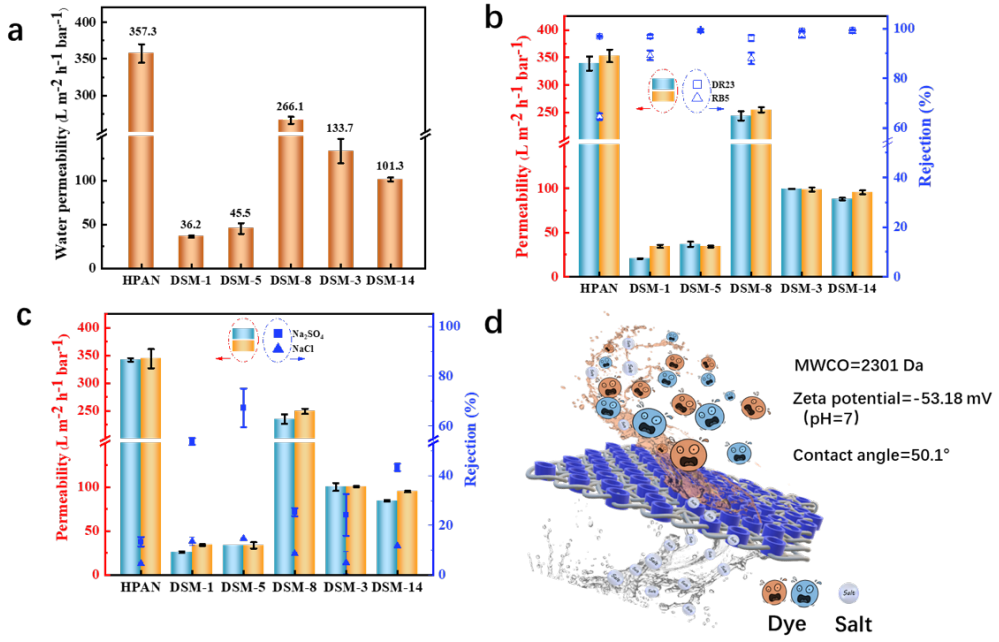

Figure 5.7 (a) DI water permeability of DSM; (b) dye solution permeability and rejection of DSM; (c) salt solution permeability and rejection of DSM; (d) schematic diagram of DSM separation of dye/salt.

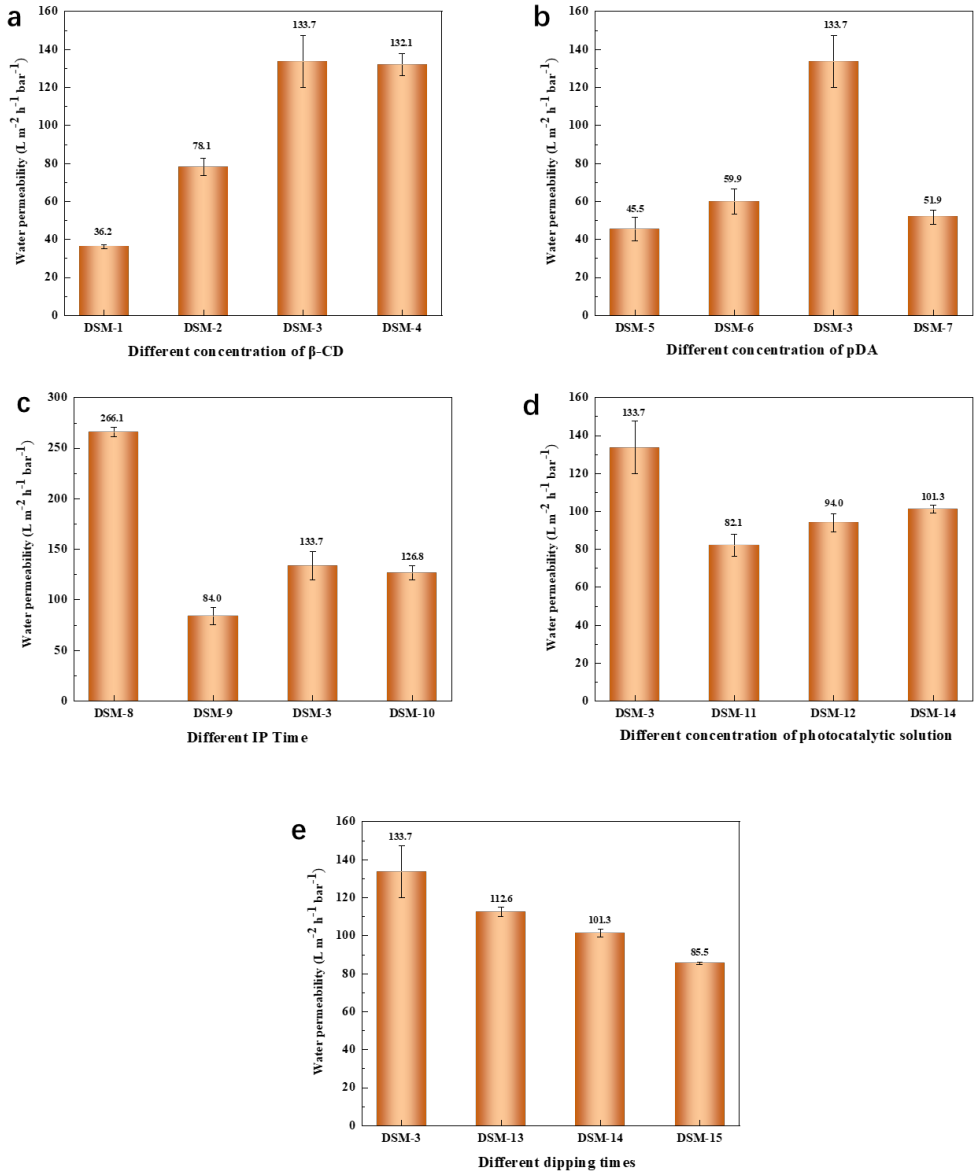

Figure 5.8 Water permeability (a) Different concentration of β-cyclodextrin; (b) Different concentration of pDA; (c) Different IP time; (d) Different concentration of photocatalytic solution; (e) Different dipping times.

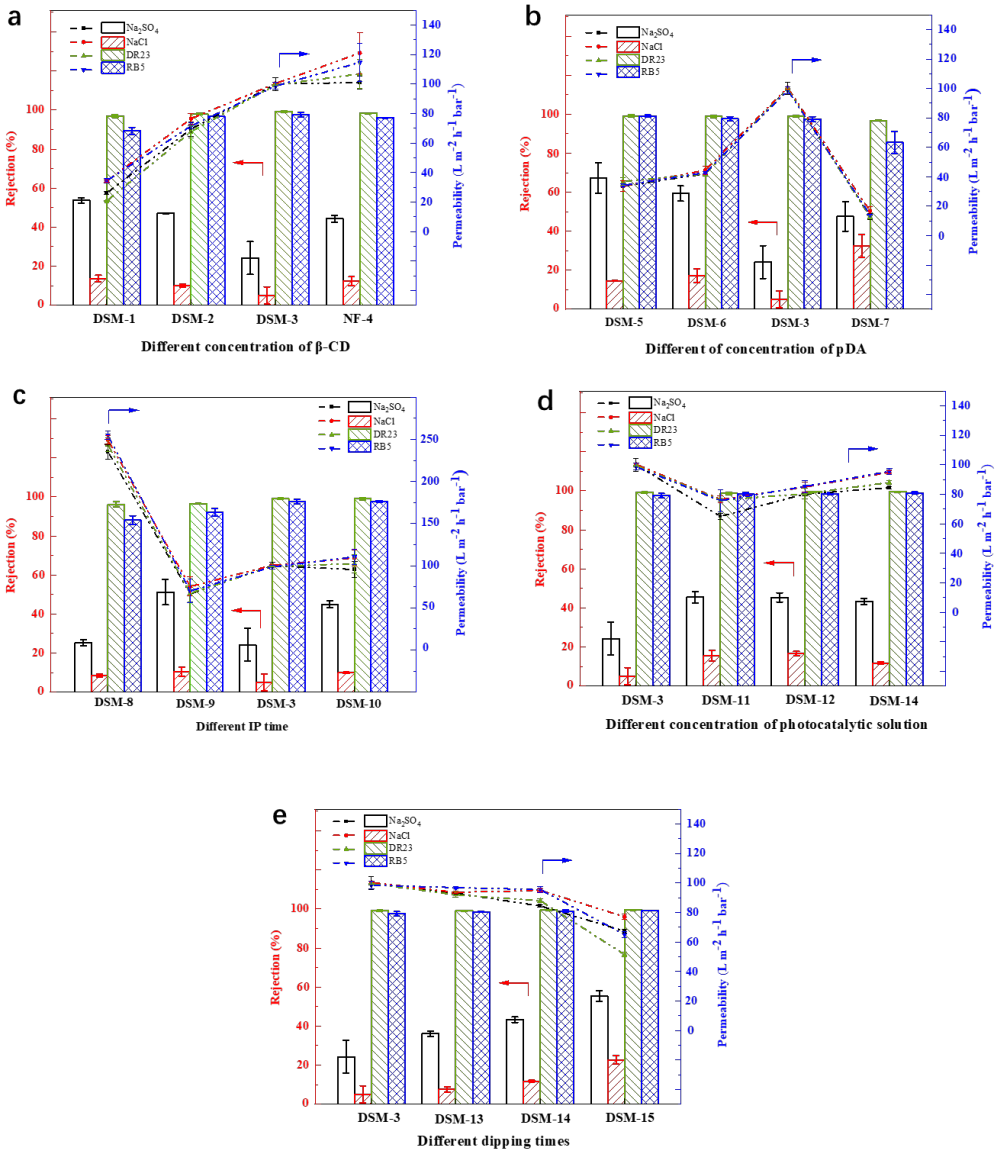

Figure 5.9 Dye/salt separation effect (a) Different concentration of β-cyclodextrin; (b) Different concentration of pDA; (c) Different IP time; (d) Different concentration of photocatalytic solution; (e) Different dipping times.

In addition, the molecular weight cut-off results could also prove this point. After the photocatalytic modification, the molecular weight cut-off of (MWCO) the membrane decreased (Fig. 5.10a). According to the results of MWCO, the MWCO before photocatalyst modification = 3308 Da, and the MWCO after modification = 2301 Da. It can be seen that the pore size changes due to the modification of the photocatalyst. In addition, the membrane filtration test was optimized by changing the synthesis conditions of pDA and β-cyclodextrin concentrations and IP time. DSM-14 was used to filter mixed solutions of NaCl and DR23 (200 ppm) with different salt concentrations to explore the influence of

different salt concentrations on the filtration process. As shown in Fig. 5.10b, the permeability of DSM to the mixed solution decreased from 79.5 to 68.6 LMH bar^{-1}, and the rejection of DR23 remained unchanged. Salits in a high concentration could be coupled with the charged dye DR23 to enhance the diffusion of dye molecules in the mixed solution[203]. Not only that, the mixed solution with high salt concentration would cause concentration polarization during the filtration process, thereby increasing the salt concentration in the mixed solution[282, 306]. Therefore, as the salt concentration increased, the rejection of NaCl by DSM-14 slightly increased. Furthermore, the long-term stability of the DSM-14 membrane was continuously tested, using DR23/NaCl to carry out a 60-hour filtration test (Fig. 5.10c). From the beginning to the 5th hour of the test, due to adsorption of DR23 by the selective layer, the permeability decreased from 84.03 to 59.54 LMH bar^{-1} and then stabilized. The rejection of DR23 and NaCl remained stable throughout the test, and the rejection of DR23 was about 99.0%, and the rejection of NaCl was about 10.0%. This can indicate that the DSM-14 has a good stability and has the characteristics of long-term stable operation. In addition, as for the filtration performance of DSM compared with previously reported, as shown in Table 5.2, DSM-3 and DSM-14 had a higher permeability and a good dye/salt separation performance. It could serve as a potential candidate for large-scale treatment of textile wastewater by membrane separation.

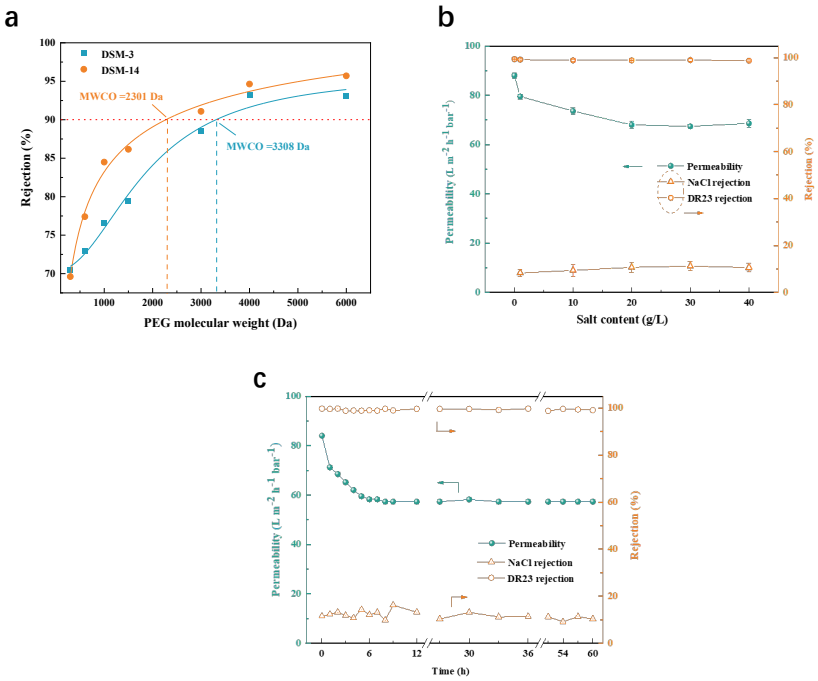

Figure 5.10 (a) The molecular weight cut-offs (MWCO) for DSM-3 and DSM-14. (b) Effect of salt content on filtration performance of dye/salt mixture solution; (c) long-term stability of DSM-14, 0.2 g/L DR 23+1 g/L Na_2SO_4.

Table 5.2 Comparison of dye/salt filtration performance.

Membrane	Method	Permeability (LMH bar^{-1})	Types of dye	Dye rejection (%)	Types of salts	Salt Rejection (%)	Refs.
Sugar-based	IP	33.7	Direct red 23 Direct red 80 Reactive black 5 Reactive orange 16 Methyl orange	99.6 99.8 98.9 97.4 91.3	Na_2SO_4 $MgSO_4$ NaCl $MgCl_2$	95.0[a] 40.0[a] 60.0[a] 18.0[a]	[87]
N-rich amine monomer	IP	95.1	Congo red Direct red 23 Reactive black 5	99.1 98.5 96.3	NaCl	5.8	[172]
Erythritol-based	IP	53.23	Congo red Direct red 23 Reactive blue 2	99.6 95.2 99.6	Na_2SO_4 NaCl	11.0 5.6	[203]
POP/TMC	IP	31.28	Reactive black 5	99.1	RB5/Na_2SO_4	15.4	[260]
Tannic acid/PEI	Co-deposition	41.5	Congo red	99.5	Na_2SO_4 NaCl	6.00 8.00	[261]
Catechol/PEI-$CuSO_4/H_2O_2$	Co-deposition	24.5	Congo red Reactive black 5 Methyl blue	99.8 99.7 99.3	Na_2SO_4 NaCl $MgCl_2$	12.5 2.0 0.6	[262]
Fe^{3+}-PEI@HPAN	In-situ self-assembly	6.0	Congo red Methyl blue Acid fuchsin Crystal violet	99.5 99.9 99.0 92.9	Na_2SO_4 NaCl $MgCl_2$ $MgSO_4$	5.9 7.5 30.5 20.6	[263]
DSM-3	Co-deposition/IP	133.7	Direct red 23 Reactive black 5	99.1 97.5	Na_2SO_4 NaCl	24.2 5.0	This work
DSM-14	Co-deposition/IP	101.3	Direct red 23 Reactive black 5	99.4 98.9	Na_2SO_4 NaCl	43.3 1.4	This work

5.2.5 Self-cleaning and photocatalytic properties of DSM

As shown in Fig. 5.11a and 5.12b, the photocatalytically modified DSM (DSM-14) was subjected to self-cleaning experiments with or without visible light irradiation. A solution containing 200 ppm DR23 was used as the feed source to explore the self-cleaning performance of the membrane. For the self-cleaning experiment carried out in the dark, the average values of water permeability (without dye) in the four cycles were 98.6, 94.0, 88.5, and 75.8 LMH bar^{-1} (Fig. 5.11a). For dye transport, the average values of the four cycles were 74.3, 63.8, 57.6, 54.3 LMH bar^{-1}, respectively. In addition, the rejection

of DR23 remains unchanged, stabilizing above 99.0%. Both water and dye permeability decreased gradually with filtration time, which indicated the appearance of membrane fouling. The dye molecules contacted the membrane surface through intermolecular interactions and remained on the membrane, blocking the solute transport channel and decreasing the permeability. In addition, after three cycles, the permeability tended to be stable, because the adsorption of DR23 on the membrane surface was saturated. Simultaneously, the filtration experiment was performed on DSM-14 under visible light (Fig. 5.11b). The average values of water permeability (without dye) of each cycle were 98.0, 97.9, 96.8, and 94.4 LMH bar^{-1}, respectively, and the corresponding average values of DR23 permeability were 74.0, 74.5, 75.5, and 75.3 LMH bar^{-1}. In addition, its rejection of DR23 had always maintained a high rejection (>99.0%). Compared with the experiment under dark conditions, the filtering under visible light had stable water and DR23 permeability. As the AgBr-Ag_3PO_4 generated *in-situ* on the surface of the DSM decomposes the DR23 adsorbed on the membrane surface to a certain extent under visible light, the molecular transport channels blocked by DR23 open again. As the filtration progressed, decomposition occurred. Furthermore, the fouling resistance ratio of DSM-14 with or without visible light is shown in Fig. 5.11c. The FRR value of DSM-14 under visible light was 96.3%, indicating that DSM-14 under visible light has a good antifouling performance. Since the photocatalyst could only catalyze the degradation of DR23 adsorbed on the surface under visible light during the filtering process, the FRR value of DSM-14 under dark conditions was much lower, only 76.9%. The total fouling ratio (R_t) was the sum of reversible fouling (R_r) and irreversible fouling (R_{ir}). Under visible light, the Rir value of DSM-14 was only 3.7%, which was much lower than under dark conditions (23.1%). Under visible light conditions, the value of R_t was 24.2% lower than under dark conditions (47.2%). Therefore, the high FRR value and low R_t value under visible light conditions indicate that DSM-14 has excellent antifouling and self-cleaning properties.

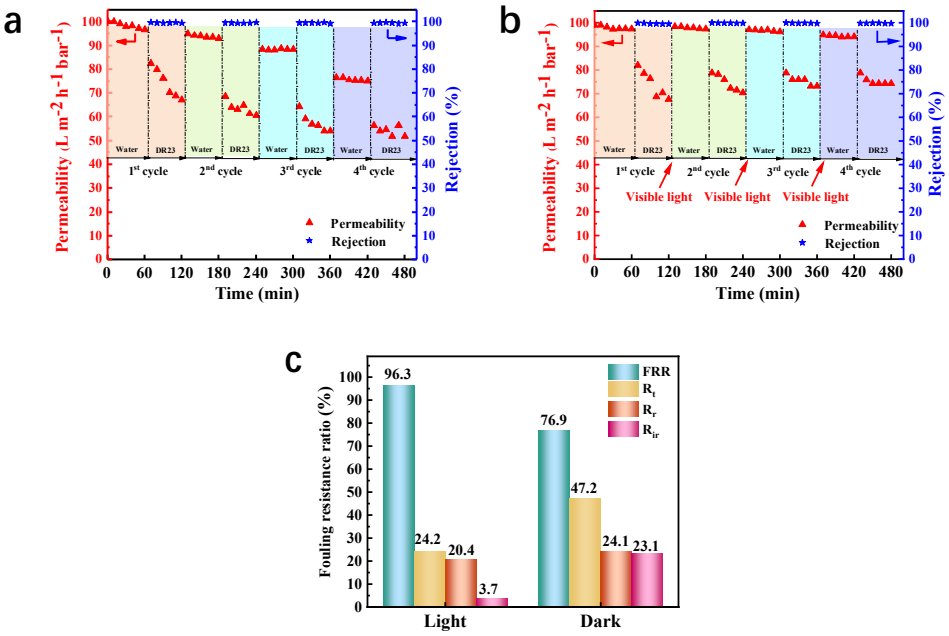

Figure 5.11 (a) Dark self-cleaning experiment of DSM-14; (b) light self-cleaning experiment of DSM-14; (c) fouling resistance ratio of DSM-14 in the dark and under visible light.

Furthermore, a static catalysis experiment was performed on the photocatalyst-modified membrane to explore the degradation efficiency of DR23 on the surface of the membrane. As shown in Fig. 5.12a, in the first 90 minutes of the photocatalytic degradation experiment, the concentration of DR23 in the solution dropped. This shows that the interface between the photocatalyst layer and the DSM has a certain adsorption performance for DR23, and DR23 can be adsorbed to the surface of the catalyst. This is related to the decrease in the hydrophilicity of the membrane surface after the photocatalyst modification of DSM. Moreover, after 60 minutes, the adsorption of DR23 by the membrane reached saturation, and the concentration of DR23 in the solution remained unchanged. Different from that under the dark, the membrane under visible light underwent a photocatalytic reaction over time, and the concentration of DR23 in the solution would decrease. After 210 minutes of reaction, the C/C_0 of DR23 in the solution dropped to 0.38, which indicated that the photocatalyst on the membrane surface had a good degradation performance for DR23. After 210 minutes, C/C_0 remained unchanged, indicating that the degradation of DR23 reached a balance. Quenching experiments using different radical scavengers were carried out to further understand the underlying reaction mechanism of DR23 degradation on Ag_3PO_4-AgBr. As shown in Fig. 5.12a, when benzoquinone was added to the reaction system as scavenger for superoxide radical, the degradation of DR23 by Ag_3PO_4-AgBr was almost terminated under visible light irradiation. Likewise, when tert-butanol as scavenger for hydroxyl radicals and ammonium oxalate as scavenger for

holes were added, significant inhibition of the photocatalytic reaction was observed. Differently, when tert-butanol and ammonium oxalate were added, the degree of photoactivity inhibition was less than that induced by benzoquinone. Therefore, it can be concluded that hydroxyl radicals, holes and superoxide radicals all have significant effects on the degradation process of DR23 by Ag_3PO_4-AgBr. Moreover, superoxide radicals play a more important role than hydroxyl radicals and holes on the photodegradation of DR23 on Ag_3PO_4-AgBr. Fig. 5.12b shows the mineralization efficiency results of DSM-14 for the 200 ppm DR23 solution. The results show that DSM-14 can efficiently mineralize the dyes in solution. The results of the mineralization test show that most dyes can be degraded into the final oxidation products H_2O and CO_2, so there will be no secondary pollution to the environment due to incomplete degradation of small molecular organic matter. Electron spin resonance (ESR) radical trapping experiments can determine the active species in the degradation of DR23 by AgBr-Ag_3PO_4, and the results are shown in Fig. 5.12c and 5.12d. The results show that under dark conditions, no signal peaks of free radicals appear. However, under visible light, the signal peaks of DMPO-•OH and DMPO-•O_2^- appeared, which also indicated that the main active free radicals were DMPO-•OH and DMPO-•O_2^- during the degradation of DR23. This also corresponds well to the results of the quenching experiments, further indicating that the generation of free radicals is the key to achieve dye degradation and self-cleaning of the modified membranes. Fig. 5.12e shows the ultraviolet-visible diffuse reflectance spectra of AgBr, AgBr-Ag_3PO_4, HPAN, DSM-3, and DSM-14. The carboxyl group in HPAN has an absorption peak at λ=204 nm. Moreover, in DSM-3 and DSM-14, many -OH and -NH_2 auxochromes will shift the absorption peak to the long-wave direction and increase the peak intensity. AgBr-Ag_3PO_4 powders have absorption properties in the visible light region. For the UV-Vis spectra of DSM-3 and DSM-14 membranes, DSM-14 has a better optical response in the visible light region due to the modification of the photocatalyst. The separation and transfer efficiency of photogenerated carriers is an important property to measure the activity and lifetime of photocatalysts. This property can be assessed using photoluminescence spectroscopy. A higher photoluminescence intensity can indicate a higher recombination efficiency of photo-generated electron-hole pairs and a shorter lifetime, implies lower photocatalytic activity of the catalyst [307]. The photoluminescence spectra of AgBr-Ag_3PO_4 powder and AgBr powder synthesized by this work at an excitation wavelength of 380 nm are shown in Fig. 5.12f. The peak intensity of AgBr-Ag_3PO_4 was significantly smaller than that of AgBr. It could be shown that the photo-generated electron-hole pair separation efficiency of the AgBr-Ag_3PO_4 hybrid was higher, and it had a higher photocatalytic

activity. To further understand the charge transfer at the contact interface between the electrode and electrolyte, electrochemical impedance spectroscopy (EIS) measurements were performed (Fig. 5.12g) [308, 309]. The results show that the impedance of the AgBr-Ag_3PO_4 composite is smaller than that of AgBr, which suggests the improved electron-hole separation efficiency. To further analyze the transfer and separation of charge carriers, photocurrent transient responses were recorded, as shown in Fig. 5.12h. The photocurrent density of AgBr-Ag_3PO_4 is higher than that of AgBr, indicating more efficient transfer of charge carriers in AgBr-Ag_3PO_4. This result is similar to the conclusion drawn from the test results of EIS and PL, which illustrates that AgBr-Ag_3PO_4 is more beneficial to photocatalytic reactions than AgBr.

Based on the band gap structure and photocatalytic degradation of AgBr-Ag_3PO_4, a degradation mechanism to degrade DR23 was proposed [310]. The band gaps of AgBr and Ag_3PO_4 are 2.53 and 2.46 eV, respectively [291, 293]. As shown in Fig. 5.12i, under visible light irradiation, the electrons in the valence band of AgBr-Ag_3PO_4 can be excited to the conduction band, leaving holes in the valence band [307]. The DR23 adsorbed on the surface of AgBr-Ag_3PO_4 is directly oxidized by the photogenerated holes. Photogenerated electrons can move to Ag_3PO_4 through the tight interfacial contact between AgBr and Ag_3PO_4, which effectively hinders the recombination of electrons and holes. Meanwhile, electrons can activate molecular oxygen to form superoxide ions ($\bullet O_2^-$) and photogenerated holes react with water (H_2O) or hydroxide ions (OH^-) and adsorb on the catalyst surface to generate hydroxyl radicals (•OH). Both $\bullet O_2^-$ and •OH have strong oxidative abilities, which are able to degrade DR23 into CO_2, H_2O and other intermediates [311].

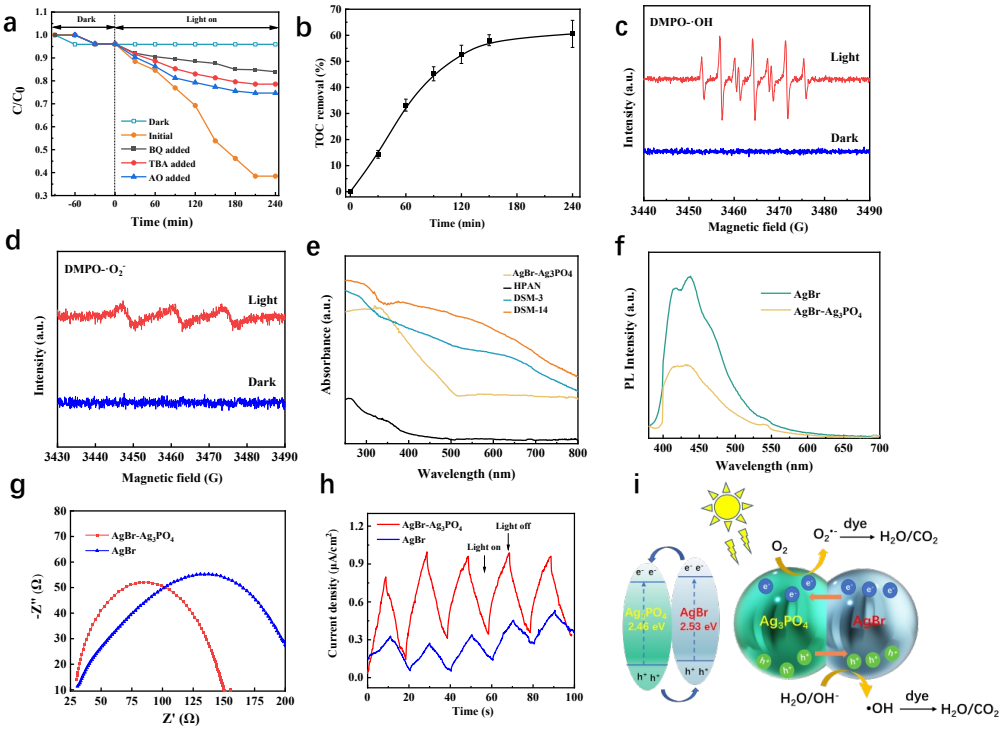

Figure 5.12 (a) static catalysis and quenching experiment of DSM-14 on DR23; (b) mineralization efficiency of DSM-14 to 200ppm DR23; (c) DMPO-•OH; (d) DMPO-•O_2^-; (e) UV-vis of AgBr, AgBr-Ag_3PO_4, HPAN, DSM-3, DSM-14; (f)photoluminescence spectra of AgBr and AgBr-Ag_3PO_4; (g) EIS Nyquist plots for AgBr and AgBr-Ag_3PO_4; (h) photocurrent transient response of AgBr and AgBr-Ag_3PO_4; (i) schematic diagram of AgBr-Ag_3PO_4 photocatalytic mechanism.

5.3 Conclusion

In summary, a fast solute transport dye/salt separation membrane was developed based on the host-guest interaction between β-cyclodextrin and pDA in supramolecular chemistry and the interfacial polymerization reaction. In addition, to address the problem of membrane fouling, AgBr-Ag_3PO_4 photocatalyst with a stable structure was generated *in-situ* on the membrane surface, so that the contaminants on the membrane surface could be quickly decomposed under visible light. High dye rejections and low salt rejections were obtained by filtration experiments with synthetic DSM membranes. In addition, during the filtration process, there was rapid solute transport. Furthermore, it is shown that the membrane has good self-cleaning and antifouling properties after photocatalyst loading. The photocatalyst synthesized in this work is also characterized, and it is proved that the synthesized AgBr-Ag_3PO_4 is not only stably supported on the membrane surface but also has a high catalytic activity. Thus, a strategy is provided for solving the resource recovery and secondary utilization in the textile wastewater treatment process.

Chapter 6: Tailoring fast mass transfer membrane: zero discharge of wastewater using visible light to increase practicality

Adapted from: *"Gao, Q., Ding, Y., Li, J., Jin, P., Xu, D., Fang, L., Wang, Y., Liu, B., Xie, Y., Bao, X., Jiang, L., Du, J., Zhu, J., Zheng, L., Su, B-L., Ng, Y.H., Xing, Y., Gui, X., Wang, C., van der Bruggen, B. with Li, J. (corresp. author), Xing, Y. (corresp. author), Wang, C. (corresp. author), van der Bruggen, B. (corresp. author) (2025). Tailoring fast mass transfer membrane: Zero discharge of wastewater using visible light. JOURNAL OF MEMBRANE SCIENCE, 717, Art.No. ARTN 123632. doi: 10.1016/j.memsci.2024.123632"*

6.1 Introduction

In December 2017, UN Member States adopted United Nations General Assembly resolution 71/222 on an International Decade for Action on 'Water for Sustainable Development' 2018-2028 [312]. This requires an ever-increasing awareness of sustainability in water purification processes. Five years on, it should be discussed how this goal has performed in practice so far. In the realm of sustainability, it is imperative to redefine wastewater not as mere "waste" but as a valuable resource [313-315]. Within the framework of a circular economy, the objective of wastewater treatment appears to be the minimization of environmental impact and the optimization of resource utilization [316]. In contemporary times, the advent of novel loose nanofiltration membranes (LNMs) appears to present a promising ecological remedy for water treatment applications, due to their well-matched pore dimensions, minimal operating pressure, better mass transfer efficacy, and outstanding separation capabilities [317]. Nevertheless, the quest persists for versatile LNMs adept at navigating intricate separation scenarios [33, 42, 318]. Using mussel-inspired polydopamine (pDA) and piperazine (PIP) to form loose nanofiltration sediment layers rapidly through Michael or Schiff base reactions demonstrated advantageous for driving an efficient separation process in wastewater treatment [319-321]. However, these membranes often contend with inadequacies in mass transport and selectivity, thereby constraining their utilization within industrial contexts, including but not limited to resource recovery endeavors [322, 323].

To promote the commercialization of LNMs, developing a facile strategy is highly desirable. AMN, a small molecule containing amino and cyano groups, holds great potential for introducing advances in the separation performance of LNMs [94]. When AMN is inserted into a PIP/pDA selective layer, the charge derived from the amino group can strengthen the Donnan effect of the selective layer, and the

cyano-assisted scaffold-like framework further expands the loose structure of the LNM [64]. Furthermore, the AMN with prebiotic-like structure acts as a bio-coating due to the bio-adhesive and antibacterial properties, which can increase the resistance of LNMs [94, 189]. During resource recovery, traditional LNMs typically recover metal ions that do not involve a change in valence state [257]. Nevertheless, factual textile wastewater typically contains heavy metal ions (e.g., Cr^{6+}1-10 mg/L), necessitating treatments that involve valence state transformations to ensure their benign remediation [153]. Coupling membranes with photocatalysts could be an effective strategy for addressing this issue because it endows photoredox reactions, by which heavy metal ions can be reduced to harmless counterparts, while organic substances are separated through the LNMs[94]. Furthermore, substances obstructing specific membrane pores during transmembrane transport can be subject to photooxidative degradation, facilitating an experimental means for self-cleaning of the membrane layer [321, 324, 325].

Here, a concept for a catalytic membrane system is explored, characterized by a synergistic effect that modulates the permeability of the selective layer to facilitate expedited mass transport through the incorporation of the small molecule AMN. Furthermore, the integration of a photocatalytic component within the conventional PIP/pDA selective layer is employed to realize self-cleaning properties and the mitigation of heavy metal ion concentrations.

6.2 Results and discussion

6.2.1 Membrane simulation predictions

Traditional PIP/pDA LNMs are produced using the co-deposition method through the Michael reaction to construct a selective layer [42, 94, 326]. To expand this approach, it can be reasoned that introducing AMN into the PIP/pDA layers could construct looser selective layers [63, 94] (Fig. 6.1). Molecular dynamics (MD) simulations were first employed to examine the membrane's structural alterations by determining the diffusion coefficient of PIP in pure water [63, 327]. The PIP diffusion coefficient was calculated from the slope of the mean-azimuth shift (MSD) curve using Einstein's relation [63]. The calculated PIP diffusion coefficients in pure water, pDA, AMN, and pDA/AMN were 4.57×10^{-11}, 4.08×10^{-11}, 2.63×10^{-11}, 2.45×10^{-11} $m^2 s^{-1}$, respectively (Fig. 6.1a and Fig. 6.2a). This indicates that both pDA and AMN slowed the diffusion rate of PIP during co-deposition to form a selective layer [328]. In addition, the diffusion rate was suppressed further after the introduction of AMN indicating that

AMN changes the deposition process of the selective layer, as well as its structure [63, 329]. The membrane free volume calculation results showed that the free volumes of pDA, pDA/PIP-AMN, and pDA/PIP-AMN were basically the same, indicating that AMN molecules do not occupy the free volume of the membrane. However, after inserting AMN, the free volume of the selective layer changed from "multi-point dispersion" to "single-point volume increase" (Fig. 6.1b). Furthermore, the pore size simulation of the membrane revealed that after AMN intercalation the pore size of the selection layer ranged from ~0.75 nm (PIP/pDA) to ~0.83 nm (PIP/pDA-AMN) (Fig. 6.1c). This fully demonstrates that the structure of the selective layer changes and the pore size increases after insertion of AMN, which is beneficial for the transport of molecules and increases the permeance of the membrane [330]. This can also be evidenced by the distribution of water molecules in different selection layers. The distribution of water molecules near pDA/PIP-AMN is significantly larger than that of the other two selection layers in the same volume of simulation box (Fig. 6.1d). The water molecule radial distribution functions (RDFs) of PIP/pDA and PIP/pDA-AMN were also investigated (Fig. 6.2b). The results showed that PIP/pDA (r = 0.28 nm) and PIP/pDA-AMN (r = 0.27 nm) exhibit the highest RDF peaks in their respective first coordination layers. The value of PIP/pDA-AMN at the peak is 5.3, which is greater than the value of 4.6 of PIP/pDA. This shows that the binding ability of PIP/pDA-AMN to water is greater than that of PIP/pDA. The introduction of AMN also increases the hydrophilicity of the selection layer [331]. These MD simulation results confirm that the insertion of AMN favors the transport of water molecules, which is expected to increase the permeance of the selective layer. At the molecular level by density functional theory (DFT), the calculation results revealed that the binding energy of water molecules changed from −0.22 eV (PIP/pDA) to −0.38 eV (PIP/pDA-AMN) after AMN intercalation (Fig. 6.1e), further indicating the increased hydrophilicity of the selection layer after AMN insertion. Consequently, the introduction of AMN increases the number of transport sites for water molecules and facilitates the transmembrane transport of water.

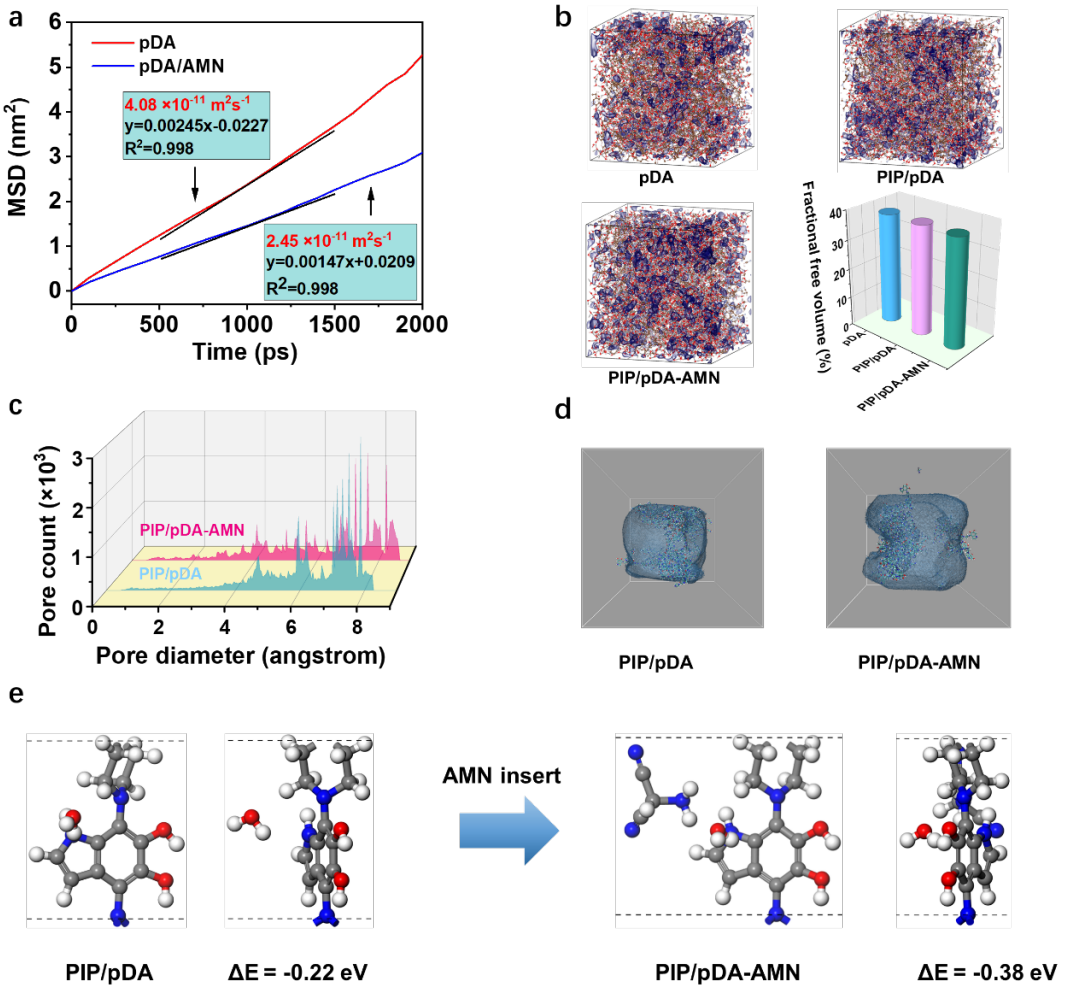

Figure 6.1 Membrane simulation results: (a) MSD curves of PIP molecules in the two simulated systems. (b) Free volume in pDA, PIP/pDA, and PIP/pDA-AMN. (c) Simulated pore size distributions of PIP/pDA and PIP/pDA-AMN. (d) Spatial distribution of water in pDA, PIP/pDA, and PIP/pDA-AMN. (e) DFT simulation of binding energy between water molecules and the two systems.

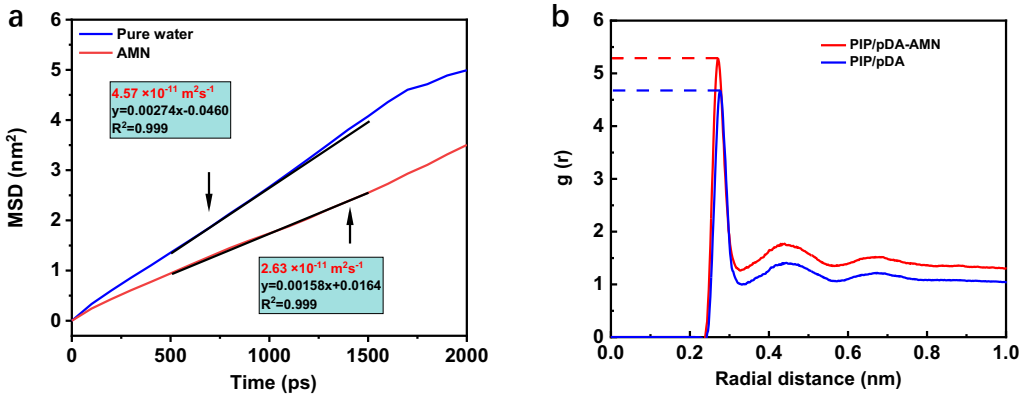

Figure 6.2 (a) MSD curves of PIP molecules: in two simulated systems with linear regression slopes ranging from 500-1500 ps. (b) Radial distribution function of water: PIP/pDA and PIP/pDA-AMN.

6.2.2 Insertion of AMN into PIP/pDA selection layer

The AMN molecules are inserted like "scaffolds" to increase membrane permeance, and changes in the PIP/pDA with AMN were experimentally examined. After AMN insertion, the thickness of the selected layer increased (from 85 to 120 nm), and the structure became looser (Fig. 6.3 and Fig. 6.4). The chemical structure of the selective layer was investigated under different synthesis conditions. FT-IR spectroscopy showed that the different selective layers had overlapping primary amine and hydroxyl peaks at approximately 3360 cm^{-1}, originating from the deposition of pDA and the amino groups in AMN (Fig. 6.3b) [94, 332, 333]. The peak at ~2245 cm^{-1} provides clear evidence for the presence of –C≡N in the PAN supporting substrate and AMN (Fig. 6.3b) [94]. The self-polymerization of dopamine was accomplished by the introduction of H_2O_2/$CuSO_4$ in the dopamine solution in Tris-buffer [94, 334]. Therefore, Cu element could be observed in the elemental composition of the selective layer (Fig. 6.5a). After AMN insertion, the –C≡N functional group was detected on the selective layer, and the N/C ratio increases compared to the PAN substrate (Fig. 6.3c-d and Fig. 6.5b) because of the abundant N element in the amino and cyano groups [94, 335]. Moreover, the newly formed PIP/pDA-AMN still has a relatively smooth structure, as confirmed by the topographical characterization of the membrane recorded by SEM and AFM (Fig. 6.6).

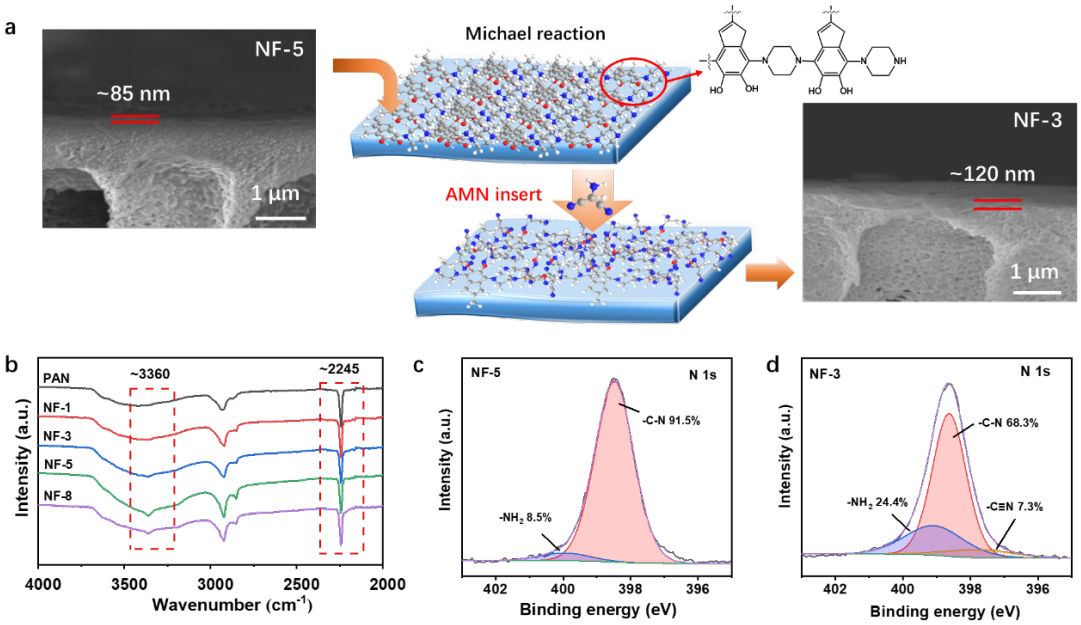

Figure 6.3 Insertion of AMN: (a) Schematic diagram of AMN insertion and the cross-sectional shape and thickness of the AMN before and after insertion, and SEM images before/after AMN insertion and membrane thickness. (b) FT-IR spectra of different selected layers. (c-d) N 1s XPS core-level scan of the selected layer before/after AMN insertion.

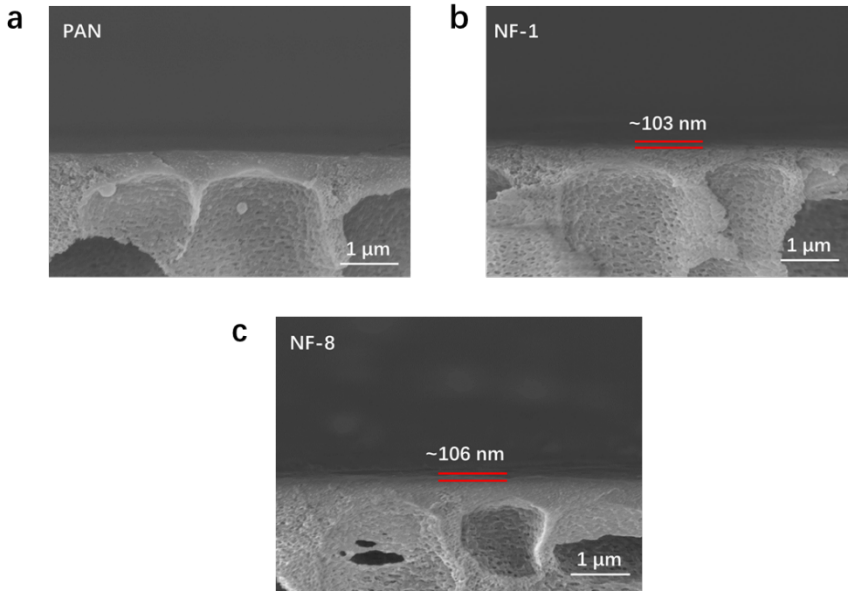

Figure 6.4 Cross-sectional morphology and thickness: (a) PAN; (b) NF-1; (c) NF-8.

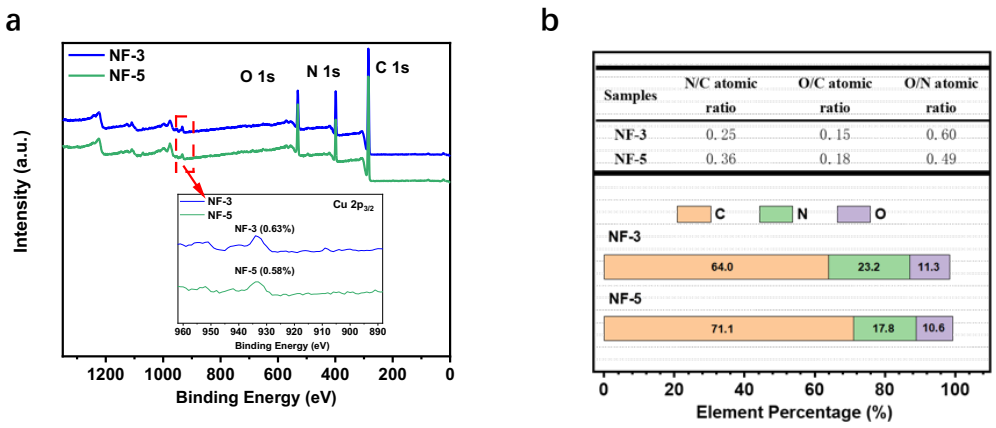

Figure 6.5 (a) XPS scan of selected layers before and after AMN insertion. (b) C, N, O element content ratio: selected layer before and after AMN insertion.

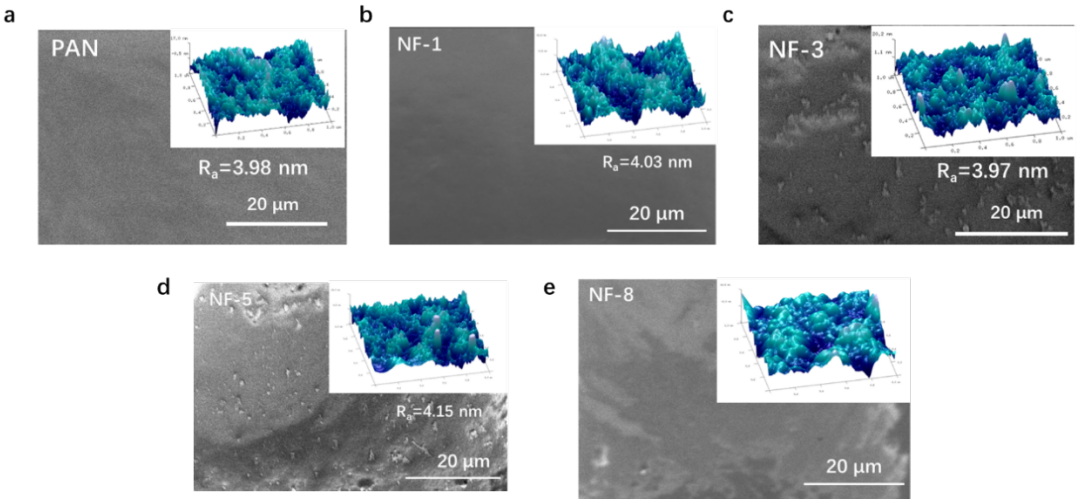

Figure 6.6 Surface morphology and roughness: (a) PAN; (b) NF-1; (c) NF-3; (d) NF-5; (e) NF-8.

6.2.3 Bifunctional Cu-TiO_2/CuO photocatalyst on the membrane

TiO_2 semiconductor material was used as the model photocatalyst because of its low-cost, non-toxic character, and commercial availability. To improve the photocatalytic performance of TiO_2, it was modified by doping Cu to TiO_2 via a facile method to obtain the Cu-TiO_2/CuO photocatalyst with a heterojunction structure [151]. Unlike conventional TiO_2 stacked into blocks (Fig. 6.7a and Fig. 6.8a), the morphology of the Cu-TiO_2/CuO is an aggregate composed of smaller stone-like nano-ions with high porosity (Fig. 6.7a) [336]. Therefore, the modified catalyst would be beneficial for mass transfer on the surface of the membrane selective layer and diffusion and charge separation of photocatalytic reactants [151]. For the modified catalyst, elemental analysis confirms the presence of Cu, Ti, and O in the modified photocatalyst, underscoring the efficacy of the modification process (Fig. 6.7b). Furthermore, the lattice spacings of TiO_2 ((101) = 0.366 nm) and CuO ((111) = 0.248 nm) in the Cu-TiO_2/CuO sample were identified (Fig. 6.7c-d) [337]. Then, TiO_2 and Cu-TiO_2/CuO photocatalysts were loaded onto the surface of the membrane to prepare a separation membrane with photocatalysts (Fig. 6.7e). The surface morphology of the membrane showed high roughness due to the well-dispersed Cu-TiO_2/CuO supported on the membrane surface, which facilitates contact with the catalytic substrate and thus improves catalytic performance (Fig. 6.8b and 6.8c) [151, 338]. Another evidence of successful Cu-TiO_2/CuO loading is apparent from the interface of the selective layer, where the catalyst layer was stably formed on the membrane surface without affecting the selective layer and without affecting the mass transfer of the membrane [94]. In comparison with the catalyst powder, the catalytic membrane showed two

characteristic peaks of CuO at 35.6° and 41.7° (red box in Fig. 6.7f), which further confirmed the successful synthesis of Cu-TiO_2/CuO nanocomposites [151, 339]. Furthermore, the presence of Ti and Cu elements in NF-14 was proven by XPS analysis (Fig. 6.7g and Fig. 6.8d and 6.8e). For the membrane loaded with TiO_2 (NF-13), the Cu peak can also be observed due to the addition of $CuSO_4$ for the self-polymerization of pDA during membrane synthesis (Fig. 6.7g). However, the Cu content and composition of NF-14 and NF-13 were different. This was revealed by the XPS spectrum of Cu 2p, where NF-3 and NF-5 (without CuO) showed a much lower intensity than those of the NF-14 and Cu-TiO_2/CuO samples (Fig. 6.8d and 6.8e). This confirms that CuO was not only present on the Cu-TiO_2 surface but was also successfully supported on the membrane.

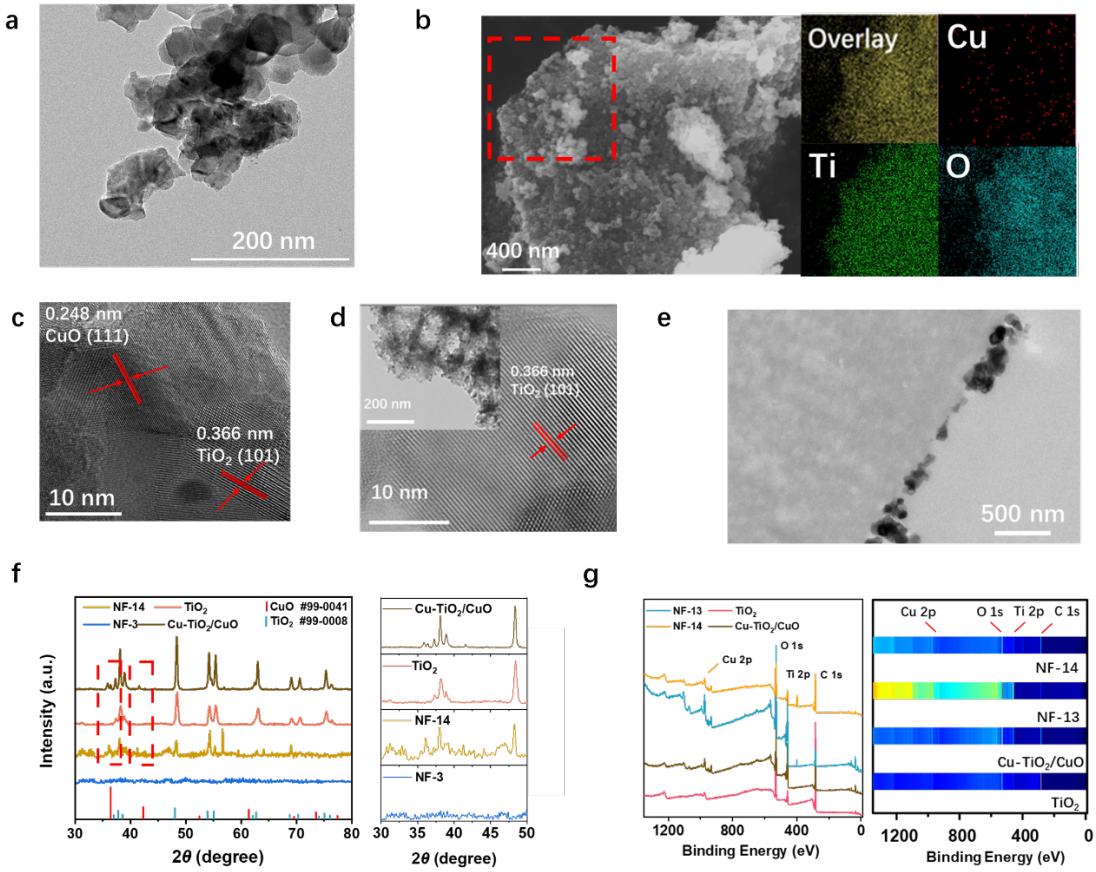

Figure 6.7 Loading of photocatalyst: (a) TEM images of Cu-TiO_2/CuO. (b) Surface morphology and element mapping of Cu-TiO_2/CuO. (c) HRTEM images and lattice spacing of Cu-TiO_2/CuO. (d) TEM cross-sectional view of the selective layer NF-14 loaded with Cu-TiO_2/CuO photocatalyst. (e) Selective layer before and after loading photocatalyst and XRD pattern of catalyst powder. (f) XPS scanning patterns of the synthesized photocatalyst and the loaded photocatalyst membrane.

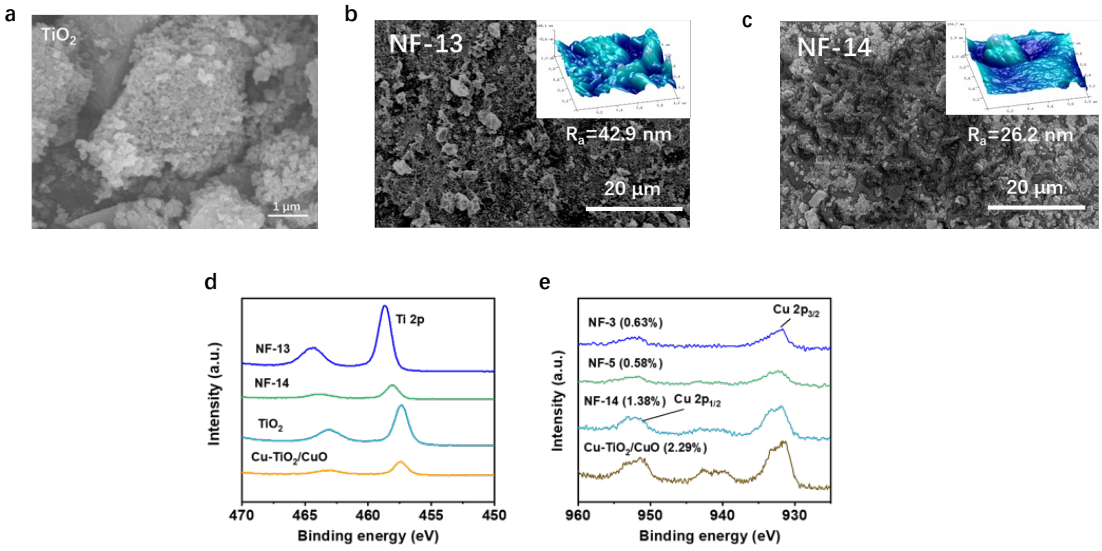

Figure 6.8 (a) Surface morphology of TiO_2. Surface morphology of the membrane loaded with photocatalyst: (b) TiO_2; (c) Cu-TiO_2/CuO. XPS scanning spectrum of: (d) Ti core-level loaded with photocatalyst selective layer and photocatalyst powder; (e) XPS scanning spectrum of Cu core-level loaded with photocatalyst selective layer and photocatalyst powder.

6.2.4 Membrane separation performance

During actual testing, the membrane synthesis conditions were optimized and filtration experiments were performed (water permeance, DR23 permeance/rejection, and Cr^{6+} permeance/rejection, where the concentrations of Cr^{6+} and dyes are comparable to that in real textile wastewater) (Fig. 6.9a and Figs. 6.10-12). The experimental results showed that the pure water permeance of the selective layer increased by 34.3% (75.3 to 114.6 LMH bar^{-1}) with the introduction of a suitable concentration of AMN, which is attributable to the fact that AMN can change the structure of the selective layer (Fig. 6.9a), thereby enhancing its sieving effect as well as its hydrophilicity to increase the mass transfer rate [335, 340]. The catalytic membrane loaded with catalyst was also investigated. Considering the particle size of the catalyst is much larger than the pore size of the selective layer, the influence of the membrane loaded with catalyst on mass transfer can be ignored. For the salt solution, the Cr^{6+} rejection of NF-3 was within 10% (Fig. 6.9b), with a good permeance due to its suitable selected layer structure. Furthermore, common salts (NaCl, Na_2SO_4, $MgCl_2$, $MgSO_4$, and $(NH_4)_2SO_4$, 1 g/L) were also filtered in textile wastewater and obtained the same effect (Fig. 6.13a) [330]. We explored the rejection of dye DR23 (200 ppm) by membranes under different synthesis conditions, and the results showed that the rejection of NF-3 reached over 99% (Fig. 6.9c). Meanwhile, the rejection of common negatively charged dyes (MO, RO16, CR, RB2, and RB5, 200 ppm) in NF-3 textile wastewater reached higher than 90% (Fig. 6.13b). Most

importantly, a comparison of the performance showed the permeance and rejection over NF-3 catalytic membrane outperforms most recently reported membranes (Table 5.2). This can be attributed to the functionality of AMN, in which the nitrogen-containing group shifts the isoelectric point on the surface of the selective layer to the right, improving the rejection of negatively charged dye molecules according to the Donnan effect (Fig. 6.9d and Fig. 6.13c) [44]. The loading of the catalyst can also move the isoelectric point on the surface of the selective layer to the right, which further increases the rejection of negatively charged dye molecules [94]. Measurement of the water contact angle further proves that insertion of AMN leads to a reduction of the water contact angle of the selective layer (36.2° to 30.7°), thereby increasing the hydrophilicity and facilitating the transport of water, which corresponds to the simulation results (Fig. 6.9e). Investigation of the actual pore size of the selective layer was performed by filtering PEG with a certain molecular weight. The results showed that the molecular weight cut-off (MWCO) of NF-3 was about 1218 Da and that the MWCO of NF-14 after loading the catalyst was 952 Da (Fig. 6.9f). Furthermore, by calculation, the pore size of the membrane is about 0.86 nm (NF-3) and 0.79 nm (NF-14) (inset in Fig. 6.9f). Interestingly, the molecular weight cut-off of NF-3 was consistent with the MD simulation pore size (0.83 nm), which indicated that the constructed MD simulation system was highly similar to the actual situation. Next, the long-term stability of NF-3 was tested with a mixed solution of Cr^{6+} (1 g/L) and DR23 (200 ppm). The results showed a compromised stability for the membrane during the cycling test, which may originate from the blocked transport channels of the selective layer caused by dye molecules during the filtration process due to the intermolecular interactions (Fig. 6.9g) [341]. In addition, tests using mixed solutions of different concentrations of Cr^{6+} and DR23 (200 ppm) were conducted; it was found that high-concentration salt solutions have negligible effect on the filtration process of NF-3, which greatly increases the practicability of NF-3 (Fig. 6.13d). Moreover, in the case of permeance and sustainable salt recovery, NF-3 and the catalyst-loaded NF-13 and NF-14 show unique advantages among those of similar studies in recent years (Fig. 6.13f). Therefore, the success of AMN insertion both enables dye/salt recovery and also provides forward-looking suggestions for this field of study.

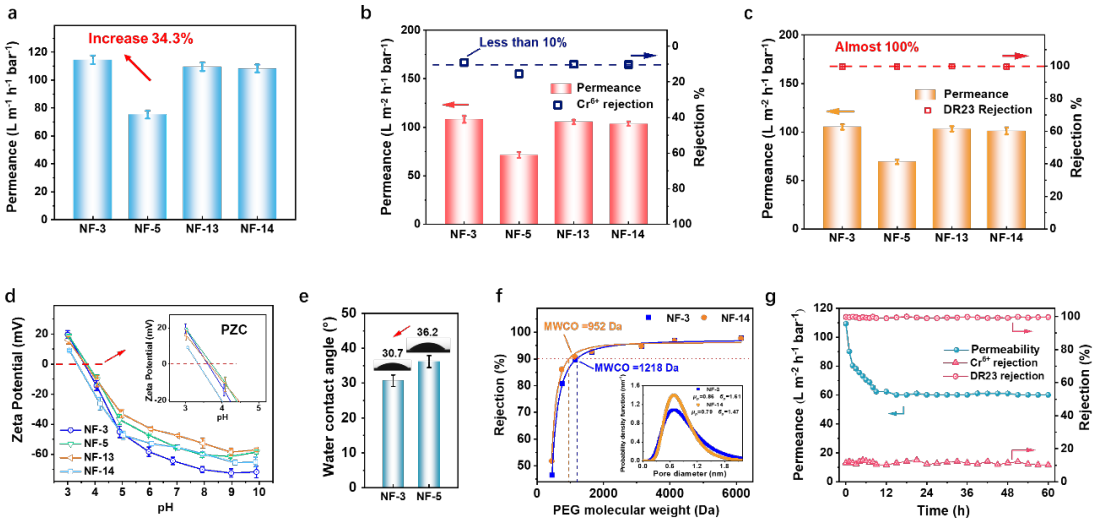

Figure 6.9 Membrane filtration performance: (a) Pure water permeance. (b) Permeance/rejection of Cr^{6+}. (c) Permeance /rejection of DR23. (d) Zeta potential and isoelectric point. (e) Water contact angle. (f) Molecular weight cut-off and pore size distribution. (g) Long-term filtration stability test for DR23/Cr^{6+} mixed solution of NF-3.

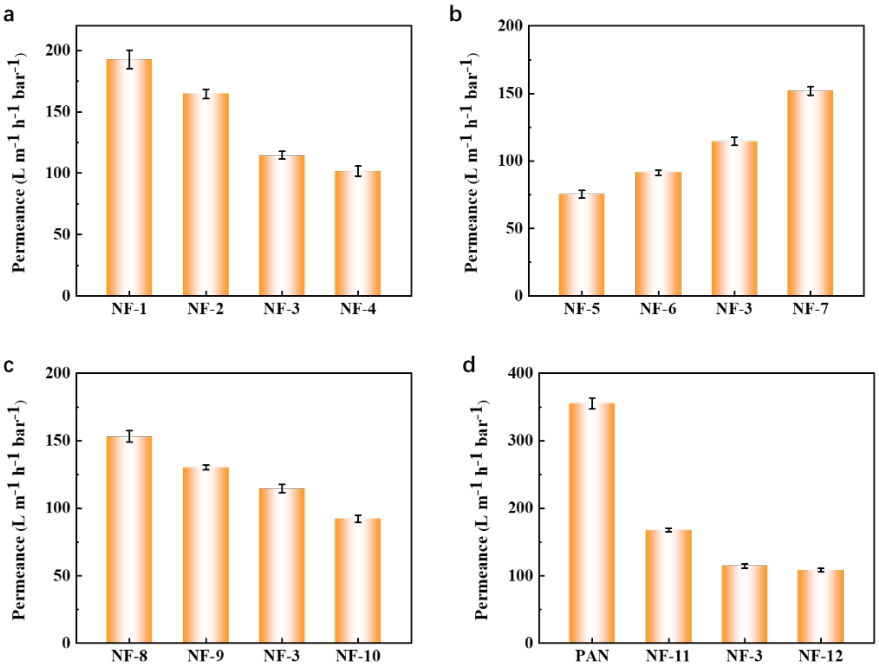

Figure 6.10 Permeance of water in selective layers: (a) DA concentrations; (b) different AMN concentrations; (c) different PIP concentrations; (d) different co-deposition time.

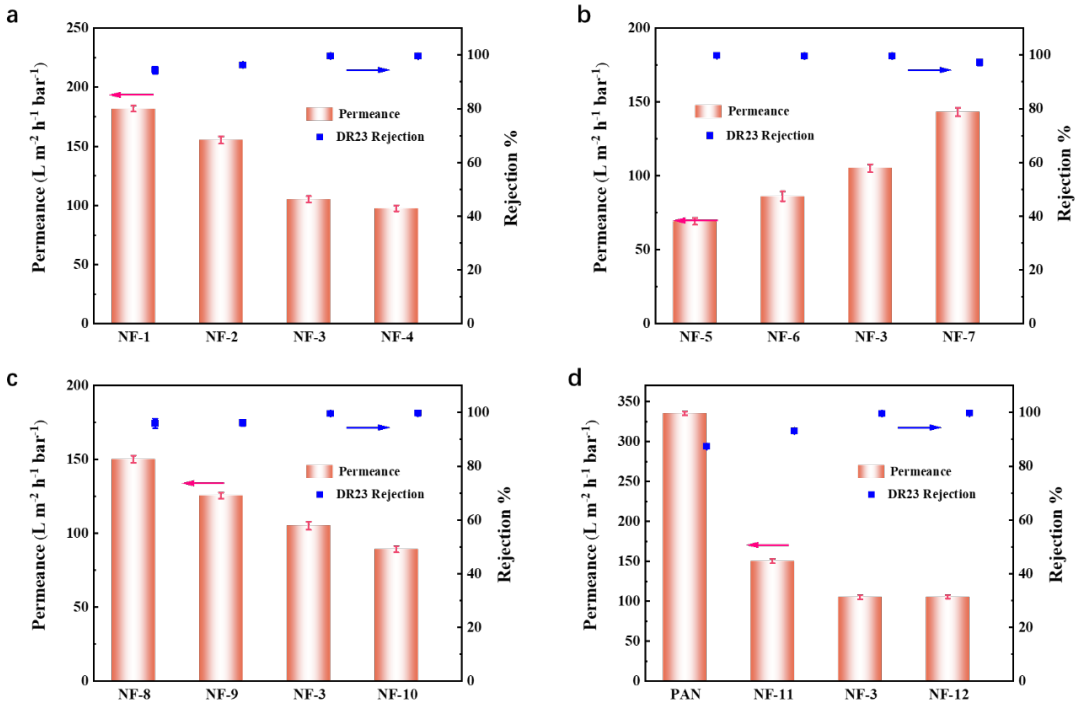

Figure 6.11 Permeance and rejection of DR23 in selective layers: (a) different pDA concentrations; (b) different AMN concentrations; (c) different PIP concentrations; (d) different co-deposition times.

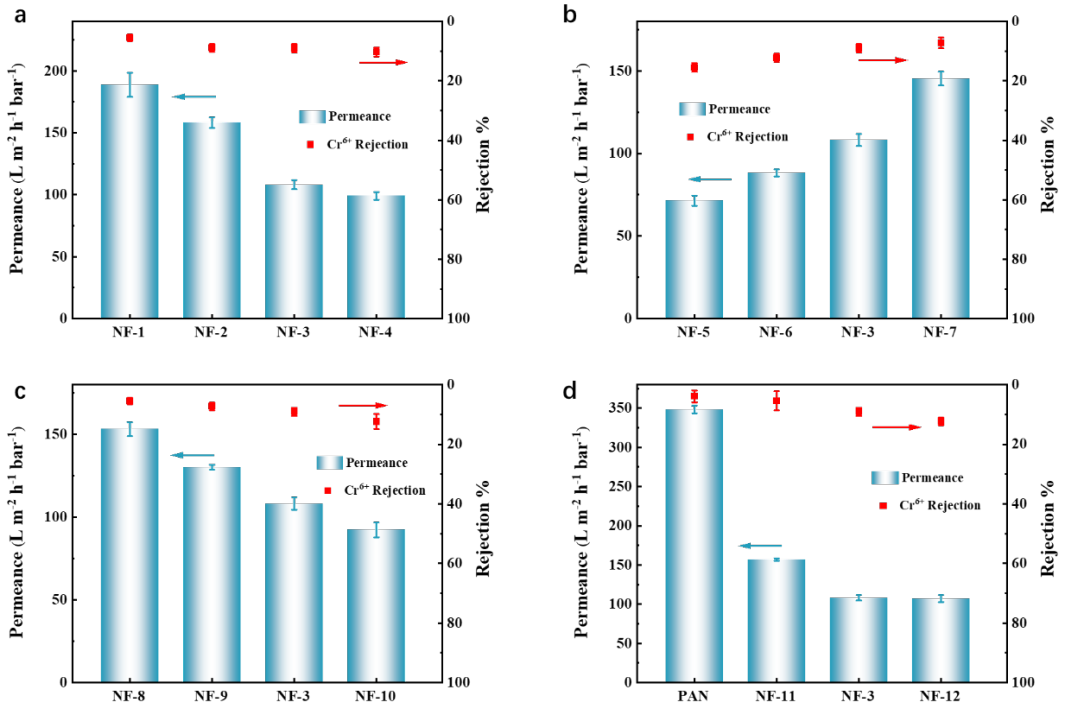

Figure 6.12 Permeance and rejection of Cr^{6+} in selective layers: (a) different pDA concentrations; (b) different AMN concentrations; (c) different PIP concentrations; (d) different co-deposition times.

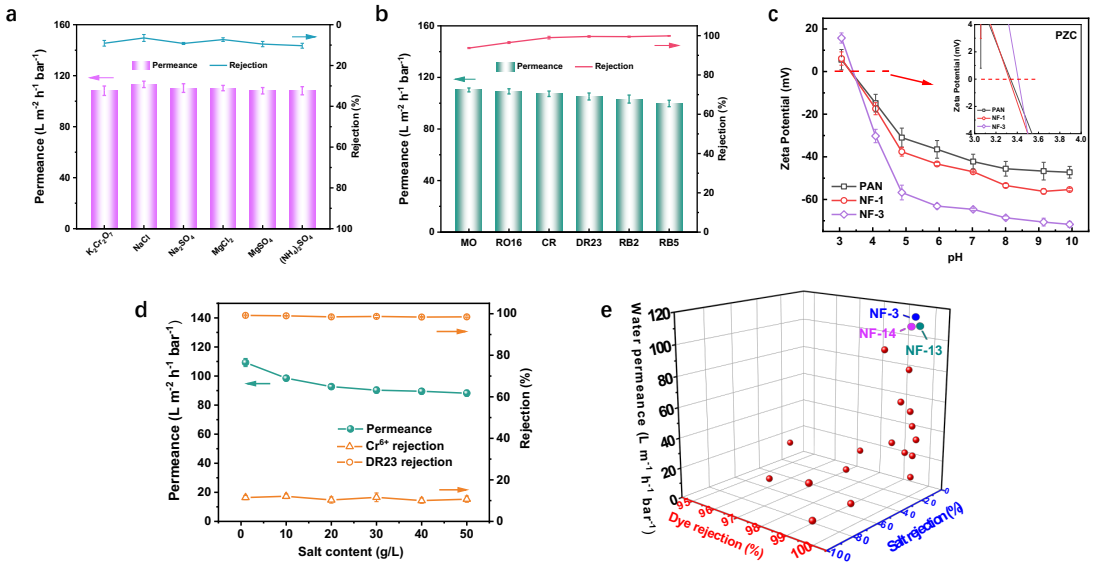

Figure 6.13 (a) Permeance and rejection of common salt in textile wastewater by NF-3. (b) Permeance and rejection of common negatively charged dyes by NF-3. (c) Zeta potential and isoelectric point. (d) Filtration test of mixed solution of with different concentrations Cr^{6+} and DR23. (e) Comparison of filtration performance: NF-3, NF-13, and NF-14 with those of recent similar reports (see Table 6.1 for specific data and references).

Table 6.1 Comparison with recently reported separation performance of similar membranes

Membrane	Permeability (LMH bar^{-1})	Types of dye	Dye rejection (%)	Types of salts	Salt rejection (%)	Refs.
NF270	12.5	Congo Red Direct Red23 Reactive Black5	99.8 99.6 99.5	Na_2SO_4 NaCl	96.3 21.7	[342]
Sugar-based	33.7	Direct red 23 Direct red 80 Reactive black 5 Reactive orange 16 Methyl orange	99.6 99.8 98.9 97.4 91.3	Na_2SO_4 $MgSO_4$ NaCl $MgCl_2$	95.0[a] 40.0[a] 60.0[a] 18.0[a]	[87]
Erythritol-based	53.23	Congo red Direct red 23 Reactive blue 2	99.6 95.2 99.6	Na_2SO_4 NaCl	11.0 5.6	[203]
POP/TMC	31.28	Reactive black 5	99.1	RB5/Na_2SO_4	15.4	[260]
Tannic acid/PEI	41.5	Congo red	99.5	Na_2SO_4 NaCl	6.00 8.00	[261]
Catechol/PEI-$CuSO_4/H_2O_2$	24.5	Congo red Reactive black 5 Methyl blue	99.8 99.7 99.3	Na_2SO_4 NaCl $MgCl_2$	12.5 2.0 0.6	[262]
Fe^{3+}-PEI@HPAN	6.0	Congo red Methyl blue Acid fuchsin Crystal violet	99.5 99.9 99.0 92.9	Na_2SO_4 NaCl $MgCl_2$ $MgSO_4$	5.9 7.5 30.5 20.6	[263]
NF-3	62.0	Direct red 23 Reactive black 5	99.6 99.2	Na_2SO_4 NaCl	20.3 12.3	[343]

CS-MMT	15.6	Reactive Black5 Reactive Red	95.0 87.0	Na_2SO_4 NaCl	22.0 5.0	[344]
PDA-rGOC3	22.8	Congo Red Reactive Blue2	99.3 99.4	Na_2SO_4 NaCl	7.4 2.5	[345]
DAT/TMC	95.1	Congo Red Direct Red	99.1 98.5	Na_2SO_4 NaCl	24.5 5.8	[172]
TA/GOQDs	11.7	Congo Red Methyl blue	99.8 97.6	Na_2SO_4 NaCl	66.7 17.2	[346]
GO/MoS2	10.2	Congo Red Methyl blue	98.5 97.4	Na_2SO_4 NaCl	65.2 43.2	[347]
3D dually charged	36.9	Congo Red Methyl blue	100.0 86.0	Na_2SO_4 NaCl	14.6 11.1	[348]
ZIF-8/PEI–HPAN	78.0	Congo Red	99.2	Na_2SO_4 NaCl	3.4 4.3	[349]
PES 30-4-0.02	15.3	Congo Red Methyl blue	97.4 99.1	Na_2SO_4 NaCl	6.0 2.7	[350]
GO/NH_2-Fe_3O_4	13.0	Congo Red Methyl blue	98.0 70.0	Na_2SO_4 NaCl	32.0 15.0	[351]
This work	114.6	Reactive Red	99.6	$K_2Cr_2O_7$	9.1	

6.2.5 Membrane self-cleaning and photocatalytic properties

Previous long-term tests showed that NF-3 has a poor antifouling performance; therefore, the antifouling abilities of NF-3, NF-13, and NF-14 were investigated under light reaction conditions. The experimental results showed that NF-13 and NF-14 loaded with the photocatalyst have good anti-fouling abilities. Under light, the photocatalyst can digest dye molecules that block the molecular transport channel of the selective layer, thereby reopening the channel (Fig. 6.14a-b and Fig. 6.15a) [94, 352]. The fouling resistance ratio (FRR) of NF-14 loaded with Cu-TiO_2/CuO can reach over 90%, which is significantly higher than that of NF-13 loaded with TiO_2 (Fig. 6.14c). In addition, radical quenching experiments and mineralization experiments of Cu-TiO_2/CuO were also conducted (Fig. 6.14d). When the experiment was carried out for 90 min, the adsorption on the membrane selective layer reached saturation. In contrast, under light conditions, the photocatalytic reaction was affected to varying degrees after the quencher was added. Among these, the addition of ert-butanol exhibited a significant impact on the catalytic system, indicating that hydroxyl radicals have the greatest impact on the system [94]. Moreover, the mineralization experiment results showed that more than 70% of DR23 can be mineralized and converted into final oxidation products. Next, *E. coli* was used to carry out an anti-biofouling test of the membrane. The experimental results showed that the anti-biofouling performance of NF-3 was attributable to the PAN support substrate because of the presence of Cu (II) element and pDA [94, 353]

(Fig. 6.14e and Fig. 6.15b). Interestingly, the Cu (II) in the NF-14 supported Cu-TiO_2/CuO photocatalyst can increase the anti-biofouling performance compared with that of NF-13. Like Bordeaux mixture (the methodology employed by viticulturists in the Bordeaux region of France during the late 19th century for addressing fungal infestations affecting grapevine cultivation), Cu (II) has been used to inhibit the activity of enzymes in microorganisms to achieve anti-biofouling [354]. Because of its excellent catalytic ability, Cu-TiO_2/CuO can reduce the harmful Cr^{6+} in the feed to Cr^{3+} after penetrating the membrane and also oxidize the dye molecules that block the molecular transport channels, resulting in a synergistic effect of oxidation and reduction. In addition, the experimental conditions were optimized to determine the best working state of NF-14 (Figs. 5.15c-d). The experimental findings demonstrate that the optimal pollutant removal efficacy is achieved when the mixed solution's concentration is below 50 mg/L and the DR23/Cr^{6+} concentration ratio is maintained at 1:1. This aligns with the dye concentration range (10-50 mg/L) and the chromium ion concentration range (1-10 mg/L) typically observed in real textile wastewater, thus imparting valuable reference potential for process feed optimization [153, 355]. Then, long-term photocatalytic filtration experiments were performed on a TiO_2 supported membrane (NF-13) and a Cu-TiO_2/CuO supported membrane (NF-14) with cross-flow mode, using membrane modules equipped with quartz glass (insert in Fig. 6.14f). The experimental results showed that both NF-13 and NF-14 had a good pollutant removal efficiency and that the removal of DR23 was close to 100% due to membrane rejection (Fig. 6.14f). Moreover, due to the photocatalytic reduction of Cu-TiO_2/CuO on NF-14, more than 70% of Cr^{6+} in the permeate was reduced, which is greater than that of TiO_2 in NF-13 (Fig. 6.14f). Its photocatalytic mechanism is discussed in the next section.

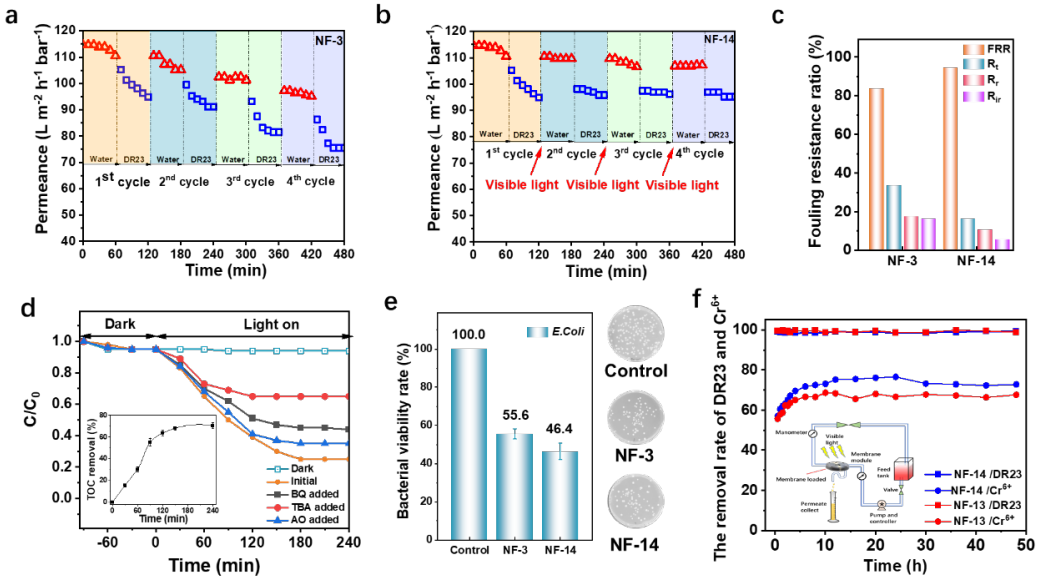

Figure 6.14 Membrane self-cleaning and photocatalytic properties: (a-b) Self-cleaning test for NF-3 and NF-14. (c) Fouling resistance ratio of NF-3 and NF-14. (d) Static catalysis and quenching experiment of Cu-TiO_2/CuO on DR23 (the inset is the mineralization efficiency of Cu-TiO_2/CuO to DR23). (e) Anti-biofouling properties of membranes and real shot of the anti-biofouling effect of the membrane in Luria–Bertani broth liquid medium. (f) Photocatalyst-loaded membranes for pollutant separation/removal by actual filtration.

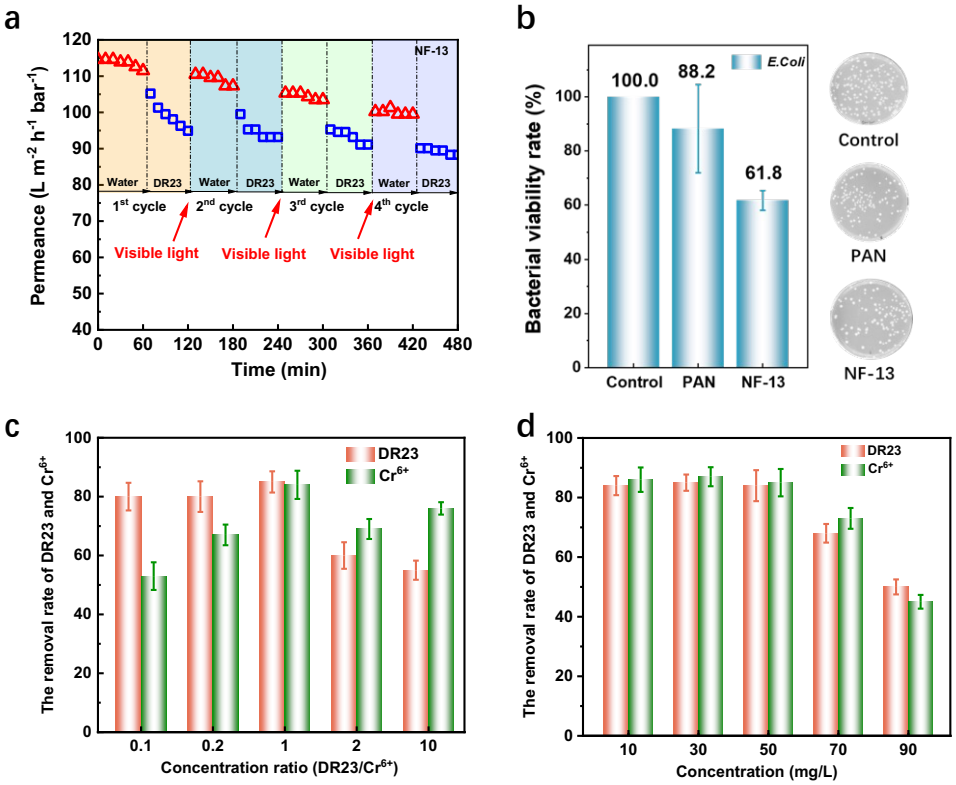

Figure 6.15 (a) Self-cleaning test for NF-13. (b) Anti-biofouling properties: membranes and real shot of the anti-biofouling effect of the membrane in Luria–Bertani broth liquid medium. (c) Photocatalytic degradation of DR23/Cr^{6+}: different concentration ratios of Cu-TiO_2/CuO powder. (d) Photocatalytic degradation of DR23/Cr^{6+}: different feed concentrations.

6.2.6 Photocatalytic mechanism

The photocatalysts (TiO_2 and Cu-TiO_2/CuO) and the corresponding loaded photocatalytic membrane have obvious absorption peaks at visible light wavelengths of 300–435 nm (Fig. 6.16a), which is different from the case of NF-3 without photocatalyst. This supports the photo-responsiveness of the membrane with the supported catalysts in the visible light range. Furthermore, the band gaps of the catalyst powder and the selective layer supporting the catalyst powder were calculated according to the converted Kubelka–Munk model (Fig. 6.17a), showing that the band gaps of the Cu-TiO_2/CuO powder and its supported NF-14 were 2.20 eV and 1.76 eV, respectively. These gaps are lower than those of TiO_2 powder (2.77 eV) and its loaded NF-13 (1.99 eV). Cu doping and intimate contact with CuO can systematically reduce the band gap of TiO_2 and enhance its visible-light absorption ability, which is beneficial for achieving high photocatalytic activity (Fig. 6.17a) [356, 357]. The carrier dynamics of the photocatalysts were explored using steady-state photoluminescence (PL) and time-resolved PL spectroscopy. The results showed that the Cu-modified photocatalyst (Cu-TiO_2/CuO) can significantly reduce the PL emission intensity of TiO_2 (Fig. 6.16b). This suggests that the suppressed recombination rate of the photogenerated charges can enhance the probability of carriers participating in photoredox reactions, thereby enhancing the catalytic activity of the photocatalysts. This is combined by time-resolved PL measurements (Fig. 6.16c), showing that Cu-TiO_2/CuO has a longer lifetime than the blank TiO_2, thus contributing to the catalytic performance [151, 358, 359]. Furthermore, the photogenerated carrier transfer efficiency of the two photocatalysts was also investigated by evaluating their transient photocurrent response (Fig. 6.16d). Clearly, the transient photocurrent intensity was significantly enhanced after using Cu to modify the TiO_2, indicating that Cu-TiO_2/CuO has a stronger separation and transfer of photoinduced carriers. This was further confirmed by linear sweep voltammetry test (Fig. 6.17b), where a higher current density was achieved on the Cu-TiO_2/CuO sample [360]. To uncover the reason, the electrochemical impedance spectroscopy (EIS) of the materials was measured. The results showed that Cu-TiO_2/CuO sample possesses a smaller semicircle radius in the Nyquist plot than TiO_2, indicating a reduced transfer resistance in the modified sample (Fig. 6.16e) [151]. In addition, to study the internal mechanism at the microscopic level, DFT calculations were performed. When Cu was incorporated into TiO_2, the band-edge charges were dispersed (Fig. 6.16f and Fig. 6.17c), so the charges were transferred more easily. Furthermore, after CuO and Cu-TiO_2 form a heterojunction, the new

interface formed is more conducive to the transport of charges (Fig. 6.16f and Fig. 6.17c) [361, 362]. These results demonstrate more efficient charge carrier generation and migration in Cu-TiO_2/CuO than in unmodified TiO_2, which thereby contributes to the photocatalytic performance enhancement. Moreover, the synergistic catalytic processes of dye degradation and heavy metal reduction were fully demonstrated for loading on the membrane.

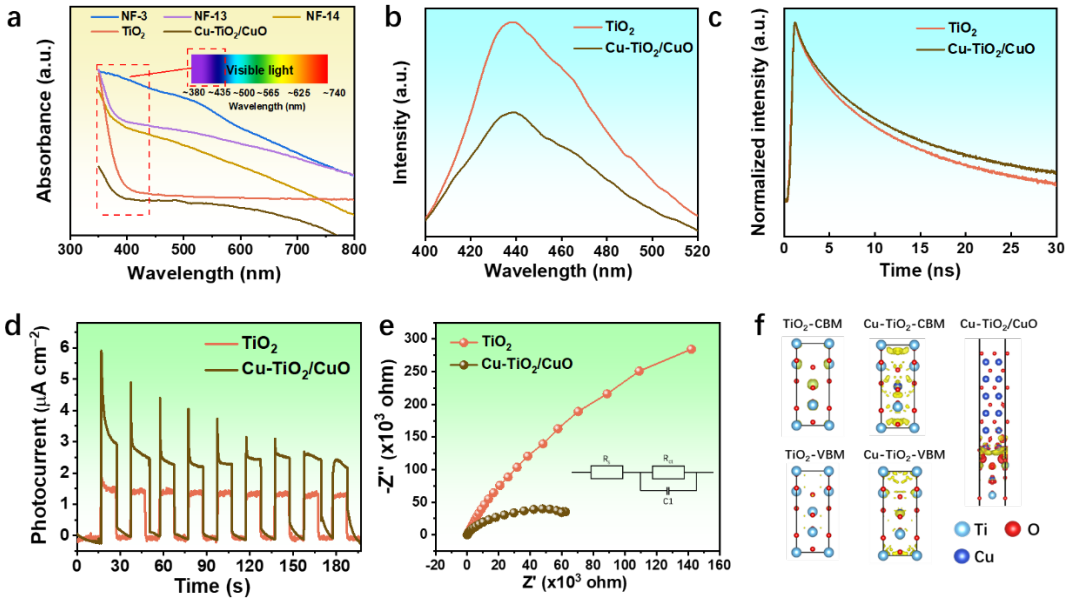

Figure 6.16 Photocatalytic mechanism investigation: (a) UV-Vis absorption spectrum of photocatalyst powders and membranes. (b) steady-state PL spectra, (c) Time-resolved PL decay traces, (d) Photocurrent curves, (e) Nyquist plots of TiO_2 and Cu-TiO_2/CuO. (f) DFT calculation results (yellow and cyan colors represent charge accumulation and depletion zones, respectively).

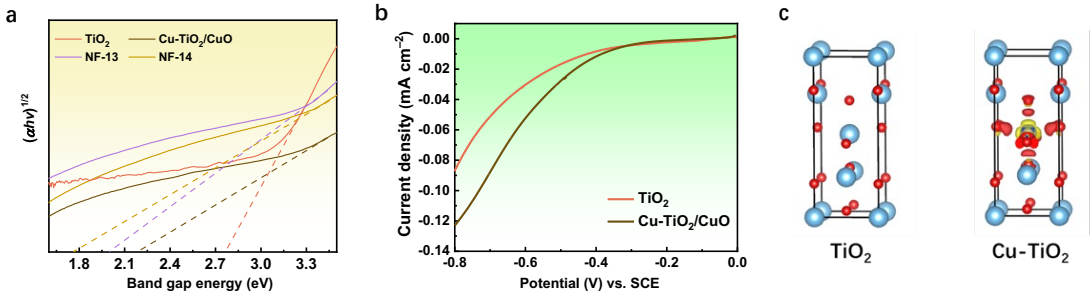

Figure 6.17 (a) Corresponding Tauc plots of photocatalyst powders and membrane bandgap values. (b) Linear sweep voltammetry (LSV) of TiO_2 and Cu-TiO_2/CuO. (c) Graphical structure during DFT calculation.

6.3 Conclusion

The insertion of AMN into the pDA/PIP selective layer to modify the membrane structure and thereby substantially enhance the membrane permeance was reported in this chapter. The synergistic photocatalyst Cu-TiO_2/CuO is introduced to engender a synergistic catalytic process that concurrently catalyzes the degradation of dye compounds and the reduction of Cr^{6+}. Thus, a synergistic photocatalytic membrane with fast mass transfer was obtained. Both experimental and simulated data (DFT and MD) confirmed the change in permeability properties of the membrane and the higher photocatalytic ability. These comprehensive features enable the membrane to achieve excellent textile wastewater treatment capabilities: high permeance (34.3% higher than conventional selective layers), high rejection of dyes, and efficient catalytic reduction of heavy metals. In addition, the membrane also showed strong robustness, mainly reflected in better self-cleaning ability, bio-fouling resistance, and long-term stability. The proposed scheme is expected to offer a guideline for next-generation non-hazardous wastewater treatment.

Chapter 7: General conclusions and further research

7.1 General Conclusions

Nanofiltration membrane separation technology has garnered considerable attention in water purification and resource recovery realms, due to its distinct advantages such as energy efficiency, environmental compatibility, absence of added chemicals, and established large-scale applicability. Nevertheless, the practicality and robustness of nanofiltration membranes significantly constrain their widespread adoption. This thesis addresses the robustness of nanofiltration membranes, particularly focusing on their antifouling properties, biological antifouling properties, and resistance to acid/alkali environments. Through targeted efforts, a series of robust nanofiltration membranes is developed to mitigate these limitations. Concerning the practicality of nanofiltration membranes, this study synthesizes a range of novel nanofiltration membranes by considering synthesis methods and the realization of sustainable water treatment solutions. The objective is to furnish nanofiltration technology with technical support for diverse applications in water treatment processes. The specific conclusions drawn from this PhD thesis are as follows:

(1) A positively charged membrane tailored for efficient dye/salt separation was developed via a straightforward procedure inspired by prebiotic chemistry. This method involved the application of an AMN coating and the Mannich reaction between PEI and THPC. The resulting membrane demonstrates a rapid mass transfer, boasting a water permeance of 30.7 LMH bar^{-1}. This allows for effective removal of dyes, achieving a remarkable rate of 99.5%, while maintaining a salt rejection of below 10%, thus facilitating resource reclamation in textile wastewater treatment processes. Through a rigorous 60-hour long-term stability assessment, the membrane showcased consistent performance in dye/salt separation and proficient separation in dye/salt mixed solutions even under high salt concentrations. Furthermore, the membrane's inherent antifouling and antibacterial attributes were verified, underscoring its resilience against fouling and microbial proliferation. In a landscape where pDA-based and interfacial polymeric membranes dominate textile wastewater treatment, this innovative 'crossover combination' approach offers fresh insights for membrane fabrication in dye/salt separation endeavors.

(2) A resilient and highly efficient solute transport membrane was synthesized through chemical cross-linking, leveraging a blend of pDA/β-cyclodextrin and host-guest interactions. This membrane facilitates rapid separation of dyes and salts present in textile wastewater, showcasing robustness adaptable to diverse applications. Its deployment aids in resource recovery during textile wastewater treatment, ensuring prolonged stability across a broad pH range. Noteworthy are its exceptional self-cleaning properties and antibacterial efficacy. By harnessing specific molecular transport channels, the membrane optimizes solute transport under consistent energy input, thereby enhancing resource recycling in textile wastewater processes. This approach stands out for its sustainability and energy efficiency, supported by the membrane's unmatched durability. Its versatility enables application across various domains, laying the groundwork for potential large-scale implementation.

(3) A swift solute transport membrane tailored for dye/salt separation was devised, leveraging the host-guest interaction between β-cyclodextrin and pDA in supramolecular chemistry, complemented by interfacial polymerization. To combat membrane fouling, an AgBr-Ag_3PO_4 photocatalyst with a stable structure was synthesized *in-situ* on the membrane surface, enabling rapid decomposition of contaminants under visible light. Filtration trials employing synthetic DSM membranes showcased high dye rejections and minimal salt rejection, alongside expedited solute transport during filtration. Moreover, the incorporated photocatalyst endowed the membrane with notable self-cleaning and antifouling characteristics. Extensive characterization of the synthesized photocatalyst affirmed its stable support on the membrane surface and demonstrated high catalytic activity. Consequently, this approach presents a promising avenue for addressing resource recovery and secondary utilization in textile wastewater treatment processes.

(4) AMN was inserted into the pDA/PIP selective layer to modify the membrane structure, resulting in a substantial enhancement of membrane permeance. Additionally, a synergistic photocatalyst, Cu-TiO_2/CuO, was introduced to facilitate a concurrent catalytic process for degrading dye compounds and reducing Cr^{6+}. This led to the development of a synergistic photocatalytic membrane with fast mass transfer. Both experimental and simulated data (utilizing DFT and MD) confirmed the change in permeability properties of the membrane and its higher photocatalytic ability. These comprehensive features enable the membrane to achieve excellent textile wastewater treatment capabilities, including high permeance (34.3% higher than conventional selective layers), high rejection of dyes, and efficient catalytic reduction of heavy metals. Additionally, the membrane

exhibited strong robustness, particularly in terms of enhanced self-cleaning ability, resistance to bio-fouling, and long-term stability. The proposed scheme is expected to offer a guideline for next-generation non-hazardous wastewater treatment.

7.2 Recommendations and future research

Although this thesis provides several better ways to improve the robustness and practicality of nanofiltration membranes, however, these efforts still have some limitations.

(1) **In chapter 3,** while this study has focused on developing electropositive membranes through the Mannich reaction of PEI and THPC, as well as the application of bioinspired AMN coatings for modification, it has encountered several significant limitations. Firstly, despite demonstrating promising potential for the simultaneous and effective separation of dyes and salts, the membrane's separation efficiency may be compromised when dealing with high-concentration salt mixtures, particularly in practical industrial scenarios such as treating dye and salt-laden wastewater from textile production, where challenges may be more intricate. Secondly, although some assessment of the membrane's long-term stability has been conducted, further protracted experimentation is necessary to substantiate its longevity and dependability under genuine operational conditions. Furthermore, while the membranes have exhibited certain capabilities in terms of antifouling and antibacterial properties, prolonged exposure to real-world industrial environments may pose heightened challenges, including the accumulation of contaminants and the presence of complex microbial communities. Hence, while this study presents an innovative approach to addressing the efficient separation of dyes and salts, additional research and refinement are imperative to ascertain its practical applicability and sustainability within industrial settings.

(2) **In chapter 4,** the examination of PBG-3 membrane filtration performance acknowledges certain constraints inherent in the study. It highlights the potential influence exerted by external variables, including alterations in feed water composition and operating parameters, on the membrane's enduring stability and efficacy. While this investigation comprehensively encompasses membrane synthesis and characterization, inquiries regarding scalability and cost-effectiveness pertinent to large-scale industrial implementation remain sparse. The membrane's specific focus on the separation of particular dyes and salts from textile effluents may restrict its broader applicability to

diverse contaminants or industrial effluent streams. Despite exhibiting promising attributes such as robustness, self-purging capabilities, pH resilience, and antimicrobial functionality, further refinement is imperative to tackle impediments such as fouling mechanisms and sustained resilience in authentic operational scenarios. Thus, although PBG-3 membranes hold promise for addressing dyeing wastewater treatment, additional research endeavors are warranted to surmount these limitations and ascertain their pragmatic viability.

(3) **In chapter 5,** while this investigation yields valuable insights into the advancement and efficacy of dye/salt separation membranes (DSM), several constraints and inadequacies merit acknowledgment. Firstly, the research predominantly centers on membrane modification and characterization, neglecting a thorough exploration of the scalability and practicability of the proposed membranes for large-scale deployment. Moreover, a comprehensive analysis of the long-term stability and durability is absent, crucial elements in evaluating the viability of DSMs within practical contexts. Additionally, a more meticulous examination of the environmental repercussions and potential hazards associated with the utilization of photocatalytic materials is warranted, considering their plausible discharge into aquatic environments during operational phases. Furthermore, this inquiry primarily scrutinizes filtration performance under controlled laboratory conditions, necessitating further validation under diverse environmental and operational variables to accurately gauge real-world applicability. Lastly, while emphasizing the efficacy of photocatalyst-modified membranes in dye contaminant degradation, elucidation of the photocatalytic degradation mechanism is essential for enhanced comprehension and optimization of membrane design to elevate performance standards.

(4) **In Chapter 6,** the development of loose nanofiltration membranes (LNMs) for water treatment is examined in depth, focusing on sustainability and resource recovery. However, several critical limitations emerge. Firstly, the reliance on laboratory-scale experiments and simulations highlights the necessity for validation in real-world scenarios through field trials or pilot-scale studies to ensure scalability and performance under practical conditions. Secondly, while the study touches upon potential environmental benefits like self-cleaning properties and reduced heavy metal ion concentrations, a comprehensive environmental impact assessment is lacking, particularly regarding energy consumption, raw material sourcing, and waste generation during membrane fabrication. Thirdly, uncertainties persist regarding the long-term stability of LNMs, especially in terms of fouling resistance and anti-biofouling properties, necessitating extended studies under continuous

operation, especially in challenging industrial wastewater treatment settings. Furthermore, the absence of substantial real-world application data, especially in textile wastewater treatment plants, impedes conclusive findings. Finally, the scalability and cost-effectiveness of membrane fabrication methods require in-depth exploration, including comparative cost-benefit analyses and techno-economic assessments. Addressing these limitations would not only enhance the robustness and applicability of the study's findings but also provide a clearer understanding of the potential of LNMs for sustainable water treatment applications.

Based on this, the following are some suggestions for further research:

Predictive modeling of nanofiltration membrane processes:

The utilization of the extended Nernst-Planck equation provides a fundamental framework for modeling the transport of numerous ions and dissolved species across nanofiltration membranes. However, prevailing modeling efforts have predominantly focused on dilute and simplified solutions containing a limited number of ions. To accurately model concentrated multicomponent electrolyte solutions relevant for industrial applications, a transition to modeling systems of genuine industrial significance is imperative. Critically evaluating the suitability of current modeling approaches, particularly for concentrated multicomponent separations crucial for industrial processes such as desalination, highlights existing shortcomings. These deficiencies include an insufficient understanding of the physical properties and physicochemical phenomena within nanopores, particularly related to activity coefficients, water layer organization at the solid-liquid interface, and basic physical properties. Addressing these challenges requires the development of new methodologies to understand complex interactions and physical phenomena such as membrane charge and particle-membrane interactions. Additionally, innovative approaches are needed to handle the intensive mathematics inherent in such systems.

Innovative methods for nanofiltration membrane manufacturing:

Advances in nanotechnology have revolutionized the manufacturing of nanofiltration membranes, with thin-film composites and nanocomposite nanofiltration membranes manufactured through interfacial polymerization becoming the benchmark. While techniques such as UV or photografting, electron beam irradiation, plasma grafting, and layer-by-layer methods have shown promise for small-

scale development in laboratory settings, challenges have arisen in scaling up production for industrial applications. The exploration of novel nanomaterials and additives to enhance membrane properties and performance emphasizes the need for further studies to elucidate their effects on membrane structure, morphology, and solute transport. Additionally, it is critical to evaluate the safety and environmental impacts of these materials, especially in drinking water treatment applications. Tailoring nanofiltration membranes to achieve specific selectivity by controlling manufacturing parameters has the potential to significantly optimize performance. In addition, the sustainability of the membrane manufacturing process cannot be ignored. Especially today when the topic of "permanent chemicals" is increasingly being discussed, it is very important to use green solvents and more sustainable support substrates. Developing green solvents and finding green polymer substrates to replace existing traditional processes are our future development directions.

Long-term techno-economic research on nanofiltration membrane processes:

Although nanofiltration membranes show promise in various applications, there are limited studies on their large-scale, long-term operation. Techno-economic evaluations, especially pilot-scale evaluations, are critical to assess process feasibility, profitability, fouling control strategies, and membrane compatibility with the complex feeds encountered in industrial settings. Integrating nanofiltration with other processes, especially in desalination applications, offers a promising approach to improving process efficiency and water quality. Reliable simulation and modeling can guide the design and operation of integrated/hybrid processes, minimizing reliance on expensive experimental studies.

New applications for nanofiltration membranes:

Known for their selectivity towards salts and organic solutes, nanofiltration membranes continue to find a variety of applications, including the removal of emerging contaminants and water recycling. Optimizing nanofiltration membrane utilization and integrating renewable energy sources in water recycling scenarios provide a path to sustainable water treatment solutions. In addition, in actual production, attention should be paid to the relevant economic and technical cost analysis, and the overall process should be grasped. In the actual process, attention should be paid to energy consumption and accounting, as well as the boundary conditions of the actual application process.

References

[1] I. Abdelfattah, A. El-Shamy, Review on the escalating imperative of zero liquid discharge (ZLD) technology for sustainable water management and environmental resilience, Journal of Environmental Management 351 (2024) 119614.

[2] S. Mousavinezhad, S. Nili, A. Fahimi, E. Vahidi, Environmental impact assessment of direct lithium extraction from brine resources: Global warming potential, land use, water consumption, and charting sustainable scenarios, Resources, Conservation and Recycling 205 (2024) 107583.

[3] Y. Shevah, Impact of persistent droughts on the quality of the middle east water resources, Separation science and technology, Elsevier2019, pp. 51-84.

[4] B. Chellaney, Water, peace, and war: Confronting the global water crisis, Rowman & Littlefield2013.

[5] M.T. Van Vliet, E.R. Jones, M. Flörke, W.H. Franssen, N. Hanasaki, Y. Wada, J.R. Yearsley, Global water scarcity including surface water quality and expansions of clean water technologies, Environmental Research Letters 16(2) (2021) 024020.

[6] A. Abdelfattah, S.S. Ali, H. Ramadan, E.I. El-Aswar, R. Eltawab, S.-H. Ho, T. Elsamahy, S. Li, M.M. El-Sheekh, M. Schagerl, Microalgae-based wastewater treatment: Mechanisms, challenges, recent advances, and future prospects, Environmental Science and Ecotechnology 13 (2023) 100205.

[7] J.P. Vareda, A.J. Valente, L. Durães, Assessment of heavy metal pollution from anthropogenic activities and remediation strategies: A review, Journal of environmental management 246 (2019) 101-118.

[8] K.H. Vardhan, P.S. Kumar, R.C. Panda, A review on heavy metal pollution, toxicity and remedial measures: Current trends and future perspectives, Journal of Molecular Liquids 290 (2019) 111197.

[9] I. Ali, Q. Cheng, T. Ding, Q. Yiguang, Z. Yuechao, H. Sun, C. Peng, I. Naz, J. Li, J. Liu, Micro- and nanoplastics in the environment: Occurrence, detection, characterization and toxicity–A critical review, Journal of Cleaner Production 313 (2021) 127863.

[10] N. Mushtaq, D.V. Singh, R.A. Bhat, M.A. Dervash, O.b. Hameed, Freshwater contamination: sources and hazards to aquatic biota, Fresh water pollution dynamics and remediation (2020) 27-50.

[11] M.U. Rehman, B. Nisar, A.M. Yatoo, N. Sehar, R. Tomar, L. Tariq, S. Ali, A. Ali, S.M. Rashid, S.B. Ahmad, After effects of Pharmaceuticals and Personal Care Products (PPCPs) on the biosphere and their counteractive ways, Separation and Purification Technology (2024) 126921.

[12] A. Ding, R. Zhang, H.H. Ngo, X. He, J. Ma, J. Nan, G. Li, Life cycle assessment of sewage sludge treatment and disposal based on nutrient and energy recovery: A review, Science of the Total Environment 769 (2021) 144451.

[13] A.J. Reid, A.K. Carlson, I.F. Creed, E.J. Eliason, P.A. Gell, P.T. Johnson, K.A. Kidd, T.J. MacCormack, J.D. Olden, S.J. Ormerod, Emerging threats and persistent conservation challenges for freshwater biodiversity, Biological reviews 94(3) (2019) 849-873.

[14] K. Gunaalan, E. Fabbri, M. Capolupo, The hidden threat of plastic leachates: A critical review on their impacts on aquatic organisms, Water Research 184 (2020) 116170.

[15] M.N. Rahman, S.H. Shozib, M.Y. Akter, A.R.M.T. Islam, M.S. Islam, M.S. Sohel, C. Kamaraj, M.R.J. Rakib, A.M. Idris, A. Sarker, Microplastic as an invisible threat to the coral reefs: sources, toxicity mechanisms, policy intervention, and the way forward, Journal of Hazardous Materials 454 (2023) 131522.

[16] L. Salamé, D.C. McKinney, J. Delli Priscoli, T. Koike, J. Moss, M. Tignino, O. McIntyre, H. Hussein, M. Motlagh, A.T. Wolf, Water discourses, Handbook of Water Resources Management: Discourses, Concepts and Examples, Springer2021, pp. 145-214.

[17] V. Bytyqi, F. Morina, The International Standards on the Protection of the Environment through Criminal Law-Special Focus on the EU Directive on Environmental Crime, Polish Journal of Environmental Studies 32(2) (2023).

[18] R. Ardiyanti, K. Azrague, G. Medema, C. Hallé, Navigating quality, health and environmental risk: A novel framework for wastewater resource recovery products, Journal of Cleaner Production 434 (2024) 140260.

[19] V. Mitsilegas, E. Fasoli, F. Giuffrida, M. Fitzmaurice, Environmental Crime at the EU Level: The Role of EU Agencies and Bodies, The Legal Regulation of Environmental Crime, Brill Nijhoff2022, pp. 233-285.

[20] M. Stanhope, J. Lancaster, Public health nursing: Population-centered health care in the community, Elsevier Health Sciences2015.

[21] S. Manikandan, R. Subbaiya, M. Saravanan, M. Ponraj, M. Selvam, A. Pugazhendhi, A critical review of advanced nanotechnology and hybrid membrane based water recycling, reuse, and wastewater treatment processes, Chemosphere 289 (2022) 132867.

[22] C.A. Quist-Jensen, F. Macedonio, E. Drioli, Membrane technology for water production in agriculture: Desalination and wastewater reuse, Desalination 364 (2015) 17-32.

[23] N.N.R. Ahmad, W.L. Ang, C.P. Leo, A.W. Mohammad, N. Hilal, Current advances in membrane technologies for saline wastewater treatment: A comprehensive review, Desalination 517 (2021) 115170.

[24] S. Li, X. Wang, Y. Guo, J. Hu, S. Lin, Y. Tu, L. Chen, Y. Ni, L. Huang, Recent advances on cellulose-based nanofiltration membranes and their applications in drinking water purification: A review, Journal of Cleaner Production 333 (2022) 130171.

[25] B. Mustafa, T. Mehmood, Z. Wang, A.G. Chofreh, A. Shen, B. Yang, J. Yuan, C. Wu, Y. Liu, W. Lu, Next-generation graphene oxide additives composite membranes for emerging organic micropollutants removal: Separation, adsorption and degradation, Chemosphere 308 (2022) 136333.

[26] N. Albayati, Z.A. Naser, H.A.B. Ahmed, M. Kadhom, P.O. Oladoye, A comprehensive review on the use of Ti3C2Tx MXene in membrane-based water treatment, Separation and Purification Technology (2024) 127448.

[27] D. Lu, Z. Yao, L. Jiao, M. Waheed, Z. Sun, L. Zhang, Separation mechanism, selectivity enhancement strategies and advanced materials for mono-/multivalent ion-selective nanofiltration membrane, Advanced Membranes 2 (2022) 100032.

[28] A.M. Nasir, M.R. Adam, S.N.E.A.M. Kamal, J. Jaafar, M.H.D. Othman, A.F. Ismail, F. Aziz, N. Yusof, M.R. Bilad, R. Mohamud, A review of the potential of conventional and advanced membrane technology in the removal of pathogens from wastewater, Separation and Purification Technology 286 (2022) 120454.

[29] S. Wang, L. Yang, G. He, B. Shi, Y. Li, H. Wu, R. Zhang, S. Nunes, Z. Jiang, Two-dimensional nanochannel membranes for molecular and ionic separations, Chemical Society Reviews 49(4) (2020) 1071-1089.

[30] S. Kim, K.H. Chu, Y.A. Al-Hamadani, C.M. Park, M. Jang, D.-H. Kim, M. Yu, J. Heo, Y. Yoon, Removal of contaminants of emerging concern by membranes in water and wastewater: A review, Chemical Engineering Journal 335 (2018) 896-914.

[31] J. Zheng, R. Zhao, A.A. Uliana, Y. Liu, D. de Donnea, X. Zhang, D. Xu, Q. Gao, P. Jin, Y. Liu, Separation of textile wastewater using a highly permeable resveratrol-based loose nanofiltration membrane with excellent anti-fouling performance, Chemical Engineering Journal 434 (2022) 134705.

[32] J. Li, L. Fang, D. Xu, X. Zhang, L. Jiang, Q. Zhu, Q. Chen, P. Jin, A. Volodine, R. Dewil, Intercalation of small molecules in the selective layer of polyamide nanofiltration membranes facilitates the separation of Mg2+/Li+, Chemical Engineering Journal 487 (2024) 150659.

[33] Y. Liu, G. Van Eygen, S. Yuan, H. Wang, M. Chi, D. Xu, Q. Gao, G. Li, J. Zheng, B. Van der Bruggen, Facile and novel fabrication of high-performance loose nanofiltration membranes for textile wastewater recovery, Separation and Purification Technology 308 (2023) 122867.

[34] X. Zhang, P. Jin, D. Xu, J. Zheng, Z.-M. Zhan, Q. Gao, S. Yuan, Z.-L. Xu, B. Van der Bruggen, Triethanolamine modification produces ultra-permeable nanofiltration membrane with enhanced removal efficiency of heavy metal ions, Journal of Membrane Science 644 (2022) 120127.

[35] A. Foglia, J. González-Camejo, S. Radini, M. Sgroi, K. Li, A.L. Eusebi, F. Fatone, Transforming wastewater treatment plants into reclaimed water facilities in water-unbalanced regions. An overview of possibilities and recommendations focusing on the Italian case, Journal of Cleaner Production (2023) 137264.

[36] G. Szekely, M.F. Jimenez-Solomon, P. Marchetti, J.F. Kim, A.G. Livingston, Sustainability assessment of organic solvent nanofiltration: from fabrication to application, Green Chemistry 16(10) (2014) 4440-4473.

[37] P. Vandezande, L.E. Gevers, I.F. Vankelecom, Solvent resistant nanofiltration: separating on a molecular level, Chemical Society Reviews 37(2) (2008) 365-405.

[38] Y.J. Lim, K. Goh, M. Kurihara, R. Wang, Seawater desalination by reverse osmosis: Current development and future challenges in membrane fabrication–A review, Journal of Membrane Science 629 (2021) 119292.

[39] T. Wei, Y. Zhao, M. Zhou, Z. Zhang, Y. Wei, A.E. Núñez, Initial concept and embodiment to develop modular constructed wetland: A unique and promising solution to sustainability transitions in water management, Journal of Cleaner Production 450 (2024) 141912.

[40] N.N.R. Ahmad, A.W. Mohammad, E. Mahmoudi, W.L. Ang, C.P. Leo, Y.H. Teow, An overview of the modification strategies in developing antifouling nanofiltration membranes, Membranes 12(12) (2022) 1276.

[41] L. Liu, Y. Liu, X. Chen, S. Feng, Y. Wan, H. Lu, J. Luo, A nanofiltration membrane with outstanding antifouling ability: exploring the structure-property-performance relationship, Journal of Membrane Science 668 (2023) 121205.

[42] Q. Gao, D. Bouwen, S. Yuan, X. Gui, Y. Xing, J. Zheng, H. Ling, Q. Zhu, Y. Wang, S. Depuydt, Robust loose nanofiltration membrane with fast solute transfer for dye/salt separation, Journal of Membrane Science 674 (2023) 121518.

[43] D. Xu, J. Zheng, X. Zhang, D. Lin, Q. Gao, X. Luo, X. Zhu, G. Li, H. Liang, B. Van der Bruggen, Mechanistic insights of a thermoresponsive interface for fouling control of thin-film composite nanofiltration membranes, Environmental Science & Technology 56(3) (2022) 1927-1937.

[44] X. Luo, Y. Wang, Y. Guo, Q. Gao, R. Zhao, Y. Liu, R. Liu, L. Jiang, Z. Mai, H. Matsuyama, Cleanable natural-sugar-alcohol-based polyester membrane for highly efficient molecular separation, Resources, Conservation and Recycling 198 (2023) 107149.

[45] Q. Gao, J. Li, P. Jin, J. Zheng, D. Xu, B. Van der Bruggen, The Practical Application Value of a Sustainable Water Purification Process Is Crucial, ACS ES&T Water 3(8) (2023) 1990-1993.

[46] A.I. Osman, Z. Chen, A.M. Elgarahy, M. Farghali, I.M. Mohamed, A. Priya, H.B. Hawash, P.S. Yap, Membrane Technology for Energy Saving: Principles, Techniques, Applications, Challenges, and Prospects, Advanced Energy and Sustainability Research (2024) 2400011.

[47] B. Ramasubramanian, S. Sundarrajan, R.P. Rao, M. Reddy, V. Chellappan, S. Ramakrishna, Novel low-carbon energy solutions for powering emerging wearables, smart textiles, and medical devices, Energy & Environmental Science 15(12) (2022) 4928-4981.

[48] N.A. Khan, E.A. López-Maldonado, A. Majumder, S. Singh, R. Varshney, J. López, P. Méndez, P.C. Ramamurthy, M.A. Khan, A.H. Khan, A state-of-art-review on emerging contaminants: Environmental chemistry, health effect, and modern treatment methods, Chemosphere (2023) 140264.

[49] R. Wang, S. Lin, Pore model for nanofiltration: History, theoretical framework, key predictions, limitations, and prospects, Journal of Membrane Science 620 (2021) 118809.

[50] A.W. Mohammad, Y. Teow, W. Ang, Y. Chung, D. Oatley-Radcliffe, N. Hilal, Nanofiltration membranes review: Recent advances and future prospects, Desalination 356 (2015) 226-254.

[51] I. Wenten, M.Z. Bazant, K. Khoiruddin, Mitigating electrodialysis membrane fouling in seawater desalination, Separation and Purification Technology (2024) 127228.

[52] I. Sadeghi, P. Kaner, A. Asatekin, Controlling and expanding the selectivity of filtration membranes, Chemistry of Materials 30(21) (2018) 7328-7354.

[53] A.S. Al-Amoudi, Factors affecting natural organic matter (NOM) and scaling fouling in NF membranes: A review, Desalination 259(1-3) (2010) 1-10.

[54] G. Blandin, A.R. Verliefde, J. Comas, I. Rodriguez-Roda, P. Le-Clech, Efficiently combining water reuse and desalination through forward osmosis—reverse osmosis (FO-RO) hybrids: a critical review, Membranes 6(3) (2016) 37.

[55] R.V. Linares, Z. Li, S. Sarp, S.S. Bucs, G. Amy, J.S. Vrouwenvelder, Forward osmosis niches in seawater desalination and wastewater reuse, Water research 66 (2014) 122-139.

[56] D.M. Warsinger, S. Chakraborty, E.W. Tow, M.H. Plumlee, C. Bellona, S. Loutatidou, L. Karimi, A.M. Mikelonis, A. Achilli, A. Ghassemi, A review of polymeric membranes and processes for potable water reuse, Progress in polymer science 81 (2018) 209-237.

[57] Y. Qi, L. Zhu, X. Shen, A. Sotto, C. Gao, J. Shen, Polythyleneimine-modified original positive charged nanofiltration membrane: removal of heavy metal ions and dyes, Separation and Purification Technology 222 (2019) 117-124.

[58] H. Wu, H. Zhao, Y. Lin, X. Liu, L. Wang, H. Yao, Y. Tang, L. Yu, H. Wang, X. Wang, Positively-charged PEI/TMC nanofiltration membrane prepared by adding a diamino-silane coupling agent for Li+/Mg2+ separation, Journal of Membrane Science 672 (2023) 121468.

[59] L.Y. Ng, A.W. Mohammad, C.Y. Ng, A review on nanofiltration membrane fabrication and modification using polyelectrolytes: Effective ways to develop membrane selective barriers and rejection capability, Advances in colloid and interface science 197 (2013) 85-107.

[60] K. Wang, X. Wang, B. Januszewski, Y. Liu, D. Li, R. Fu, M. Elimelech, X. Huang, Tailored design of nanofiltration membranes for water treatment based on synthesis–property–performance relationships, Chemical Society Reviews 51(2) (2022) 672-719.

[61] C. Ji, S. Xue, Y.-J. Tang, X.-H. Ma, Z.-L. Xu, Polyamide membranes with net-like nanostructures induced by different charged mofs for elevated nanofiltration, ACS Applied Polymer Materials 2(2) (2019) 585-593.

[62] M. Vallet-Regí, F. Schüth, D. Lozano, M. Colilla, M. Manzano, Engineering mesoporous silica nanoparticles for drug delivery: where are we after two decades?, Chemical Society Reviews 51(13) (2022) 5365-5451.

[63] Q. Gao, B. Weng, P. Jin, S. Yuan, X. Gui, J. Zheng, D. Xu, Y. Wang, A. Volodine, L. Sun, Rapid solute transfer photocatalytic membrane: The combination of host–guest interaction and photocatalyst load, Chemical Engineering Journal 446 (2022) 137316.

[64] J. Luo, Y. Wan, Mix-charged nanofiltration membrane: Engineering charge spatial distribution for highly selective separation, Chemical Engineering Journal 464 (2023) 142689.

[65] L. Yang, X. Xiao, S. Shen, J. Lama, M. Hu, F. Jia, Z. Han, H. Qu, L. Huang, Y. Wang, Recent advances in graphene oxide membranes for nanofiltration, ACS Applied Nano Materials 5(3) (2022) 3121-3145.

[66] H. Adenusi, G.A. Chass, S. Passerini, K.V. Tian, G. Chen, Lithium batteries and the solid electrolyte interphase (SEI)—progress and outlook, Advanced Energy Materials 13(10) (2023) 2203307.

[67] S. Al Aani, T.N. Mustafa, N. Hilal, Ultrafiltration membranes for wastewater and water process engineering: A comprehensive statistical review over the past decade, Journal of Water Process Engineering 35 (2020) 101241.

[68] T.D. Lu, Q. Wang, S.S. Gu, S.P. Sun, Beyond Symmetry: Exploring Asymmetric Electrospun Nanofiber Membranes for Liquid Separation, Advanced Functional Materials 34(10) (2024) 2310218.

[69] P. Goh, T. Matsuura, A. Ismail, N. Hilal, Recent trends in membranes and membrane processes for desalination, Desalination 391 (2016) 43-60.

[70] Z. Wan, Y. Jiang, Synthesis-structure-performance relationships of nanocomposite polymeric ultrafiltration membranes: A comparative study of two carbon nanofillers, Journal of Membrane Science 620 (2021) 118847.

[71] Y. Sun, S. Zhou, G. Qin, J. Guo, Q. Zhang, S. Li, S. Zhang, A chemical-induced crystallization strategy to fabricate poly (ether ether ketone) asymmetric membranes for organic solvent nanofiltration, Journal of Membrane Science 620 (2021) 118899.

[72] Y. Zhao, T. Tong, X. Wang, S. Lin, E.M. Reid, Y. Chen, Differentiating solutes with precise nanofiltration for next generation environmental separations: a review, Environmental Science & Technology 55(3) (2021) 1359-1376.

[73] P. Marchetti, M.F. Jimenez Solomon, G. Szekely, A.G. Livingston, Molecular separation with organic solvent nanofiltration: a critical review, Chemical reviews 114(21) (2014) 10735-10806.

[74] C. Liu, W. Bi, D. Chen, S. Zhang, H. Mao, Positively charged nanofiltration membrane fabricated by poly (acid–base) complexing effect induced phase inversion method for heavy metal removal, Chinese journal of chemical engineering 25(11) (2017) 1685-1694.

[75] Q. Zhao, Q.F. An, Y. Ji, J. Qian, C. Gao, Polyelectrolyte complex membranes for pervaporation, nanofiltration and fuel cell applications, Journal of membrane science 379(1-2) (2011) 19-45.

[76] J. Borges, J.F. Mano, Molecular interactions driving the layer-by-layer assembly of multilayers, Chemical reviews 114(18) (2014) 8883-8942.

[77] J. Lee, Y. Shin, C. Boo, S. Hong, Performance, limitation, and opportunities of acid-resistant nanofiltration membranes for industrial wastewater treatment, Journal of Membrane Science 666 (2023) 121142.

[78] M.O. Mavukkandy, S.A. McBride, D.M. Warsinger, N. Dizge, S.W. Hasan, H.A. Arafat, Thin film deposition techniques for polymeric membranes–A review, Journal of membrane science 610 (2020) 118258.

[79] L. Wang, N. Wang, J. Li, J. Li, W. Bian, S. Ji, Layer-by-layer self-assembly of polycation/GO nanofiltration membrane with enhanced stability and fouling resistance, Separation and Purification Technology 160 (2016) 123-131.

[80] C. Ding, X. Qin, Y. Tian, B. Cheng, PES membrane surface modification via layer-by-layer self-assembly of GO@ TiO2 for improved photocatalytic performance, Journal of Membrane Science 659 (2022) 120789.

[81] F. Zhang, J.b. Fan, S. Wang, Interfacial polymerization: from chemistry to functional materials, Angewandte Chemie International Edition 59(49) (2020) 21840-21856.

[82] X. Li, Z. Wang, X. Han, Y. Liu, C. Wang, F. Yan, J. Wang, Regulating the interfacial polymerization process toward high-performance polyamide thin-film composite reverse osmosis and nanofiltration membranes: A review, Journal of Membrane Science 640 (2021) 119765.

[83] D. Wu, Y. Huang, S. Yu, D. Lawless, X. Feng, Thin film composite nanofiltration membranes assembled layer-by-layer via interfacial polymerization from polyethylenimine and trimesoyl chloride, Journal of membrane science 472 (2014) 141-153.

[84] Y. Liu, Z. Xin, M. Wang, X. Wang, H. Zhang, Z. Wang, Optimizing separation layer structure of polyamide composite membrane for high permselectivity based on post-treatment: A review, Desalination (2024) 117585.

[85] G.M. Shi, Y. Feng, B. Li, H.M. Tham, J.-Y. Lai, T.-S. Chung, Recent progress of organic solvent nanofiltration membranes, Progress in Polymer Science 123 (2021) 101470.

[86] L.E. Peng, Z. Yang, L. Long, S. Zhou, H. Guo, C.Y. Tang, A critical review on porous substrates of TFC polyamide membranes: Mechanisms, membrane performances, and future perspectives, Journal of Membrane Science 641 (2022) 119871.

[87] J. Zheng, Y. Liu, J. Zhu, P. Jin, T. Croes, A. Volodine, S. Yuan, B. Van der Bruggen, Sugar-based membranes for nanofiltration, Journal of Membrane Science 619 (2021) 118786.

[88] J. Luo, B. Zhou, C. Dong, R. He, Y. Zhang, T. He, Effect of substrate morphology on characteristics of layer-by-layer self-assembly nanofiltration membrane for micropollutants removal, Desalination 574 (2024) 117229.

[89] W. Lau, A. Ismail, P. Goh, N. Hilal, B. Ooi, Characterization methods of thin film composite nanofiltration membranes, Separation & Purification Reviews 44(2) (2015) 135-156.

[90] T.M. Joseph, H.E. Al-Hazmi, B. Śniatała, A. Esmaeili, S. Habibzadeh, Nanoparticles and nanofiltration for wastewater treatment: From polluted to fresh water, Environmental Research (2023) 117114.

[91] K. Sathya, K. Nagarajan, G. Carlin Geor Malar, S. Rajalakshmi, P. Raja Lakshmi, A comprehensive review on comparison among effluent treatment methods and modern methods of treatment of industrial wastewater effluent from different sources, Applied Water Science 12(4) (2022) 70.

[92] N. Diaz-Elsayed, N. Rezaei, T. Guo, S. Mohebbi, Q. Zhang, Wastewater-based resource recovery technologies across scale: a review, Resources, Conservation and Recycling 145 (2019) 94-112.

[93] S. Khan, A. Malik, Environmental and health effects of textile industry wastewater, Environmental deterioration and human health: Natural and anthropogenic determinants (2014) 55-71.

[94] Q. Gao, Q. Zhu, J. Zheng, S. Yuan, Y. Wang, R. Zhao, Y. Liu, X. Gui, C. Wang, A. Volodine, Positively charged membranes for dye/salt separation based on a crossover combination of Mannich reaction and prebiotic chemistry, Journal of Hazardous Materials 440 (2022) 129744.

[95] P. Mondal, A. Nandan, S. Ajithkumar, N.A. Siddiqui, S. Raja, A.K. Kola, D. Balakrishnan, Sustainable application of nanoparticles in wastewater treatment: Fate, current trend & paradigm shift, Environmental Research (2023) 116071.

[96] S. Natarajan, Resource recovery from dye wastewaters using nanofiltration systems, Resource Recovery in Industrial Waste Waters, Elsevier2023, pp. 229-252.

[97] J. Lin, W. Ye, H. Zeng, H. Yang, J. Shen, S. Darvishmanesh, P. Luis, A. Sotto, B. Van der Bruggen, Fractionation of direct dyes and salts in aqueous solution using loose nanofiltration membranes, Journal of Membrane Science 477 (2015) 183-193.

[98] C. Xing, J. Han, X. Pei, Y. Zhang, J. He, R. Huang, S. Li, C. Liu, C. Lai, L. Shen, Tunable graphene oxide nanofiltration membrane for effective dye/salt separation and desalination, ACS Applied Materials & Interfaces 13(46) (2021) 55339-55348.

[99] L. Yang, X. Liu, X. Zhang, T. Chen, Z. Ye, M.S. Rahaman, High performance nanocomposite nanofiltration membranes with polydopamine-modified cellulose nanocrystals for efficient dye/salt separation, Desalination 521 (2022) 115385.

[100] N.N.R. Ahmad, W.L. Ang, Y.H. Teow, A.W. Mohammad, N. Hilal, Nanofiltration membrane processes for water recycling, reuse and product recovery within various industries: A review, Journal of Water Process Engineering 45 (2022) 102478.

[101] W. Ye, R. Liu, X. Chen, Q. Chen, J. Lin, X. Lin, B. Van der Bruggen, S. Zhao, Loose nanofiltration-based electrodialysis for highly efficient textile wastewater treatment, Journal of membrane science 608 (2020) 118182.

[102] J. Dasgupta, J. Sikder, S. Chakraborty, S. Curcio, E. Drioli, Remediation of textile effluents by membrane based treatment techniques: a state of the art review, Journal of environmental management 147 (2015) 55-72.

[103] N.H.H. Hairom, C.F. Soon, R.M.S.R. Mohamed, M. Morsin, N. Zainal, N. Nayan, C.Z. Zulkifli, N.H. Harun, A review of nanotechnological applications to detect and control surface water pollution, Environmental Technology & Innovation 24 (2021) 102032.

[104] J. Hoslett, T.M. Massara, S. Malamis, D. Ahmad, I. van den Boogaert, E. Katsou, B. Ahmad, H. Ghazal, S. Simons, L. Wrobel, Surface water filtration using granular media and membranes: A review, Science of the Total Environment 639 (2018) 1268-1282.

[105] C. Zwiener, Trihalomethanes (THMs), Haloacetic Acids (HAAs), and Emerging Disinfection By-products in Drinking Water, Organic Pollutants in the Water Cycle: Properties, Occurrence, Analysis and Environmental Relevance of Polar Compounds (2006) 251-286.

[106] G. Moradi, R. Heydari, S. Zinadini, M. Rahimi, F. Gholami, High-performance nanofiltration membranes consisting of the new functionalized mesoporous for enhanced antifouling attributes and simultaneous removal of salts, dyes and heavy metals, Environmental Technology & Innovation 24 (2021) 101929.

[107] Z. Stevanović, Karst waters in potable water supply: a global scale overview, Environmental Earth Sciences 78(23) (2019) 662.

[108] T.L. Silva, S. Morales-Torres, S. Castro-Silva, J.L. Figueiredo, A.M. Silva, An overview on exploration and environmental impact of unconventional gas sources and treatment options for produced water, Journal of environmental management 200 (2017) 511-529.

[109] A. Podder, A.A. Sadmani, D. Reinhart, N.-B. Chang, R. Goel, Per and poly-fluoroalkyl substances (PFAS) as a contaminant of emerging concern in surface water: A transboundary review of their occurrences and toxicity effects, Journal of hazardous materials 419 (2021) 126361.

[110] M.N. Soliman, F.Z. Guen, S.A. Ahmed, H. Saleem, M.J. Khalil, S.J. Zaidi, Energy consumption and environmental impact assessment of desalination plants and brine disposal strategies, Process Safety and Environmental Protection 147 (2021) 589-608.

[111] A. Srivastava, R. Singh, V.D. Rajput, T. Minkina, S. Agarwal, M.C. Garg, A systematic approach towards optimization of brackish groundwater treatment using nanofiltration (NF) and reverse osmosis (RO) hybrid membrane filtration system, Chemosphere 303 (2022) 135230.

[112] D. Zhou, L. Zhu, Y. Fu, M. Zhu, L. Xue, Development of lower cost seawater desalination processes using nanofiltration technologies—A review, Desalination 376 (2015) 109-116.

[113] I. Owusu-Agyeman, J. Shen, A.I. Schäfer, Renewable energy powered membrane technology: Impact of pH and ionic strength on fluoride and natural organic matter removal, Science of the total environment 621 (2018) 138-147.

[114] P. Nativ, O. Leifman, O. Lahav, R. Epsztein, Desalinated brackish water with improved mineral composition using monovalent-selective nanofiltration followed by reverse osmosis, Desalination 520 (2021) 115364.

[115] Y.-N. Wang, K. Goh, X. Li, L. Setiawan, R. Wang, Membranes and processes for forward osmosis-based desalination: Recent advances and future prospects, Desalination 434 (2018) 81-99.

[116] P. Goh, W. Lau, M. Othman, A. Ismail, Membrane fouling in desalination and its mitigation strategies, Desalination 425 (2018) 130-155.

[117] Y. Song, X. Gao, T. Li, C. Gao, J. Zhou, Improvement of overall water recovery by increasing RNF with recirculation in a NF–RO integrated membrane process for seawater desalination, Desalination 361 (2015) 95-104.

[118] A. Matin, T. Laoui, W. Falath, M. Farooque, Fouling control in reverse osmosis for water desalination & reuse: Current practices & emerging environment-friendly technologies, Science of the total Environment 765 (2021) 142721.

[119] A. Abou-Shady, H. El-Araby, Electro-agric, a novel environmental engineering perspective to overcome the global water crisis via marginal water reuse, Natural Hazards Research 1(4) (2021) 202-226.

[120] S.F. Anis, R. Hashaikeh, N. Hilal, Reverse osmosis pretreatment technologies and future trends: A comprehensive review, Desalination 452 (2019) 159-195.

[121] S. Dutta, B.M. Patel, Y. Singh, G. Hegde, S. Bose, Photocatalytic driven ‘self-cleaning’IPN membranes infused with a ‘host-guest’pair consisting of metal-organic framework encapsulated anionic ‘nano-clusters’ for water remediation, Journal of Membrane Science 694 (2024) 122422.

[122] A. Asatekin, E.A. Olivetti, A.M. Mayes, Fouling resistant, high flux nanofiltration membranes from polyacrylonitrile-graft-poly (ethylene oxide), Journal of Membrane Science 332(1-2) (2009) 6-12.

[123] I. Michael-Kordatou, C. Michael, X. Duan, X. He, D. Dionysiou, M. Mills, D. Fatta-Kassinos, Dissolved effluent organic matter: characteristics and potential implications in wastewater treatment and reuse applications, Water Research 77 (2015) 213-248.

[124] K. Elsaid, A. Olabi, A. Abdel-Wahab, A. Elkamel, A.H. Alami, A. Inayat, K.-J. Chae, M.A. Abdelkareem, Membrane processes for environmental remediation of nanomaterials: Potentials and challenges, Science of The Total Environment 879 (2023) 162569.

[125] A. Mahto, K. Aruchamy, R. Meena, M. Kamali, S.K. Nataraj, T.M. Aminabhavi, Forward osmosis for industrial effluents treatment–sustainability considerations, Separation and purification technology 254 (2021) 117568.

[126] A. Azarafza, M.A. Islam, Y. Golpazirsorkheh, I. Efteghar, M. Sadrzadeh, M. Kamkar, A.F. Shojaei, M. Younas, T.M. Aminabhavi, M. Rezakazemi, Aquaporin‐Based Biomimetic Membranes for Low Energy Water Desalination and Separation Applications, Advanced Functional Materials 33(21) (2023) 2213326.

[127] D.S. Mallya, S. Abdikheibari, L.F. Dumée, S. Muthukumaran, W. Lei, K. Baskaran, Removal of natural organic matter from surface water sources by nanofiltration and surface engineering membranes for fouling mitigation–A review, Chemosphere 321 (2023) 138070.

[128] X. Shi, G. Tal, N.P. Hankins, V. Gitis, Fouling and cleaning of ultrafiltration membranes: A review, Journal of Water Process Engineering 1 (2014) 121-138.

[129] R.R. Choudhury, J.M. Gohil, S. Mohanty, S.K. Nayak, Antifouling, fouling release and antimicrobial materials for surface modification of reverse osmosis and nanofiltration membranes, Journal of Materials Chemistry A 6(2) (2018) 313-333.

[130] A. Al-Amoudi, R.W. Lovitt, Fouling strategies and the cleaning system of NF membranes and factors affecting cleaning efficiency, Journal of membrane science 303(1-2) (2007) 4-28.

[131] Y. Song, Q. Hu, T. Li, Y. Sun, X. Chen, J. Fan, Fabrication and characterization of phosphorylated chitosan nanofiltration membranes with tunable surface charges and improved selectivities, Chemical Engineering Journal 352 (2018) 163-172.

[132] J.M. Solaiman, N. Rajamohan, M. Yusuf, H. Kamyab, Nanocomposite ceramic membranes as novel tools for remediation of textile dye waste water–A review of current applications, machine learning based modeling and future perspectives, Journal of Environmental Chemical Engineering (2024) 112353.

[133] E.M. Hoek, M. Elimelech, Cake-enhanced concentration polarization: a new fouling mechanism for salt-rejecting membranes, Environmental science & technology 37(24) (2003) 5581-5588.

[134] Y. Cao, X. Chen, S. Feng, Y. Wan, J. Luo, Nanofiltration for decolorization: membrane fabrication, applications and challenges, Industrial & Engineering Chemistry Research 59(45) (2020) 19858-19875.

[135] V. Geraldes, P. Henriques, M.D. Afonso, A.M. Alves, R.F. Pires, M. Faria, B. Van der Bruggen, M. Rodrigues, fDesigning Centrifugal Membrane Filters with Uniform-Pressure for UF/NF/RO separations, Journal of Membrane Science (2024) 122752.

[136] H.-R. Zuo, P. Shi, M. Duan, A review on thermally stable membranes for water treatment: Material, fabrication, and application, Separation and Purification Technology 236 (2020) 116223.

[137] M.U. Farid, J.A. Kharraz, J. Sun, M.W. Boey, M.A. Riaz, P.W. Wong, M. Jia, X. Zhang, B.J. Deka, N.K. Khanzada, Advancements in nanoenabled membrane distillation for a sustainable water-energy-environment nexus, Advanced Materials 36(17) (2024) 2307950.

[138] D. Wu, J. Martin, J.R. Du, Y. Zhang, D. Lawless, X. Feng, Effects of chlorine exposure on nanofiltration performance of polyamide membranes, Journal of membrane science 487 (2015) 256-270.

[139] A. Yusuf, A. Sodiq, A. Giwa, J. Eke, O. Pikuda, G. De Luca, J.L. Di Salvo, S. Chakraborty, A review of emerging trends in membrane science and technology for sustainable water treatment, Journal of cleaner production 266 (2020) 121867.

[140] T. Chidambaram, Y. Oren, M. Noel, Fouling of nanofiltration membranes by dyes during brine recovery from textile dye bath wastewater, Chemical Engineering Journal 262 (2015) 156-168.

[141] C. Laberty-Robert, K. Valle, F. Pereira, C. Sanchez, Design and properties of functional hybrid organic–inorganic membranes for fuel cells, Chemical Society Reviews 40(2) (2011) 961-1005.

[142] L. Qiu, X. Zhang, W. Yang, Y. Wang, G.P. Simon, D. Li, Controllable corrugation of chemically converted graphene sheets in water and potential application for nanofiltration, Chemical communications 47(20) (2011) 5810-5812.

[143] H. Zhu, W. Luo, P.N. Ciesielski, Z. Fang, J. Zhu, G. Henriksson, M.E. Himmel, L. Hu, Wood-derived materials for green electronics, biological devices, and energy applications, Chemical reviews 116(16) (2016) 9305-9374.

[144] M.A. Shannon, P.W. Bohn, M. Elimelech, J.G. Georgiadis, B.J. Marinas, A.M. Mayes, Science and technology for water purification in the coming decades, Nature 452(7185) (2008) 301-310.

[145] A. Raza, J.Z. Hassan, A. Mahmood, W. Nabgan, M. Ikram, Recent advances in membrane-enabled water desalination by 2D frameworks: Graphene and beyond, Desalination 531 (2022) 115684.

[146] Z. Wang, F. He, J. Guo, S. Peng, X.Q. Cheng, Y. Zhang, E. Drioli, A. Figoli, Y. Li, L. Shao, The stability of a graphene oxide (GO) nanofiltration (NF) membrane in an aqueous environment: Progress and challenges, Materials Advances 1(4) (2020) 554-568.

[147] A. Escriba, B.A.T.T. Da Silva, S.A. Lourenco, C.E. Cava, Incorporation of nanomaterials on the electrospun membrane process with potential use in water treatment, Colloids and Surfaces A: Physicochemical and Engineering Aspects 624 (2021) 126775.

[148] H. Saleem, L. Trabzon, A. Kilic, S.J. Zaidi, Recent advances in nanofibrous membranes: Production and applications in water treatment and desalination, Desalination 478 (2020) 114178.

[149] W.-H. Chen, T.-Y. Liao, H. Thissen, W.-B. Tsai, One-step aminomalononitrile-based coatings containing zwitterionic copolymers for the reduction of biofouling and the foreign body response, ACS Biomaterials Science & Engineering 5(12) (2019) 6454-6462.

[150] X. Meng, J. Ren, J. Chen, J. Song, H. Zheng, L. Wang, D. Huang, Ag3PO4 composite nanofiltration membrane and its visible-light photocatalytic properties, Journal of Membrane Science 631 (2021). https://doi.org/10.1016/j.memsci.2021.119334.

[151] Y. Ding, S. Maitra, C. Wang, R. Zheng, T. Barakat, S. Roy, L.-H. Chen, B.-L. Su, Bi-functional Cu-TiO2/CuO photocatalyst for large-scale synergistic treatment of waste sewage containing organics and heavy metal ions, Science China Materials 66(1) (2023) 179-192.

[152] X. Zhu, X. Tang, X. Luo, Z. Yang, X. Cheng, Z. Gan, D. Xu, G. Li, H. Liang, Stainless steel mesh supported thin-film composite nanofiltration membranes for enhanced permeability and regeneration potential, Journal of Membrane Science 618 (2021) 118738.

[153] D. Çetin, S. Dönmez, G. Dönmez, The treatment of textile wastewater including chromium (VI) and reactive dye by sulfate-reducing bacterial enrichment, Journal of environmental management 88(1) (2008) 76-82.

[154] M.J. Abraham, T. Murtola, R. Schulz, S. Páll, J.C. Smith, B. Hess, E. Lindahl, GROMACS: High performance molecular simulations through multi-level parallelism from laptops to supercomputers, SoftwareX 1 (2015) 19-25.

[155] T. Lu, F. Chen, Multiwfn: A multifunctional wavefunction analyzer, Journal of computational chemistry 33(5) (2012) 580-592.

[156] K. Zimmermann, ORAL: All purpose molecular mechanics simulator and energy minimizer, Journal of computational chemistry 12(3) (1991) 310-319.

[157] T.F. Willems, C.H. Rycroft, M. Kazi, J.C. Meza, M. Haranczyk, Algorithms and tools for high-throughput geometry-based analysis of crystalline porous materials, Microporous and Mesoporous Materials 149(1) (2012) 134-141.

[158] P. Giannozzi, S. Baroni, N. Bonini, M. Calandra, R. Car, C. Cavazzoni, D. Ceresoli, G.L. Chiarotti, M. Cococcioni, I. Dabo, A. Dal Corso, S. de Gironcoli, S. Fabris, G. Fratesi, R. Gebauer, U. Gerstmann, C. Gougoussis, A. Kokalj, M. Lazzeri, L. Martin-Samos, N. Marzari, F. Mauri, R. Mazzarello, S. Paolini, A. Pasquarello, L. Paulatto, C. Sbraccia, S. Scandolo, G. Sclauzero, A.P. Seitsonen, A. Smogunov, P. Umari, R.M. Wentzcovitch, QUANTUM ESPRESSO: a modular and open-source software project for quantum simulations of materials, J Phys Condens Matter 21(39) (2009) 395502. https://doi.org/10.1088/0953-8984/21/39/395502.

[159] O.T. Muldoon, K. Trew, P. Devine, Flagging difference: Identification and emotional responses to national flags, Journal of Applied Social Psychology 50(5) (2020) 265-275.

[160] R. Meldola, S.U. Pickering, H.W. Hake, R. Tatlock, J.C. Brown, Obituary notices: William Henry Perkin, 1838–1907; Robert Warington, 1838–1907; August Dupré, 1835–1907; John Clark, Ph. D., FIC, 1844–1907; Frederick James Montague Page, 1848–1907; Sir David Gamble, Bart., KCB, 1823–1907, Journal of the Chemical Society, Transactions 93 (1908) 2214-2281.

[161] P. Nidheesh, G. Divyapriya, F.E. Titchou, M. Hamdani, Treatment of textile wastewater by sulfate radical based advanced oxidation processes, Separation and Purification Technology 293 (2022) 121115.

[162] T. Fazal, A. Razzaq, F. Javed, A. Hafeez, N. Rashid, U.S. Amjad, M.S.U. Rehman, A. Faisal, F. Rehman, Integrating adsorption and photocatalysis: A cost effective strategy for textile wastewater treatment using hybrid biochar-TiO2 composite, Journal of hazardous materials 390 (2020) 121623.

[163] Q. Gao, P. Jin, L. Wang, Y. Xing, X. Gui, P. Van Puyvelde, B. Van der Bruggen, Removal of organic pollutants in coking wastewater based on coal-based adsorbents: A pilot-scale study of static adsorption and flotation, Journal of Environmental Chemical Engineering 9(6) (2021) 106844. https://doi.org/10.1016/j.jece.2021.106844.

[164] E. GilPavas, I. Dobrosz-Gómez, M.-Á. Gómez-García, Optimization and toxicity assessment of a combined electrocoagulation, H2O2/Fe2+/UV and activated carbon adsorption for textile wastewater treatment, Science of the Total Environment 651 (2019) 551-560.

[165] N. Cao, C. Yue, Z. Lin, W. Li, H. Zhang, J. Pang, Z. Jiang, Durable and chemical resistant ultra-permeable nanofiltration membrane for the separation of textile wastewater, Journal of Hazardous Materials 414 (2021) 125489.

[166] G. Moradi, S. Zinadini, L. Rajabi, A.A. Derakhshan, Removal of heavy metal ions using a new high performance nanofiltration membrane modified with curcumin boehmite nanoparticles, Chemical Engineering Journal 390 (2020) 124546.

[167] S. Zhou, X. Feng, J. Zhu, Q. Song, G. Yang, Y. Zhang, B. Van der Bruggen, Self-cleaning loose nanofiltration membranes enabled by photocatalytic Cu-triazolate MOFs for dye/salt separation, Journal of Membrane Science 623 (2021). https://doi.org/10.1016/j.memsci.2021.119058.

[168] W. Zhang, H. Xu, F. Xie, X. Ma, B. Niu, M. Chen, H. Zhang, Y. Zhang, D. Long, General synthesis of ultrafine metal oxide/reduced graphene oxide nanocomposites for ultrahigh-flux nanofiltration membrane, Nature Communications 13(1) (2022) 1-10.

[169] J. Zheng, Y. Li, D. Xu, R. Zhao, Y. Liu, G. Li, Q. Gao, X. Zhang, A. Volodine, B. Van der Bruggen, Facile fabrication of a positively charged nanofiltration membrane for heavy metal and dye removal, Separation and Purification Technology 282 (2022) 120155.

[170] L. Huang, S. Huang, S.R. Venna, H. Lin, Rightsizing nanochannels in reduced graphene oxide membranes by solvating for dye desalination, Environmental science & technology 52(21) (2018) 12649-12655.

[171] Z. Guo, K. Zhang, H. Guan, M. Liu, S. Yu, C. Gao, Improved separation efficiency of polyamide-based composite nanofiltration membrane by surface modification using 3-aminopropyltriethoxysilane, Separation and Purification Technology 274 (2021) 119142.

[172] X. Feng, D. Liu, H. Ye, D. Peng, J. Wang, S. Han, Y. Zhang, High-flux polyamide membrane with improved chlorine resistance for efficient dye/salt separation based on a new N-rich amine monomer, Separation and Purification Technology 278 (2021) 119533.

[173] P. Jin, V. Mattelaer, S. Yuan, M. Bassyouni, K. Simoens, X. Zhang, F. Ceyssens, K. Bernaerts, R. Dewil, B. Van der Bruggen, Hydrogel supported positively charged ultrathin polyamide layer with antimicrobial properties via Ag modification, Separation and Purification Technology 284 (2022) 120295.

[174] M.T. Hoang, T.D. Pham, D. Verheyen, M.K. Nguyen, T.T. Pham, J. Zhu, B. Van der Bruggen, Fabrication of thin film nanocomposite nanofiltration membrane incorporated with cellulose nanocrystals for removal of Cu (II) and Pb (II), Chemical Engineering Science 228 (2020) 115998.

[175] S. Yuan, X. Li, J. Zhu, G. Zhang, P. Van Puyvelde, B. Van der Bruggen, Covalent organic frameworks for membrane separation, Chemical Society Reviews 48(10) (2019) 2665-2681.

[176] A. Metecan, A. Cihanoğlu, S.A. Altinkaya, A positively charged loose nanofiltration membrane fabricated through complexing of alginate and polyethyleneimine with metal ions on the polyamideimide support for dye desalination, Chemical Engineering Journal 416 (2021) 128946.

[177] J. Li, S. Yuan, J. Zhu, B. Van der Bruggen, High-flux, antibacterial composite membranes via polydopamine-assisted PEI-TiO2/Ag modification for dye removal, Chemical Engineering Journal 373 (2019) 275-284.

[178] Y. Pan, R. Xu, Z. Lü, S. Yu, M. Liu, C. Gao, Enhanced both perm-selectivity and fouling resistance of poly(piperazine-amide) nanofiltration membrane by incorporating sericin as a co-reactant of aqueous phase, Journal of Membrane Science 523 (2017) 282-290. https://doi.org/10.1016/j.memsci.2016.10.011.

[179] F. Oulad, S. Zinadini, A.A. Zinatizadeh, A.A. Derakhshan, Fabrication and characterization of a novel tannic acid coated boehmite/PES high performance antifouling NF membrane and application for licorice dye removal, Chemical Engineering Journal 397 (2020) 125105.

[180] Y.-C. Chiang, Y.-Z. Hsub, R.-C. Ruaan, C.-J. Chuang, K.-L. Tung, Nanofiltration membranes synthesized from hyperbranched polyethyleneimine, Journal of Membrane Science 326(1) (2009) 19-26.

[181] P. Li, H. Lan, K. Chen, X. Ma, B. Wei, M. Wang, P. Li, Y. Hou, Q.J. Niu, Novel high-flux positively charged aliphatic polyamide nanofiltration membrane for selective removal of heavy metals, Separation and Purification Technology 280 (2022) 119949.

[182] S.T. Lazar, T.J. Kolibaba, J.C. Grunlan, Flame-retardant surface treatments, Nature Reviews Materials 5(4) (2020) 259-275.

[183] I.S. Zope, S. Foo, D.G. Seah, A.T. Akunuri, A. Dasari, Development and evaluation of a water-based flame retardant spray coating for cotton fabrics, ACS applied materials & interfaces 9(46) (2017) 40782-40791.

[184] C. Mannich, W. Krosche, The mannich reaction revisited, Arch, Pharm 250 (1912) 647.

[185] Y. Qu, L. Qin, M. Guo, X. Liu, Y. Yang, Multilayered molecularly imprinted composite membrane based on porous carbon nanospheres/pDA cooperative structure for selective adsorption and separation of phenol, Separation and Purification Technology 280 (2022) 119915.

[186] J. Gu, T. Chen, P. Xiao, F. Ni, L. Yan, Y. Nie, T. Chen, Constructing oxidized carbon spheres-based heterogeneous membrane with high surface energy for energy-free water purification, Chemical Engineering Journal 431 (2022) 134132.

[187] Y. Zhang, X. Chen, C. Luo, J. Gu, M. Li, M. Chao, X. Chen, T. Chen, L. Yan, X. Wang, Column-to-Beam Structure House Inspired MXene-Based Integrated Membrane with Stable Interlayer Spacing for Water Purification, Advanced Functional Materials 32(22) (2022) 2111660.

[188] P. Gao, P. Jin, R. Dumas, J. Huang, A.B. Asha, R. Narain, B. Van der Bruggen, X. Yang, A prebiotic chemistry inspired one-step functionalization of zwitterionic nanofiltration membranes for efficient molecular separation, Journal of Membrane Science Letters 2(1) (2022) 100013.

[189] D.J. Menzies, A. Ang, H. Thissen, R.A. Evans, Adhesive prebiotic chemistry inspired coatings for bone contacting applications, ACS Biomaterials Science & Engineering 3(5) (2017) 793-806.

[190] T.-Y. Liao, C.D. Easton, H. Thissen, W.-B. Tsai, Aminomalononitrile-assisted multifunctional antibacterial coatings, ACS Biomaterials Science & Engineering 6(6) (2020) 3349-3360.

[191] A.J. Wagner, D.G. Blackmond, The future of prebiotic chemistry, ACS Publications, 2016.

[192] J. Jung, D. Menzies, H. Thissen, C. Easton, R. Evans, R. Henry, A. Deletic, D. McCarthy, New prebiotic chemistry inspired filter media for stormwater/greywater disinfection, Journal of hazardous materials 378 (2019) 120749.

[193] D. Xu, J. Zheng, X. Zhang, D. Lin, Q. Gao, X. Luo, X. Zhu, G. Li, H. Liang, B. Van der Bruggen, Mechanistic Insights of a Thermoresponsive Interface for Fouling Control of Thin-Film Composite Nanofiltration Membranes, Environ Sci Technol 56(3) (2022) 1927-1937. https://doi.org/10.1021/acs.est.1c06156.

[194] Q. Gao, B. Weng, P. Jin, S. Yuan, X. Gui, J. Zheng, D. Xu, Y. Wang, A. Volodine, L. Sun, Rapid solute transfer photocatalytic membrane: the combination of host-guest interaction and photocatalyst load, Chemical Engineering Journal 466 (2022) 137316.

[195] Y. Zhang, H. Sun, H. Sadam, Y. Liu, L. Shao, Supramolecular chemistry assisted construction of ultra-stable solvent-resistant membranes for angstrom-sized molecular separation, Chemical Engineering Journal 371 (2019) 535-543. https://doi.org/10.1016/j.cej.2019.04.096.

[196] G. Zhang, Y. Li, A. Gao, Q. Zhang, J. Cui, S. Zhao, X. Zhan, Y. Yan, Bio-inspired underwater superoleophobic PVDF membranes for highly-efficient simultaneous removal of insoluble emulsified oils and soluble anionic dyes, Chemical Engineering Journal 369 (2019) 576-587.

[197] V. Kumar, R. Rudra, S. Hait, Sulfonated polyvinylidene fluoride-crosslinked-aniline-2-sulfonic acid as ion exchange membrane in single-chambered microbial fuel cell, Journal of Environmental Chemical Engineering 9(6) (2021) 106467.

[198] H.M. Park, H. Takaba, Y.T. Lee, Preparation and characterization of TFC NF membrane with improved acid resistance behavior, Journal of Membrane Science 616 (2020) 118620.

[199] X. Zhang, J. Zheng, P. Jin, D. Xu, S. Yuan, R. Zhao, S. Depuydt, Y. Gao, Z.-L. Xu, B. Van der Bruggen, A PEI/TMC membrane modified with an ionic liquid with enhanced permeability and antibacterial properties for the removal of heavy metal ions, Journal of Hazardous Materials 435 (2022) 129010.

[200] B. Zhao, T.J. Kolibaba, S. Lazar, J.C. Grunlan, Environmentally-benign, water-based covalent polymer network for flame retardant cotton, Cellulose 28(9) (2021) 5855-5866.

[201] C. Chung, K.J. Lampe, S.C. Heilshorn, Tetrakis (hydroxymethyl) phosphonium chloride as a covalent cross-linking agent for cell encapsulation within protein-based hydrogels, Biomacromolecules 13(12) (2012) 3912-3916.

[202] H. Peng, W.H. Zhang, W.S. Hung, N. Wang, J. Sun, K.R. Lee, Q.F. An, C.M. Liu, Q. Zhao, Phosphonium modification leads to ultrapermeable antibacterial polyamide composite membranes with unreduced thickness, Advanced Materials 32(23) (2020) 2001383.

[203] P. Jin, J. Zhu, S. Yuan, G. Zhang, A. Volodine, M. Tian, J. Wang, P. Luis, B. Van der Bruggen, Erythritol-based polyester loose nanofiltration membrane with fast water transport for efficient dye/salt separation, Chemical Engineering Journal 406 (2021) 126796.

[204] R.J. Toh, R. Evans, H. Thissen, N.H. Voelcker, M. d'Ischia, V. Ball, Deposition of aminomalononitrile-based films: kinetics, chemistry, and morphology, Langmuir 35(30) (2019) 9896-9903.

[205] Y.-T. Shi, X. Meng, L. Yao, M. Tian, A full-scale study of nanofiltration: Separation and recovery of NaCl and Na2SO4 from coal chemical industry wastewater, Desalination 517 (2021) 115239.

[206] N.S. Naik, M. Padaki, A.M. Isloor, K. Nagaraja, K. Vishnumurthy, Poly (ionic liquid)-Based charge and size selective loose nanofiltration membrane for molecular separation, Chemical Engineering Journal 418 (2021) 129372.

[207] F. Sheng, X. Li, Y. Li, N.U. Afsar, Z. Zhao, L. Ge, T. Xu, Cationic covalent organic framework membranes for efficient dye/salt separation, Journal of Membrane Science 644 (2022) 120118.

[208] H. Wang, H. Wang, H. Jiang, A. Sheng, Z. Wei, Y. Li, C. Wu, H. Li, Positively Charged Polysulfonamide Nanocomposite Membranes Incorporating Hydrophilic Triazine-Structured COFs for Highly Efficient Nanofiltration, ACS Applied Nano Materials 3(9) (2020) 9329-9339. https://doi.org/10.1021/acsanm.0c01961.

[209] N. Zhang, B. Jiang, L. Zhang, Z. Huang, Y. Sun, Y. Zong, H. Zhang, Low-pressure electroneutral loose nanofiltration membranes with polyphenol-inspired coatings for effective dye/divalent salt separation, Chemical Engineering Journal 359 (2019) 1442-1452.

[210] Y. Kang, J. Jang, S. Kim, J. Lim, Y. Lee, I.S. Kim, PIP/TMC interfacial polymerization with electrospray: novel loose nanofiltration membrane for dye wastewater treatment, ACS Applied Materials & Interfaces 12(32) (2020) 36148-36158.

[211] Y. Song, Y. Wang, N. Zhang, X. Li, X. Bai, T. Li, Quaternized carbon-based nanoparticles embedded positively charged composite membranes towards efficient removal of cationic small-sized contaminants, Journal of Membrane Science 630 (2021) 119332.

[212] X.-p. Wang, J. Hou, F.-s. Chen, X.-m. Meng, In-situ growth of metal-organic framework film on a polydopamine-modified flexible substrate for antibacterial and forward osmosis membranes, Separation and Purification Technology 236 (2020) 116239.

[213] K. Cheng, N. Zhang, N. Yang, S. Hou, J. Ma, L. Zhang, Y. Sun, B. Jiang, Rapid and robust modification of PVDF ultrafiltration membranes with enhanced permselectivity, antifouling and antibacterial performance, Separation and Purification Technology 262 (2021) 118316.

[214] H. Kim, R. Patel, J.H. Kim, Review on Membranes Containing Silver Nanoparticles with Antibacterial and Antifouling Properties, Membrane Journal 31(5) (2021) 293-303.

[215] C. Bushdid, M.O. Magnasco, L.B. Vosshall, A. Keller, Humans can discriminate more than 1 trillion olfactory stimuli, Science 343(6177) (2014) 1370-1372.

[216] S. Li, B. Mu, X. Wang, A. Wang, Recent researches on natural pigments stabilized by clay minerals: A review, Dyes and Pigments 190 (2021) 109322.

[217] J. Wen, X. Lu, M. Jiang, X. Shao, Creativity of Nanofiber Materials and Application in the Expressive Power of Manual Tie-Dyeing Process, Advances in Materials Science and Engineering 2022 (2022).

[218] Y. Yang, W. Yan, Y. Yang, STEAM Activity Design Based on 4C Education Concept——Take tie-dye of traditional culture as an example, Frontiers in Educational Research 3(12) (2020).

[219] W.H. Perkin, I. On mauve or aniline-purple, Proceedings of the Royal Society of London (12) (1863) 713-715.

[220] D. Tamburini, C.M. Shimada, B. McCarthy, The molecular characterization of early synthetic dyes in E. Knecht et al's textile sample book “A Manual of Dyeing”(1893) by high performance liquid chromatography-Diode array detector-Mass spectrometry (HPLC-DAD-MS), Dyes and Pigments 190 (2021) 109286.

[221] R.J. Burton, The potential impact of synthetic animal protein on livestock production: The new “war against agriculture”?, Journal of Rural Studies 68 (2019) 33-45.

[222] S.A. Hien, C. Trellu, N. Oturan, A.S. Assémian, B.G.H. Briton, P. Drogui, K. Adouby, M.A. Oturan, Comparison of homogeneous and heterogeneous electrochemical advanced oxidation processes for treatment of textile industry wastewater, Journal of Hazardous Materials (2022) 129326.

[223] R.-t. Guo, J. Wang, Z.-x. Bi, X. Chen, X. Hu, W.-g. Pan, Recent advances and perspectives of g–C3N4–based materials for photocatalytic dyes degradation, Chemosphere (2022) 133834.

[224] D. Xu, X. Luo, P. Jin, J. Zhu, X. Zhang, J. Zheng, L. Yang, X. Zhu, H. Liang, B. Van der Bruggen, A novel ceramic-based thin-film composite nanofiltration membrane with enhanced performance and regeneration potential, Water Research 215 (2022) 118264.

[225] D. Xu, X. Zhu, X. Luo, Y. Guo, Y. Liu, L. Yang, X. Tang, G. Li, H. Liang, MXene nanosheet templated nanofiltration membranes toward ultrahigh water transport, Environmental Science & Technology 55(2) (2020) 1270-1278.

[226] Y. Song, X. Chen, Y. Li, C. Meng, S. Ma, T. Li, C. Hu, Synchronous Removal of Small-Sized Antibiotics by a Bifunctional Photocatalytic Nanofiltration Membrane in a Continuous Flow-Through Process under Multiple Influent Matrices, ACS ES&T Water (2022).

[227] F. Kramer, R. Shang, S. Scherrenberg, L. Rietveld, S. Heijman, Quantifying defects in ceramic tight ultra-and nanofiltration membranes and investigating their robustness, Separation and Purification Technology 219 (2019) 159-168.

[228] S. Yadav, I. Ibrar, A. Altaee, A.K. Samal, J. Zhou, Surface modification of nanofiltration membrane with kappa-carrageenan/graphene oxide for leachate wastewater treatment, Journal of Membrane Science 659 (2022) 120776.

[229] D.J. Johnson, N. Hilal, Nanocomposite nanofiltration membranes: State of play and recent advances, Desalination 524 (2022) 115480.

[230] M. Chen, J. Luo, Y. Wan, X. Chen, X. Liang, Probing the influence of shape and loading of CeO2 nanoparticles on the separation performance of thin-film nanocomposite membranes with an interlayer, Separation and Purification Technology 291 (2022) 120930.

[231] H. Zhang, Y. Chen, S. Tang, H. Sun, P. Li, Y. Hou, Q.J. Niu, Regulation of interfacial polymerization process based on reversible enamine reaction for high performance nanofiltration membrane, Journal of Membrane Science (2022) 121070.

[232] S. Xu, P. Wang, Z. Sun, C. Liu, D. Lu, J. Qi, J. Ma, Dual-functionalization of polymeric membranes via cyclodextrin-based host-guest assembly for biofouling control, Journal of Membrane Science 569 (2019) 124-136.

[233] A.A. Ivanov, C. Falaise, K. Laouer, F. Hache, P. Changenet, Y.V. Mironov, D. Landy, Y. Molard, S. Cordier, M.A. Shestopalov, Size-Exclusion Mechanism Driving Host–Guest Interactions between Octahedral Rhenium Clusters and Cyclodextrins, Inorganic Chemistry 58(19) (2019) 13184-13194.

[234] H. Li, B. Jiang, J. Li, Recent advances in dopamine-based materials constructed via one-pot co-assembly strategy, Advances in Colloid and Interface Science 295 (2021) 102489.

[235] J. Zhu, M.T. Tsehaye, J. Wang, A. Uliana, M. Tian, S. Yuan, J. Li, Y. Zhang, A. Volodin, B. Van der Bruggen, A rapid deposition of polydopamine coatings induced by iron (III) chloride/hydrogen peroxide for loose nanofiltration, Journal of colloid and interface science 523 (2018) 86-97.

[236] Y.-y. Yao, T. Wang, L.-g. Wu, H.-l. Chen, PES mixed-matrix membranes incorporating ZIF-8@ MXene nanocomposite for the efficient dye/salt separation, Desalination 543 (2022) 116116.

[237] X. Zhang, Y. Dong, Q. Wang, H. Yu, C. Gao, L. Xue, Structures and performance of alcohol activated thin film composite polyamide (TFC-PA) nanofiltration (NF) membranes prepared with and without Co (II) modulation, Desalination (2022) 116242.

[238] M. Liu, J. Wu, B. Ma, S. Yu, C. Gao, Selective layer reconstruction of deteriorated polyamide membrane by surface chemical deposition for desalination performance restoration and simultaneous antifouling and anti-chlorine, Desalination 547 (2023) 116224.

[239] D. Zou, Y. Zhou, W. Yan, Y. Zhou, C. Gao, Boric acid-loosened polyvinyl alcohol/glutaraldehyde membrane with high flux and selectivity for monovalent/divalent salt separation, Journal of Membrane Science 662 (2022) 120954.

[240] K. Zhao, M. Chen, Y. Zhang, J. Miao, J. Jiang, W. Xie, Z. Yang, L. Lin, W. Zhang, R. Chu, Anti-fouling and anti-bacterial graphene oxide/calcium alginate hybrid hydrogel membrane for efficient dye/salt separation, Desalination 538 (2022) 115908.

[241] B. Qin, S. Zhang, Q. Song, Z. Huang, J.F. Xu, X. Zhang, Supramolecular interfacial polymerization: a controllable method of fabricating supramolecular polymeric materials, Angewandte Chemie 129(26) (2017) 7747-7751.

[242] S.A.N. Mehrabani, V. Vatanpour, I. Koyuncu, Green solvents in polymeric membrane fabrication: A review, Separation and Purification Technology 298 (2022) 121691.

[243] C. Shi, A. Zhou, D. Fang, T. Lu, J. Wang, Y. Song, L. Lyu, W. Wu, C. Huang, W. Li, Oregano essential oil/β-cyclodextrin inclusion compound polylactic acid/polycaprolactone electrospun nanofibers for active food packaging, Chemical Engineering Journal 445 (2022) 136746.

[244] Y. Zhang, W. Chen, X. Yan, F. Zhang, X. Wang, X. Wu, B. Pang, J. Wang, G. He, Ether spaced N-spirocyclic quaternary ammonium functionalized crosslinked polysulfone for high alkaline stable anion exchange membranes, Journal of Membrane Science 598 (2020) 117650.

[245] M. Zhang, J. Cui, T. Lu, G. Tang, S. Wu, W. Ma, C. Huang, Robust, functionalized reduced graphene-based nanofibrous membrane for contaminated water purification, Chemical Engineering Journal 404 (2021) 126347.

[246] T.A.C. Balbino, C.R. Bellato, A.D. da Silva, J.d.O.M. Neto, L. de Moura Guimarães, Magnetic cross-linked chitosan modified with ethylenediamine and β-cyclodextrin for removal of phenolic compounds, Colloids and Surfaces A: Physicochemical and Engineering Aspects 602 (2020) 125119.

[247] R. Su, S. Li, W. Wu, C. Song, G. Liu, Y. Yu, Recent progress in electrospun nanofibrous membranes for oil/water separation, Separation and Purification Technology 256 (2021) 117790.

[248] L. Pino-Soto, A. Schwarz, C. Vargas, F. Saravia, H. Horn, R. Bórquez, Influence of multivalent-electrolyte metal solutions on the superficial properties and performance of a polyamide nanofiltration membrane, Separation and Purification Technology 272 (2021) 118846.

[249] S.F. Seyedpour, M. Dadashi Firouzjaei, A. Rahimpour, E. Zolghadr, A. Arabi Shamsabadi, P. Das, F. Akbari Afkhami, M. Sadrzadeh, A. Tiraferri, M. Elliott, Toward sustainable tackling of biofouling implications and improved performance of TFC FO membranes modified by Ag-MOF nanorods, ACS applied materials & interfaces 12(34) (2020) 38285-38298.

[250] Y. Lu, H. Zhang, J.Y. Chan, R. Ou, H. Zhu, M. Forsyth, E.M. Marijanovic, C.M. Doherty, P.J. Marriott, M.M.B. Holl, Homochiral MOF–polymer mixed matrix membranes for efficient separation of chiral molecules, Angewandte Chemie 131(47) (2019) 17084-17091.

[251] X. Tu, F. Gao, X. Ma, J. Zou, Y. Yu, M. Li, F. Qu, X. Huang, L. Lu, Mxene/carbon nanohorn/β-cyclodextrin-Metal-organic frameworks as high-performance electrochemical sensing platform for sensitive detection of carbendazim pesticide, Journal of Hazardous Materials 396 (2020) 122776.

[252] T. Pei, M. Deng, C. Ma, H. Yan, A. Zhu, L. Ye, Q. Liu, Q. Zhang, Loose nanofiltration membranes based on interfacial glutaraldehyde-amine polymerization for fast and highly selective dye/salt separation, Chemical Engineering Journal 450 (2022) 138057.

[253] N. Zhang, K. Cheng, J. Zhang, N. Li, X. Yang, Z. Wang, A dual-biomimetic strategy to construct zwitterionic anti-fouling membrane with superior emulsion separation performance, Journal of Membrane Science 660 (2022) 120829.

[254] Y. Wang, Y. Yang, J. Wang, Z. Wang, S. Zhao, Supramolecular enzymatic membranes comprising of β-cyclodextrin and laccase for efficient removal and desalination of small molecules, Desalination 546 (2023) 116198.

[255] J. Zhang, L. Yang, Z. Wang, S. Yang, P. Li, P. Song, M. Ban, A highly permeable loose nanofiltration membrane prepared via layer assembled in-situ mineralization, Journal of Membrane Science 587 (2019) 117159.

[256] Z. Liu, Y. Wu, F. Lan, G. Xie, M. Zhang, C. Ma, J. Jia, Improvement of permeability and antifouling performance of PVDF membranes via dopamine-assisted deposition of zwitterionic copolymer, Colloids and Surfaces A: Physicochemical and Engineering Aspects (2022) 130505.

[257] S. Guo, Y. Wan, X. Chen, J. Luo, Loose nanofiltration membrane custom-tailored for resource recovery, Chemical Engineering Journal 409 (2021) 127376.

[258] Y.-F. Mi, G. Xu, Y.-S. Guo, B. Wu, Q.-F. An, Development of antifouling nanofiltration membrane with zwitterionic functionalized monomer for efficient dye/salt selective separation, Journal of Membrane Science 601 (2020) 117795.

[259] B. Zhu, R. Shao, N. Li, C. Min, S. Liu, Z. Xu, X. Qian, L. Wang, Progress of cyclodextrin based membranes in water treatment: special 3D bowl-like structure to achieve excellent separation, Chemical Engineering Journal (2022) 137013.

[260] R. Li, Z. Mai, D. Peng, S. Xu, J. Wang, J. Zhu, Y. Zhang, In situ formation of porous organic polymer-based thin polyester membranes for loose nanofiltration, Journal of Membrane Science (2021) 120074.

[261] Q. Li, Z. Liao, X. Fang, D. Wang, J. Xie, X. Sun, L. Wang, J. Li, Tannic acid-polyethyleneimine crosslinked loose nanofiltration membrane for dye/salt mixture separation, Journal of Membrane Science 584 (2019) 324-332.

[262] J. Wang, R. He, X. Han, D. Jiao, J. Zhu, F. Lai, X. Liu, J. Liu, Y. Zhang, B. Van Der Bruggen, High performance loose nanofiltration membranes obtained by a catechol-based route for efficient dye/salt separation, Chemical Engineering Journal 375 (2019) 121982.

[263] P. Li, Z. Wang, L. Yang, S. Zhao, P. Song, B. Khan, A novel loose-NF membrane based on the phosphorylation and cross-linking of polyethyleneimine layer on porous PAN UF membranes, Journal of Membrane Science 555 (2018) 56-68.

[264] Y. Wu, M. Chen, H.-J. Lee, M. A. Ganzoury, N. Zhang, C.-F. de Lannoy, Nanocomposite Polymeric Membranes for Organic Micropollutant Removal: A Critical Review, ACS ES&T Engineering 2(9) (2022) 1574-1598.

[265] Q. Feng, Y. Zhan, W. Yang, H. Dong, A. Sun, L. Li, X. Chen, Y. Chen, Ultra-high flux and synergistically enhanced anti-fouling Ag@ MXene lamellar membrane for the fast purification of oily wastewater through nano-intercalation, photocatalytic self-cleaning and antibacterial effect, Separation and Purification Technology 298 (2022) 121635.

[266] X. Wang, M. Sun, Y. Zhao, C. Wang, W. Ma, M.S. Wong, M. Elimelech, In situ electrochemical generation of reactive chlorine species for efficient ultrafiltration membrane self-cleaning, Environmental Science & Technology 54(11) (2020) 6997-7007.

[267] L. Zhang, H. Jia, J. Wang, H. Wen, J. Li, Characterization of fouling and concentration polarization in ion exchange membrane by in-situ electrochemical impedance spectroscopy, Journal of Membrane Science 594 (2020) 117443.

[268] J. Zhang, F. Zhou, S. Li, Y. Wan, J. Luo, Surface functionalization of nanofiltration membrane by catechol-amine codeposition for enhancing antifouling performance, Journal of Membrane Science 635 (2021) 119451.

[269] T. Fan, J. Miao, Z. Li, B. Cheng, Bio-inspired robust superhydrophobic-superoleophilic polyphenylene sulfide membrane for efficient oil/water separation under highly acidic or alkaline conditions, Journal of hazardous materials 373 (2019) 11-22.

[270] D.S. Dlamini, C. Matindi, G.D. Vilakati, J.M. Tesha, M.M. Motsa, J.M. Thwala, B.B. Mamba, E. Hoek, J. Li, Fine-tuning the architecture of loose nanofiltration membrane for improved water flux, dye rejection and dye/salt selective separation, Journal of Membrane Science 621 (2021) 118930.

[271] J. Ju, L. Hao, S. Yang, D. Wang, Y. Zhang, H. Yuan, X. Yin, Y. Tan, Designing robust, breathable, and antibacterial multifunctional porous membranes by a nanofluids templated strategy, Advanced Functional Materials 30(46) (2020) 2006544.

[272] S. Xiong, C. Han, A. Phommachanh, W. Li, S. Xu, Y. Wang, High-performance loose nanofiltration membrane prepared with assembly of covalently cross-linked polyethyleneimine-based polyelectrolytes for textile wastewater treatment, Separation and Purification Technology 274 (2021) 119105.

[273] G. Van der Snickt, K.A. Dooley, J. Sanyova, H. Dubois, J.K. Delaney, E.M. Gifford, S. Legrand, N. Laquiere, K. Janssens, Dual mode standoff imaging spectroscopy documents the painting process of the Lamb of God in the Ghent Altarpiece by J. and H. Van Eyck, Science advances 6(31) (2020) eabb3379.

[274] G. Noirbent, F. Dumur, Photoinitiators of polymerization with reduced environmental impact: Nature as an unlimited and renewable source of dyes, European Polymer Journal 142 (2021) 110109.

[275] Y. Yuan, X.-a. Ning, Y. Zhang, X. Lai, D. Li, Z. He, X. Chen, Chlorobenzene levels, component distribution, and ambient severity in wastewater from five textile dyeing wastewater treatment plants, Ecotoxicology and environmental safety 193 (2020) 110257.

[276] Y. Li, Q. Fan, X. Wang, G. Liu, L. Chai, L. Zhou, J. Shao, Y. Yin, Shear-Induced Assembly of Liquid Colloidal Crystals for Large-Scale Structural Coloration of Textiles, Advanced Functional Materials 31(19) (2021) 2010746. https://doi.org/https://doi.org/10.1002/adfm.202010746.

[277] P. Goh, K. Wong, A. Ismail, Membrane technology: A versatile tool for saline wastewater treatment and resource recovery, Desalination 521 (2022) 115377.

[278] T. Yao, Y. Gan, Q. Li, M. Tan, X. Shi, Removal and recovery of triphenylmethane dyes from wastewater with temperature-sensitive magnetic ionic liquid aqueous two-phase system, Journal of Cleaner Production (2021) 129648.

[279] Q. Gao, P. Jin, L. Wang, Y. Xing, X. Gui, P. Van Puyvelde, B. Van der Bruggen, Removal of organic pollutants in coking wastewater based on coal-based adsorbents: A pilot-scale study of static adsorption and flotation, Journal of Environmental Chemical Engineering 9(6) (2021). https://doi.org/10.1016/j.jece.2021.106844.

[280] S. Leaper, A. Abdel-Karim, T.A. Gad-Allah, P. Gorgojo, Air-gap membrane distillation as a one-step process for textile wastewater treatment, Chemical Engineering Journal 360 (2019) 1330-1340.

[281] P. Chanikya, P. Nidheesh, D.S. Babu, A. Gopinath, M.S. Kumar, Treatment of dyeing wastewater by combined sulfate radical based electrochemical advanced oxidation and electrocoagulation processes, Separation and Purification Technology 254 (2021) 117570.

[282] J. Zheng, Y. Li, D. Xu, R. Zhao, Y. Liu, G. Li, Q. Gao, X. Zhang, A. Volodine, B. Van der Bruggen, Facile fabrication of a positively charged nanofiltration membrane for heavy metal and dye removal, Separation and Purification Technology 282 (2022). https://doi.org/10.1016/j.seppur.2021.120155.

[283] M. Liu, Q. He, K. Zhang, Z. Guo, Z. Lü, S. Yu, C. Gao, Carbodiimide-assisted zwitterionic modification of poly (piperazine amide) thin-film composite membrane for enhanced separation and anti-depositing performances to cationic/anionic dye aqueous solutions, Journal of hazardous materials 396 (2020) 122582.

[284] J. Cai, J. Huang, S. Wang, J. Iocozzia, Z. Sun, J. Sun, Y. Yang, Y. Lai, Z. Lin, Crafting Mussel-Inspired Metal Nanoparticle-Decorated Ultrathin Graphitic Carbon Nitride for the Degradation of Chemical Pollutants and Production of Chemical Resources, Advanced Materials 31(15) (2019) 1806314.

[285] Y. Zhang, X. Cheng, X. Jiang, J.J. Urban, C.H. Lau, S. Liu, L. Shao, Robust natural nanocomposites realizing unprecedented ultrafast precise molecular separations, Materials Today 36 (2020) 40-47. https://doi.org/10.1016/j.mattod.2020.02.002.

[286] Z. Wang, Y. Zou, Y. Li, Y. Cheng, Metal-Containing Polydopamine Nanomaterials: Catalysis, Energy, and Theranostics, Small 16(18) (2020) 1907042.

[287] N. Gao, J. Yang, Y. Wu, J. Yue, G. Cao, A. Zhang, L. Ye, Z. Feng, β-Cyclodextrin functionalized coaxially electrospun poly(vinylidene fluoride) @ polystyrene membranes with higher mechanical performance for efficient removal of phenolphthalein, Reactive and Functional Polymers 141 (2019) 100-111. https://doi.org/10.1016/j.reactfunctpolym.2019.05.001.

[288] J. Xue, J. Shen, R. Zhang, F. Wang, S. Liang, X. You, Q. Yu, Y. Hao, Y. Su, Z. Jiang, High-flux nanofiltration membranes prepared with β-cyclodextrin and graphene quantum dots, Journal of Membrane Science 612 (2020). https://doi.org/10.1016/j.memsci.2020.118465.

[289] J. Domenzain-Gonzalez, J.J. Castro-Arellano, L.A. Galicia-Luna, M. Rodriguez-Cruz, R.T. Hernandez-Lopez, L. Lartundo-Rojas, Photocatalytic membrane reactor based on Mexican Natural Zeolite: RB5 dye removal by photo-Fenton process, Journal of Environmental Chemical Engineering 9(4) (2021). https://doi.org/10.1016/j.jece.2021.105281.

[290] A. Fauzi, A. Jalil, N. Hassan, F. Aziz, M. Azami, I. Hussain, R. Saravanan, D.-V. Vo, A critical review on relationship of CeO2-based photocatalyst towards mechanistic degradation of organic pollutant, Chemosphere 286 (2022) 131651.

[291] S. Wang, Y. Wang, J. Wan, Y. Ma, Z. Yan, G. Zhang, Dual channel carrier transfer based on Ti3C2Tx improves carrier utilization of Z-scheme Ag3PO4/AgBr heterojunction photocatalyst, Separation and Purification Technology 253 (2020) 117486.

[292] Y.-J. Lee, J.-K. Kang, S.-J. Park, C.-G. Lee, J.-K. Moon, P.J. Alvarez, Photocatalytic degradation of neonicotinoid insecticides using sulfate-doped Ag3PO4 with enhanced visible light activity, Chemical Engineering Journal 402 (2020) 126183.

[293] S.-w. Xiong, Y. Yu, P. Wang, M. Liu, S.-h. Chen, X.-z. Yin, L.-x. Wang, H. Wang, Growth of AgBr/Ag3PO4 Heterojunction on Chitosan Fibers for Degrading Organic Pollutants, Advanced Fiber Materials 2(5) (2020) 246-255. https://doi.org/10.1007/s42765-020-00042-y.

[294] X. Wang, J. Jian, Z. Yuan, J. Zeng, L. Zhang, T. Wang, H. Zhou, In situ loading of polyurethane/negative ion powder composite film with visible-light-responsive Ag3PO4@ AgBr particles for photocatalytic and antibacterial applications, European Polymer Journal 125 (2020) 109515.

[295] S. Ghattavi, A. Nezamzadeh-Ejhieh, A visible light driven AgBr/g-C3N4 photocatalyst composite in methyl orange photodegradation: Focus on photoluminescence, mole ratio, synthesis method of g-C3N4 and scavengers, Composites Part B: Engineering 183 (2020). https://doi.org/10.1016/j.compositesb.2019.107712.

[296] L. Chen, S. Yang, Y. Huang, B. Zhang, F. Kang, D. Ding, T. Cai, Degradation of antibiotics in multi-component systems with novel ternary AgBr/Ag3PO4@ natural hematite heterojunction photocatalyst under simulated solar light, Journal of hazardous materials 371 (2019) 566-575.

[297] P. Zhu, J. Xu, M. Duan, R. Wang, L. Xie, M. Hu, P. Wang, Fabrication of a double Z-type g-C3N4/AgBr/Ag3PO4 composite with enhanced visible-light photocatalytic activity for organic dye elimination, Optical Materials 107 (2020) 110076.

[298] J. Zhu, S. Yuan, A. Uliana, J. Hou, J. Li, X. Li, M. Tian, Y. Chen, A. Volodin, B.V. der Bruggen, High-flux thin film composite membranes for nanofiltration mediated by a rapid co-deposition of polydopamine/piperazine, Journal of Membrane Science 554 (2018) 97-108. https://doi.org/10.1016/j.memsci.2018.03.004.

[299] Z. Yang, H. Guo, Z.K. Yao, Y. Mei, C.Y. Tang, Hydrophilic Silver Nanoparticles Induce Selective Nanochannels in Thin Film Nanocomposite Polyamide Membranes, Environ Sci Technol 53(9) (2019) 5301-5308. https://doi.org/10.1021/acs.est.9b00473.

[300] P. Jin, J. Zhu, S. Yuan, G. Zhang, A. Volodine, M. Tian, J. Wang, P. Luis, B. Van der Bruggen, Erythritol-based polyester loose nanofiltration membrane with fast water transport for efficient dye/salt separation, Chemical Engineering Journal 406 (2021). https://doi.org/10.1016/j.cej.2020.126796.

[301] W. Li, X.-s. Chu, S.-a. He, X.-c. Wang, C.-y. Wang, A gourd-like hollow mesoporous silica particle-supported Ag/AgBr Schottky junction for highly efficient mineralization of tetracycline hydrochloride, Environmental Science: Nano 7(9) (2020) 2654-2668.

[302] W. Kong, L. Huang, X. Quan, Z. Zhao, G.L. Puma, Efficient production of acetate from inorganic carbon (HCO3–) in microbial electrosynthesis systems incorporating Ag3PO4/g-C3N4 anaerobic photo-assisted biocathodes, Applied Catalysis B: Environmental 284 (2021) 119696.

[303] P. Jin, V. Mattelaer, S. Yuan, M. Bassiouni, K. Simoens, X. Zhang, F. Ceyssens, K. Bernaerts, R. Dewil, B. Van der Bruggen, Hydrogel supported positively charged ultrathin polyamide layer with antimicrobial properties via Ag modification, Separation and Purification Technology (2021) 120295.

[304] J. Liu, D. Hua, Y. Zhang, S. Japip, T.S. Chung, Precise Molecular Sieving Architectures with Janus Pathways for Both Polar and Nonpolar Molecules, Adv Mater 30(11) (2018). https://doi.org/10.1002/adma.201705933.

[305] S. Wu, J. Shi, X. Nie, Y. Yao, F. Jiang, Q. Wei, F. Huang, Microporous Cyclodextrin Film with Funnel-type Channel Polymerized on Electrospun Cellulose Acetate Membrane as Separators for Strong Trapping Polysulfides and Boosting Charging in Lithium–Sulfur Batteries, Energy & Environmental Materials 6(2) (2023) e12319.

[306] P. Jin, S. Chergaoui, J. Zheng, A. Volodine, X. Zhang, Z. Liu, P. Luis, B. Van der Bruggen, Low-pressure highly permeable polyester loose nanofiltration membranes tailored by natural carbohydrates for effective dye/salt fractionation, Journal of Hazardous Materials 421 (2022) 126716.

[307] B. Sun, F. Tao, Z. Huang, W. Yan, Y. Zhang, X. Dong, Y. Wu, G. Zhou, Ti3C2 MXene-bridged Ag/Ag3PO4 hybrids toward enhanced visible-light-driven photocatalytic activity, Applied Surface Science 535 (2021). https://doi.org/10.1016/j.apsusc.2020.147354.

[308] S. Lu, B. Weng, A. Chen, X. Li, H. Huang, X. Sun, W. Feng, Y. Lei, Q. Qian, M.-Q. Yang, Facet engineering of Pd nanocrystals for enhancing photocatalytic hydrogenation: Modulation of the schottky barrier height and enrichment of surface reactants, ACS Applied Materials & Interfaces 13(11) (2021) 13044-13054.

[309] C. Wang, B. Weng, M. Keshavarz, M.-Q. Yang, H. Huang, Y. Ding, F. Lai, I. Aslam, H. Jin, G. Romolini, Photothermal Suzuki Coupling Over a Metal Halide Perovskite/Pd Nanocube Composite Catalyst, ACS Applied Materials & Interfaces (2022).

[310] H. Yu, D. Wang, B. Zhao, Y. Lu, X. Wang, S. Zhu, W. Qin, M. Huo, Enhanced photocatalytic degradation of tetracycline under visible light by using a ternary photocatalyst of Ag3PO4/AgBr/g-C3N4 with dual Z-scheme heterojunction, Separation and Purification Technology 237 (2020) 116365.

[311] B. Weng, K.-Q. Lu, Z. Tang, H.M. Chen, Y.-J. Xu, Stabilizing ultrasmall Au clusters for enhanced photoredox catalysis, Nature communications 9(1) (2018) 1-11.

[312] U. Secretary-General, Implementation of General Assembly resolution 71/243 on the quadrennial comprehensive policy review of operational activities for development of the United Nations system, 2018: report of the Secretary-General, (2018).

[313] S. Pi, W. Yang, W. Feng, R. Yang, W. Chao, W. Cheng, L. Cui, Z. Li, Y. Lin, N. Ren, Solar-driven waste-to-chemical conversion by wastewater-derived semiconductor biohybrids, Nature Sustainability (2023) 1-12.

[314] J. Lin, W. Ye, M. Xie, D.H. Seo, J. Luo, Y. Wan, B. Van der Bruggen, Environmental impacts and remediation of dye-containing wastewater, Nature Reviews Earth & Environment (2023) 1-19.

[315] Z. Yang, Low-cost and rapid sensors for wastewater surveillance at low-resource settings, Nature Water (2023) 1-3.

[316] Z. Hu, L. Li, X. Cen, M. Zheng, S. Hu, X. Wang, Y. Song, K. Xu, Z. Yuan, Integrated urban water management by coupling iron salt production and application with biogas upgrading, Nature Communications 14(1) (2023) 6405.

[317] Y. Zhang, H. Wang, J. Guo, X. Cheng, G. Han, C.H. Lau, H. Lin, S. Liu, J. Ma, L. Shao, Ice-confined synthesis of highly ionized 3D-quasilayered polyamide nanofiltration membranes, Science 382(6667) (2023) 202-206.

[318] R. Zhao, P. Jin, J. Zhu, Y. Li, G. Li, A. Volodine, Y. Liu, J. Zheng, B. Van der Bruggen, Amino acid-based loose polyamide nanofiltration membrane with ultrahigh water permeance for efficient dye/salt separation, Journal of Membrane Science 673 (2023) 121477.

[319] A. Zhao, M. Zhang, Y. Bao, L. Zhao, G. Liu, Y. Jiang, P. Zhang, X. Cao, Loose nanofiltration membrane constructed via interfacial polymerization using porous organic cage RCC3 for dye/salt separation, Journal of Membrane Science 664 (2022) 121081.

[320] X. Feng, D. Peng, J. Zhu, Y. Wang, Y. Zhang, Recent advances of loose nanofiltration membranes for dye/salt separation, Separation and Purification Technology 285 (2022) 120228.

[321] J. Li, Y. Xie, L. Cheng, X. Li, F. Liu, Z. Wang, Photo-Fenton reaction derived self-cleaning nanofiltration membrane with MOFs coordinated biopolymers for efficient dye/salt separation, Desalination 553 (2023) 116459.

[322] Y. Yang, Z. Tian, J. Zhang, Z. Cui, H. Wang, N. Han, X. Ma, J. Li, Fabrication of hollow fiber loose nanofiltration separation layers based on nucleophilic addition and Schiff base reactions and the investigation on separation performance of low molecular weight dye/salt systems, Journal of Membrane Science 640 (2021) 119761.

[323] D. Liu, F. Yu, L. Zhong, T. Zhang, Y. Xu, Y. Qin, J. Ma, W. Wang, Armor-Structured Interconnected-Porous Membranes for Corrosion-Resistant and Highly Permeable Waste Ammonium Resource Recycling, Environmental Science & Technology 56(10) (2022) 6658-6667.

[324] D.L. Zhao, H. Jin, Q. Zhao, Y. Xu, L. Shen, H. Lin, T.-S. Chung, Smart integration of MOFs and CQDs to fabricate defect-free and self-cleaning TFN membranes for dye removal, Journal of Membrane Science 679 (2023) 121706.

[325] M. Ge, Z. Jia, Y. Yang, P. Dong, C. Peng, X. Zhang, R. Dewil, Y. Zhao, B. Van der Bruggen, J. Zhang, In situ assembly of graphitic carbon nitride/polypyrrole in a thin-film nanocomposite membrane with highly enhanced permeability and durability, Desalination 555 (2023) 116566.

[326] Y. Yang, Y. Li, Q. Li, Y. Wang, C.H. Tan, R. Wang, Rapid co-deposition of graphene oxide incorporated metal-phenolic network/piperazine followed by crosslinking for high flux nanofiltration membranes, Journal of Membrane Science 588 (2019) 117203.

[327] S. Yuan, G. Zhang, J. Zhu, N. Mamrol, S. Liu, Z. Mai, P. Van Puyvelde, B. Van der Bruggen, Hydrogel assisted interfacial polymerization for advanced nanofiltration membranes, Journal of Materials Chemistry A 8(6) (2020) 3238-3245.

[328] Z. Li, S. Peng, W. Zhang, J. Zhang, Y. Jiao, R. Li, L. Shen, H. Lin, Y. Xu, Innovative role of polyvinylpyrrolidone in tailoring polyamide layer for high-performance nanofiltration membranes, Desalination (2023) 116767.

[329] D. Wang, N. Zhang, J. Zhang, Y. Qin, S. Wang, C.Y. Tang, Z. Wang, Hydrogel-regulated interfacial polymerization: A gateway to effective nanostructure tuning of polyamide nanofiltration membranes, Desalination 556 (2023) 116593.

[330] S. Li, L. Bai, J. Ding, Z. Liu, G. Li, H. Liang, Nanofiltration Membranes with Salt-Responsive Ion Valves for Enhanced Separation Performance in Brackish Water Treatment: A Battle against the Limitation of Salt Concentration, Environmental Science & Technology (2023).

[331] X. Li, G. Zhang, H. Liu, H. Lan, J. Qu, Sequential Demulsification through the Hydrophobic-Hydrophilic-Hydrophobic Filtration Layer toward High-Performing Oil Recovery, Environmental Science & Technology 57(32) (2023) 12083-12093.

[332] A. Hu, C. Sun, C. Li, Z. Sun, J. Fan, M. Zheng, Q. Dong, A Novel Metal–Organic-Framework-Based Composite Solid Electrolyte for Lithium Metal Batteries, ACS Applied Materials & Interfaces 15(29) (2023) 35034-35042.

[333] J. Zhu, S. Yuan, A. Uliana, J. Hou, J. Li, X. Li, M. Tian, Y. Chen, A. Volodin, B. Van der Bruggen, High-flux thin film composite membranes for nanofiltration mediated by a rapid co-deposition of polydopamine/piperazine, Journal of membrane science 554 (2018) 97-108.

[334] R. Liu, Q. Chen, M. Cao, J. Lin, F. Lin, W. Ye, P. Luis, B. Van der Bruggen, S. Zhao, Robust bio-inspired superhydrophilic and underwater superoleophobic membranes for simultaneously fast water and oil recovery, Journal of Membrane Science 623 (2021) 119041.

[335] P. Gao, P. Jin, R. Dumas, J. Huang, A.B. Asha, R. Narain, I. Vankelecom, B. Van der Bruggen, X. Yang, High-performance zwitterionic membranes via an adhesive prebiotic chemistry-inspired coating strategy: A demonstration in dye/salt fractionation, Journal of Membrane Science 676 (2023) 121572.

[336] G.Y. Yoo, R. Azmi, C. Kim, W. Kim, B.K. Min, S.-Y. Jang, Y.R. Do, Stable and colorful perovskite solar cells using a nonperiodic SiO2/TiO2 multi-nanolayer filter, ACS nano 13(9) (2019) 10129-10139.

[337] X.-l. Wang, Q. Wang, Y.-x. Xue, B. Zhang, S.-r. Han, H. Zhang, K.-y. Zhao, W. Wang, J.-f. Wei, Preparation of composite nanofiltration membrane with interlayer for pharmaceutical rejection, Separation and Purification Technology 312 (2023) 123411.

[338] N.L. Reddy, M. Shankar, S. Sharma, G. Nagaraju, One-pot synthesis of Cu–TiO2/CuO nanocomposite: application to photocatalysis for enhanced H2 production, dye degradation & detoxification of Cr (VI), International Journal of Hydrogen Energy 45(13) (2020) 7813-7828.

[339] L. Li, D. Mao, J. Yu, X. Guo, Highly selective hydrogenation of CO2 to methanol over CuO–ZnO–ZrO2 catalysts prepared by a surfactant-assisted co-precipitation method, Journal of Power Sources 279 (2015) 394-404.

[340] H. Zeng, F. Sun, J. Zhang, Y. Wang, S. Yang, D. Xing, Gradient crosslinking optimization for the selective layer to prepare polyvinyl alcohol (PVA) nanofiltration (NF) membrane: The enhanced filtration performance and potential rejection for EDCs, Journal of Membrane Science 675 (2023) 121548.

[341] H. Wang, M. Wang, X. Liang, J. Yuan, H. Yang, S. Wang, Y. Ren, H. Wu, F. Pan, Z. Jiang, Organic molecular sieve membranes for chemical separations, Chemical Society Reviews 50(9) (2021) 5468-5516.

[342] W.-P. Zhu, J. Gao, S.-P. Sun, S. Zhang, T.-S. Chung, Poly (amidoamine) dendrimer (PAMAM) grafted on thin film composite (TFC) nanofiltration (NF) hollow fiber membranes for heavy metal removal, Journal of Membrane Science 487 (2015) 117-126.

[343] Q. Gao, D. Bouwen, S. Yuan, X. Gui, Y. Xing, J. Zheng, H. Ling, Q. Zhu, Y. Wang, S. Depuydt, Robust loose nanofiltration membrane with fast solute transfer for dye/salt separation, Journal of Membrane Science (2023) 121518.

[344] J. Zhu, M. Tian, Y. Zhang, H. Zhang, J. Liu, Fabrication of a novel “loose” nanofiltration membrane by facile blending with Chitosan–Montmorillonite nanosheets for dyes purification, Chemical Engineering Journal 265 (2015) 184-193.

[345] J. Zhu, J. Wang, A.A. Uliana, M. Tian, Y. Zhang, Y. Zhang, A. Volodin, K. Simoens, S. Yuan, J. Li, Mussel-inspired architecture of high-flux loose nanofiltration membrane functionalized with antibacterial reduced graphene oxide–copper nanocomposites, ACS applied materials & interfaces 9(34) (2017) 28990-29001.

[346] C. Zhang, K. Wei, W. Zhang, Y. Bai, Y. Sun, J. Gu, Graphene oxide quantum dots incorporated into a thin film nanocomposite membrane with high flux and antifouling properties for low-pressure nanofiltration, ACS applied materials & interfaces 9(12) (2017) 11082-11094.

[347] P. Zhang, J.-L. Gong, G.-M. Zeng, B. Song, W. Cao, H.-Y. Liu, S.-Y. Huan, P. Peng, Novel “loose” GO/MoS2 composites membranes with enhanced permeability for effective salts and dyes rejection at low pressure, Journal of Membrane Science 574 (2019) 112-123.

[348] Y. Cao, H. Zhang, S. Guo, J. Luo, Y. Wan, A robust dually charged membrane prepared via catechol-amine chemistry for highly efficient dye/salt separation, Journal of Membrane Science 629 (2021) 119287.

[349] L. Yang, Z. Wang, J. Zhang, Highly permeable zeolite imidazolate framework composite membranes fabricated via a chelation-assisted interfacial reaction, Journal of Materials Chemistry A 5(29) (2017) 15342-15355.

[350] L. Zhang, H. Guan, N. Zhang, B. Jiang, Y. Sun, N. Yang, A loose NF membrane by grafting TiO2-HMDI nanoparticles on PES/β-CD substrate for dye/salt separation, Separation and Purification Technology 218 (2019) 8-19.

[351] L. Dong, M. Li, S. Zhang, X. Si, Y. Bai, C. Zhang, NH2-Fe3O4-regulated graphene oxide membranes with well-defined laminar nanochannels for desalination of dye solutions, Desalination 476 (2020) 114227.

[352] M. Vazquez-Gonzalez, I. Willner, Aptamer-functionalized micro-and nanocarriers for controlled release, ACS Applied Materials & Interfaces 13(8) (2021) 9520-9541.

[353] Y. Zeng, P. Wang, B. He, S. Liu, Q. Ye, F. Zhou, Fabrication of zwitterionic polymer-functionalized MXene nanosheets for anti-bacterial and anti-biofouling applications, Progress in Organic Coatings 183 (2023) 107727.

[354] S.K. Estreicher, Wine and France: A Brief History, European Review 31(2) (2023) 91-179.

[355] D. Yaseen, M. Scholz, Textile dye wastewater characteristics and constituents of synthetic effluents: a critical review, International journal of environmental science and technology 16 (2019) 1193-1226.

[356] Y. Yang, L.C. Yin, Y. Gong, P. Niu, J.Q. Wang, L. Gu, X. Chen, G. Liu, L. Wang, H.M. Cheng, An unusual strong visible-light absorption band in red anatase TiO2 photocatalyst induced by atomic hydrogen-occupied oxygen vacancies, Advanced Materials 30(6) (2018) 1704479.

[357] R. Hao, G. Wang, H. Tang, L. Sun, C. Xu, D. Han, Template-free preparation of macro/mesoporous g-C3N4/TiO2 heterojunction photocatalysts with enhanced visible light photocatalytic activity, Applied Catalysis B: Environmental 187 (2016) 47-58.

[358] H. Zhao, J. Liu, C.F. Li, X. Zhang, Y. Li, Z.Y. Hu, B. Li, Z. Chen, J. Hu, B.L. Su, Meso-microporous nanosheet - constructed 3DOM perovskites for remarkable photocatalytic hydrogen production, Advanced Functional Materials 32(22) (2022) 2112831.

[359] Y.-Y. Wang, Y.-X. Chen, T. Barakat, Y.-J. Zeng, J. Liu, S. Siffert, B.-L. Su, Recent advances in non-metal doped titania for solar-driven photocatalytic/photoelectrochemical water-splitting, Journal of Energy Chemistry 66 (2022) 529-559.

[360] K.M. Chahrour, F. Yam, A. Eid, A.A. Nazeer, Enhanced photoelectrochemical properties of hierarchical black TiO2-x nanolaces for Cr (VI) photocatalytic reduction, International Journal of Hydrogen Energy 45(43) (2020) 22674-22690.

[361] C. Feng, L. Tang, Y. Deng, J. Wang, J. Luo, Y. Liu, X. Ouyang, H. Yang, J. Yu, J. Wang, Synthesis of leaf-vein-like g-C3N4 with tunable band structures and charge transfer properties for selective photocatalytic H2O2 evolution, Advanced Functional Materials 30(39) (2020) 2001922.

[362] S. Wang, L. Pan, J.-J. Song, W. Mi, J.-J. Zou, L. Wang, X. Zhang, Titanium-defected undoped anatase TiO2 with p-type conductivity, room-temperature ferromagnetism, and remarkable photocatalytic performance, Journal of the American Chemical Society 137(8) (2015) 2975-2983.

Curriculum Vitae

PERSONAL DATA



First Name: Qieyuan

Family Name: Gao

Date of Birth: 14th Oct 1994

Gender: Male

CONTACT

Process Engineering for Sustainable System (ProcESS)

Department of Chemical Engineering, KU Leuven

Chem & Tech, Celestijnenlaan 200F, 3001 Heverlee, Belgium

Mobile phone: (+32) 485 650575

E-mail address: qieyuan.gao@kuleuven.be

EDUCATION

Oct. 2020-present	Ph.D.	Chemical Engineering, KU Leuven, Belgium
Sep. 2017-Jun. 2020	M.Eng.	Mineral Processing Engineering, China University of Mining and Technology, China
Sep. 2013-Jun. 2017	B.Sc.	Chemical Engineering and technology, Changzhou University, China

RESEARCH INTERESTS

Qieyuan's primary research interests revolve around the future-oriented applications of membrane materials in water treatment and resource recovery, targeted design and optimization of membrane molecules across various scenarios, and the continuous process design leveraging advanced separation technology.

PUBLICATIONS

1. **Gao, Q.,** Weng, B., Jin, P., Yuan, S., Gui, X., Zheng, J., Xu, D., Wang, Y., Volodine, A., Sun, L., Van der Bruggen, B. with Jin, P. (corresp. author), Van der Bruggen, B. (corresp. author) (2022). Rapid solute transfer photocatalytic membrane: The combination of host-guest interaction and photocatalyst load. *CHEMICAL ENGINEERING JOURNAL*, *446*, Art.No. ARTN 137316. doi: 10.1016/j.cej.2022.137316
2. **Gao, Q.,** Zhu, Q., Zheng, J., Yuan, S., Wang, Y., Zhao, R., Liu, Y., Gui, X., Wang, C., Volodine, A., Jin, P., Van der Bruggen, B. with Jin, P. (corresp. author), Van der Bruggen, B. (corresp. author) (2022). Positively charged membranes for dye/salt separation based on a crossover combination of Mannich reaction and prebiotic chemistry. *JOURNAL OF HAZARDOUS MATERIALS*, *440*, Art.No. ARTN 129744. doi: 10.1016/j.jhazmat.2022.129744
3. **Gao, Q.,** Bouwen, D., Yuan, S., Gui, X., Xing, Y., Zheng, J., Ling, H., Zhu, Q., Wang, Y., Depuydt, S., Li, J., Volodine, A., Jin, P., Van der Bruggen, B. with Jin, P. (corresp. author), Van der Bruggen, B. (corresp. author) (2023). Robust loose nanofiltration membrane with fast solute transfer for dye/salt separation. *JOURNAL OF MEMBRANE SCIENCE*, *674*, Art.No. ARTN 121518. doi: 10.1016/j.memsci.2023.121518
4. **Gao, Q.,** Ding, Y., Li, J., Jin, P., Xu, D., Fang, L., Wang, Y., Liu, B., Xie, Y., Bao, X., Jiang, L., Du, J., Zhu, J., Zheng, L., Su, B-L., Ng, Y.H., Xing, Y., Gui, X., Wang, C., van der Bruggen, B. with Li, J. (corresp. author), Xing, Y. (corresp. author), Wang, C. (corresp. author), van der Bruggen, B. (corresp. author) (2025). Tailoring fast mass transfer membrane: Zero discharge of wastewater using visible light. *JOURNAL OF MEMBRANE SCIENCE*, 717, Art.No. ARTN 123632. doi: 10.1016/j.memsci.2024.123632
5. **Gao, Q.,** Jin, X., Zhang, X., Li, J., Liu, P., Li, P., Luo, X., Gong, W., Xu, D., Dewil, R., Liang, H., van der Bruggen, B. with Xu, D. (corresp. author), van der Bruggen, B. (corresp. author) (2024). Catalytic membrane with dual-layer structure for ultrafast degradation of emerging contaminants in surface water treatment. *JOURNAL OF HAZARDOUS MATERIALS*, 480, Art.No. ARTN 136333. doi: 10.1016/j.jhazmat.2024.136333
6. **Gao, Q.,** Li, J., Jin, P., Zheng, J., Xu, D., van der Bruggen, B. with Gao, Q. (corresp. author), van der Bruggen, B. (corresp. author) (2023). The Practical Application Value of a Sustainable Water Purification Process Is Crucial. *ACS ES&T WATER*, *3* (8), 1990-1993. doi: 10.1021/acsestwater.3c00301
7. **Gao, Q.,** Jin, P., Wang, L., Xing, Y., Gui, X., Van Puyvelde, P., Van der Bruggen, B. with Gui, X. (corresp. author), Van der Bruggen, B. (corresp. author) (2021). Removal of organic pollutants in coking wastewater based on coal-based adsorbents: A pilot-scale study of static adsorption and flotation. *JOURNAL OF ENVIRONMENTAL CHEMICAL ENGINEERING*, *9* (6), Art.No. ARTN 106844. doi: 10.1016/j.jece.2021.106844
8. **Gao, Q.,** Wang, L., Li, Z., Xie, Y., He, Q., Wang, Y. with Wang, L. (corresp. author), Wang, Y. (corresp. author) (2019). Adsorptive Removal of Pyridine in Simulation Wastewater Using Coke Powder. *Processes*, *7* (7), Art.No. 459. doi: 10.3390/pr7070459
9. Zhu, X., Gao, Q.(co-first author), Lou, M., Bai, Y., Xu, X., Li, F., Van der Bruggen, B. with Li, F. (corresp. author) (2024). GO-based membranes with enhanced stability and permeability by implanting etched-MXene nanosheets: The role of binding energy in stabilizing 2D membranes. *JOURNAL OF MEMBRANE SCIENCE*, 707, Art.No. ARTN 122983. doi: 10.1016/j.memsci.2024.122983

10. Li, J., Fang, L., Xu, D., Zhang, X., Jiang, L., Zhu, Q., Chen, Q., Jin, P., Volodine, A., Dewil, R., Gui., X. (corresp. author), **Gao, Q. (corresp. author),** Van der Bruggen, B(corresp. author). Intercalation of small molecules in the selective layer of polyamide nanofiltration membranes facilitates the separation of Mg2+/Li+. *CHEMICAL ENGINEERING JOURNAL*, 487, 150659. doi: 10.1016/j.cej.2024.150659
11. Li, J., Song, Y., Xu, D., Zhang, X., Du, J., Liu, R., Zhao, R., Chen, Q., Volodine, A., Dewil, R., Gao, Q., van der Bruggen, B. with **Gao, Q. (corresp. author)**, van der Bruggen, B. (corresp. author) (2024). Choline chloride modification of nanofiltration membranes for improving heavy metal ions separation in wastewater. *JOURNAL OF MEMBRANE SCIENCE*, 708, Art.No. ARTN 123079. doi: 10.1016/j.memsci.2024.12307
12. Xu, D., Xie, Y., Jin, X., Zheng, J., **Gao, Q.,** Jin, P., Zhu, X., Zhang, Z., Li, X., Li, G., Liang, H., Van der Bruggen, B. (2024). Polyphenol-mediated defect patching of graphene oxide membranes for sulfonamide contaminants removal and fouling control. *JOURNAL OF HAZARDOUS MATERIALS*, *469*. doi: 10.1016/j.jhazmat.2024.133890
13. Luo, X., Wang, Y., Guo, Y., **Gao, Q.,** Zhao, R., Liu, Y., Liu, R., Jiang, L., Mai, Z., Matsuyama, H., Jin, P. with Jin, P. (corresp. author) (2023). Cleanable natural-sugar-alcohol-based polyester membrane for highly efficient molecular separation. *RESOURCES CONSERVATION AND RECYCLING*, *198*, Art.No. ARTN 107149. doi: 10.1016/j.resconrec.2023.107149
14. Liu, Y., Van Eygen, G., Yuan, S., Wang, H., Chi, M., Xu, D., **Gao, Q.,** Li, G., Zheng, J., Van der Bruggen, B. with Zheng, J. (corresp. author) (2023). Facile and novel fabrication of high-performance loose nanofiltration membranes for textile wastewater recovery. *SEPARATION AND PURIFICATION TECHNOLOGY*, *308*, Art.No. ARTN 122867. doi: 10.1016/j.seppur.2022.122867
15. Zheng, J., Zhao, R., Uliana, A.A., Liu, Y., Zhang, D., Zhang, X., Xu, D., **Gao, Q.,** Jin, P., Liu, Y., Volodine, A., Zhu, J., Van der Bruggen, B. with Zhu, J. (corresp. author), Van der Bruggen, B. (corresp. author) (2022). Separation of textile wastewater using a highly permeable resveratrol-based loose nanofiltration membrane with excellent anti-fouling performance. *CHEMICAL ENGINEERING JOURNAL*, *434*, Art.No. ARTN 134705. doi: 10.1016/j.cej.2022.134705
16. Zhang, X., Jin, P., Xu, D., Zheng, J., Zhan, Z-M., **Gao, Q.,** Yuan, S., Xu, Z-L., van der Bruggen, B. with Jin, P. (corresp. author), van der Bruggen, B. (corresp. author) (2022). Triethanolamine modification produces ultra-permeable nanofiltration membrane with enhanced removal efficiency of heavy metal ions. *JOURNAL OF MEMBRANE SCIENCE*, *644*, Art.No. ARTN 120127. doi: 10.1016/j.memsci.2021.120127
17. Zheng, J., Li, Y., Xu, D., Zhao, R., Liu, Y., Li, G., **Gao, Q.,** Zhang, X., Volodine, A., Van der Bruggen, B. (2022). Facile fabrication of a positively charged nanofiltration membrane for heavy metal and dye removal. *SEPARATION AND PURIFICATION TECHNOLOGY*, 282, Art.No. 120155. doi: 10.1016/j.seppur.2021.120155
18. Xu, D., Zheng, J., Zhang, X., Lin, D., **Gao, Q.,** Luo, X., Zhu, X., Li, G., Liang, H., Van der Bruggen, B. with Liang, H. (corresp. author), Van der Bruggen, B. (corresp. author) (2022). Mechanistic Insights of a Thermoresponsive Interface for Fouling Control of Thin-Film Composite Nanofiltration Membranes. *ENVIRONMENTAL SCIENCE & TECHNOLOGY*, 56 (3), 1927-1937. doi: 10.1021/acs.est.1c06156
19. Zhu, X., Liu, F., Meng, L., **Gao, Q.,** Wang, X., Lou, M., Xu, X., Zhang, W., Li, F. (corresp. author) (2025), Van der Bruggen, B., MXene membranes inserted with tannic acid etched MOF nanocrystals

for ultrafast water permeation: Elucidating the water transportmechanism in nanoconfined interlaminar channels, *NANO LETTERS.* (Accepted)

20. Jin, P., Zheng, J., **Gao, Q.,** Kyoungjin An A., Van der Bruggen, B. (corresp. author) (2022) Loose Nanofiltration Membranes for the Treatment of Textile Wastewater: A Review. *JOURNAL OF MEMBRANE SCIENCE AND RESEARCH*, 8(3), Art.No. ARTN 249018. doi: 10.22079/JMSR.2022.538529.1492
21. Xie, Y., Zhang, C., Yuan, L., **Gao, Q.,** Liang, H., Lu, N. with Zhang, C. (corresp. author) (2020). Fast start-up of PN/A process in a single-stage packed bed and mechanism of nitrogen removal. *ENVIRONMENTAL SCIENCE AND POLLUTION RESEARCH*, 27 (32), 40483-40494. doi: 10.1007/s11356-020-10030-9
22. Wang, L., **Gao, Q.,** Li, Z., Wang, Y. with Wang, L. (corresp. author), Wang, Y. (corresp. author) (2020). Improved Removal of Quinoline from Wastewater Using Coke Powder with Inorganic Ions. *PROCESSES*, 8 (2), Art.No. ARTN 156. doi: 10.3390/pr8020156
23. Bian, Y., Sun, H., Luo, Y., **Gao, Q.,** Li, G., Wang, Y. with Wang, Y. (corresp. author) (2018). Effect of inorganic salt ions on the adsorption of quinoline using coal powder. *WATER SCIENCE AND TECHNOLOGY*, 78 (3), 496-505. doi: 10.2166/wst.2018.300

CONFERENCES

1. **Gao, Q.,** Jin, P., Van der Bruggen, B. (2023). Mannich reaction-based smart membrane of prebiotic chemistry for the desalination of positively charged dyes. Presented at the 13th International Congress on Membranes and Membrane Processes (ICOM 2023), Chiba, Japan.
2. **Gao, Q.,** Jin, P., Van der Bruggen, B. (2023). Robust and self-cleaning properties of loose nanofiltration membranes for rapid mass transfer dye/salt separations. Presented at the 13th International Congress on Membranes and Membrane Processes (ICOM 2023), Chiba, Japan.
3. **Gao, Q.,** Jin, P., Van der Bruggen, B. (2023). Robust loose nanofiltration membrane with fast solute transfer for dye/salt separation. Presented at the 13th International Congress on Membranes and Membrane Processes (ICOM 2023), Chiba, Japan.
4. **Gao, Q.,** Jin, P., Van der Bruggen, B. (2022). Improvement of robustness of loose nanofiltration membranes for dye/salt separation. Presented at the International Congress on Separation and Purification Technology 2022 (ISPT2022), Online.

MAIN AWARDS

1. Chinese government scholarship for master's degree in 2019.
2. Gold award of the 12th "Challenge Cup" national College students' entrepreneurship plan competition.
3. Silver award of the 8th national college students' "Internet +" competition.
4. Second prize of “Challenge Cup” national college student curricular academic science and technology works comptition.
5. Third prize of national college students' social practice of energy conservation and emission reduction and science and technology competition.
6. First prize of Jiangsu province college student curricular academic science and technology works competition.
7. Gold award of the 11th "Challenge Cup" Jiangsu province college students' entrepreneurship plan competition.

8. Bronze award of Jiangsu province college student business plan competition.
9. Third prize of Jiangsu chemical industry innovation competition.